

Extending Full-Plate Tectonic Models into Deep Time: Linking the Neoproterozoic and the Phanerozoic

Andrew S. Merdith^{1,*}, Simon E. Williams², Alan S. Collins³, Michael G. Tetley¹, Jacob A. Mulder⁴, Morgan L. Blades³, Alexander Young⁵, Sheree E. Armistead⁶, John Cannon⁷, Sabin Zahirovic⁷ and R. Dietmar Müller⁷

1 UnivLyon, Université Lyon 1, Ens de Lyon, CNRS, UMR 5276 LGL-TPE, F-69622, Villeurbanne, France

2 Northwest University, Xi'an, China

3 Tectonics and Earth Systems (TES) Group, Department of Earth Sciences, The University of Adelaide, Adelaide, SA 5005, Australia

4 School of Earth, Atmosphere and Environment, Monash University, Clayton, Victoria 3168, Australia

5 GeoQuEST Research Centre, School of Earth, Atmospheric and Life Sciences, University of Wollongong, Northfields Avenue, NSW 2522, Australia

6 Geological Survey of Canada, 601 Booth Street, Ottawa, Ontario, Canada & Metal Earth, Harquail School of Earth Sciences, Laurentian University, Sudbury, Ontario, Canada

7 Earthbyte Group, School of Geosciences, University of Sydney, Sydney, New South Wales, 2006, Australia

Andrew.merdith@univ-lyon1.fr @AndrewMerdith

simon.williams@nwu.edu.cn

Alan.collins@adelaide.edu.au @geoAlanC

michaelgtetley@gmail.com @mikegtet

jack.mulder@monash.edu

morgan.blades@adelaide.edu.au

ajy321@uowmail.edu.au

sarmistead@laurentian.ca @geoSheree

john.cannon@sydney.edu.au

sabin.zahirovic@sydney.edu.au @tectonicSZ

dietmar.muller@sydney.edu.au @MullerDietmar

This is the unformatted accepted manuscript published in Earth-Science Reviews
<https://www.journals.elsevier.com/earth-science-reviews>

DOI:

<https://doi.org/10.1016/j.earscirev.2020.103477>

1 **Extending Full-Plate Tectonic Models into Deep Time: Linking the Neoproterozoic and the** 2 **Phanerozoic**

3
4 Andrew S. Merdith^{1,*}, Simon E. Williams², Alan S. Collins³, Michael G. Tetley¹, Jacob A. Mulder⁴, Morgan
5 L. Blades³, Alexander Young⁵, Sheree E. Armistead⁶, John Cannon⁷, Sabin Zahirovic⁷ and R. Dietmar
6 Müller⁷

7 1 UnivLyon, Université Lyon 1, Ens de Lyon, CNRS, UMR 5276 LGL-TPE, F-69622, Villeurbanne, France

8 2 Northwest University, Xi'an, China

9 3 Tectonics and Earth Systems (TES) Group, Department of Earth Sciences, The University of Adelaide, Adelaide, SA 5005, Australia

10 4 School of Earth, Atmosphere and Environment, Monash University, Clayton, Victoria 3168, Australia

11 5 GeoQuEST Research Centre, School of Earth, Atmospheric and Life Sciences, University of Wollongong, Northfields Avenue, NSW 2522,
12 Australia

13 6 Geological Survey of Canada, 601 Booth Street, Ottawa, Ontario, Canada & Metal Earth, Harquail School of Earth Sciences, Laurentian
14 University, Sudbury, Ontario, Canada

15 7 Earthbyte Group, School of Geosciences, University of Sydney, Sydney, New South Wales, 2006, Australia

16 * Corresponding author: Andrew.merdith@univ-lyon1.fr

17 18 **Abstract**

19
20 Recent progress in plate tectonic reconstructions has seen models move beyond the classical idea of
21 continental drift by attempting to reconstruct the full evolving configuration of tectonic plates and plate
22 boundaries. A particular problem for the Neoproterozoic and Cambrian is that many existing interpretations
23 of geological and palaeomagnetic data have remained disconnected from younger, better-constrained
24 periods in Earth history. An important test of deep time reconstructions is therefore to demonstrate the
25 continuous kinematic viability of tectonic motions across multiple supercontinent cycles. We present, for
26 the first time, a continuous full-plate model spanning 1 Ga to the present-day, that includes a revised and
27 improved model for the Neoproterozoic–Cambrian (1000–520 Ma) that connects with models of the
28 Phanerozoic, thereby opening up pre-Gondwana times for quantitative analysis and further regional
29 refinements. In this contribution, we first summarise methodological approaches to full-plate modelling
30 and review the existing full-plate models in order to select appropriate models that produce a single
31 continuous model. Our model is presented in a palaeomagnetic reference frame, with a newly-derived
32 apparent polar wander path for Gondwana from 540 to 320 Ma, and a global apparent polar wander path
33 from 320 to 0 Ma. We stress, though while we have used palaeomagnetic data when available, the model
34 is also geologically constrained, based on preserved data from past-plate boundaries. This study is intended
35 as a first step in the direction of a detailed and self-consistent tectonic reconstruction for the last billion
36 years of Earth history, and our model files are released to facilitate community development.

37

38 **1 Introduction**

39

40 Plate tectonics is a unifying theory of modern geology, explicitly connecting the evolution and processes
41 that bridge the mantle, lithosphere, hydrosphere and atmosphere. Tectonic forces control the rates of uplift
42 and erosion where continents collide or separate (England and Molnar, 1990) and modulate the flow of
43 energy between oceans, lithosphere and mantle as continental configurations evolve (Bebout, 1995; Karlsen
44 et al., 2019; Müller et al., 2008). Evolving plate tectonic configurations also determine changes in how
45 species are distributed across different landmasses (McKenzie et al., 2014; Meert and Lieberman, 2008)
46 and infer the rates of chemical flux between the Earth's surface and the deep interior (Gernon et al., 2016;
47 Jarrard, 2003).

48

49 Global reconstructions have traditionally focussed on the positions of the major continents and geological
50 terranes preserved within them. Data acquired from modern oceans provide a powerful constraint on the
51 breakup of the supercontinent Pangea over the last ca. 200 Ma, and form the basis of continuous models of
52 plate configurations from the Mesozoic to present (e.g. Müller et al., 2016; Seton et al., 2012). These 'full-
53 plate' reconstructions use geological and geophysical data to determine the configurations and motions of
54 both continental and oceanic lithosphere, and the nature of the plate boundaries that separate neighbouring
55 plates. Together with the development of free software tools (Boyden et al., 2011; Müller et al., 2018), full-
56 plate reconstructions permit quantitative estimates of tectonic processes through time within a continuous,
57 consistent kinematic framework, opening up portions of Earth's history to quantitative analysis (e.g. Bower
58 et al., 2013; Brune et al., 2017; Dutkiewicz et al., 2019; Hounslow et al., 2018; Karlsen et al., 2019; Merdith
59 et al., 2019a).

60

61 Plate tectonic processes are thought to have been the dominant control on Earth's paleogeography possibly
62 since 3.2 Ga (Brenner et al., 2020; Brown et al., 2020a; Cawood et al., 2018a; Gerya, 2014; Palin et al.,
63 2020). Studies of the pre-Pangean Earth have led to the proposal that Pangea was preceded by the
64 Proterozoic supercontinents Rodinia (Dalziel, 1991; Hoffman, 1991; Moores, 1991) and Nuna/Columbia
65 (Meert, 2002; Rogers and Santosh, 2002; Zhao et al., 2002) and earlier Archaean 'supercratons' (e.g.
66 Bleeker, 2003; Pehrsson et al., 2013; Smirnov et al., 2013), reflecting transient aggregations of continental
67 blocks interspersed between other phases of Earth's history when the continents were more dispersed. The
68 absence of a pre-Mesozoic ocean floor record necessitates that reconstructing the pre-Pangean Earth relies
69 on the fragmented geological record preserved within the continents. Early studies of Proterozoic
70 supercontinents provide individual snapshots of continental configurations; though there are differences

71 between competing interpretations. More recently, attempts have been made to reconcile Neoproterozoic
72 continental motions within a continuous kinematic framework (Cawood et al., 2020; Collins and
73 Pisarevsky, 2005; Li et al., 2008). To further infer the extent and nature of tectonic boundaries covering all
74 of Earth's surface in the Proterozoic requires methodical extrapolation of available observations and is
75 subject to major uncertainties. Despite this, these reconstructions are valuable in that they make testable
76 predictions about regions and time periods where observations are lacking.

77
78 Full-plate models published over the last decade collectively span the last 1 Ga. However, each of these
79 models cover different time periods or areas of the world and each model is based on different assumptions
80 and hypotheses, and place differing emphases on subsets of the geological record. Thus, although
81 continental motions and plate boundary evolution have been categorised in some manner for the past 1 Ga,
82 there is no fully continuous model defining Earth's tectonic history for this time. A fundamental test of any
83 tectonic reconstruction for the Precambrian is that the configurations of continents, terranes and plate
84 boundaries can evolve continuously as to seamlessly merge with reconstructed configurations for more
85 recent times that are better constrained and ultimately tied to the present-day Earth. The absence of such
86 continuous reconstructions highlights a critical uncertainty for assessing interpretations of Neoproterozoic
87 palaeogeography, tectonics and geodynamics.

88
89 Our key motivations for this study are three-fold. Firstly, a 1 Ga model will permit, for the first time,
90 Neoproterozoic and Cambrian quantitative analysis that constrains (bio)geochemical and volatile fluxes,
91 palaeoclimatic studies and the nature of earth systems, during times of biological evolution and extreme
92 climate change (Gernon et al., 2016; Godd ris et al., 2017; Mills et al., 2011, 2019). Second, a full-plate
93 model would be a starting point for future studies to constrain both the tectonic (e.g. supercontinent cycle
94 (Li et al., 2019; Merdith et al., 2019b)) and geodynamic (e.g. core-lithosphere-mantle connection (Heron et
95 al., 2020; Tetley et al., 2019)) nature and evolution of the Earth. Third, a consistent model for the
96 Neoproterozoic and Cambrian that coherently links with younger models can be used as a framework to
97 support future regional studies that test and enhance the resolution of the model or spawn alternative models
98 that can be used for hypothesis testing. We stress that our reconstruction is intended to capture the main
99 aspects of global tectonics across the last billion years and consequently lacks many details that could be
100 incorporated for individual regions. Just as the earliest full-plate models for the Cenozoic and Mesozoic
101 (Seton et al., 2012) and late Palaeozoic (Domeier and Torsvik, 2014) have provided valuable open-access
102 resources for numerous other studies to test and improve, we intend that the global framework provided by
103 our reconstruction will form the basis for future studies that will generate improved reconstructions by
104 incorporating new or different observations and ideas.

105

106 This paper is organised as follows: first, we provide a review of the concepts behind full-plate
107 reconstructions, including the types of observations and assumptions on which they are based. We then
108 summarise the previously published reconstruction models and justify which elements of these existing
109 studies we have chosen to include in our reconstruction. Finally, we present the main outcome of our study:
110 the first continuous and self-consistent full-plate model from 1 Ga to present day with a single set of
111 polygons, Euler rotations and plate boundaries.

112

113 **2 Full-plate reconstruction models**

114 There are two broad categories of models that can be constructed to describe Earth's tectonic or
115 palaeogeographic history. The first category we refer to as 'continental drift' type models (Fig. 1a), as they
116 model the motion of continents drifting across the Earth's surface and tend to explicitly reflect
117 palaeogeography rather than tectonic evolution. The second type we refer to as 'full-plate models' (Fig.
118 1b), which, in addition to tracking the motion of continents, trace the evolution of plate boundaries and by
119 implication, the evolution of tectonic plates themselves (Gurnis et al., 2012). In effect, continental drift type
120 models are the precursor to full-plate models, but rather than supersede continental drift models, both types
121 of models complement each other and provide different avenues for research. Continental drift type models
122 are useful for analysing palaeomagnetic data, for contextualising regional studies or as a ground-breaking
123 study where there is little preserved data on plate boundaries. Comparably, full-plate models are more
124 encompassing, but are also much harder to iterate over and generate alternative models from. If one simply
125 requires the distribution of continental crust and not of plate boundaries, then it is much easier and simpler
126 to build a continental drift style model than categorically describe and model plate boundaries through time.
127 However, both types of models use the same reconstruction framework.

128

129

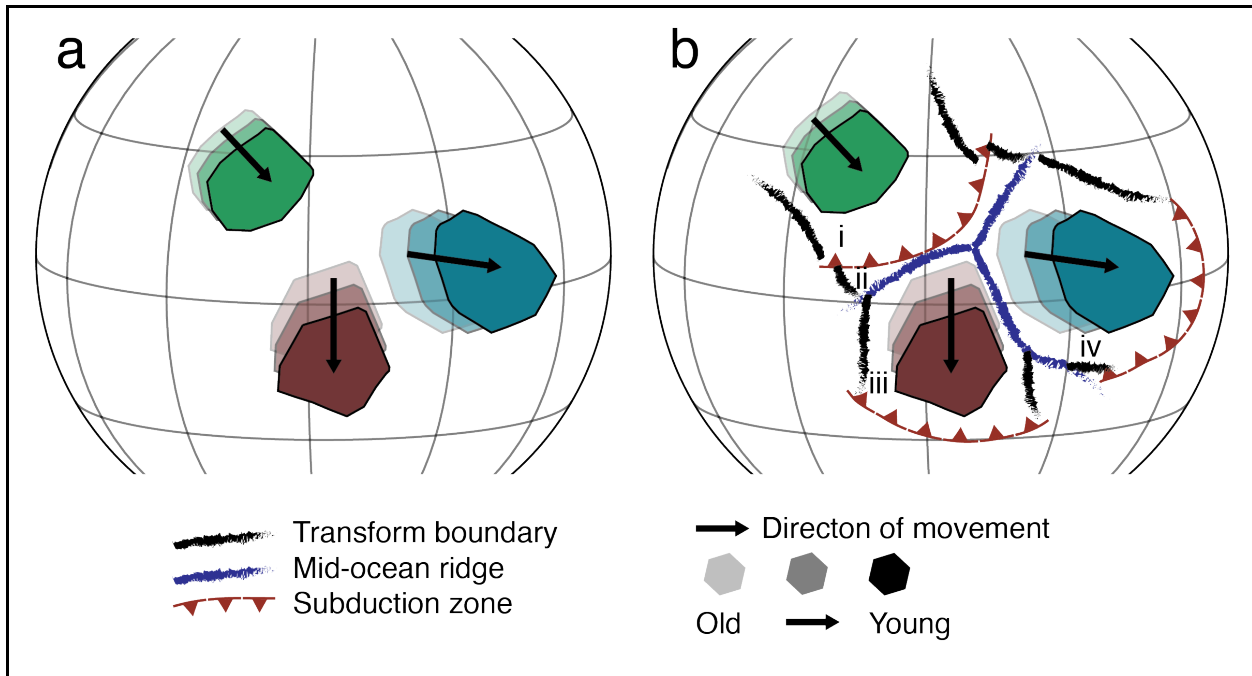


Figure 1
 Schematic comparison of evolution of plate tectonic modelling. (a) ‘Continental drift’/palaeogeographic type models and (b) full-plate models; (i)–(iv) identify separate plates. Palaeomagnetic data are the primary constraint of the movement of continents in both (a) and (b) however, the inclusion of geological data into the model in (b) preserves the relative type of motion between two continents (divergence, convergence or transform) and allows for the construction of plate boundaries.

130

131 2.1 Reconstruction Framework

132

133 The essential characteristic of any plate reconstruction is the reconstruction framework (or network
 134 (Domeier and Torsvik, 2017)), which is the organisation of data used to describe the motion of rigid objects
 135 on a sphere using Euler’s rotation theorem (McKenzie and Parker, 1967; Morgan, 1968). In plate
 136 reconstructions, the rigid objects in motion are the plates themselves and, in addition to requiring the
 137 temporal and spatial components of moving plates (i.e. the time period of motion, latitude, longitude and
 138 angle of rotation) the theorem also requires that each rotation be defined relative to another object. This
 139 rotation of one object relative to another forms the basis of a ‘relative plate motion model’. It is also
 140 desirable for these relative rotations to be tied to something (relatively) immutable within, or around, the
 141 Earth (e.g. the core, mantle, or the spin-axis) thus, transforming the model into an ‘absolute plate motion
 142 model’. For the Mesozoic and Cenozoic, plates are described in a relative framework due to the preservation
 143 of oceanic lithosphere within oceans formed since the breakup of Pangea. In this way each plate’s motion
 144 history is described as moving relative to another plate, with the African plate typically at the top of the
 145 hierarchy (e.g. (Ross and Scotese, 1988; Torsvik et al., 2008); Fig. 2a, b). The motion of the African plate

146 can then be defined absolutely (though using observations from many or all plates, and not just Africa) to
147 the deep Earth through alternative methods such as hotspot chains (Müller et al., 1993; O'Neill et al., 2005),
148 seismic imaging of subducted slabs (van der Meer et al., 2010), palaeomagnetic data (with or without true
149 polar wander corrections, Torsvik et al., 2012) or methods jointly evaluating the characteristics of multiple
150 constraints including plate velocities, hotspot chains and subduction trench migration (Tetley et al., 2019).
151 Regardless of which method is chosen, the result is a global reference frame defined as a sequence of
152 absolute motions of the African plate, which, together with the relative motions between plate-pairs
153 arranged within a hierarchy (Fig. 2), define the absolute motions of all plates. An exception to all plates
154 being tied to Africa occurs for the Mesozoic Pacific Ocean. Before 83 Ma (and the opening of the West
155 Antarctic spreading centre) the motion of the Pacific plate is preserved and reconstructed absolutely to the
156 spin axis through hotspot motion, rather than through Africa. Plate models can also be described in a purely
157 relative framework, in which case a single continent (or plate) is fixed to its present-day position and all
158 other continents or plates are rotated relative to the fixed plate. This approach is commonly used for
159 localised studies or to easily highlight the difference between two contrasting models (Fig. 2c).

160

161 Before the Mesozoic era, it is not possible to use preserved, *in situ* oceanic lithosphere, hotspot motions
162 and seismic imaging of slabs. Therefore, the logical arrangement of connections within the rotational
163 framework changes (Domeier and Torsvik, 2017), however the general principles of plate reconstructions
164 remain the same. For these times, the only quantitative information on the positions of plates is through
165 palaeomagnetism, which describes the palaeolatitude of continents with respect to the Earth's spin axis. In
166 these cases, where the absolute motions are more directly constrained than relative motions, rotation models
167 traditionally favour a simpler hierarchy, rather than the complex hierarchies used for post-Pangea times (e.g
168 Fig. 3a, b). The motion of major continents relative to the spin axis is determined using their own
169 palaeomagnetic data (Fig. 3a, b). Within this data set, continents can be grouped together in localised
170 hierarchies where there is evidence that they have remained together or close to one another or, in instances
171 where paleomagnetic data are lacking from some of the blocks if geological constraints permit.

172

173 Finally, although Euler's rotation theorem is based on the motion of rigid bodies, this is a simplification
174 because the lithosphere is deformable. Recent advancements in plate modelling (Gurnis et al., 2018) have
175 allowed for the development of deforming plate models where rigid plates are able to deform along their
176 edges.

177

178

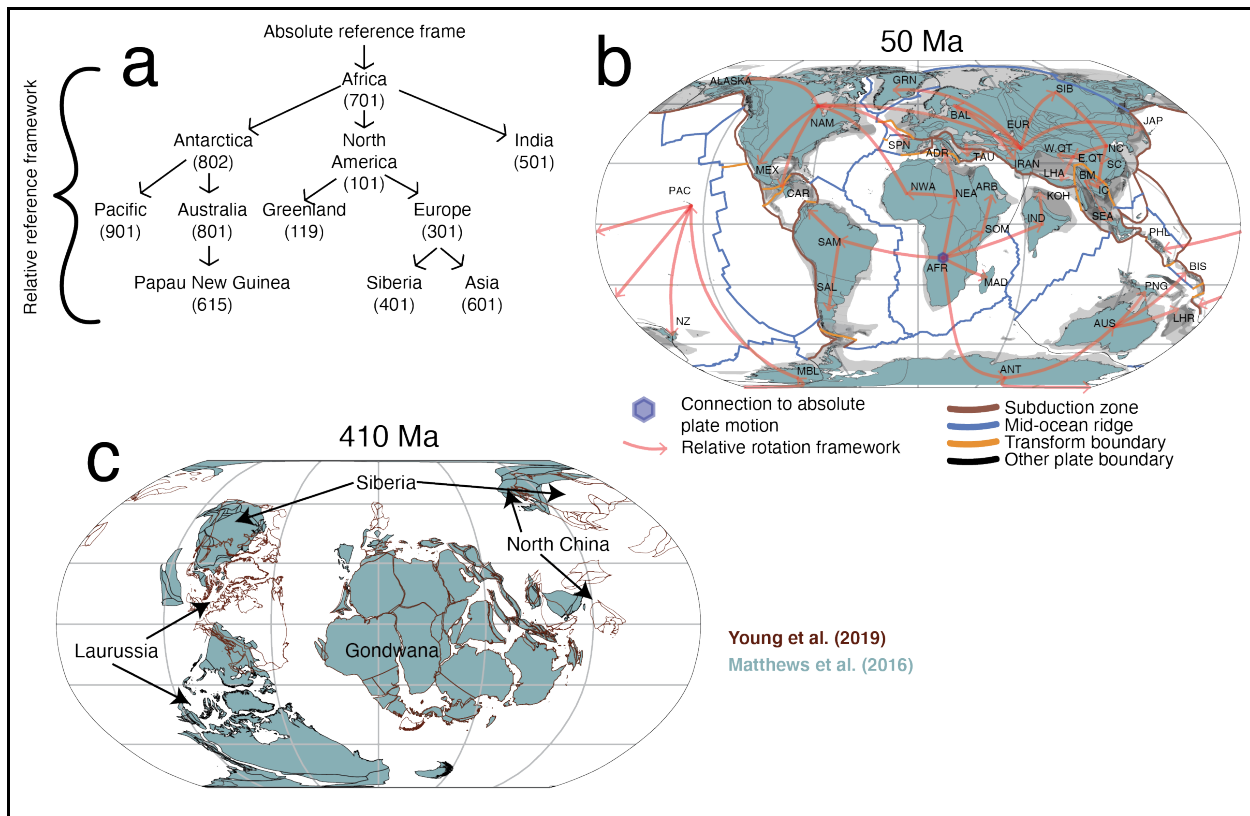


Figure 2

Overview of the rotational framework of a relative plate motion model. (a) Schematic of the ‘tree’ like hierarchy (e.g. Ross and Scotese, 1988) from the Matthews et al. (2016) reconstruction, where the motion of all plates are defined relative to the African plate at 50 Ma. (b) A simplified map view of the hierarchy in (a). The African stage pole (blue hexagon) is at the top of the hierarchy and connected to the absolute plate motion model that describes the movement of the African plate (in this case, as a proxy for the entire globe) to the deep earth. (c) Example of plate motion with a continent (Africa) fixed in its present-day position. Fixed plate presentations enable observations of relative motions between the fixed continent or plate and another. Hence, they are useful to constrain relative plate motions and also compare two or more different plate models. In this instance, a key difference between the model of Young et al. (2019) and Matthews et al. (2016) is highlighted in the spatial relationship between Laurussia and Gondwana at 410 Ma. In Domeier and Torsvik (2014) (which is preserved in Matthews et al. (2016)) Laurussia is proximal to southwest Gondwana while in Young et al. (2019) it is positioned to the northwest. ADR, Adria; AFR, Africa; ARB, Arabia; AUS, Australia; BAL, Baltica (cratonic Europe); BM, Burma; CAR, Caribbean; E.QT, East Qiangtang; EUR, Europe; GRN, Greenland; IC, Indochina; IND, India; JAP, Japan; KOH, Kohistan arc; LHA, Lhasa; LHR, Lord Howe Rise; MAD, Madagascar; MBL, Marie Byrd Land; MEX, Mexico; NAM, North America; NC, North China; NEA, Northeast Africa; NWA, Northwest Africa; NZ, New Zealand; PAC, Pacific; PHL, Philippines; PNG, Papua New Guinea; SAL, Salado Microplate; SAM, South America; SC, South China; SEA, Southeast Asia; SIB, Siberia; SOM, Somalia; SPN, Spain; TAU, Taurides; W.QT, West Qiangtang.

181 2.2 Palaeolatitude

182

183 Palaeolatitude is determined through the study of palaeomagnetic data and is the only method to
184 quantitatively constrain the absolute latitudinal position of a continent for pre-Jurassic times. If sufficient
185 data are present from a single continent, an apparent polar wander path (APWP) can be constructed that
186 describes the motion of that continent through time (Torsvik et al., 2012). If there are very good geological
187 constraints on the relative positioning between multiple continents, then poles from these continents can be
188 merged to form composite apparent polar wander paths. This merging is done by rotating the poles of
189 multiple continents into the coordinate frame of a single continent, typically found higher in the framework
190 (e.g. Africa, Fig. 2a). If this process is done using all global data it is known as a global apparent polar
191 wander path (GAPWaP). GAPWaPs provide the potential for a more rigorous description of the evolution
192 of a suite of continents as more data are available.

193

194 There are, however, many caveats and uncertainties associated with GAPWaPs and APWPs that contain
195 data sourced from more than one continent (e.g. APWP for Gondwana). In particular, they are strongly
196 dependent on the relative position of continents, as even minor changes in these relative positions can result
197 in large differences in the resulting wander paths. They also are directly dependent on the quality and
198 abundance of palaeomagnetic data, thus a degree of subjectivity can be introduced by what criteria are used
199 for selecting and filtering poles (Van der Voo, 1990; see a new approach in Wu et al., 2020). For example,
200 in the Gondwana APWP of Torsvik et al. (2012) (and also for the APWP we construct in this paper), there
201 is one pole for Gondwana between 440 and 400 Ma that constrains the motion of over half of all known
202 continental crust at the time. In the Precambrian, the geological uncertainty of exactly how two cratons (or
203 continents) fit together limits the usefulness of GAPWaPs and APWPs that are defined by multiple
204 continents in conjunction with one another. Instead individual APWPs can be constructed using available
205 palaeomagnetic data for continents and then these are all balanced together globally to produce a coherent
206 kinematic continental model (e.g. Li et al., 2008; Pisarevsky et al., 2014). In this manner, it is possible to
207 build continental drift models purely from palaeomagnetic data.

208

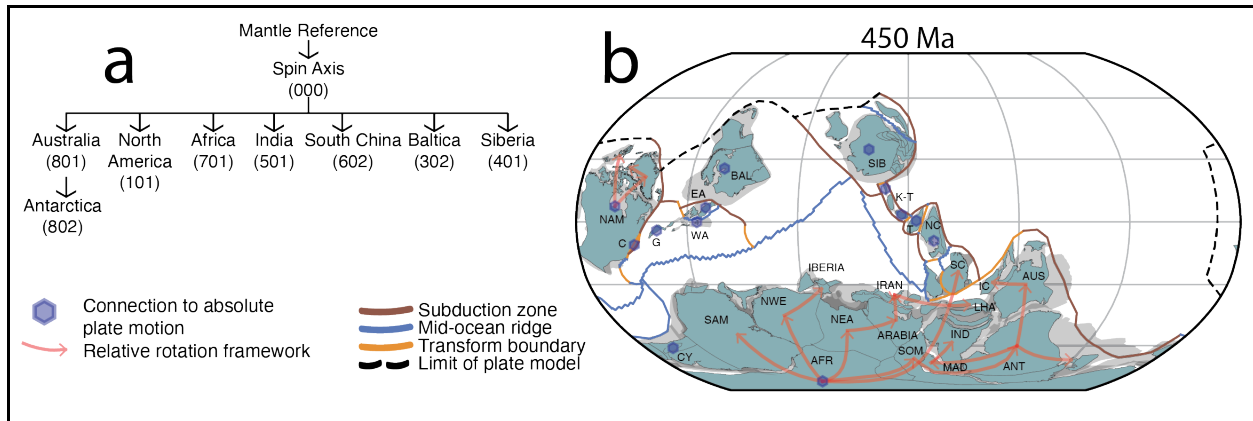


Figure 3
 Overview of the rotational framework of an absolute plate motion model. (a) Schematic of a flat hierarchy where the motion of all plates is defined relative to Africa. (b) Map view of the schematic at 450 Ma from Domeier (2018, 2016). Many different plates (blue hexagons) sit at the top of the hierarchy and connect to the deep earth. AFR, Africa; ANT, Antarctica; AUS, Australia; BAL, Baltica; C, Carolina; CY, ; EA, East Avalonia; G, Ganderia; IC, Indochina; IND, India; K-T, Kazakh-Tianshan; LHA, Lhasa; MAD, Madagascar; NAM, North America; NC, North China; NEA, Northeast Africa; NWA, Northwest Africa; SAM, South America; SC, South China; SIB, Siberia; SOM, Somalia; T, Tarim; WA, West Avalonia.

209

2.3 True Polar Wander

210

211
 212 True polar wander (TPW) is the motion of the entire solid Earth (mantle-lithosphere) with respect to the
 213 spin axis due to centrifugal forces from Earth's orbit acting on mass anomalies in the upper mantle, wherein
 214 positive anomalies are driven towards the equator and negative anomalies towards the poles (Evans, 2003).
 215 Since TPW is inherent in palaeomagnetic data, all APWP are a composite of both plate motions and some
 216 component of TPW. Thus, in the strictest sense, to properly use a plate model for geodynamic modelling,
 217 a correction that removes any component of detected TPW should be applied (i.e. the mantle reference
 218 frame). Further, as the mass anomalies in the mantle are thought to arise from the flow induced by subducted
 219 oceanic lithosphere and the associated return flows, TPW excursions are closely linked to the
 220 supercontinent cycle (Zhong et al., 2007).

221

222 Raub et al. (2007) identified three types of TPW summarised briefly below, though only the latter two are
 223 relevant here. Type 0 TPW operates on short ($< 10^3$ a) timescales as a response to elastic deformation within
 224 the lithosphere arising from seismic events (Soldati et al., 2001) and so has a negligible effect on plate
 225 motions on the timescales pertinent here (Evans, 2003; Raub et al., 2007). Type 1 TPW is the most
 226 important to consider, and is broadly defined as the slow motion of the solid Earth (mantle and lithosphere)
 227 readjusting to mass anomalies in the mantle. Type 1 TPW is what is commonly detected and corrected in

228 plate motion models (Steinberger and Torsvik, 2008; Torsvik et al., 2012) in order to constrain geodynamic
229 relationships between deep Earth processes and tectonics (Mitchell et al., 2012). Type 2 TPW (Inertial-
230 Interchange True Polar Wander, IITPW) was originally described by Kirschvink (1997) and is a hypothesis
231 where the mantle and crust are rapidly displaced over large distances relative to the spin axis as the moment
232 of minimum inertia (I_{min}) approaches the maximum moment of inertia (I_{max}) resulting in an interchange
233 between the two (i.e. I_{min} becomes I_{max} and vice versa). IITPW has been linked to supercontinent breakup
234 as continental lithosphere and subduction zones move away from the upwelling, known as a superswell,
235 developing beneath the supercontinent, which is assumed to remain quasi-stable (Li et al., 2004). In the Li
236 et al. (2004) model, the superswell is likely to maintain the I_{max} , but as all the continents move away I_{min}
237 approaches I_{max} , thus they are speculated to interchange with each other.

238
239 The primary challenge of subtracting the effects of TPW from APW paths is identifying and separating
240 TPW components from continental motion. Methods of detecting TPW vary, either isolating it directly
241 from palaeomagnetic data (Mitchell et al., 2012) or deconstructing the APWP of continents by comparing
242 the kinematic motions of all continental lithosphere on the globe to isolate TPW (Steinberger and Torsvik,
243 2008). Both approaches require *a priori* assumptions stemming from the choice of plate model being
244 analysed, which makes it impossible to apply a TPW correction from one model to another. For example,
245 fitting a great circle to palaeomagnetic data following the approach of Mitchell et al. (2012) is dependent
246 on knowing the relative continental configuration from which the palaeomagnetic data are sampled.
247 Alternatively, deconstructing the motions of the continents after Steinberger and Torsvik (2008) is
248 dependent on constraining absolute palaeolongitude to separate TPW from apparent polar wander. In order
249 to support their arguments, both methods are dependent on having some form of absolute palaeolongitudinal
250 control.

251

252 **2.4 Palaeolongitude**

253

254 There is no well-established method to compute the absolute palaeolongitude of any given plate that is
255 applicable to pre-Jurassic times. However, two hypotheses have been proposed for establishing absolute
256 palaeolongitude for pre-Pangea reconstructions (Torsvik and Cocks, 2017): (i) the plume generation zone
257 method (PGZ) (Torsvik et al., 2014) and (ii) the orthoversion model of the supercontinent cycle (Mitchell
258 et al., 2012).

259

260 The PGZ method is based on reconstructing the surface locations of kimberlites and large igneous provinces
261 (LIPs) to the margins of the large low shear velocity provinces (LLSVPs) (Burke and Torsvik, 2004;

262 Torsvik et al., 2010a) situated on the core-mantle boundary (CMB) (Garnero et al., 2007; Li and McNamara,
263 2013). The foundation for this method is the observation that kimberlites and LIPs, when restored to a
264 mantle reference frame at the time of eruption, are positioned preferentially above the margins of the
265 LLSVPs (Burke and Torsvik, 2004; Torsvik et al., 2010a). LLSVPs are regions of anomalously slow
266 (slower than ambient mantle) seismic velocities, close to the core–mantle boundary. Since large-scale
267 mantle structure is intimately related to the supercontinent cycle, LLSVPs (Li and Zhong, 2009) are thought
268 to exist for (at least) a similar time frame as the supercontinent itself (i.e. present-day LLSVPs are thought
269 to have existed at least back to 320 Ma) (Li and Zhong, 2009), but not necessarily maintaining their present-
270 day geometry (Flament et al., 2017; Zhang et al., 2010; Zhong and Rudolph, 2015).

271
272 The PGZ method to establish absolute palaeolongitude therefore assumes: (i) the geometric stability of the
273 present-day positions of LLSVPs back to the time of interest, and (ii) that there is a positive statistical
274 correlation with margins of LLSVPs and the extrusion of LIPs and kimberlites at the Earth’s surface.
275 Adopting the PGZ method allows one to position continents longitudinally by reconstructing the positions
276 of LIPs and kimberlites to overlie the margins of LLSVPs while simultaneously utilising TPW-corrected
277 palaeomagnetic data (Torsvik et al., 2014). In this way, models with explicitly defined and reproducible
278 absolute plate motions can be created (Domeier and Torsvik, 2014). However, a number of recent studies
279 have raised questions about the assumptions implicit in the PGZ approach. For example Flament et al.
280 (2017) and correspondence by Torsvik and Domeier (2017), Doucet et al. (2020), Zhong and Rudolph
281 (2015) and Zhong and Liu (2016) on long term LLSVP stability and Austermann et al. (2014), Davies et
282 al. (2015), with response by Doubrovine et al. (2016) on the statistical correlation. Consequently, while
283 utilising the PGZ method for plate reconstructions in the Palaeozoic is currently an open area of research,
284 the theoretical and practical application for Precambrian times remains untested.

285
286 The other proposed method of determining absolute palaeolongitude for deep time reconstructions is known
287 as the ‘orthoversion model’ and suggests that successive supercontinents coalesce orthogonally (90°
288 longitude) above the downwelling formed by subduction at the margin of the previous supercontinent
289 (Mitchell et al., 2012). Mitchell et al. (2012) test their model by first determining the minimum moment of
290 inertia (I_{min}) during each phase of supercontinent assembly. This is done by rotating the available
291 paleomagnetic data into a relative reference frame of a fixed continent (Africa for the Phanerozoic,
292 Laurentia for the Neoproterozoic) and then fitting a great circle to the resulting poles. I_{min} is defined as the
293 orthogonal axes (or pole) of the great circle and is taken to approximate the TPW axis. Mitchell et al. (2012)
294 fitted great circles to palaeomagnetic data for a selection of time periods (1165–1015 Ma, 805–790 Ma,
295 550–490 Ma and 220–90 Ma) and calculated that the angle between each successive I_{min} was $\sim 90^\circ$; as

296 expected in the orthoversion model. The initial (palaeolongitudinal) placement of Pangea is constrained
297 from its position at ~90 Ma (centroid of I_{min} at 0°N, 10°E) when the most recent TPW episode finished
298 (Steinberger and Torsvik, 2008). Therefore, during Rodinia and Gondwana, when I_{min} was 90° from present
299 day, Mitchell et al. (2012) proposed that the centre of mass of both was positioned at 100°E.

300
301 As with the PGZ, a number of limitations are apparent with the orthoversion model. In particular, the
302 method of Mitchell et al. (2012) does not separate continental motion from true polar wander when
303 calculating I_{min} , thus it assumes that during these times TPW is the primary signal recovered from
304 palaeomagnetic data and not continental motion. Secondly, the orthoversion model is inherently dependent
305 on both the quality and abundance of palaeomagnetic data (e.g. the Rodinia I_{min} in Mitchell et al. (2012) is
306 based on only three poles), as well as the continental configuration of the time (as the continental
307 configurations can determine the relative position of palaeomagnetic data when rotated into a specific
308 reference frame). Torsvik and Cocks (2017) highlight this succinctly by using slightly different
309 palaeomagnetic data, and a slightly different Gondwana configuration to produce an I_{min} between 550 and
310 490 Ma of 50°S, 64°E (compared to the estimate of Mitchell et al. (2012) of 30°S, 75°E). Finally, the
311 calculation of I_{min} at each time step occurs within a fixed relative reference frame (i.e. Fig. 2c), meaning
312 that the I_{min} itself cannot be restored to an absolute palaeogeographic position. Thus, the longitudinal centre
313 of Rodinia at 100°E is not explicitly proven by Mitchell et al. (2012). Instead, since the calculated
314 successive I_{min} 's are 90° apart, it is inferred to be in this location.

315 316 **2.5 Geology**

317
318 Geology is unfortunately silent on the absolute positioning of continents in time, except in circumstances
319 such as the PGZ method discussed above. However, it contains a wealth of information of relative plate
320 motions in the Mesozoic and Cenozoic (e.g. seafloor spreading), and in deeper time through the temporal
321 evolution of sedimentary basins and facies, and tectonic affinities inferred from geochemistry, zircon
322 arrays, magmatism and metamorphism. However, geology does have an advantage over palaeomagnetic
323 data in that there are many different types of data available, especially from small and minor terranes in the
324 Precambrian that are otherwise unconstrained palaeomagnetically. Given the wealth of geological data,
325 especially in the Neoproterozoic, there is a general hierarchy of use that is a reflection of the scale of the
326 problem. Our approach is to start by building a global framework and work progressively to finer resolution
327 to inform the localised nature of that framework.

328

329 The first and most important geological data to gather is evidence of rifts and arcs, as they describe
330 separation (usually leading to seafloor spreading) and convergence, respectively and can therefore put in
331 place the framework for plate motions and subsequent interpretation of geological data. Secondly,
332 identifying piercing points where geological boundaries can be matched on now separate continents (e.g.
333 Appalachians and Gondwana forming orogenies), or ways of fitting two continents together in a stable
334 configuration. These piercing points are important because reconstructing continental configurations with
335 high confidence allows the generation of more rigorous APWPs and they help to constrain the location and
336 orientation of both rifts and arcs on the periphery of continents. Unfortunately, due to deformation and
337 progressive alteration of continental crust (e.g. changes of continent-ocean boundaries (COBs)), in pre-
338 Gondwana times it is difficult to be more precise than matching the margins of large continents and for
339 smaller cratons and terranes it is almost impossible. A pertinent example of this are the four different
340 proposed configurations of Australia and Laurentia during Rodinia (see reviews by Li et al., 2008; Meredith
341 et al., 2017b), which all broadly match the same margins against each other (east coast of Australia with
342 the west coast Laurentia, with or without an intervening continent) but place them in different relative
343 positions.

344
345 After arcs and rifts, we can loosely (but not exhaustively) group geological features and data based on their
346 applications. Sedimentary basins, dyke swarms, detrital minerals, geochemical signatures and fossils are
347 typically used to determine provenance or latitudinal band and align once contiguous regions. The time-
348 scales and conditions of metamorphism together with structural data can be used to infer the tectonic setting
349 and polarity of collisional events or help constrain the nature of indeterminate plate margins such as
350 transform boundaries. These types of data assist in increasing the resolution of a plate model by
351 understanding the geology at smaller scales within the framework of a specific tectonic setting, such as an
352 arc or rift. We stress here that the relationship between detailed regional geology and the broader framework
353 of a plate model is not a 'one-way street' but is highly iterative. If, for example, a detailed geological study
354 determines that an interval of magmatism and sedimentation that was originally interpreted as a failed rift,
355 in fact led to seafloor spreading, then the broader scale tectonic framework and plate model must be re-
356 evaluated. Finally, due to the qualitative nature of most geological data, the iteration and implementation
357 of these data into the plate model typically necessitates qualitative decisions that others may disagree with.
358 Iteration over the model continues until we approach tectonic congruency within the model (i.e. data-based
359 iterations in one part of the world do not nullify data in other areas of the world). We stress that this does
360 not mean our model is 'correct' or 'true', just that it is internally consistent with as much data as possible.
361 Consequently, we consider the model presented here a viable, but non-unique interpretation of
362 Neoproterozoic data.

363

364 A specific example of the importance of interpreting geology within a full-plate framework is given by
365 recent work on the Stenian–Cryogenian evolution of the East African Orogen. Although arc-related
366 magmatism has been recognised in the northern East African Orogen for a number of decades (e.g. Stern,
367 1994), the recognition of similar-aged arc magmatism in the higher-grade southern East African Orogen of
368 Madagascar, Southern India and East Antarctica has been more controversial and under-appreciated until
369 recently (Archibald et al., 2018, 2017; Armistead et al., 2019; Plavsa et al., 2015; Ruppel et al., 2018). In
370 one particular example, work over the last decade on Western Dronning Maud Land in East Antarctica has
371 identified an extensive Stenian–Tonian juvenile arc system (named TOAST; (Elburg et al., 2015; Jacobs et
372 al., 2015; Ruppel et al., 2018)). This discovery has gone hand-in-hand with the recognition of a similar
373 region in western Madagascar, known as the Dabolava Arc (Archibald et al., 2017; Tucker et al., 2011)
374 (e.g. Fig. 8). These arcs are now separated by a considerable distance, but their reconstructed position in
375 the Neoproterozoic and their similarity has led to us interpreting them as part of one continuous subduction
376 system that was active for the Stenian and Tonian. In this manner, we now include TOAST as another part
377 of Azania and have reworked a number of the plate boundaries in Merdith et al. (2017a) to reflect these
378 new geological data and tectono-geographic interpretations.

379

380 **2.6 Kinematic considerations**

381

382 The final line of reasoning used to create full plate models are plate kinematic constraints. These are not
383 defined explicitly through geological or geophysical data of the types outlined above, but rather come from
384 the idea that the evolution of plate motions through time must follow the broad principles of plate tectonics
385 in a way that would seem reasonable; for example, by equivalency with more recent and well-constrained
386 plate motions. The most basic requirement is that continental blocks cannot pass through or significantly
387 overlap other continents and we must be able to describe the position and motion of each continental block
388 for as long as the crust within that block is thought to have existed. While this may seem obvious, these
389 considerations present a powerful method for discriminating between competing reconstruction scenarios.
390 Models constructed for deep time that cannot evolve towards more recent and present-day configurations
391 of continents cannot be considered correct. Similarly, models requiring an implausible kinematic evolution
392 in order to meet present-day configurations cannot be correct. A tangible example is Rodinia, for which a
393 range of configurations could be permissible based on available paleomagnetic and geological data (see
394 reviews in Evans, 2013; Li et al., 2008; Merdith et al., 2017b). However, analysing the sequence of plate
395 motions required to translate each continent to their (better constrained) positions during the Palaeozoic is
396 more plausible in some of these scenarios than others, such as not requiring individual terranes or blocks to

397 cross multiple ocean basins or navigate their way around a stable continent (Merdith et al., 2017b). Further
398 examples where kinematic constraints add useful insights are when constructing models that explicitly trace
399 the evolution of plate boundaries and tectonic plates. An example is expressed in the logic of Domeier
400 (2018) who inferred that the longitudinal position of Tarim, North China and South China during the late
401 Cambrian–Devonian must have remained stable relative to one another, because palaeolatitudes from
402 palaeomagnetic data overlapped and therefore must be consistent with their end position in the more well
403 constrained Devonian–Triassic.

404
405 Finally, we take a uniformitarian view of tectonic evolution, in that we assume that plate tectonics and
406 relative plate motions were operating on similar principles in the Neoproterozoic to what we can observe
407 in the Mesozoic and Cenozoic. During more recent times, the motion of plates remains relatively constant
408 for time lengths on the order of 10–100 Ma, with changes in motion occurring comparatively quickly (< 3
409 Ma) and tied to an event further afield, such as terrane collision in a subduction zone, subduction onset,
410 rifting onset or ridge subduction (e.g. Austermann et al., 2011; Cawood et al., 2016; Cawood and Buchan,
411 2007; Knesel et al., 2008). The representation of this within a conceptual framework is that a single
412 continent or plate may move for time lengths on the order of 10–100 Ma around a single Euler pole, before
413 a plate re-organisation event triggers a change in direction and velocity of the plate (Gordon et al., 1984).
414 Within palaeomagnetic data, this approach is exemplified in Torsvik et al. (2008), where filtered
415 compilations of data result in smooth APWP segments punctuated by cusps in motion and velocity, and
416 more recently by Wu et al. (2020). For the Neoproterozoic, which has much more sparse palaeomagnetic
417 data coverage than the Phanerozoic, the logic can be applied by linking changes in plate direction (as
418 suggested or necessitated by palaeomagnetic data) directly to geological evidence of a change in tectonic
419 regime within the region of interest (e.g. Merdith et al., 2017b).

420

421 **2.7 Synthetic Ocean Plates**

422
423 A complete full-plate model by definition includes a representation of the evolution of ocean basins through
424 time. This is the most uncertain part of any full-plate model. With a few exceptions (e.g. Granot, 2016), no
425 pre-Jurassic ocean crust is preserved *in situ*, so that even where we can infer the presence of divergent plate
426 boundaries (for example, following continental breakup), the precise geometry and spreading rates at these
427 boundaries are conjectural. Consequently, there are no unique solutions to the definition of these boundaries
428 and the synthetic ocean plates constructed from them. The main aim in the reconstruction of ancient ocean
429 basins is to ensure that the synthetic plates and plate boundaries are at least consistent with sparse
430 observations preserved on the continents.

431
432 Firstly, although we have little data on the creation of oceanic lithosphere for pre-Jurassic times, the
433 geological record does preserve data on the consumption of oceanic lithosphere at subduction zones. The
434 most important criteria that therefore must be met are that (i) (sub-) orthogonal divergence occurs at mid-
435 ocean ridges and that (ii) convergence occurs at subduction zones (Domeier and Torsvik, 2014). The former
436 of these two criteria typically occurs between continents during supercontinent breakup or when small
437 terranes rift from a continent (Dalziel, 1997). The latter of these includes subduction along the margins of
438 continents as well as within intra-oceanic arcs. Thus, these two criteria necessitate the extrapolation of
439 known plate boundary positions (e.g. preserved continental arcs, rift zones) into larger areas to ensure the
440 tectonic congruency of the model (in this case, that convergence or divergence at one location doesn't
441 nullify the same criteria in another location). It is this step, in particular, that requires significant iteration
442 when constructing a model. Maintaining tectonic congruency for a model is best achieved when the
443 extrapolation of plate boundaries is done as simply as possible. For example, in reconstructing an ocean
444 basin without any continental crust (e.g. Pacific Ocean, Panthalassa Ocean), a triple junction is usually the
445 simplest expression of a ridge system that ensures divergence in all directions and convergence at its
446 margins (Domeier and Torsvik, 2014). The evolution of such a triple junction could also be seen in the
447 Ediacaran opening of the Iapetus Ocean (e.g. Pisarevsky et al., 2008; Robert et al., 2020),

448

449 **3 Model selection and justification**

450

451 **3.1 Existing plate models**

452

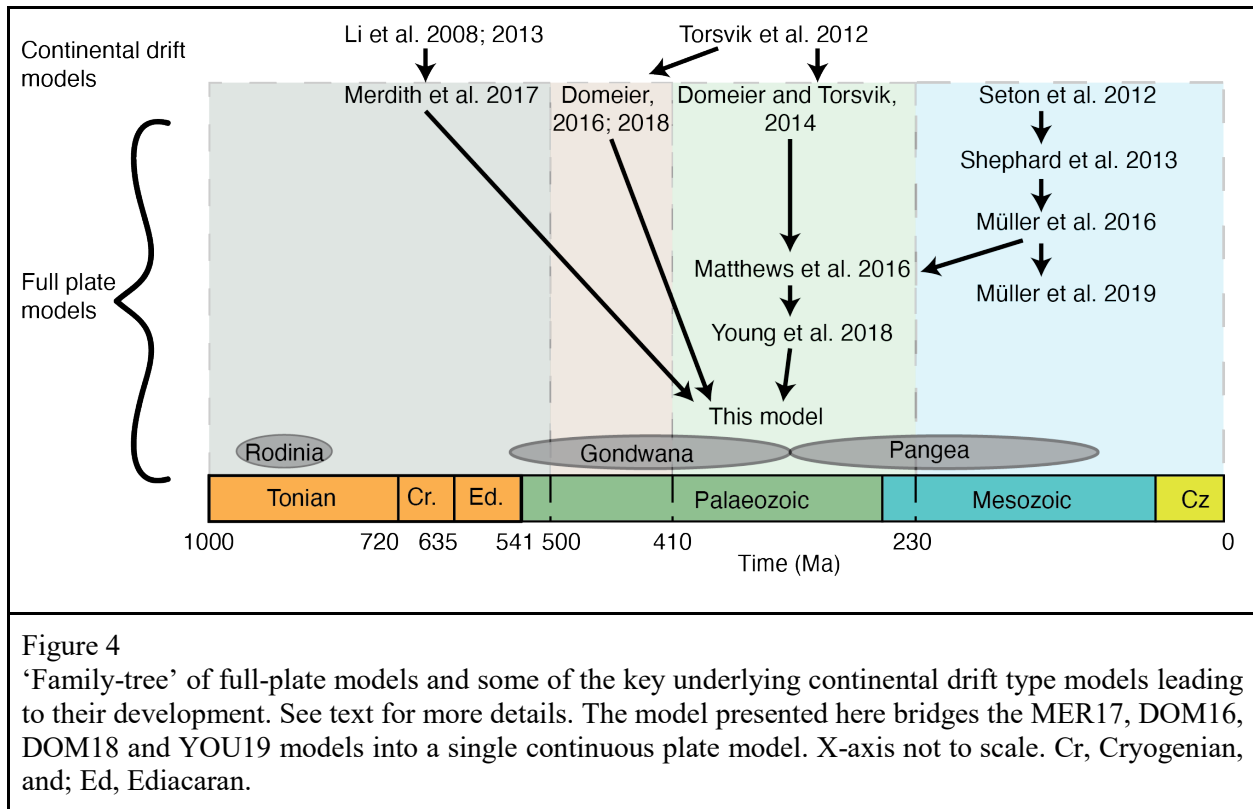
453 The selection of which full-plate model to assist in solving a problem is dependent on the nature of the
454 problem, as each published plate model is constructed using a different approach and has a different
455 reconstruction framework. For example, a study looking at absolute plate motions of the Cenozoic has little
456 use for models connected to the Palaeozoic or Neoproterozoic. Instead, such studies typically include a
457 comparison with previously published models as well as a rigorous mantle reference frame. Similarly, a
458 study that traces the latitudinal distribution of continental arcs through the Phanerozoic has no need for a
459 mantle reference frame and a study investigating the changes in net rotation through time would be
460 concerned with small, localised improvements from regional models but more focussed on capturing the
461 large scale changes that occur when continents breakup. Although newer plate models typically address the
462 shortcomings of previous models or implement more refined updates of regional areas, this does not
463 necessarily make them better for all applications. Older plate models have been more rigorously tested and
464 used by the community and as one travels further back in geological time, the data are more ambiguous and

465 can invite alternative interpretations. For the purpose of this study, the existing plate models we consider
466 are only those that are publicly released with fully self-consistent with coherent plate motions and plate
467 boundaries. Thus, we omit many models that provide only continental motions (Scotese, 2016; Torsvik and
468 Cocks, 2016), alternative or regional Rodinia configurations (Evans, 2013) or regional refinements of
469 global models for the Mesozoic and Cenozoic (e.g. Vaes et al., 2019).

470
471 The major step forward for producing full-plate models was the construction of open-source computer
472 software specifically designed to work with full-plate reconstructions (e.g. GPLates; (Gurnis et al., 2012).
473 Following their development, GPLates-compatible global models for the Early Jurassic to present (Seton et
474 al., 2012; Shephard et al., 2013) and a model for the Late Palaeozoic (Domeier and Torsvik, 2014) soon
475 followed (hereafter, SET12 and DT14, respectively). Subsequent work by Matthews et al. (2016) (MAT16)
476 bridged the gap between the Palaeozoic and Jurassic, linking a slightly modified version of DT14 with an
477 updated SET12 model, the Müller et al. (2016) model (MUL16). Further back in time, two models for the
478 Early Palaeozoic (500 to 410 Ma) now exist: Domeier (2016) (DOM16), which encompasses the evolution
479 of the Iapetus and Rheic Oceans, as well as the motion of Gondwana, and Domeier (2018) (DOM18), which
480 models the evolution of the first generations of Tethyan Oceans and Central Asian blocks (Siberia, North
481 and South China, Tarim). For the Neoproterozoic, Merdith et al. (2017a) (MER17) produced a full-plate
482 model from 1000 to 520 Ma, using the models of continental motion presented by Li et al. (2013, 2008) as
483 a base. An alternative reconstruction from the late Palaeozoic to present-day has been presented by Young
484 et al. (2019) (YOU19). YOU19 offers an alternative full-plate model for the Palaeozoic to the DT14 and
485 MAT16 models that does not rely on the PGZ method. Finally, a deforming plate model was produced
486 (Müller et al., 2019) (MUL19) that modelled rift and convergence deformation from 250 to 0 Ma. Table 1
487 summaries the main features of these models.

488

489



491

492 **3.2 Cenozoic and Mesozoic plate models**

493

494 We consider three plate models for the Cenozoic and Mesozoic: SET12, MUL16, and MUL19 (Fig. 4). The
 495 SET12 model spans from present-day to 200 Ma, with MUL16 and MUL19 extending back to 230 and 240
 496 Ma, respectively. The main geological constraint of these models are the magnetic lineations preserved in
 497 oceanic crust that describe the relative movement between the pairs of continents breaking apart during the
 498 fragmentation of Pangea. The evolution of the Atlantic, Indian, Southern, Arctic and Cenozoic Pacific
 499 oceans are consistent, to the first order, across all three models. Larger differences between the models arise
 500 in regions where oceanic crust has been subducted, upon which they then rely on a combination of
 501 geometric (e.g. assumption of symmetrical spreading), geological, seismic and palaeomagnetic data to
 502 constrain the motion and evolution of terranes that open and close ocean basins (e.g. Liu et al., 2010, 2008;
 503 Sigloch and Mihalynuk, 2013). In these regions, the tectonic histories, even for Cenozoic times, remain the
 504 subject of ongoing research and the scenarios embedded in the global models used in this study represent
 505 one candidate amongst many competing models. For example, the extent of subduction systems within the
 506 Tethyan domain and the nature of India-Eurasia collision is still hotly debated (Hu et al., 2016; Parsons et
 507 al., 2020; van Hinsbergen et al., 2020, 2012). Similar combinations of methods have been used to propose

508 alternative interpretations for circum-Pacific regions, especially for the Cretaceous and earlier times in the
509 northwest Pacific (Domeier et al., 2017; Konstantinovskaya, 2002; Shapiro and Solov'ev, 2009; Vaes et
510 al., 2019; Wu et al., 2016), the southwest Pacific (Hochmuth et al., 2015; Matthews et al., 2015; Schellart
511 et al., 2006; Sutherland et al., 2020) and the northeast Pacific (Clennett et al., 2020; Sigloch and Mihalyuk,
512 2013). All of these regions invite competing models and alterations to existing global models and it is
513 notable that many of the studies mentioned above have benefited from using the resources made available
514 by previous global studies, beginning with SET12, as a starting point for detailed regional analysis.

515
516 All three models employ a relative hierarchy (Fig. 2a), in which a fully relative plate motion model is tied
517 to an absolute plate motion model through Africa. The relative hierarchies are similar across the models
518 because of the preserved oceanic crust. These global relative motion hierarchies are then linked to an
519 absolute reference frame tied to the mantle, though the details of these reference frames differ between
520 models. SET12 uses a hybrid reference frame, using a moving hotspot reference frame for 100–0 Ma
521 (O'Neill et al., 2005) and a true-polar wander corrected palaeomagnetic reference frame for 200–100 Ma
522 (Steinberger and Torsvik, 2008). MUL16 also adopts a hybrid absolute reference frame, but uses the
523 moving hotspot model of Torsvik et al. (2008) instead of that of O'Neill et al. (2005) based on an assessment
524 of the geodynamic plausibility of a range of alternative mantle reference frames by Williams et al. (2015).
525 MUL19 departs from both SET12 and MUL16 in that it uses an absolute reference frame derived by Tetley
526 et al. (2019). The method of Tetley et al. (2019) optimises absolute plate motions through a joint inversion
527 involving trench motion, fitting hotspot motion tracks and net rotation to determine the motion of Africa
528 (at the top of the relative hierarchy) that simultaneously best fits all three criteria. Despite the emphasis on
529 mantle reference frames in these previous global models, the same relative plate motion hierarchies can
530 also be tied to a pure paleomagnetic reference frame (e.g. Cao et al., 2019; Torsvik et al., 2008).

531
532 In this study, we rely on palaeomagnetic data as the main basis for linking absolute plate configurations
533 continuously from the Cenozoic to the early Neoproterozoic, when tying plate configurations to the mantle
534 is far more problematic. Nonetheless, some aspects of the more recent plate motions still rely on
535 observations from hotspot trails—specifically, the motion of the Pacific Plate and other oceanic plates that
536 have bordered it. During the Early Cretaceous, these plates lay within the Panthalassa ocean basin that was
537 entirely surrounded by subduction zones, meaning that we cannot tie the motions of the oldest crust of the
538 Pacific Plate to the continents by seafloor spreading anomalies.

539
540 Finally, with regard to Mesozoic-Cenozoic global plate models, we note that MUL19, while containing the
541 same relative framework as SET12 and MUL16, also contains deforming plates. In MUL19, deformation

542 of rifts and collisional zones are modelled explicitly, making it the first plate model to step away from the
543 simplification of rigid plates that all other models assume. However, the reconstruction here relies on the
544 simpler, rigid approximation used in SET12, MUL16, and other previous studies.

545

546 **3.3 Mid-late Palaeozoic plate models**

547

548 The progression of the three Palaeozoic plate models (all modelling 410–250 Ma) is slightly more nuanced
549 than in the Mesozoic and Cenozoic because of the absence of preserved oceanic crust. DT14 is the original
550 model and both MAT16 and YOU19 used DT14 as the basis of their Palaeozoic models and then connect
551 to MUL16 for the Mesozoic and Cenozoic. In effect, MAT16 is the connection of DT14 (i.e. minimal
552 changes) to MUL16, while YOU19 is an alternate version of DT14 for the Palaeozoic.

553

554 DT14 is heavily based on work by Torsvik et al. (2012) and models the amalgamation of Pangea through
555 the collision of Laurussia and Gondwana and the evolution of the Palaeo-Tethys and opening of the Meso-
556 Tethys oceans. The model has a flat hierarchy (Fig. 3a) with APWPs defined for each individual continent
557 and each continent being tied directly to the spin axis. Domeier and Torsvik (2014) also use the PGZ method
558 to constrain absolute palaeolongitude. Therefore, their model assumes the stable, immutable nature of the
559 present-day LLSVPs within the mantle back to 410 Ma. DT14 is presented in both a mantle and a
560 palaeomagnetic reference frame, with the mantle reference frame being corrected for TPW after Torsvik et
561 al. (2014) .

562

563 MAT16 adopted the DT14 model, with minor amendments required to link it with MUL16 (see Matthews
564 et al. (2016) for details). A key difference between the two models is that MAT16 translated the flat
565 hierarchy of DT14 into a fully relative reference frame (i.e. converted the structure from Fig. 3a into Fig.
566 2a), where the motion of all plates is tied to Africa, which is then tied to an absolute plate motion model.
567 The absolute plate motion model of MAT16 is the same as in both MUL16 (i.e. a hybrid between hotspots,
568 slabs and palaeomagnetic data) and DT14 (i.e. absolute latitude and longitude, corrected for TPW). Thus,
569 MAT16 also invokes the PGZ method.

570

571 YOU19, while starting from MAT16 as a base, differs much more from MAT16 than MAT16 does from
572 DT14. This is because YOU19 uses a different base assumption, leading to notable changes in the actual
573 plate model itself. The most important difference is that YOU19 does not assume that LLSVPs were fixed
574 and stable back to 410 Ma. They abandon the PGZ method for constraining palaeolongitude and thus argue
575 that they can better accommodate geological and kinematic (plate speed and trench migration) criteria more

576 strongly than either DT14 or MAT16. The two key changes that YOU19 implemented (relative to DT14
577 and MAT16) are shifting Laurussia in latitude and longitude to be closer to its position in Pangea against
578 Gondwana, thus removing a dextral motion between the Patagonian margin of South America and Laurussia
579 (e.g. Fig. 2c), and removing easterly drift of South China during the Carboniferous–Permian. The
580 implementation of both in DT14 (and then in MAT16) is a consequence of the PGZ method, since the
581 longitudinal position of Laurussia and South China is based on fitting preserved eruptions to the edges of
582 LLSVPs (Domeier and Torsvik, 2014). YOU19 argue that the interpretations of DT14 introduce unrealistic
583 kinematic scenarios: 8000 km of relative dextral motion between Laurussia and the Patagonian margin of
584 Gondwana (e.g. Fig 2c) at a relative plate velocity of 30 cm/a and South China moving at plate speeds of
585 40 cm/a between 260 and 250 Ma in MAT16 (Young et al., 2019). The dextral motion between Gondwana
586 and Laurussia of DT14 and MAT16 that that YOU19 removed is not a transition from the Pangea B to
587 Pangea A configuration, which is explicitly defined as dextral motion after Pangea formed (Domeier et al.,
588 2012). Rather, all three models adopt a Pangea A configuration and include *some* component of dextral
589 motion between Laurussia and Columbian–Mexican margin of Gondwana in the Devonian. However, the
590 position of Laurussia in YOU19 is unsupported palaeomagnetically by $\sim 30^\circ$ (Section 4.2 and 5.1), which
591 is problematic as there is an abundance of data from both Laurentia and Baltica to constrain its position at
592 this time.

593
594 Recently, Wu et al. (2020) have also proposed an integrated geological and palaeomagnetic model for the
595 amalgamation of Pangea. Their study used a different selection of palaeomagnetic data (all three mid-late
596 Palaeozoic full-plate models discussed here used the compilation of Torsvik et al. (2012) as a base) and a
597 new method of APWP generation that weighted poles based on their quality and uncertainty. The model of
598 Wu et al. (2020) also suggested that the formation of Pangea was originally initiated by collision between
599 Laurussia and a promontory of Gondwana consisting of the Variscan Massifs at ca. 400 Ma. In their model,
600 the promontory formed by the scissor-like opening of the Palaeotethys Ocean off the northern margin of
601 Gondwana. In principle this model would be very compatible with the one we present here, however as the
602 model of Wu et al. (2020) is currently only palaeogeographic, we do not consider it as an option for merging
603 in this study.

604
605 YOU19, like MAT16, uses a relative plate hierarchy with Africa as the root of the hierarchy. Africa is
606 connected to an absolute plate motion model using the Torsvik and Van der Voo (2002) APWP for the
607 Palaeozoic, before the model transition to the absolute plate motion model of MUL16. Because the model
608 has no absolute palaeolongitude control, YOU19 does not constrain or correct for TPW in the Palaeozoic
609 and is therefore presented in a purely palaeomagnetic reference frame.

610

611 **3.4 Early Palaeozoic plate models**

612

613 Two separate models exist for part of the Early Palaeozoic between 500 and 410 Ma. Each of these two
614 models focus on a separate area of the Earth at the time. DOM16 focuses on the evolution of the Iapetus
615 and Rheic oceans and the amalgamation of Laurussia (Baltica, Laurentia and Avalonia). DOM18 models
616 the evolution of Siberia, Gondwana, the terranes that now make up the Central Asian Orogenic Belt and
617 the Chinese cratons (Tarim, North and South China). While each model focuses on a different area, the
618 overarching assumptions and framework of both models are identical. Both models follow the approach of
619 DT14, possessing a flat hierarchy with APWPs being defined for most continents, such that they all move
620 independently from each other. The model extends the assumptions of the PGZ method back to 500 Ma,
621 using the location of LIPs and kimberlites to constrain absolute palaeolongitude. Both models therefore
622 have a TPW correction, and are presented in a mantle and palaeomagnetic reference frame.

623

624 **3.5 Neoproterozoic**

625

626 Only one full plate model exists for the Neoproterozoic (MER17, Meredith et al., 2017a). MER17 is based
627 on Li et al. (2013, 2008) and models the evolution of Rodinia; it's breakup and the amalgamation of
628 Gondwana (1000–520 Ma). There are, however, a number of important considerations that differentiate
629 MER17 from Phanerozoic full-plate models. Firstly, MER17 used a hybrid plate rotation hierarchy,
630 defining two separate nodes that move independently from each other using palaeomagnetic data tied
631 directly to the spin axis (India as one and Laurentia, as the centre of Rodinia, as the second) (Fig. 5a, b). In
632 this model, India and Laurentia both act as separate roots that then constrain a series of relative plate
633 rotations that collectively describe the rest of the world. Secondly, the continental drift model of Li et al.
634 (2013) invokes the orthoversion model of determining palaeolongitude, where they fix the I_{min} of Rodinia
635 to be at 100°E. As MER17 adopted these rotations as their base, there is an element of the orthoversion
636 model preserved between models. However, MER17 also drastically changed the configuration of Rodinia,
637 as well as the timing of breakup, compared to Li et al. (2013), relative rotations within the Laurentian (i.e.
638 Rodinian) node and absolute rotation of Laurentia itself in order to fit geological and kinematic constraints.
639 They did not recalculate TPW and the I_{min} of Rodinia, thus MER17 does not have a strict absolute
640 palaeolongitude control. Finally, there is no correction for TPW in MER17 and no mantle reference frame;
641 the model is presented purely in a palaeomagnetic reference frame.

642

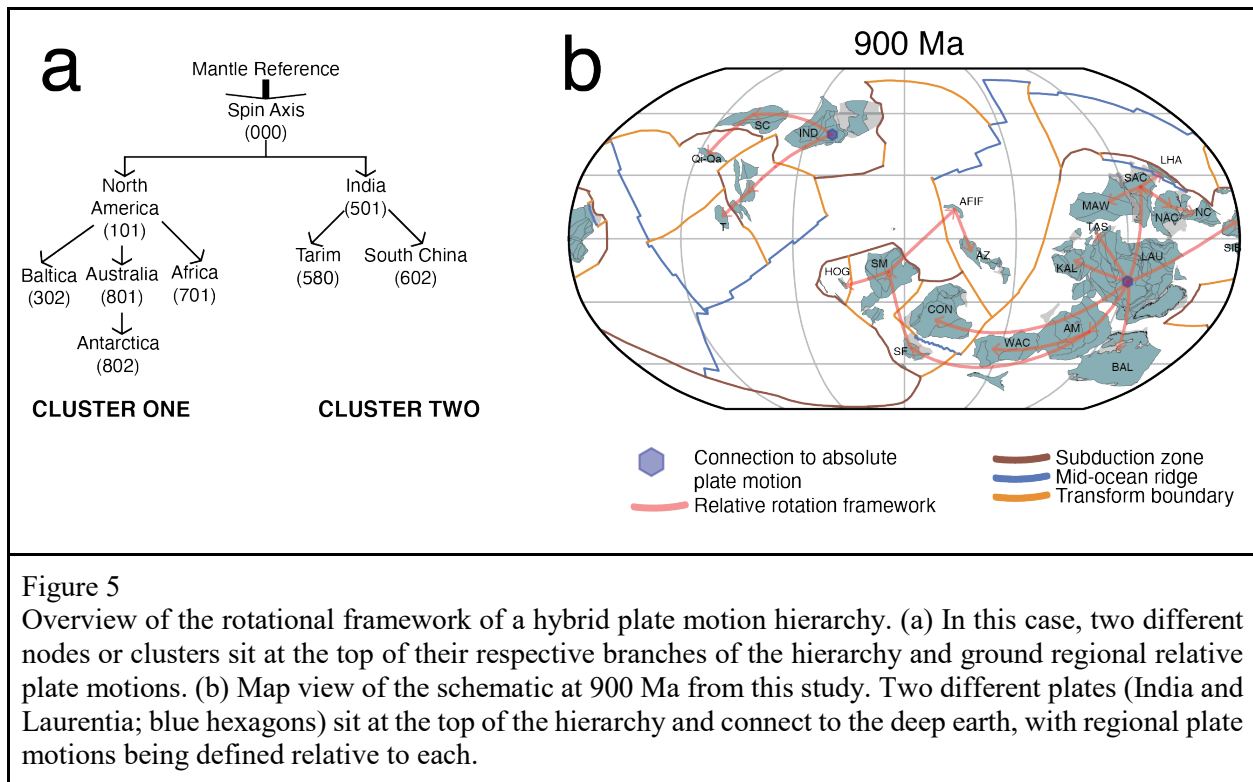


Figure 5
Overview of the rotational framework of a hybrid plate motion hierarchy. (a) In this case, two different nodes or clusters sit at the top of their respective branches of the hierarchy and ground regional relative plate motions. (b) Map view of the schematic at 900 Ma from this study. Two different plates (India and Laurentia; blue hexagons) sit at the top of the hierarchy and connect to the deep earth, with regional plate motions being defined relative to each.

643

644 3.6 Model selection

645

646 In order to produce a coherent global model, we must select from the models described above that best
647 align with our goals: (i) open the Neoproterozoic and Cambrian up for quantitative tectonic analysis; (ii)
648 create a framework that can support local or regional studies for the Neoproterozoic and (iii) a foundation
649 for future studies looking at long timescale (> 10–100 Ma) trends in either tectonics or geodynamics.

650

651 As our aim is to produce a model back to 1 Ga, three choices are already made for us because they are the
652 only models that exist for those time periods: MER17 for 1000–520 Ma, and DOM16 and DOM18 for 500–
653 410 Ma. For the remaining time period, MAT16 (an extension of DT14) and YOU19 are viable options.
654 Both models link to the MUL16 model and choosing between them requires considering the reconstruction
655 framework (e.g. hierarchy, reference frame) of our model with respect to our intent. To satisfy our goals,
656 we need a model in a palaeomagnetic reference frame. We acknowledge the value and potential in exploring
657 hypotheses for constraining palaeolongitude. However, since tectonic reconstruction models, such as the
658 one we are presenting here, are a required starting point for exploring the long-term evolution of mantle,
659 we have kept the model conservative by not assuming the fixity of LLSVPs or that TPW dictates
660 supercontinent position. Therefore, we elect to leave palaeolongitude unconstrained by either PGZ or
661 orthoversion methods. Thus, we selected the YOU19 model, as it has removed the absolute palaeolongitude

662 controls adopted in MAT16. We stress that our approach is deliberately conservative and requires the fewest
663 *a priori* assumptions, but anticipate that future developments will see improvements in the model presented
664 and that a comparison of several end member models would be useful for evaluating the long-term
665 connection between lithosphere and mantle. One promising way forward could be to optimise tectonic
666 parameters, such as subduction zone migration and plate velocity in the manner of Tetley et al. (2019) to
667 define a mantle reference frame. The model we present is an essential precursor for such techniques. Our
668 model is constructed with a palaeomagnetic reference frame, that is, even at younger times, there is no
669 mantle reference frame. For studies needing such a reference frame, which only exists since the Cretaceous,
670 we suggest people use either SET12, MUL16 or MUL19.

671

672 **3.6.1 Our approach to plate modelling**

673

674 Here we outline our approach to merging individual plate models into a coherent global plate model
675 spanning the past 1 Ga. As detailed above, our goal is a geologically constrained model within a
676 palaeomagnetic framework. In addition to reconstructing plate motions, we also model plate boundaries,
677 which requires us to also focus on the relative motion between plates. The evolution of plate boundaries is
678 commonly preserved in the geological record such as passive margins marking divergent boundaries and
679 magmatic arcs recording convergence. Palaeomagnetic data, although providing a quantitative absolute
680 constraint on the position of a craton, have varying uncertainty that allow some manipulation and flexibility.
681 For example, continental drift models (and APWPs) typically fit the data as tightly as possible. However
682 recent studies have analysed the effect of exploring both the temporal (i.e. age constraints) and statistical
683 uncertainty to create alternative APWPs (Tetley et al., 2019; Wu et al., 2020). Given this, we use a hybrid
684 approach that adopts parts of both the flat, palaeomagnetic hierarchy traditionally used for Precambrian
685 reconstructions and the relative framework used in more recent times.

686

687 Using this approach, our model has multiple clusters of related cratonic elements moving together (Fig. 5a).
688 Whether a specific cratonic element moves relative to another is dependent on their geological relationship.
689 For example, if they are separated by an incipient ocean basin as indicated by geological data then we
690 suggest that it is easiest for them to be moving relative to each other (within the bounds of whatever
691 available palaeomagnetic data), because the relative relationship of divergence (expressed as a mid-ocean
692 ridge) is preserved. The hierarchy is defined by geological precedence, where terranes move relative to
693 blocks, blocks move relative to cratons and cratons move relative to ‘supercontinents’. In this manner,
694 generally (but not necessarily exclusively), crust with more preserved data should always be placed above
695 crust with less preserved data in the hierarchy, because we have more confidence in the geological evolution

696 (and also likely palaeomagnetic constraints) from these continents. Alternatively, if continents are separated
697 by a large ocean basin, we form a new cluster. This cluster-approach has an added benefit in the more
698 uncertain Neoproterozoic, as it means that we can simply introduce a new cluster for Rodinia, which has
699 Laurentia as the root of the relative hierarchy, instead of maintaining Africa or the Congo craton at the top
700 of the cluster (which are the roots of Pangea and Gondwana, respectively) and can also introduce a cluster
701 for India and South China which, in our interpretation, move separately to Rodinia on the other side of the
702 globe.

703
704 A full-plate reconstruction models both continents (palaeomagnetic data) and plate boundaries (geological
705 data). Therefore, we use both data simultaneously to iterate towards a solution. Palaeomagnetic data are
706 used initially to build a continental drift framework (e.g. (Li et al., 2013, 2008). If palaeomagnetic data are
707 abundant and of high quality, then either an APWP or GAPWaP are constructed, which we do for the
708 Phanerozoic. We then introduce geological data in the form of plate boundaries (e.g. compilation of rifts
709 and arcs (Merdith et al., 2017b)) and use the compilation to manipulate the model in a manner that still fits
710 the palaeomagnetic data, but also accommodates geological data. Structural and metamorphic constraints
711 are used here principally to infer (where possible): (i) polarity of subduction, (ii) collision timing and (iii)
712 orientation of rifting. Once the broader tectonic framework is implemented, we begin introducing smaller
713 blocks and terranes into this framework. This approach allows us to increase the resolution of the model
714 within key areas while maintaining the tectonic coherency of the model as a whole. For example, where the
715 broader tectonic framework models subduction leading to collision, the introduction of terranes and smaller
716 blocks that preserve evidence suggesting a two-stage collision or accretion of an oceanic arc can be used to
717 more finely model the plate boundary network. Other pieces of geological data, such as faunal provinces
718 (e.g. Burrett et al., 1990), isotopic signatures (e.g. Collins et al., 2011) and detrital zircons (e.g. Cawood et
719 al., 1999) are used here to assist with connecting disparate terranes to larger blocks that they share affinity
720 with or to infer the presence of a plate boundary not directly preserved in the geological record (such as by
721 a diverging fossil record).

722
723 Because our model contains geological data in the form of plate boundaries, we are particularly interested
724 in ensuring the forwards and backwards compatibility of any decision made around geological data,
725 especially for terranes or blocks that have limited palaeomagnetic data. For example, if the data support
726 two or three interpretations in the early Neoproterozoic, but only one of those is consistent with an
727 Ediacaran (or younger position), then we consider that position more reliable than the other two. However,
728 we argue that this logic also works in reverse; if a number of positions are deemed viable in the Ediacaran
729 for a terrane based on the data available, but only one of those also fits what data are available in the early

730 Neoproterozoic, then we will use the older data to force an interpretation of the younger data (e.g. Evans,
731 2009). This argument is highlighted by the concept of ‘world uncertainty’ (the percentage of total crust
732 (oceanic and continental) on the earth at any one time that is also preserved at present-day) of Torsvik et
733 al. (2010b). Because time is asymmetrical, this means that the level of confidence we have at present-day
734 is 100%, but decreases linearly back in time to ~70% at 200 Ma (i.e. 70% of all crust at 200 Ma is no longer
735 preserved). At 400 Ma, the world certainty is ~73% (Domeier and Torsvik, 2017), and using estimates of
736 continental crustal volumes, at 600 Ma it is between 75 and 80% (Cawood et al., 2013a). Therefore, for the
737 Mesozoic and Cenozoic, data from younger times are much more compelling to force interpretations of
738 older data because of how much more confident one can be in the last 20 Ma. Comparably, the difference
739 in this measure of uncertainty is much smaller between the Neoproterozoic and Cambrian, thus we suggest
740 that models in this time period should simultaneously use older and younger data to iterate towards a
741 solution.

742

743 **4 Palaeomagnetic Data**

744

745 A major problem in comparing the Phanerozoic models is that they all use different rotational frameworks,
746 including reference trees (i.e. flat vs hierarchical) and different absolute reference frames. In order to
747 properly synthesise the DOM16, DOM18 and YOU19 models into a single reconstruction, we first need to
748 lay a coherent groundwork in defining an absolute plate motion model for the largest continents during this
749 time in order to merge the individual models. To do this, we first derive a new APWP for Gondwana (540–
750 320 Ma) and GAPWaP for Pangea (320–0 Ma) using the palaeomagnetic compilation of Torsvik et al.
751 (2012) to provide an absolute palaeomagnetic reference frame for 540 to 0 Ma. We also apply the GAPWaP
752 to the MUL16 portion (i.e. the Mesozoic and Cenozoic) of the YOU19 model. We do this to ensure
753 compatibility between the Cenozoic and Palaeozoic, and also because our goals for this model are broad
754 scale (> 10–100 Ma) trends, mostly focussed on the Neoproterozoic. The method we follow to calculate
755 our APWP and GAPWaP is outlined below. For the Neoproterozoic, and non-Gondwana constituents of
756 the Palaeozoic, we use the compilations of palaeomagnetic data as presented in MER17, DOM16 and
757 DOM18, along with some other additions. Palaeomagnetically derived alterations to the models are also
758 discussed below.

759

760 **4.1 APWP and GAPWaP construction**

761

762 The absolute reference frames for Gondwana (540–320 Ma) and Pangea (320–0 Ma) used in this study are
763 derived using the method and velocity-optimised global palaeomagnetic data of Tetley (2018). APWPs are

764 routinely constructed using poles assigned averaged or nominal ages, which particularly for older times,
765 where palaeomagnetic constraint becomes increasingly limited, contribute to spurious apparent polar
766 wander behaviours. This method directly evaluate individual palaeomagnetic pole age and associated
767 uncertainty in combination with calculated pole A95 latitude and longitude uncertainties to derive optimised
768 APWPs that minimise predicted plate velocities and plate velocity gradients (instantaneous accelerations).
769 The resulting rate of apparent polar wander in optimised APWPs was reduced globally by an average of
770 56% by comparison to existing APWPs, resulting in predicted Phanerozoic plate motions displaying greater
771 kinematic consistency with present-day plate motion behaviours.

772

773 Optimised APWPs were produced for the 15 major continental blocks of Amazonia, Australia, Colorado,
774 East Antarctica, Greenland, India-Pakistan, Madagascar, Meseta, North America, Northeast Africa,
775 Northwest Africa, Panama, Patagonia, Somalia, and Stable Europe. Applying the method as described in
776 Torsvik et al. (2012, 2008) and the data provided in Torsvik et a. (2012), optimised continental pole data
777 from all 15 continents were rotated from their individual source coordinate frames into a consistent South
778 African coordinate frame using the rotation model from this study. Now in a consistent coordinate frame,
779 a GAPWaP for Pangea was produced using all poles aged 320-0 Ma (due to the collision of Laurussia and
780 Gondwana during the Late Carboniferous), with a second GAPWaP produced using poles aged 540-320
781 Ma associated with Gondwana (South America, Africa, India, Antarctica and Australia) only. For both
782 GAPWaP reference frames, the *GMAP* software was used (Torsvik et al., 2012, 2008; Torsvik and
783 Smethurst, 1989), applying a running mean method using a window size of 20 Ma and a step size of 10 Ma.

784

785 **4.2 Palaeomagnetic compilation**

786

787 A compilation of palaeomagnetic data was used to constrain the position of all continental blocks during
788 the Neoproterozoic and for non-Gondwanan continental blocks during the early and middle Palaeozoic.
789 The Neoproterozoic data are presented in Table 2 and a GPlates compatible file of the data is also presented
790 in the Supplementary Material. Figure 6a–c shows the great circle misfit of our model to the selected poles.
791 As the majority of the data have already been used in the MER17, DOM16 and DOM18 reconstructions,
792 we point readers to those publications for in-depth discussion of the data. Here, we discuss two alterations
793 to the base models that we implemented based on palaeomagnetic data: Tarim at ca. 700 Ma and Laurussia
794 at ca. 420–400 Ma.

795

796 The MER17 model omitted Tarim prior to 700 Ma due to its pre-700 Ma palaeomagnetic data nullifying
797 the position that placed it outboard of Australia. We rectify this and include a robust, time-sensitive

798 geological argument for its position against India-South China during the Tonian (1000–720 Ma) and
799 Cryogenian (720–635 Ma) (Section 5.4.2). The rationale for placing Tarim in this position is to allow for a
800 significant 180° rotation required by paleomagnetic data. Two well-dated and high-quality poles; the 760–
801 720 Ma Qiaoenbrak Formation (Wen et al., 2013) and the 770–717 Ma Baiyisi Volcanics (Huang et al.,
802 2005) are internally consistent and require Tarim to be inverted 180° from its present-day position (i.e.
803 northern margin facing south). A third pole, assumed to be pre 700 Ma, from the Aksu Dykes (Chen et al.,
804 2004) is rejected for poor age constraints and the possibility of remagnetisation (Wen et al., 2017).
805 Comparably, three younger poles: the 635–550 Ma Sugetbrak Formation (Zhan et al., 2007), the ca. 635
806 Ma Tereeken Cap Carbonate (Zhao et al., 2014) and the 621–609 Ma Zhamoketi Andesite (Zhao et al.,
807 2014) are all consistent with each other and indicate that Tarim was in its present-day orientation. A recent
808 pole by Wen et al. (2017) from the Lower Sugetbrak formation (640–615 Ma) stands in conflict with these
809 three poles, suggesting a ~50° rotational difference in the orientation of Tarim, while maintaining the same
810 palaeolatitude. Wen et al. (2017) dismiss the three earlier poles due to similarity to Silurian–Devonian poles
811 for the Sugetbrak Formation and possible remagnetisation for the latter two poles, respectively.

812
813 Successfully fitting the two older poles with either the three younger poles or the single pole of Wen et al.
814 (2017) is not possible in a model in which Tarim is surrounded by continental lithosphere for the
815 Neoproterozoic or in a scenario where Tarim is attached to the north-western or northern margin of
816 Australia or the northern margin of India (e.g. instead of South China). An accommodation of the data can
817 be obtained by placing Tarim in a ‘Missing-Link’ position (between Australia and Laurentia) with breakout
818 and rotation of Tarim from ca. 700 Ma; as argued by Wen et al. (2018, 2017). However, beyond the
819 kinematic issues with Missing-Link style models (Merdith et al., 2017b), it is difficult to account for the
820 formation of the 760 Ma Aksu Blueschist if Tarim was located in the centre of an assembled Rodinia (see
821 comment by Song and Li (2019) and reply by Wen et al. (2019)). In the present model, we use the pole of
822 Wen et al. (2017) due to its greater reliability, though our model could easily be adapted to fit the other
823 three poles if necessary (Section 5.4.2.). We also note that although we argue that India-South China were
824 separate from the rest of Rodinia, our preferred Neoproterozoic position for Tarim is also compatible with
825 models in which India-South China formed part of Rodinia (e.g. Cawood et al., 2013b).

826
827 In the YOU19 model, Laurussia was moved ~30° further north in latitude relative to its position in DT14
828 and MAT16 (Section 3.3). The consequence of this decision by YOU19 is that Laurussia is not in a
829 palaeomagnetically constrained position in the late Silurian and early Devonian. For this model, in addition
830 to the compilation of palaeomagnetic data in Torsvik et al. (2012), we also used palaeomagnetic data from
831 mainland Baltica (Table 2) to constrain the late Silurian to early Devonian position of Laurussia. We

832 implement these alterations to produce a coherent motion of Laurentia (later Laurussia) and Gondwana that
833 fits palaeomagnetic data, while also ensuring that the relative motion between Gondwana and Laurussia is
834 convergent, rather than dextral transform (e.g. Fig. 2c).
835

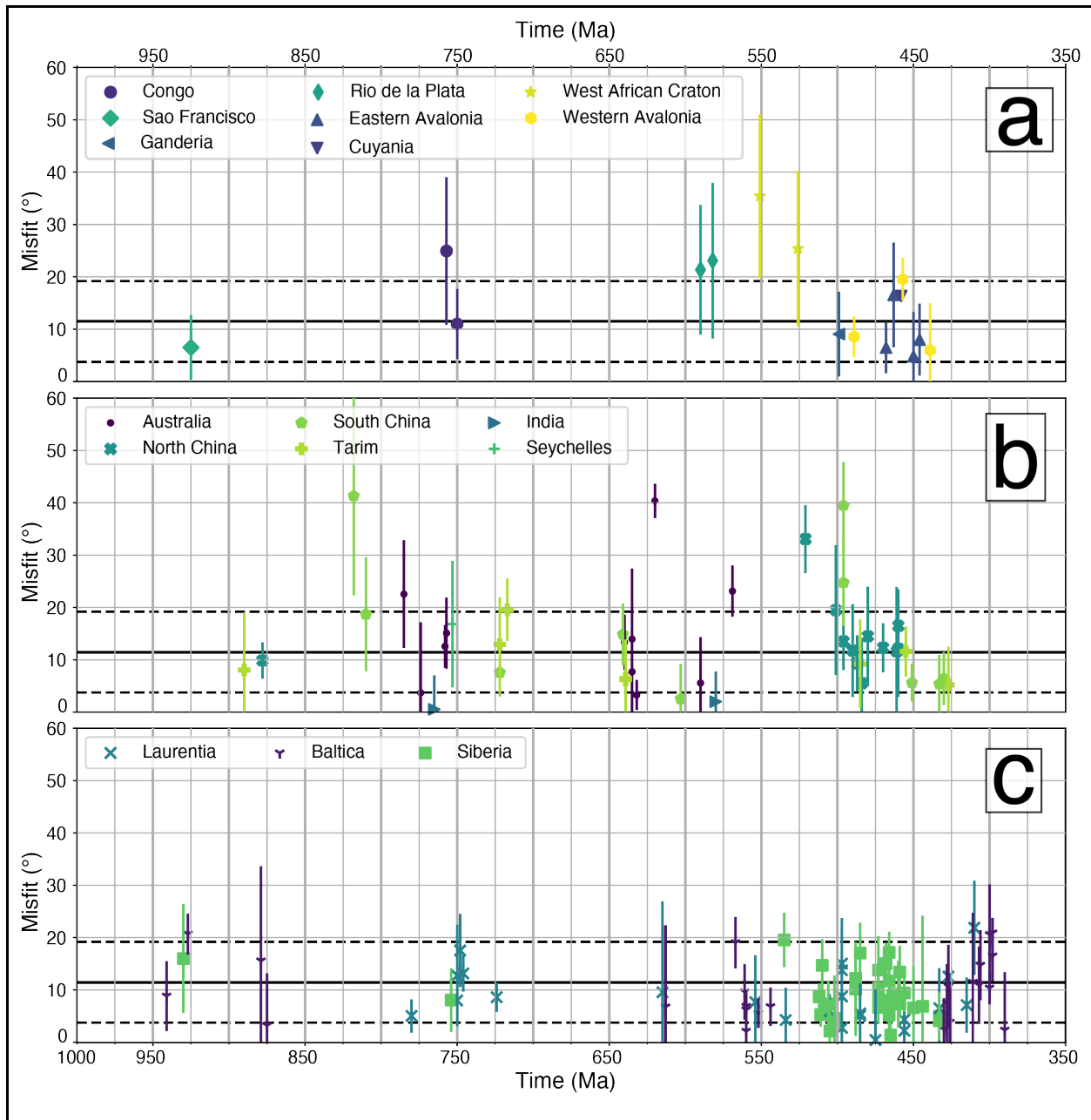


Figure 6

Summary of the fit of palaeomagnetic data to our model for 1000 to 400 Ma (omitting poles used to construct the Gondwana APWP). Misfit is the minimum great circle distance (in degrees) within the valid time range between the palaeomagnetic pole and the geographic north pole. The error bar on each point is the pole 95% confidence limit (A_{95}). Solid line is the mean misfit of all poles, with the dashed lines representing the standard deviation of the mean. Poles marked as 'not used' or 'inclination only' in Table 1 are not included in this figure. (a) Poles from the constituent cratons of western Gondwana and the Avalonian terranes; (b) poles from the constituent cratons of eastern Gondwana and present-day Asia, and; (c) poles from Laurussia and Siberia.

838 **5 Alterations to models**

839

840 We describe the alterations made to individual models separately for clarity, however, we stress that no
841 single model was treated in isolation. Each alteration, whether during the Tonian or Devonian, was
842 evaluated both forwards and backwards in time in order to ensure continuity with both older and younger
843 geological and/or palaeomagnetic evidence. We begin our discussion with the alterations made to YOU19,
844 followed by alterations to DOM16, DOM18 and MER17. The alterations to DOM16 and DOM18 are
845 discussed together, as the two models essentially form a single global model between 500 and 410 Ma. The
846 most significant changes, and the focus of much of the discussion, occurred in MER17. This is because,
847 firstly, connecting this model with younger models in order to validate Neoproterozoic tectonic-geography
848 is a primary goal of this study, and secondly, because many of the alterations are completely new and have
849 never been incorporated into a plate model before. Figure 7a–b displays a latitudinal overview of the major
850 and minor cratons in our model, with a comparison to the DOM-MAT models for the Phanerozoic, and the
851 model of Li et al. (2013, 2008) for the Neoproterozoic. Figures 8, 9 and 10 show overviews of our
852 reconstruction at 1000 Ma, 500 Ma and present-day with relevant terranes and blocks highlighted.

853

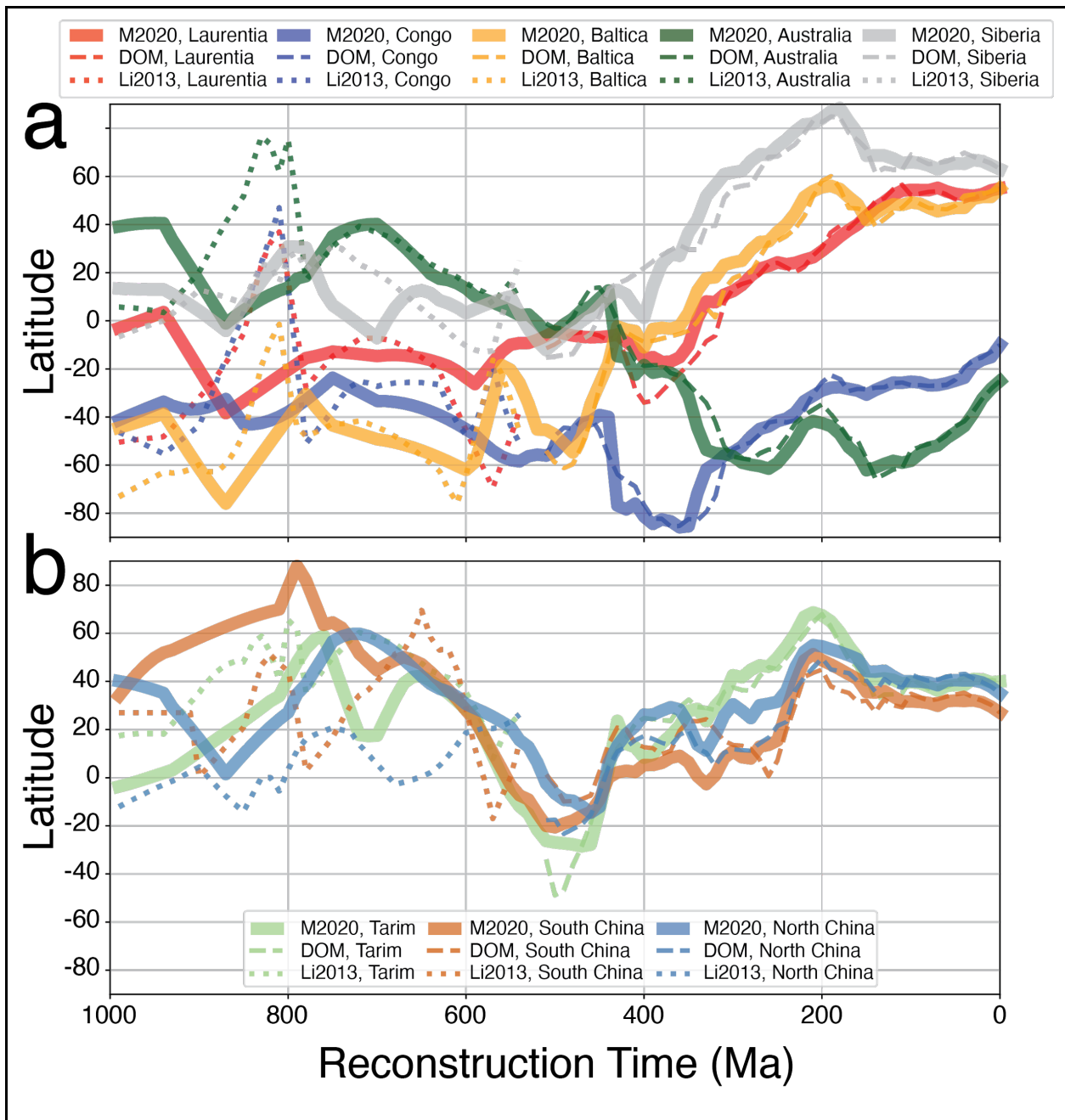


Figure 7

Comparison of palaeolatitude of major cratons (a) and Chinese cratons (b) from 1000–0 Ma between three models; (i) This model, M2020; (ii) DOM16/18 (500–410 Ma) and MAT16 (410–0 Ma), and; (iii) Li et al. (2013, 2008) (1000–550 Ma). The notable excursion at 800 Ma in the Li et al. (2013, 2008) model is due to their adoption of IITPW at this time (Li et al., 2004).

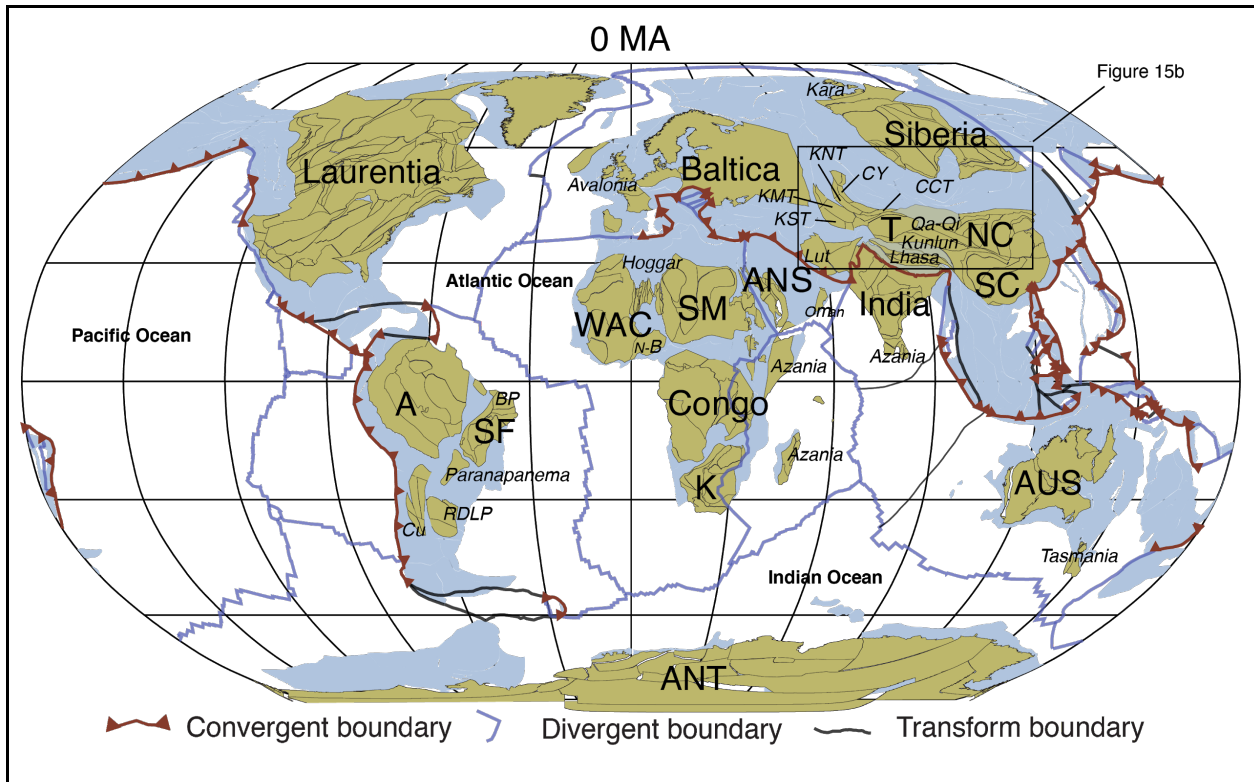


Figure 8

(a) Distribution of continental crust, ocean basins and plate boundaries in our plate model at 0 Ma, based on MUL16. Tan polygons are areas of continental lithosphere in the Neoproterozoic that we model, blue polygons are areas of present-day continental lithosphere. Abbreviations as Figures 8 and 9. A, Amazonia; Ant, Antarctica; AUS, Australia; BP, Borborema Province; CCT, Chinese Central Tianshan; Cu, Cuyania; CY, Chu Yili; K, Kalahari; KMT, Krygyz Middle Tianshan; KNT, Krygyz North Tianshan; N-B, Nigeria-Benin; NC, North China; P, Paranapanema; ANS, Arabian Nubian Shield; Qa, Qaidam; Qi, Qilian; RDLP, Rio de la Plata; SC, South China; SM, Sahara Metacraton; T, Tarim.

856

857

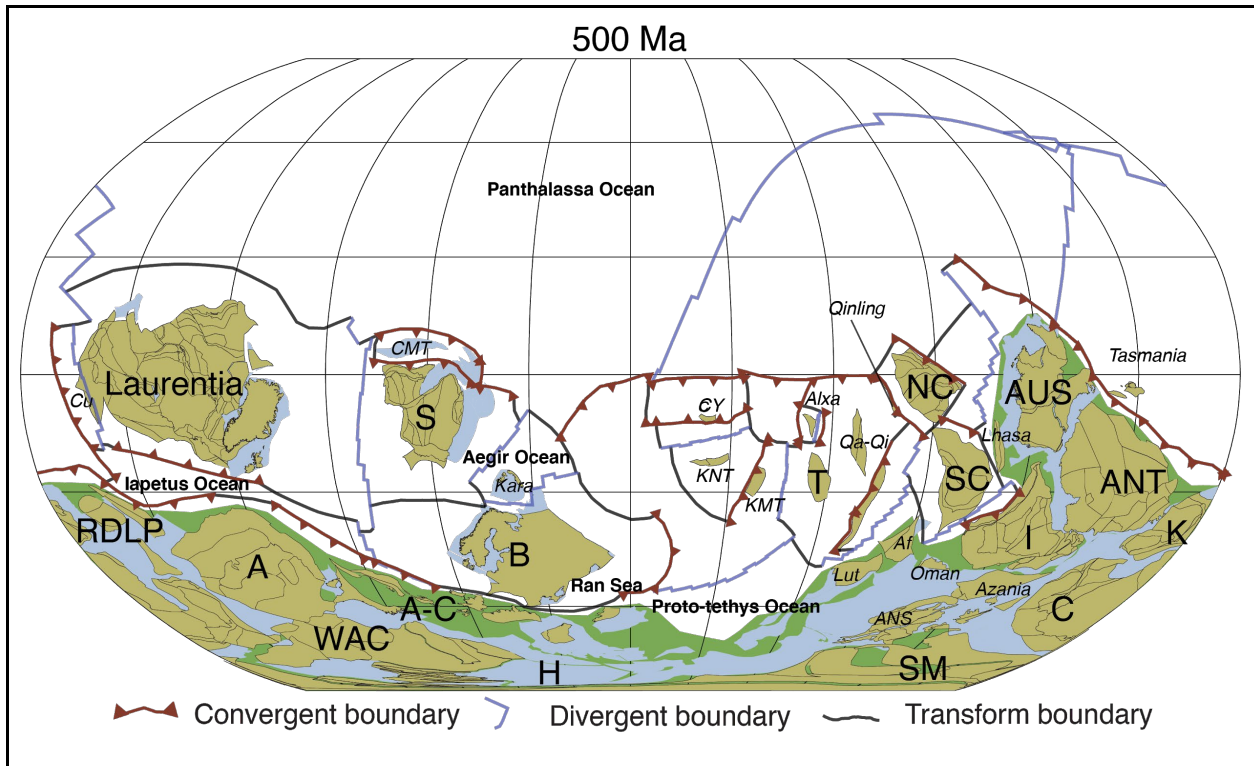


Figure 9
 Distribution of continental crust, ocean basins and plate boundaries in this plate model at 500 Ma, based on DOM16 and DOM18 (e.g. Figs. 12 and 13). Tan polygons are areas of continental lithosphere in the Neoproterozoic that we model, blue polygons are areas of present-day continental lithosphere that are inferred to exist during the Neoproterozoic, but without having firm geological evidence or that have been effected by subsequent deformation (e.g. the distance between a present-day coastline and COB). Green polygons represent a schematic interpretation of congruent continental lithosphere, with intervening crust being subsequently deformed during future tectonic cycles. Abbreviations as Figure 8, in addition to; Af, Afghanistan; B, Baltica; C, Congo; H, Hoggar; I, India; S, Siberia.

858

859

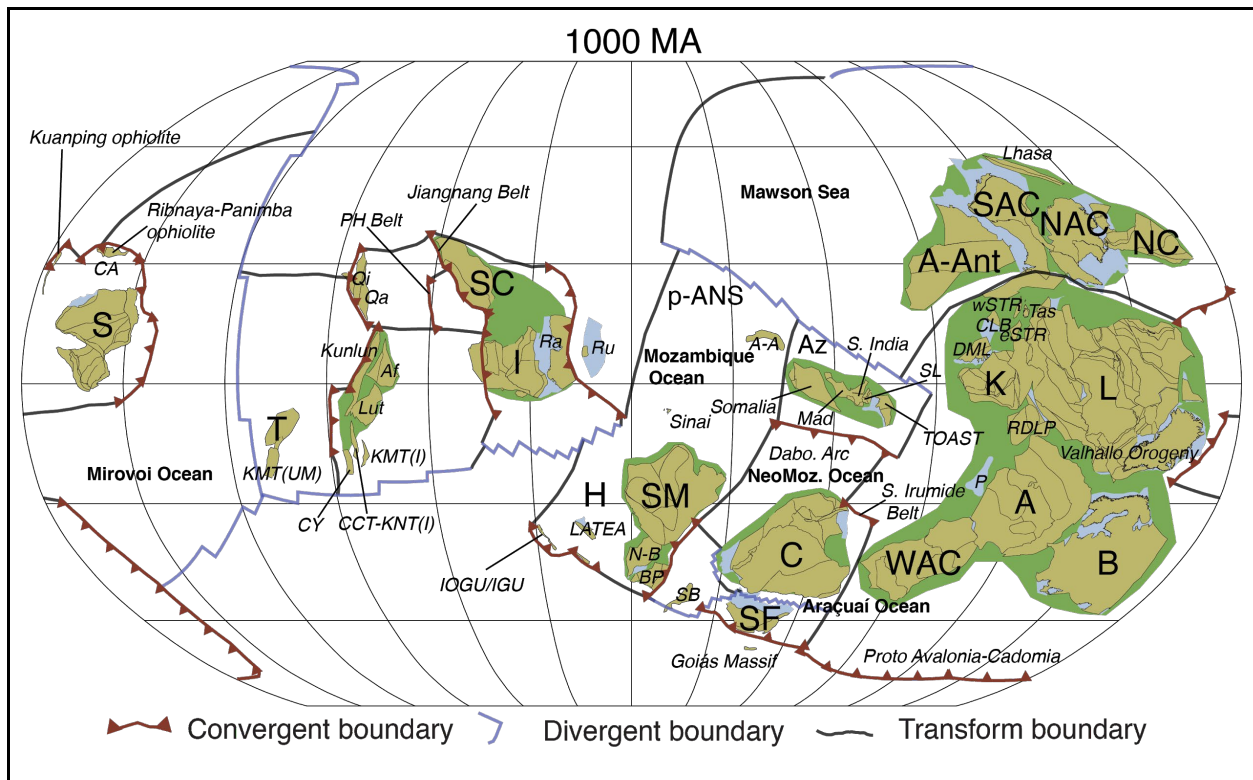


Figure 10
 Distribution of continental crust, ocean basins and plate boundaries in our plate model at 1 Ga. Tan polygons are areas of continental lithosphere in the Neoproterozoic that we model, blue polygons are areas of present-day continental lithosphere that are inferred to exist during the Neoproterozoic, but without having firm geological evidence or that have been affected by subsequent deformation (e.g. the distance between a present-day coastline and COB). Green polygons represent a schematic interpretation of congruent continental lithosphere, with intervening crust being subsequently deformed during future tectonic cycles. A-Ant, Austral-Antarctica; Az, Azania; BP, Borborema Province; CLB, Coats Land Block; Dabo. Arc, Dabolava Arc; DML, Dronning Maud Land; eSTR, Eastern South Tasman Rise; IOGU, In Ouzal Granulite Unit; IGU, Iforas Granulite Unit; KMT(I), Krygyz Middle Tianshan (Issedonian); KMT(UM), Krygyz Middle Tianshan (Ulutau-Moyunkum); KNT(I), Krygyz North Tianshan (Issedonian); Mad, Madagascar; NAC, North Australian Craton; NeoMoz. Ocean, NeoMozambique Ocean; NC, North China; p-ANS, proto-Arabian Nubian Shield; Ra, Rayner Province; Ru, Ruker Block; SAC, South Australian Craton; SB, Southern Borborema; SL, Sri Lanka; Tas, Tasmania; wSTR, Western South Tasman Rise.

860

861 5.1 YOU19

862 The primary change we made to YOU19 was the implementation of a new APWP for Gondwana from 540
 863 to 320 Ma and a GAPWaP for 320 to 0 Ma (Tetley, 2018). We also adjusted the position of Laurussia
 864 during the Devonian in order to better fit palaeomagnetic data and implemented an alternative position for
 865 Lhasa (against northwest Australia) that we consider to be more consistent with geological data in the
 866 Neoproterozoic (Section 5.4.1).

867

868 In the YOU19 reconstruction, Laurussia is rotated roughly 40° counter-clockwise compared to the DT14
869 and MAT16 reconstructions (Fig. 11). While these changes improved the global kinematic integrity of the
870 model (Young et al., 2019), the position of Baltica in this configuration conflicts with palaeomagnetic data,
871 which indicates it lay at more southerly latitudes (Torsvik et al., 2012). We used the compilation of Torsvik
872 et al. (2012) as a base, however, as many of the poles in that dataset for the late Silurian to early Devonian
873 were taken from the British Isles (c.f. Jeleńska et al., 2015), we supplement it with some data from cratonic,
874 continental Europe (Table 2, S. Pisarevsky pers. comm.). We modify the position of Laurussia from that
875 used in YOU19 such that it fits the cluster of poles at this time (Fig. 11b). This modification places it in a
876 similar latitudinal position to DT14 and MAT16 (e.g. Fig. 7a), however, we shift it further east relative to
877 DT14, so that it is closer to its final position in Pangea. This position then satisfies the kinematic and
878 structural issues outlined in YOU19, while maintaining Baltica and Laurussia at a palaeolatitude permitted
879 by palaeomagnetic data.
880

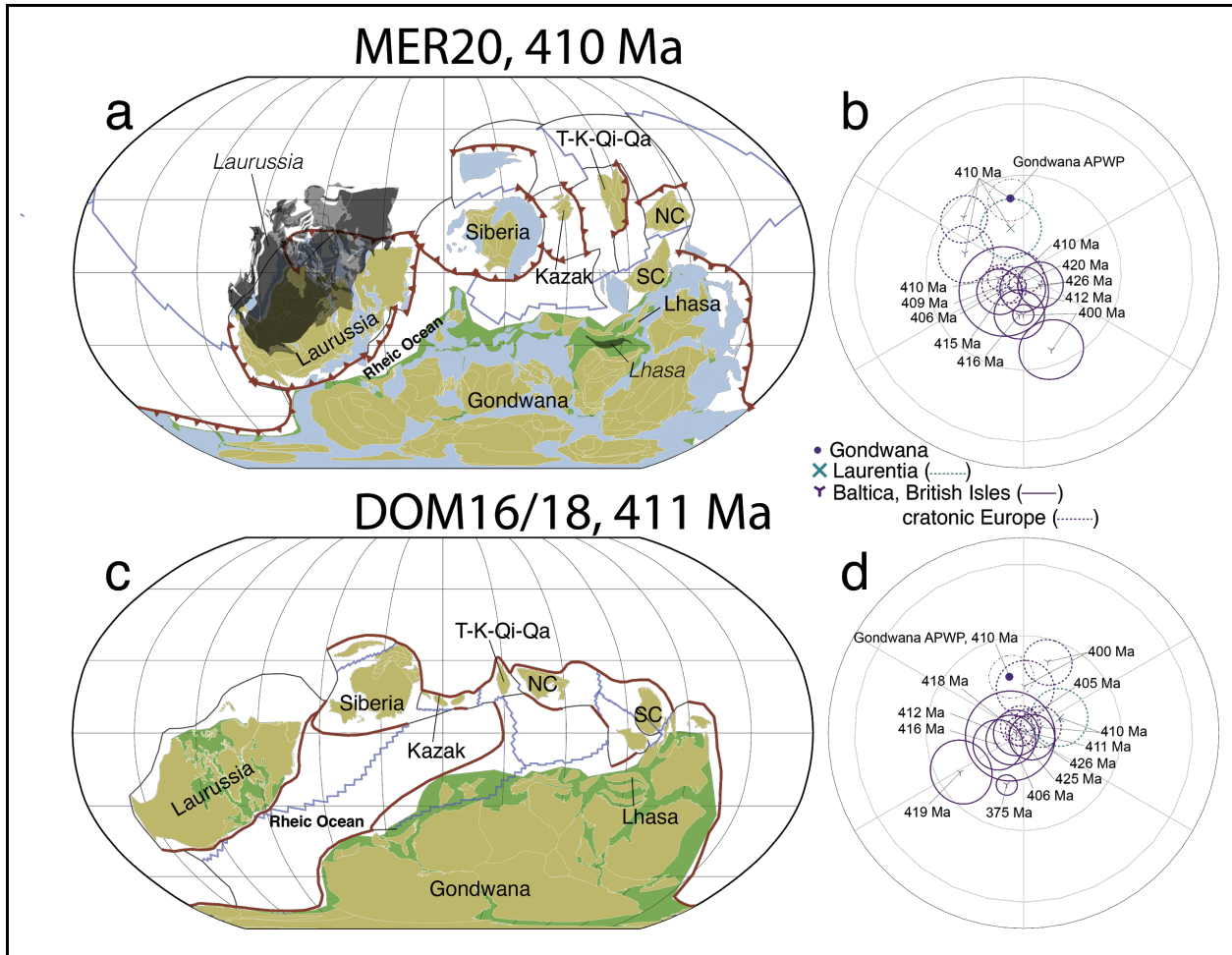


Figure 11

Comparison of our model (a, b) with Domeier (2018, 2016) (c, d) at 411–410 Ma to highlight the latitudinal changes implemented for Laurussia in our model. Dark outline of Laurussia and Lhasa (italicised labels) in (a) are their original positions in YOU19. Palaeomagnetic data are shown at time of best fit for both models (i.e. map projection view of Fig. 6). Tan polygons are areas of continental lithosphere in the Neoproterozoic that we model, blue polygons are areas of present-day continental lithosphere that are inferred to exist during the Neoproterozoic, but without having firm geological evidence or that have been affected by subsequent deformation (e.g. the distance between a present-day coastline and COB). Green polygons represent a schematic interpretation of congruent continental lithosphere, with intervening crust being subsequently deformed during future tectonic cycles. The DOM16/18 models extend until 410.1 Ma (so displayed at 411 Ma), while YOU19 begins at 410 Ma. NC, North China; SC, South China; T-K-Qi-Qa, Tarim-Kunlun-Qilian-Qaidam.

882

883 The Lhasa block, currently preserved in the Tibetan Plateau between India and Tarim, is an E-W elongated
 884 block consisting of Precambrian metamorphic basement, overlain by predominantly Palaeozoic
 885 sedimentary rocks and Mesozoic and Cenozoic volcanic assemblages (Yin and Harrison, 2000; Zhu et al.,
 886 2013). The Precambrian basement is established only in the southern and central terranes of Lhasa (Zhu et

887 al., 2013) and in the Amdo micro-block that is preserved in the Mesozoic northern Lhasa terrane (e.g. Fig.
888 10b). Lhasa is typically placed outboard of the Tethyan Himalayan terranes, off the northern margin of
889 India within Gondwana (e.g. Domeier and Torsvik, 2014). However, an alternative position outboard of
890 northwest Australia is also supported; a scenario consistent with tectonic affinities interpreted from zircon
891 age spectra and Hf isotopic signatures (Burrett et al., 2014; Zhu et al., 2011). We find a position off
892 northwest Australia more consistent with the Neoproterozoic geological record of Lhasa (Section 5.4.1)
893 that preserves magmatism interpreted to represent the existence of a subduction zone and back-arc (Guynn
894 et al., 2012; Hu et al., 2018), which would otherwise be impossible to produce if it was land-locked between
895 India and South China. We therefore alter the position of Lhasa from YOU19 to outboard of NW Australia.
896 For simplicity, we infer Lhasa's motion to follow the drift of the Cimmerian terranes, but recognise that the
897 palaeolatitudes need further refinement in the Jurassic and Cretaceous following syntheses such as Li et al.
898 (2017, 2016) and others.

899

900 **5.2 DOM16 and DOM18**

901

902 We sought to preserve, as closely as possible, the palaeolatitudes and the tectonic interpretations (i.e. history
903 of collisions, rifting, subduction and ocean basin evolution) of the DOM16 and DOM18 reconstructions.
904 The position of Gondwana (both in Early Palaeozoic and the older times covered by MER17) has been
905 adjusted to inherit the Gondwana position at 410 Ma from the new Gondwana APWP path described above.
906 Relative rotations of smaller blocks to Gondwana were calculated from DOM16/18 and translated into the
907 new position of Gondwana. Further adjustments to all continental polygons have been implemented to
908 smooth the transition from the late Palaeozoic configurations inherited from the adjusted YOU19 model
909 (adj-YOU19). The following sections detail adjustments to the DOM16/18 models made for the late
910 Cambrian–Devonian.

911

912 Figure 11 shows a direct comparison between the DOM16/18 reconstructions and our adj-YOU19 model
913 at 411/410 Ma. The primary differences between the models are longitudinal, as our adj-YOU19 model
914 shifts Laurussia, Siberia, Kazak, Taimr and North China $\sim 30^\circ$ longitudinally to the east compared to
915 DOM16/18 (as well as when compared to DT14 and MAT16, which link closely to DOM16/18), in order
916 to better model the amalgamation of Laurussia and Gondwana. This results in a far narrower Rheic Ocean
917 at 410 Ma in our model and a much simpler collision between Laurussia and Gondwana (e.g. Wu et al.,
918 2020; Young et al., 2019). This change is discussed further in context in the following section.

919

920 The motions of Baltica, Laurentia, and Siberia are tied directly to the spin axis through their own individual
921 palaeomagnetic reference frame, in contrast to the younger parts of the reconstruction where we retain the
922 hierarchy inherited from YOU19. For minor cratons (Tarim, North China, South China) and smaller blocks
923 (e.g. Tianshan, Kara), we model their motion within a relative hierarchy for the practical reason that this
924 makes it easier to preserve the consistency of their geological history, as they share multiple plate
925 boundaries with Gondwana. For all these cratons and blocks, we sought to preserve the palaeolatitudes from
926 the parent studies to a reasonable degree allowing for data uncertainties (e.g. Fig. 6). Figure 7 provides a
927 quantitative comparison between the paleolatitudes of the DOM16/18 models and our incorporation of them
928 into our adjusted reconstruction.

929

930 *5.2.1 Deviations from DOM16*

931

932 The key deviation between DOM16 and our model is a difference in the orientation of Baltica in the late
933 Cambrian (Fig. 12a), where our model has Baltica rotated 90° counter clockwise relative to DOM16. As
934 the DOM16 model only begins at 500 Ma it does not have to explicitly consider the earlier Neoproterozoic
935 history of Baltica. In our opinion the position of Baltica in DOM16 is more congruent with an inverted
936 Baltica (relative to Laurentia) during the Neoproterozoic (Hartz and Torsvik, 2002), where the southern-
937 peri Urals are connected to Greenland. In comparison, MER17 connects Baltica to Rodinia through the
938 Sveconorwegian margin in an upright position relative to the present-day (e.g. Cawood et al., 2003; Dalziel,
939 1992; Weil et al., 1998). The inverted Neoproterozoic Baltica position of Hartz and Torsvik (2002) results
940 in simpler kinematic motions during the late Ediacaran and Early Palaeozoic, whereas the ‘traditional’
941 Neoproterozoic coupling of Baltica-Laurentia requires a more complex motion path in order to fit
942 palaeomagnetic data. However, in our opinion the ‘upright’ coupling of Baltica and Laurentia is far more
943 geologically and palaeomagnetically robust (Cawood and Pisarevsky, 2006; c.f. Slagstad et al., 2019) in
944 the Neoproterozoic than the alternative, and as such we adopt this configuration at ca. 600 Ma (as in
945 MER17) during the opening of the Iapetus Ocean; necessitating a more complex kinematic evolution for
946 Baltica between 600 and 470 Ma (Fig. 12a ,b). Our reconstruction of Baltica is therefore quite different to
947 that of DOM16 during the late Cambrian and early Ordovician as we have to implement a ~90° rotation
948 between 520 and 475 Ma of Baltica to fit the same series of palaeomagnetic data at 470 Ma as DOM16.

949

950 Baltic palaeomagnetic data compiled by Meert et al. (2014), Torsvik et al. (2012) and Domeier (2016) were
951 used to ensure its latitudinal position remained valid between 550 and 470 Ma (Table 2). Importantly, only
952 two poles—one from the Andarum Shale (Torsvik and Rehnström, (2001) categorised as C-grade quality
953 by Meert (2014)) and the other from the Narva sediments, (Khramov and Iosifidi, (2009), categorised as B-

954 grade quality by Meert (2014))—are identified for Baltica between 530 and 480 Ma, both with a nominal
955 age of 500 Ma. Despite coeval ages, the poles are $\sim 35^\circ$ apart from one another and Meert (2014) identified
956 unresolved issues, specifically: few samples constraining the pole and a (possible) effect of inclination
957 shallowing (even after correction for inclination shallowing a $\sim 25^\circ$ mismatch remains). A strict fitting of
958 the Narva sediments pole would require Baltica to rotate by $\sim 2^\circ/\text{Ma}$ between 550 and 500 Ma; a situation
959 we consider implausible and likely reflecting underlying issues in the palaeomagnetic data. As such, our
960 model does not fit either pole explicitly, though our reconstructed position of Baltica is consistent with the
961 latitude suggested by the inclination data of both poles. By 460–440 Ma, our model closely resembles the
962 DOM16 model, with similar sized Rheic oceans, latitudinal positions and orientations of Gondwana, Baltica
963 and Laurentia (Fig. 12c, d). At 410 Ma, when DOM16 finishes, the only difference is the relative position
964 of Laurussia and Gondwana due to differences in palaeolongitude (Fig. 2c; 11). In our model, Laurussia is
965 much closer to Gondwana resulting in a far narrower Rheic Ocean at 410 Ma than in DOM16/18, DT14
966 and MAT16 (e.g. Fig. 2c, see also Wu et al. (2020)).

967
968 The width of the Rheic ocean is poorly constrained (c.f. Dalziel and Dewey, 2019; Domeier, 2018; Wu et
969 al., 2020) especially because of palaeolongitudinal uncertainty. The problem is compounded by the fact
970 that there is only one reliable palaeomagnetic pole constraining our Gondwana APWP between 430 and
971 400 Ma (Aïr intrusives in Niger, age at 410 Ma, (Hargraves et al., 1987)), meaning the early Devonian
972 portion of the APWP has large uncertainty. Because of this uncertainty, the methods used to create APWPs
973 tend to dampen the effect of this pole (which is true for our APWP). Nonetheless, even with the effect of
974 this pole being dampened, reconstructed palaeomagnetic data (without considering longitudinal constraints)
975 at 410 Ma allow placement of Laurussia and Gondwana to within a few thousand kilometres of one another
976 (e.g. Fig. 11a, see also Wu et al. (2020)). At first glance, this seems problematic, because one might expect
977 that the forces related to subduction zones modelled along the craton margins facing each other would draw
978 the cratons to each other. DOM16, DT14 and MAT16 (along with Torsvik et al., (2014)) solve this problem
979 by changing the palaeolongitude of Laurussia to 90° east relative to Gondwana, allowing for a much wider
980 ocean basin. This position is justified and necessitated in these models by their use of the PGZ method,
981 where Laurussia is reconstructed over the eastern arm of the present-day position of the Pacific LLSVP.
982 However, this position then requires > 8000 km of dextral motion between Laurussia and the Patagonian
983 margin of Gondwana from 400 and 340 Ma (e.g. Fig. 3c). As we do not adopt the PGZ method, our position
984 of Laurussia at 410 Ma relative to Gondwana is much closer to its final collision place and the resulting
985 relative motion between Laurussia and Gondwana between 410 and 340 Ma is of sub-orthogonal–
986 orthogonal collision along the southern Appalachian zone (Hopper et al., 2017), with some dextral
987 transform motion between north-east Laurentia and the northwest margin of Gondwana (e.g. Murphy et al.,

988 2011) and between southern Baltica and north Gondwana (e.g. Arthaud and Matte, 1977). From 340 to 320
989 Ma YOU19, MAT16 and DT14 have a similar configuration between Laurussia and Gondwana. We stress
990 that while our model this differs from the adopted DOM16 model, it is not a particularly novel interpretation
991 and many continental reconstructions show a similar scenario (e.g. McKerrow et al., 2000; Scotese, 2004;
992 Stampfli and Borel, 2002). A more detailed geological and kinematic justification of this interpretation is
993 presented in Young et al. (2019) and a discussion of the palaeomagnetic challenges in amalgamating Pangea
994 are presented in Domeier et al. (2020, 2012) which we encourage interested readers to.
995

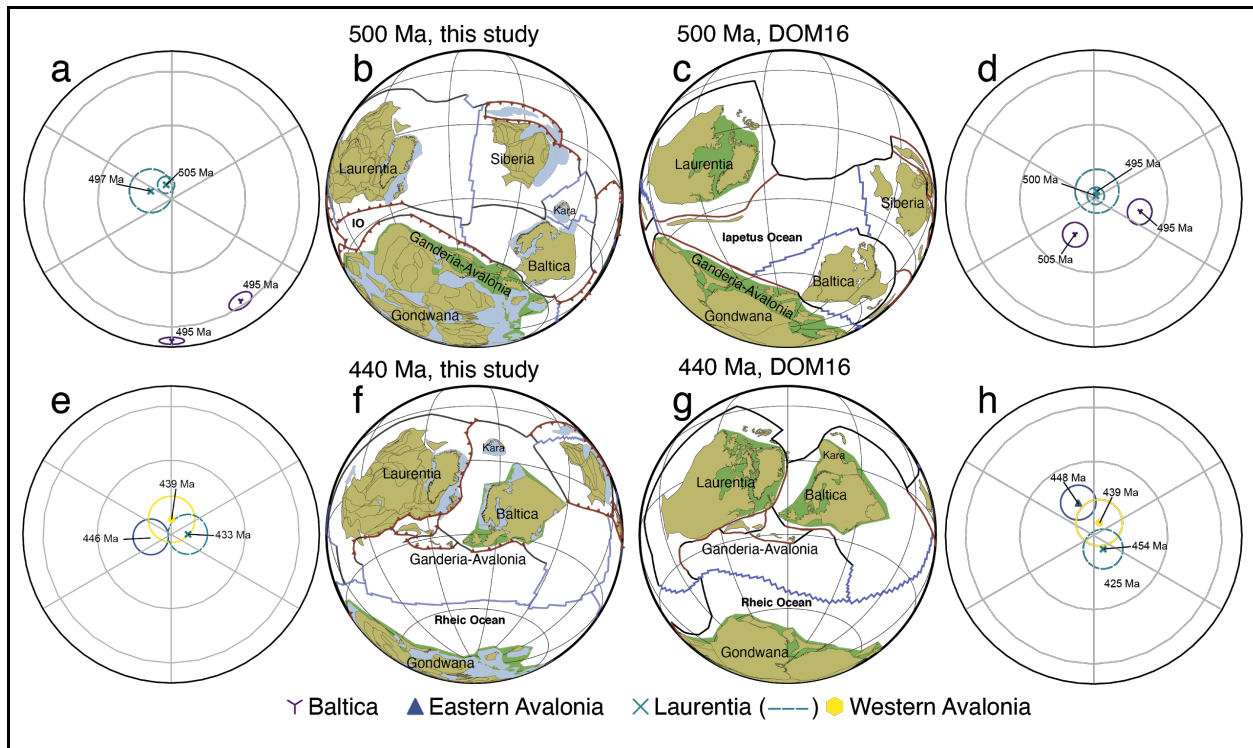


Figure 12

Comparison of the evolution of the Rheic Ocean between our model (a, 500 Ma; c, 440 Ma) and DOM16 (b, 500 Ma; d, 440 Ma) during the early Palaeozoic. We point out the rotational difference (but similar latitude) in Baltica at 500 Ma in our model relative to DOM16, discussed in text. Palaeolongitude is constrained absolutely in DOM16 but not in our model. Subduction polarities are not provided in the GPlates files of DOM16. Tan polygons are areas of continental lithosphere in the Neoproterozoic that we model, blue polygons are areas of present-day continental lithosphere that are inferred to exist during the Neoproterozoic, but without having firm geological evidence or that have been affected by subsequent deformation (e.g. the distance between a present-day coastline and COB). Green polygons represent a schematic interpretation of congruent continental lithosphere, with intervening crust being subsequently deformed during future tectonic cycles. IO, Iapetus Ocean.

997

998 5.2.2 Deviations from DOM18

999

1000 Two salient points made by Domeier (2018) pertaining to relative longitude and his model are also of
 1001 interest here, and worth reiterating when merging DOM18 into the adj-YOU19 model and then extending
 1002 the adj-YOU19 model into the Neoproterozoic. Firstly, a long lived south-dipping subduction zone,
 1003 preserved in the northern Kazakhstan terranes of Urumbai, Selety and Erementau (Degtyarev, 2011;
 1004 Domeier, 2018; Windley et al., 2007) was longitudinally distributed from Siberia through to the
 1005 northernmost margin of Gondwana (i.e. North Australia, Papua New Guinea) and secondly, the broader
 1006 framework of Baltica-Siberia-Gondwana provides geological, spatial and temporal limits on the evolution
 1007 of this area. These two aspects of the model allowed DOM18 to infer with some certainty the relative

1008 palaeolongitude of many of the smaller terranes within the broader absolute palaeolongitudinal constraints
1009 imposed by (principally) Siberia, Baltica, Laurentia and Gondwana. Likewise, even though we do not adopt
1010 the absolute longitudinal framework of DOM18, we can use the positions of the major cratons to provide a
1011 relative control on the possible kinematic evolution of the Chinese cratons and terranes. We follow DOM18
1012 by reconstructing a quasi-stable south-dipping subduction zone to delimit the northerly extent of the Palaeo-
1013 Tethys Ocean and this, coupled with the palaeomagnetic data from these cratons and terranes between 500
1014 and 410 Ma, make longitudinal re-ordering of these blocks unlikely. The unlikeliness of longitudinal re-
1015 ordering is one of the main constraints and pieces of evidence that lead to significant revision of the
1016 positions of Tarim and North China in MER17 that are discussed in the following section (5.4).

1017
1018 The relative positions of terranes (Tianshan, Qaidam-Qilian, Kunlun etc.) can also be considered in a similar
1019 manner to how we conceive of the relative ordering of the Chinese cratons during the Early Palaeozoic. In
1020 particular, the ca. 470 Ma suturing of Tianshan-Chu Yili (Alexeiev et al., 2019) and the 440–430 Ma
1021 suturing of Kunlun, Qaidam, Qilian and Alxa to Tarim (Xiao et al., 2009) both necessitate an internally
1022 consistent relative position between these terranes and Tarim and Siberia in order to be consistent with the
1023 geological record. That is, relative to present-day Tarim, Tianshan, Chu-Yili and other Kazakh terranes
1024 should be reconstructed somewhere north of the *northern* margin of Tarim during the Ediacaran–
1025 Ordovician, but south of Siberia. Similarly, Kunlun, Qaidam, Qilian and Alxa need to be reconstructed to
1026 the *south* and *east* of Tarim in the same time period. In a plate model framework, this means that the
1027 longitudinal structure of the Proto-Tethyan ocean basin should reconstruct (from west to east): Siberia—
1028 Chu-Yili-Kazak-Tianshan—Tarim—Alxa-Qaidam-Qilian-Kunlun—North China—South China (e.g. Fig.
1029 13f, g). Further back in time, we also maintain this same configuration to minimise any terrane re-
1030 organising, such that their relative positioning is broadly reminiscent of present-day (e.g. Figs. 9; 16). In
1031 this manner, we use these relative longitudinal constraints to infer a configuration for the nuclei of these
1032 terranes in the Neoproterozoic, thereby connecting the present-day with their Precambrian history.

1033
1034 The fundamental difference between DOM18 and our implementation of the model is the longitudinal width
1035 of the Proto-Tethyan ocean basin, bounded by Siberia in the west, Gondwana in the east and south and the
1036 aforementioned south-dipping subduction zone in the north (e.g. Fig. 13b, c, f, g). The latitudinal extent of
1037 the ocean basin remains similar in both models (30–50°), constrained by palaeomagnetic data from
1038 Gondwana, Siberia and the Chinese cratons (e.g. Table 2, Fig. 13a, d, e, h). In our model, this ocean basin
1039 is much wider (longitudinally) in the late Cambrian and Ordovician than in DOM18, narrowing in size as
1040 it evolves due to our implemented easterly drift of Siberia from the Cambrian through to the Devonian. The
1041 size of the ocean basin is then similar at 410 Ma (Fig. 11), due to the adopted similarity of the YOU19 from

1042 the DT14 reconstruction (Young et al., 2019). The key reason for the difference in width at 500 Ma is
1043 because DOM18 places Laurussia further east at 500 Ma than we do (Section 5.2.1). This then forces a
1044 narrower ocean basin between 500 and 410 Ma in DOM18 than in our model. The following paragraphs
1045 will discuss the regional longitudinal constraints of this ocean basin by considering the position of
1046 Gondwana and Siberia.

1047
1048 The Early Palaeozoic position of Siberia in our model is a function of palaeomagnetic data and its position
1049 in, and breakout from, Rodinia. In isolation, the simplest explanation of Siberia's journey is that sometime
1050 during the late Tonian–Cryogenian (750–700 Ma) Siberia rifted off the northern margin of Laurentia
1051 (somewhere near Greenland, see Pisarevsky and Natapov (2003) and Pisarevsky et al. (2013)). At this time
1052 Siberia was located equatorially and rotated 60° clockwise from its present-day orientation (Pisarevsky et
1053 al., 2013). Palaeomagnetic data are sparse for the remainder of the Neoproterozoic, with the few calculated
1054 poles having either poor age constraints or unresolved tectonic coherence with the Siberian craton (Pavlov
1055 et al., 2015), and are therefore typically omitted from syntheses (Cocks and Torsvik, 2007; Li et al., 2008;
1056 Merdith et al., 2017a). However, from the mid-Cambrian the palaeomagnetic record of Siberia is reasonable
1057 (Cocks and Torsvik, 2007) and broadly congruent with the palaeolatitude of the 750 Ma pole (that is,
1058 equatorial–sub-equatorial). From the mid-Cambrian, the data suggest a slow northward drift and counter-
1059 clockwise rotation (Cocks and Torsvik, 2007), with the orientation of Siberia at ca. 530 Ma inverted relative
1060 to present-day. This then requires a ~120° clockwise rotation between 720 and 530 Ma in order to fit its
1061 Neoproterozoic position (Metelkin et al., 2012). For the Cryogenian and Cambrian, Siberia's motion can be
1062 inferred indirectly using data from Baltica, as outlined in the next paragraph.

1063
1064 The position of Baltica is constrained by clusters of palaeomagnetic data during the Ediacaran and early
1065 Cambrian. Furthermore, its latitudinal position places limits on the possible position of Siberia. The
1066 equatorial excursion of Baltica in the latest Ediacaran places Baltica at a latitude similar to Siberia. As they
1067 cannot be positioned on the same longitude (Merdith et al., 2017a), Siberia must be located either
1068 longitudinally east or west of Baltica between 600 and 500 Ma (with Laurentia also occurring on a similar
1069 palaeolatitude but further east than either Siberia or Baltica). Domeier (2018) presented similar arguments
1070 for the second latitudinal excursion of Baltica (it returns to a high latitude during the Ordovician–Silurian)
1071 when it collided with Laurentia to form Laurussia at ca. 440–430 Ma. He argued that the overlapping
1072 palaeolatitudes of Siberia and Baltica at this time then requires Siberia to be located more easterly than
1073 Baltica by ca. 470 Ma (Domeier, 2018). We also adopt this logic, thus providing a rough relative
1074 longitudinal framework for Laurentia-Baltica-Siberia relations from 700 to 450 Ma.

1075

1076 Our model requires the motion of Siberia to be predominantly longitudinal between 700 and 450 Ma (the
1077 available palaeomagnetic data do not suggest more than 30° latitudinal movement). We constrain this to
1078 two broad phases of movement, defined by Baltica's two latitudinal excursions (at ca. 560 Ma and 450 Ma).
1079 In the first excursion (750–550 Ma), we keep Siberia longitudinally between Laurentia and Baltica, because
1080 to move it further east than Baltica at 550 Ma would require relative plate motion greater than 30 cm/a,
1081 which we deem unlikely. By 470 Ma palaeomagnetic data from Baltica suggest it has started drifting north
1082 again, so we therefore reconstruct Siberia to also be moving east longitudinally between 550 and 470 Ma,
1083 such that by 470 Ma it is located along the same longitude as Baltica; by 450 Ma it is further east than
1084 Baltica, such that Laurussia can form by 430 Ma. Our model is therefore similar to that of DOM18 in
1085 concept and adherence to available observations, however the different absolute longitudinal positions
1086 create a notably different ocean basin in the late Cambrian and Ordovician, within which the Chinese
1087 cratons and terranes are then arranged.

1088

1089 Domeier (2018) does not explicitly consider the Neoproterozoic or Early Palaeozoic evolution of the
1090 Chinese cratons in his model. At 500 Ma, the DOM18 model places North China off the northern margin
1091 of India, and South China off northern Australia. However, retaining these relationships in the
1092 Neoproterozoic is invalidated by what Neoproterozoic palaeomagnetic data exists for each craton (e.g. Fu
1093 et al., 2015; Li et al., 2004), and also conflicts with interpreted geological histories (Cawood et al., 2018b,
1094 2013b). Consequently, our model, which balances both older and younger times, alters the kinematic
1095 evolution in order to fit older constraints (Fig. 13, Sections 5.4.1 and 5.4.2).

1096

1097

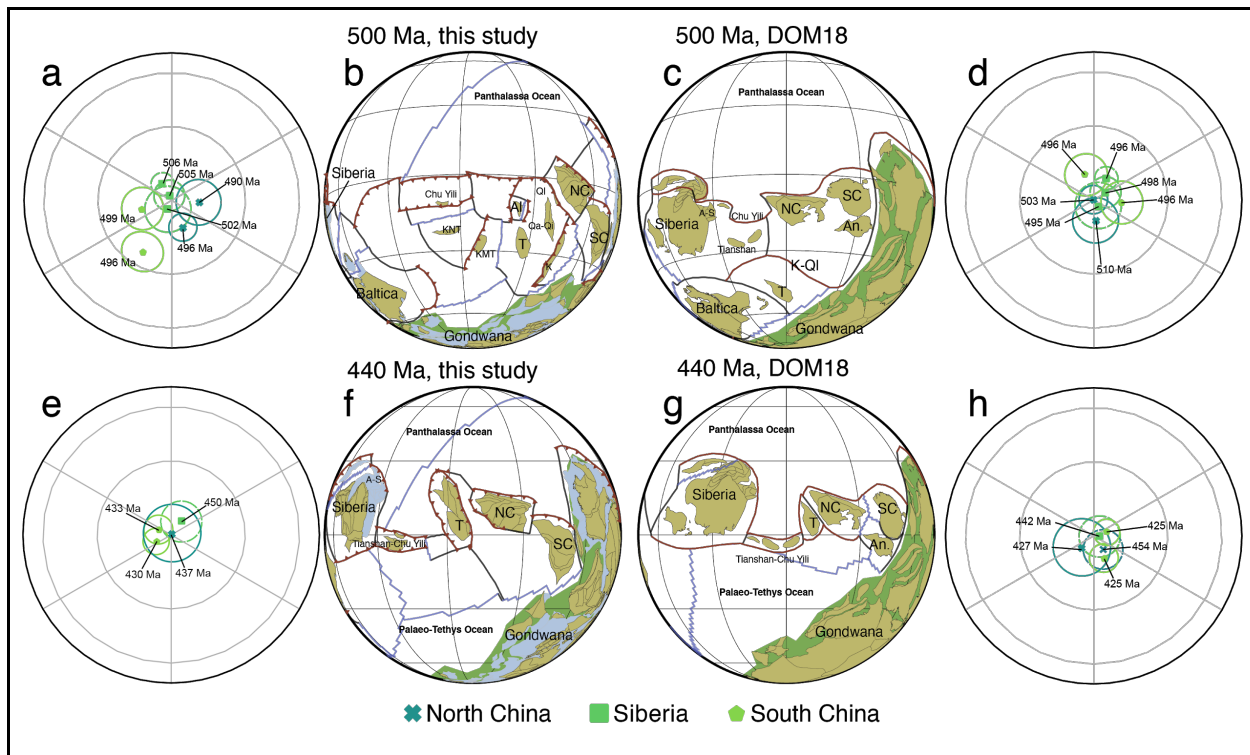


Figure 13

Comparison of our model (a, c) with DOM18 (b, d) to highlight changes made. Annamia (Indochina, Sibumasu) is not explicitly modelled in our reconstruction. L, Lut (Iran); F, Farah (Afghanistan); T, Tarim. Tan polygons are areas of continental lithosphere in the Neoproterozoic that we model, blue polygons are areas of present-day continental lithosphere that are inferred to exist during the Neoproterozoic, but without having firm geological evidence or that have been affected by subsequent deformation (e.g. the distance between a present-day coastline and COB). Green polygons represent a schematic interpretation of congruent continental lithosphere, with intervening crust being subsequently deformed during future tectonic cycles. Al, Alxa; An, Annamia; A-S, Altai-Sinai; SC, South China; K, Kunlun; KMT, Krygyz Middle Tianshan; KNT, Krygyz North Tianshan; NC, North China; Qa-Qi, Qaidam-Qilian; QL, Qinling; T, Tarim.

1098

1099 5.4 MER17

1100 5.4.1 Australia, North China, Lhasa and Tasmania

1101 Significant alterations to MER17 were made between 1000 and 900 Ma along the north-western, western
 1102 and south-western margins of Laurentia, affecting the motions and positions of Australia, North China,
 1103 Siberia, Tasmania and Lhasa. We adopt the model of Wen et al. (2018) in having a dextral shear zone
 1104 between Australia-Antarctica (A-A) and Laurentia during the early Tonian. Wen et al. (2018) argued for
 1105 placing Tarim against the eastern margin of Laurentia, separating Laurentia from Australia in a ‘Missing
 1106 Link’ position (cf. (Li et al., 2008, 1995), with the dextral shear zone transecting Tarim. However, we
 1107 consider this position for Tarim is incompatible both with geological data (the 760 Ma Aksu Blueschist
 1108 (C.-L. Zhang et al., 2013)) and with the kinematic constraints that would be necessary to move Tarim from

1109 this position to its Palaeozoic position (e.g. Merdith et al., 2017b). We therefore use the alteration of Wen
1110 et al.'s (2018) model presented in Mulder et al. (2018b), who place a dextral boundary separating the
1111 Antarctic crust of Australian affinity exposed in Terre Adélie Land from the Antarctic crust of Laurentian
1112 affinity in the Nimrod Igneous Province (Fig. 14a, see also Goodge et al., (2017)).

1113
1114 North China and northern Australia share a similar Mesoproterozoic and early Tonian sedimentary record
1115 and both preserve contemporaneous ca. 1.33–1.31 Ga magmatism (Bodorkos et al., 2020; Yang et al., 2020;
1116 Zhang et al., 2017) that is interpreted as a large igneous province. Yang et al. (2019) also demonstrated the
1117 similarity in detrital zircon ages and hafnium isotope compositions between the Tonian strata of both areas.
1118 We find that this position of North China in the latest Mesoproterozoic is remarkably compatible with the
1119 few reliable palaeomagnetic data for North China in the Neoproterozoic (e.g. Fig 6, (e.g. Fig. 6, Fu et al.,
1120 2015) and places North China in a position readily compatible with its Palaeozoic constraints where the
1121 same species of distinctive tommotiid fossils have recently been reported (Pan et al., 2018). A distinct Sino-
1122 Australian Cambro–Ordovician faunal province was identified by Burrett et al. (1990) that suggests some
1123 proximity in the early Palaeozoic. Cambrian–Ordovician rifting in the Arafura Basin north of northern
1124 Australia may represent the initial separation of North China from this margin of Gondwana (Ahmad and
1125 Munson, 2013). Palaeomagnetic data necessitate some relative motion between Australia and North China
1126 in the Early Palaeozoic from its inferred Mesoproterozoic–Neoproterozoic position (e.g. Domeier, 2018).
1127 Given there is no evidence of orogenesis between North China and northern Australia in the Phanerozoic,
1128 we infer that North China slowly drifts off this margin from the Cambrian, remaining in close enough
1129 proximity to share the identified Cambro–Ordovician faunal provinces (e.g. Fig. 13).

1130
1131 Dong and Santosh (2016) and Dong et al. (2014) describe a 1000 to 900 Ma suture between the Qinling
1132 Terrane and North China, preserved as the Kuanping Ophiolite (Fig. 14a–c). As Siberia and Australia are
1133 reconstructed adjacent to each other in Rodinia (Pisarevsky et al., 2013), the position of North China along
1134 the northern margin of Australia suggests that the Qinling terrane could feasibly be an extension of the
1135 Central Angara terrane, where there is a similarly aged (but sparsely described) ophiolite, the Ribnaya-
1136 Panimba ophiolite (Vernikovskiy et al., 2004, 2003). In our model, the subduction zones represented by
1137 these two ophiolites consume the oceanic lithosphere between Australia, Siberia and Laurentia (the
1138 Kuanping Ocean) during the early Tonian. Mulder et al. (2018b) ceased motion at 900 Ma in their model
1139 but, we adjust this cessation to 930 Ma wherein the Qinling Terrane rotates to fit against the North China
1140 block. This is because we also reconstruct the Lhasa block along the western margin of Australia ((Zhu et
1141 al., 2011), see Section 5.1) and here magmatism is preserved from ca. 925 Ma (Guynn et al., 2012, 2006;
1142 Hu et al., 2018; Zeng et al., 2018) (Fig. 14d,e). Consequently, we suggest that this subduction initiated after

1143 the closure of the interior Kuanping Ocean and collision of North China-Australia-Antarctica with Siberia-
1144 Laurentia along the Qinling-Central Angaran Terrane. The subduction zone then connects northwards
1145 through to subduction preserved in Taimyr outboard of Siberia (Vernikovsky et al., 2004; Vernikovsky and
1146 Vernikovskaya, 2001) and southward into an oceanic arc outboard of the Mawson Craton of Antarctica,
1147 possibly preserved in the southernmost Tonian Oceanic Arc Super Terrane (TOAST) or between Indo-
1148 Antarctica and Australia-Antarctica). In our model, Australia sits in a typical SWEAT (South West United
1149 States, East Antarctica) configuration (Moores, 1991). We made this change to better fit the arguments put
1150 forward by Mulder et al. (2018b), while still maintaining integrity of relative plate kinematics following
1151 the reasoning of Merdith et al. (2017b).

1152
1153 Our revised model also incorporates recent refinements to the Proterozoic and early Palaeozoic
1154 paleogeography of the Western Tasmania Terrane. The Western Tasmania Terrane, comprising the
1155 Proterozoic geology of Tasmania and the East and West South Tasman Rises (Berry et al., 2008), occupies
1156 an important position in deciphering the geological relationship between Laurentia and Australia-Antarctica
1157 in Rodinia, and also in understanding the transition between Rodinia to Gondwana. The Western Tasmania
1158 Terrane represents an exotic Proterozoic microcontinent that was accreted onto the Pacific margin of eastern
1159 Gondwana in the late Cambrian during the Ross-Delamerian orogenic cycle (Berry et al., 2008; Cayley,
1160 2011). The terrane has geological affinities with the central Transantarctic Mountains of East Antarctica
1161 and the western margin of Laurentia, including overlapping Palaeoproterozoic basement ages,
1162 contemporaneous Mesoproterozoic magmatic and fluid-flow events, and correlated Mesoproterozoic
1163 sedimentary strata (Berry et al., 2008; Fioretti et al., 2005; Halpin et al., 2014; Mulder et al., 2015, 2018b).
1164 Based on these geological connections, the Western Tasmania Terrane was likely located between East
1165 Antarctica and western Laurentia within an assembled Rodinia. The breakout of the Western Tasmania
1166 Terrane from its central position within Rodinia is recorded by widespread Tonian–Ediacaran
1167 sedimentation and rift-related magmatism (Mulder et al., 2020). The onset of Neoproterozoic rifting of the
1168 Western Tasmania Terrane is marked by 780–750 Ma intraplate magmatism (Black, 1997; Calver et al.,
1169 2013) and latest Tonian (750–730 Ma) siliciclastic and carbonate sedimentation (Calver et al., 2014; Mulder
1170 et al., 2018a). Following deposition of Cryogenian rift-related strata and glaciogenic intervals (Calver,
1171 2011; Calver et al., 2014) a final pulse of Neoproterozoic rifting is recorded by voluminous ca. 580 Ma rift-
1172 related basalts in northwest Tasmania (Direen and Crawford, 2003; Meffre et al., 2004). Geological
1173 correlations permit the Western Tasmania Terrane to have remained attached to either the western margin
1174 of Laurentia or the eastern margin of Australia-Antarctica following the opening of the Pacific Ocean (Fig.
1175 10f), prior to being isolated as a microcontinent during ca. 580 Ma rifting and accretion onto its present-
1176 day position along the margin of Gondwana by the late Cambrian (Fig. 10g; Berry et al., 2008; Mulder et

1177 al., 2020). We follow Mulder et al. (2020) in having Tasmania rift from the Antarctic margin (rather than
 1178 the alternative scenario of Laurentia), thus implying that some further unknown micro-continents rifted
 1179 from the western margin of Laurentia at the same time in order to account for that passive margin (e.g. Fig.
 1180 14f, g Macdonald et al., 2013) (see also Colpron et al., 2002; Cox et al., 2018; Eyster et al., 2019).
 1181

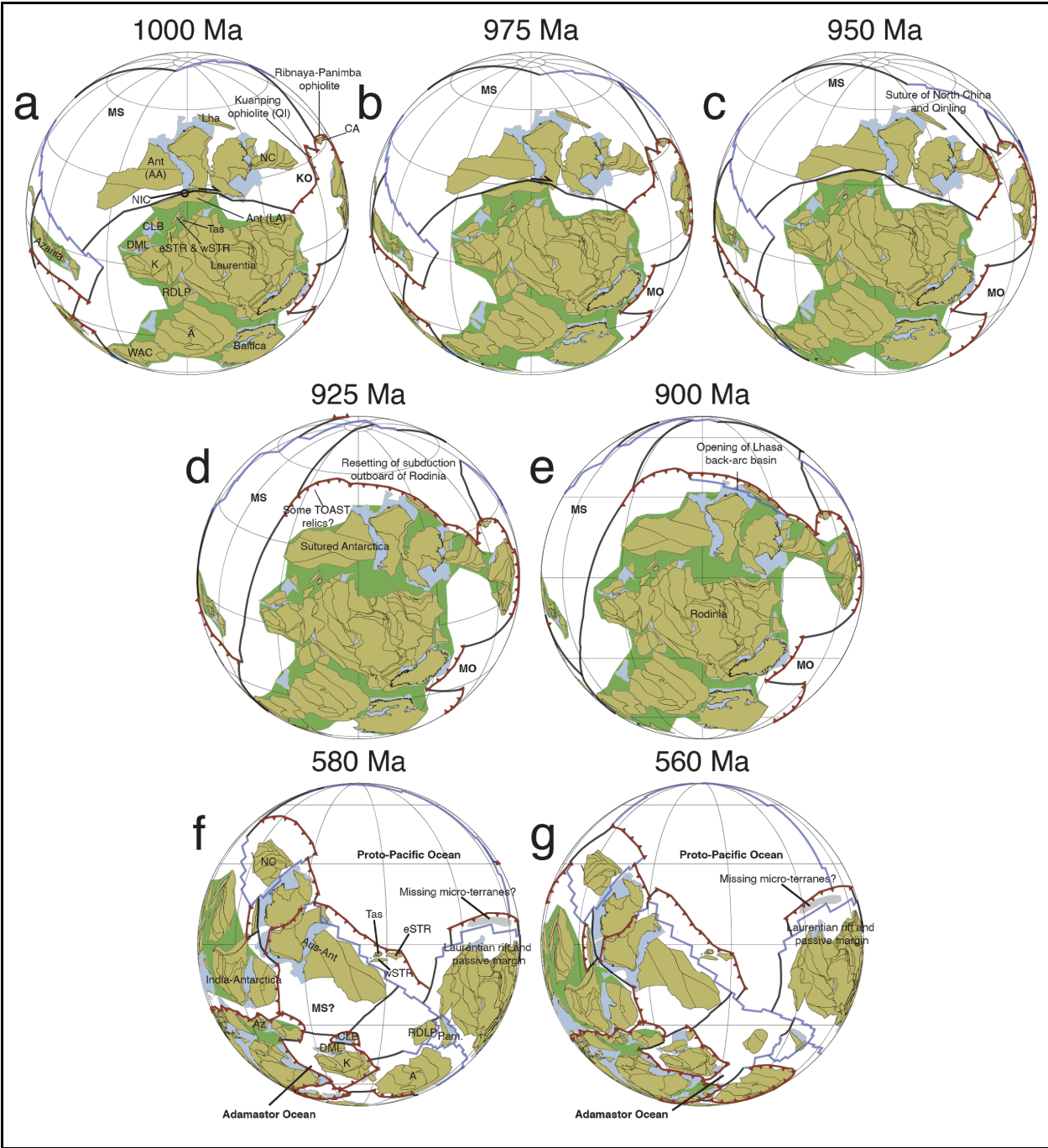


Figure 14

Snapshots of plate reconstructions showing our updated model for Australia-Laurentia at key time intervals, along with palaeomagnetic data. (a) 1000 Ma; (b) 975 Ma; (c) 950 Ma; (e) 925 Ma; (f) 900 Ma; (h) 580 Ma and (i) 560 Ma. The Tonian model (a–f) follows arguments laid out in Mulder et al. (2018b), while the Ediacaran-Cambrian evolution is after Mulder et al. (2020). Times in these panels reflex the nominal time of best fit for each pole. Tan polygons are areas of continental lithosphere in the Neoproterozoic that we model, blue polygons are areas of present-day continental lithosphere that are inferred to exist during the Neoproterozoic, but without having firm geological evidence or that have been affected by subsequent deformation (e.g. the distance between a present-day coastline and COB). Green polygons represent a schematic interpretation of congruent continental lithosphere, with intervening crust being subsequently deformed during future tectonic cycles. CLB: Coats Land Block; DML, Dronning Maud Land; eSTR: Eastern South Tasman Rise; MO, Mirovoi Ocean; MS, Mawson Sea; Tas: Tasmania; wSTR: Western South Tasman Rise; RDLP: Río de la Plata; WAC, West African Craton.

1182

1183 *5.4.2 India-South China Accretionary Belt*

1184 We preserve the MER17 interpretation of a tight India-South China connection (after Cawood et al., 2013b).
1185 This possible connection was suggested previously by Jiang et al. (2003) who noted the similarity between
1186 sequence stratigraphy in rift basins preserved in both South China and the Indian Lesser Himalaya (Fig.
1187 15a), as well as by Hofmann et al. (2011) who suggested a geological similarity based on detrital zircon
1188 analysis. Arguments for this connection are succinctly summarised in Cawood et al. (2018b) and are not
1189 repeated here—instead we focus our discussion of this margin on the relative position of outboard terranes
1190 during the Neoproterozoic (Fig. 15), which are based predominantly on their Palaeozoic positions
1191 (Domeier, 2018). Here we have sought to preserve their relative internal positions in order to minimise
1192 reshuffling of terranes during the Neoproterozoic (e.g. Fig. 16). For example, Kunlun, which is currently
1193 preserved south of Tarim and west of Qaidam-Qilian, is always reconstructed with the same internal
1194 consistency. Although we note that this may not be an accurate reflection of the ordering and positioning
1195 of the terranes, it ensures consistency within the model and minimises terrane shuffling which can preclude
1196 unrealistic scenarios, where terranes have to kinematically skirt one another precariously. Figure 16 gives
1197 a schematic overview of our conceptualisation and implementation of this model.

1198

1199 Following Alessio et al. (2018) and Armistead et al. (2019), the northwest margin of India is here interpreted
1200 as an extensive Stenian-Tonian accretionary margin that extends as far as the Omani basement and
1201 northernmost Madagascar. The pre-Ediacaran basement rocks in Rajasthan and Pakistan share similarities
1202 with those of Oman. Granitoids have been dated from Rajasthan and from Nagar Parkar in eastern Sind
1203 (Pakistan) at ca. 1.1 Ga (Meert et al., 2013; Raza et al., 2012). There is no evidence of older crust occurs
1204 west of the Western Margin Fault of the Aravalli-Delhi Orogen, where the Marwar terrane accreted to India
1205 in the latest Mesoproterozoic (Meert et al., 2010) (Fig. 15b). Tonian granitoids and rhyolites occur in inliers

1206 through northwest India and Pakistan, where they cluster into crystallisation ages of ca. 990–970 Ma
1207 (Haldar and Deb, 2001; Pandit et al., 2003), ca. 860–820 Ma (Davies and Crawford, 1971; Deb et al., 2001;
1208 Just et al., 2011; Van Lente et al., 2009) and ca. 775–760 Ma (Ashwal et al., 2013; Gregory et al., 2009;
1209 Meert et al., 2013; Van Lente et al., 2009). The latter magmatic and extrusive phase forms one of the largest
1210 felsic igneous provinces on the planet—the Malani Igneous Suite—which is also traced to the Seychelles
1211 (Fig. 15c–e) (Torsvik et al., 2001; Tucker et al., 2001). Arc accretion continued outboard to Oman where
1212 two main phases of subduction and arc magmatism occur, at ca. 850 Ma and ca. 770 Ma (Blades et al.,
1213 2019a). The latter phase focussed in the southern Mirbat area and interpreted here as the arc that formed
1214 ocean-ward of the more back-arc Malani Igneous Suite. Further outboard still, and later accreting onto the
1215 Indian margin, the Bobakindro Terrane of northern Madagascar (Armistead et al., 2019) consists of juvenile
1216 magmatism that dates from ca. 750–705 Ma (Armistead et al., 2019; Collins, 2006; Thomas et al., 2009).

1217
1218 Many terranes currently preserved north of South China and south of Siberia have Neoproterozoic or older
1219 cores. They have not been previously considered in global models (Li et al., 2008; Merdith et al., 2017a)
1220 due to the sparsity of data and small size of terranes, which invites many competing and conflicting
1221 interpretations of their history. However, in the construction of this continuous plate model, where spatial
1222 and temporal continuity is vital, the most compatible Tonian position for these terranes was outboard of the
1223 afore-discussed large accretionary subduction zone of South China and India. This position places them in
1224 the most favourable kinematic, palaeomagnetic and geologically plausible positions for their (more well
1225 constrained) Palaeozoic journeys (e.g. Charvet et al., 2011; Domeier, 2018; Xiao et al., 2013). Below we
1226 summarise some geological evidence for this, with particular reference to the Tarim Craton, as it is the only
1227 block that has multiple reliable palaeomagnetic data from the Neoproterozoic that act as a another line of
1228 evidence. We also note that Huang et al. (2019) recently proposed a location outboard of Greenland for the
1229 Yili-Tianshan Block on the basis of similar detrital zircon age spectra. However, more work would have to
1230 be done to determine whether this Tonian position is consistent with the kinematic evolution necessary for
1231 these blocks to fit their Palaeozoic constraints.

1232

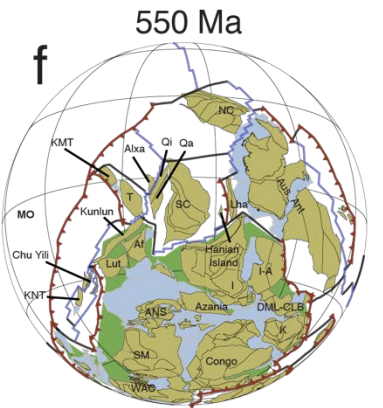
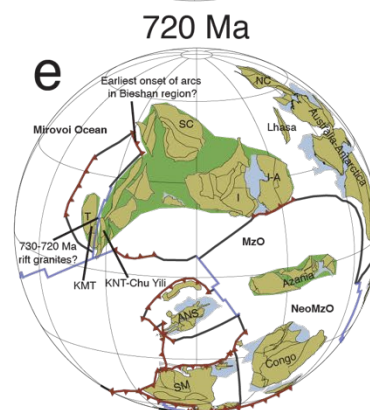
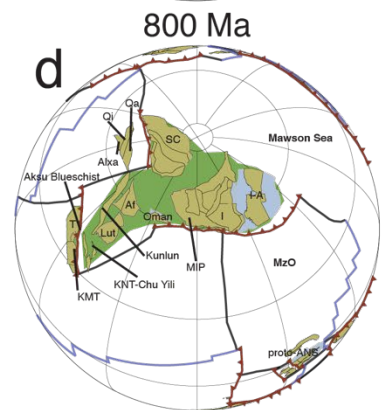
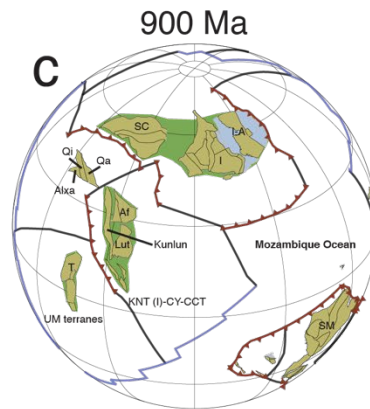
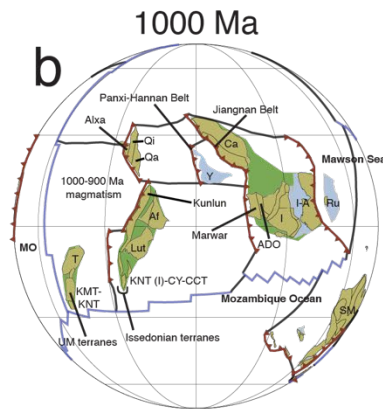
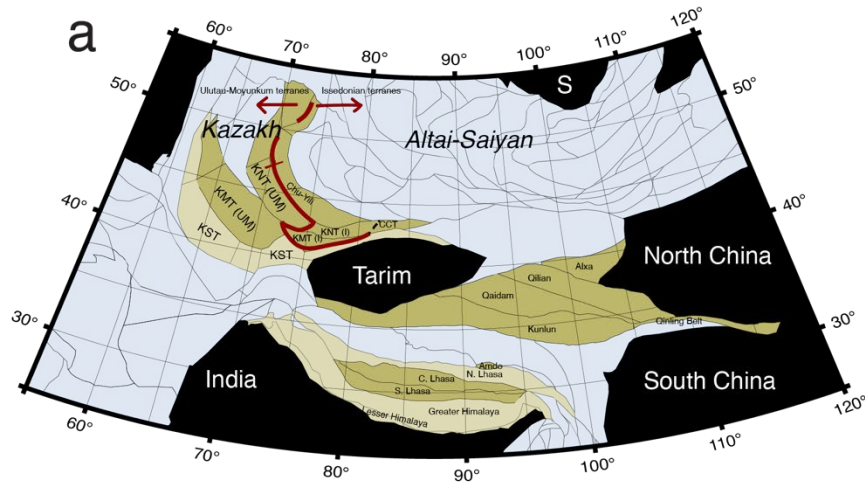


Figure 15

(a) Regional map at present day of Central Asian Orogenic Belt with modelled terranes highlighted in tan. Light tan terranes are not explicitly modelled but are referred to in the main text. Black areas represent the cratonic components. For the Kazakh area, we use polygons consistent with their Palaeozoic structure. The size, orientation and distribution of crust in these terranes in the Neoproterozoic is unknown due to the subsequent reworking of the terranes. Therefore, the precise position (along a margin), orientation, size and shape of these terrane polygons in the reconstruction figures are speculative and should be treated cautiously. (b–f) Evolution of the India–South China system during the Tonian–Cryogenian at key times. Tan polygons are areas of continental lithosphere in the Neoproterozoic that we model, blue polygons are areas of present-day continental lithosphere that are inferred to exist during the Neoproterozoic, but without having firm geological evidence or that have been affected by subsequent deformation (e.g. the distance between a present-day coastline and COB). Green polygons represent a schematic interpretation of congruent continental lithosphere, with intervening crust being subsequently deformed during future tectonic cycles. ADO = Aravalli–Delhi Orogen; Af, Afghanistan; Aus-Ant, Australia–Antarctica; Ca, Cathaysia; DML-CLN, Dronning Maud Land–Coats Land Block; I, India; I-A, Indo–Antarctica; KNT (I/UM), Krygyz North Tianshan (Issendonian/Ulutau–Moyunkum); KMT (I/UM), Krygyz Middle Tianshan (Issendonian/Ulutau–Moyunkum); MIP, Malani Igneous Province; MO, Mirovoi Ocean; MzO, Mozambique Ocean; NC, North China; NeoMzO, Neomozambique Ocean; Qa, Qaidam; Qi, Qilian; Ru, Ruker; SC, South China; SM, Sahara Metacraton; T, Tarim; WAC, West African Craton; Y, Yangtze.

1233
1234 Early Tonian age (1000–900 Ma) magmatism and high-pressure metamorphism is preserved in the
1235 basements of the Qilian–Qaidam (Qi–Qa), Kunlun and Tianshan–Chu Yili terranes (Song et al., 2012; Tung
1236 et al., 2007; Wu et al., 2017). Importantly Song et al. (2012) identified an early Tonian event preserved in
1237 a high-pressure metamorphic belt in Qi–Qa. Here, a ~200 km linear belt of granitic gneisses,
1238 metamorphosed in the Palaeozoic, have crystallisation ages between ca. 1000 and 900 Ma (Song et al.,
1239 2012). Zircons recovered from pelitic and psammitic gneisses from the same belt possess multiple
1240 generations of growth, as suggested through cathodoluminescence imaging, and return ages of the (first
1241 generation) to between ca. 940 and 900 Ma (Song et al., 2012). These are interpreted to represent a period
1242 of granulite facies metamorphism from a continental arc indicating that subduction was active during the
1243 Early Tonian (Song et al., 2012). Song et al. (2012) and others (e.g. Zhang et al., 2008) suggested a link
1244 between these two blocks and South China on the basis of similar-aged magmatism and metamorphism.
1245 However, as the Qi–Qa preserves a different Palaeozoic tectonic history to South China, as opposed to
1246 fragments of older lithosphere preserved in the Panxi–Hannan Belt of the Yangtze Craton, we suggest that
1247 a subduction zone was located outboard of Qi–Qa while a secondary, smaller ocean was closing between
1248 Qi–Qa and the accretionary orogen of the Panxi–Hannan Belt (Fig. 11a–c). Upon the suturing of Yangtze
1249 with Cathaysia (ca. 900 Ma, Fig. 11b), subduction relocated outboard of South China and began to close
1250 the ocean between Qa–Qi and South China. Similar to the Qi–Qa, the Kunlun terrane preserves scattered
1251 magmatic ages of S-type granites and protoliths of orthogneiss and amphibolites ranging between ca. 1000
1252 and 900 Ma (Chen et al., 2008; He et al., 2018; and Chen et al., 2006a; 2006b—both cited in Chen et al.,
1253 2008; He et al., 2018). We interpret these rocks and ages as an extension of the same subduction zones

1254 outboard of Qi-Qa, and extend it further to the south where (again) similar-aged magmatism is also
1255 preserved in the North Tianshan and Chu-Yili (Degtyarev et al., 2017).

1256
1257 The Kazakh terranes (including Krygyz Tianshan and Chu-Yili, Fig. 15a) have poorly constrained
1258 Neoproterozoic histories, with only a handful of ages from outcropping magmatic rocks and sedimentary
1259 successions. We predominantly follow the summary of Degtyarev et al. (2017) in offering a possible
1260 tectonic interpretation of their Neoproterozoic geological history that is linked to the wider globe.
1261 Degtyarev et al. (2017) note that there are two broad categories of Precambrian terranes preserved in the
1262 Krygyz-Tianshan-Yuli area; the Issedonian and Ulutau-Moyunkum terranes. The Issedonian terranes,
1263 preserved in the northeast of the western Central Asian Orogenic Belt, include Chu-Yili and the Chinese
1264 Central Tianshan and are characterised by late Mesoproterozoic magmatism (e.g. Degtyarev et al., 2011),
1265 thick (> 1000 m) 1050–950 Ma quartzite-schist successions followed by ongoing magmatism from ca. 960–
1266 890 Ma (e.g. Degtyarev et al., 2008; Gao et al., 2015; Huang et al., 2015). Comparably, the Ulutau-
1267 Moyunkum terranes are preserved only in the west (in Krygyz) within Krygyz Middle Tianshan and Krygyz
1268 North Tianshan (e.g. Fig. 10b), and consist of a Palaeoproterozoic basement, with predominantly
1269 sedimentary Mesoproterozoic and early Neoproterozoic rocks (Degtyarev et al., 2017). Magmatism,
1270 between 840 and 760 Ma (Kröner et al., 2012) and granulite facies metamorphism from 800–760 Ma
1271 (Degtyarev et al., 2017; Tretyakov et al., 2016) are recorded only in the late Tonian. Both sets of terranes
1272 preserve distinct differences in their Mesoproterozoic histories, minor differences in the Early
1273 Neoproterozoic histories but similar histories from the mid-Neoproterozoic (ca. 700 Ma) onwards,
1274 suggesting proximity sometime during the late Tonian (800 to 700 Ma?) (Degtyarev et al., 2017). We
1275 interpret the Issedonian terranes to be the southernmost extent of the subduction zone spanning Qi-Qa and
1276 Eastern Kunlun, as the magmatism preserved in the Issedonian terranes has a continental arc signature
1277 (Huang et al., 2014) and is broadly coeval. Comparably, the Ulutau-Moyunkum terranes, which share
1278 Mesoproterozoic similarities to Tarim and record no magmatism in the early Neoproterozoic, are located
1279 on the opposite side (lower plate) of a closing ocean basin. This culminates with the collision of Tarim
1280 (with the Ulutau-Moyunkum terranes) and the combined India-South China continent at ca. 800–760 Ma
1281 along the Issendonian margin (Fig. 11d, e). The sparse data and age constraints from these terranes means
1282 much of their Neoproterozoic history is conjectural. Although the specific orientation and positioning of
1283 the terranes along the margin is speculative our interpretation is that it places the Kazakh terranes in a
1284 favourable position for their Palaeozoic evolution which is, comparably, much better constrained.

1285
1286 Two clusters of Neoproterozoic-aged palaeomagnetic data from Tarim make it difficult to elucidate a
1287 consistent position with other palaeomagnetic data from Rodinian constituents. Three poles from the Tonian

1288 and Cryogenian require a 90° rotation of Tarim in order to fit the younger pole of Wen et al. (2017), or a
1289 180° rotation to fit the cluster of three poles in the Ediacaran to Cambrian (see Merdith et al. (2017a) and
1290 Section 4.2 for a discussion). Within a self-consistent kinematic plate boundary framework, this motion is
1291 not permissible if Tarim is positioned either against north-western Australia (e.g. Zhang et al., 2012) or as
1292 an extension of the ‘Missing-Link’ model (Li et al., 2004 for the original proposal of the “Missing-Link”
1293 model; Wen et al., 2018, 2017). A plausible position where these palaeomagnetic criteria are met, along
1294 with satisfying key geological evidence, such as the 800–760 Ma Aksu Blueschist preserved on the northern
1295 margin of Tarim (C.-L. Zhang et al., 2013), is outboard of the India-South China accretionary belt, where it
1296 acts as the final piece of continental lithosphere accreted to the margin. In our model, we suggest the
1297 metamorphism recorded by the Aksu Blueschist marks the accretion of Tarim to Chu-Yili and the Tianshan
1298 (see Xia et al. (2017) for the most recent discussion, but see also data and discussion from Zhang et al.
1299 (2012, 2009). To accommodate the change in position suggested by the palaeomagnetic data, we introduce
1300 a ~120° rotation of Tarim and Southern Tianshan away from this margin, such that Tarim’s southern margin
1301 collides with the outboard margin of Alxa-Qaidam-Qilian, so its northern margin faces an open ocean basin,
1302 allowing it to rift northward facing as Gondwana forms towards its more well constrained Palaeozoic
1303 position (Fig. 16).

1304
1305 To support this interpretation of Tarim’s evolution we present the following geological observations in
1306 support of this model. Firstly, there is an absence of extensive magmatism on either the northern or southern
1307 margin of the Tarim craton between 1000 and 850 Ma, which makes it difficult to include as a part of the
1308 upper-plate circum-Rodinian subduction girdle (Cawood et al., 2016). Previous studies, including MER17,
1309 place Tarim on the margin of Rodinia typically also include the Chu Yili and Tianshan crust attached in a
1310 quasi-present-day configuration to the northern margin of Tarim. In such cases their record of Tonian
1311 magmatism supports the interpretation that they formed part of the circum-Rodinian subduction girdle (Ge
1312 et al., 2014) however, this location is inconsistent with available palaeomagnetic data (e.g. (Wen et al.,
1313 2018). Secondly, rift related granitoids preserved in the Southern Tianshan (Degtyarev et al., 2017; Gao et
1314 al., 2015) are here interpreted as evidence of the re-adjustment of Tarim between 730 and 680 Ma to account
1315 for the change in palaeolatitude and orientation inferred from palaeomagnetic data (Fig. 11e). In addition,
1316 extensive rifting in the southwest of Tarim (Wang et al., 2015) is interpreted to reflect the rearrangement
1317 of subduction after Tarim/India-South China amalgamation. This motion is similar to the adjustment of
1318 Baltica relative to Laurentia in the latest Mesoproterozoic proposed by Cawood et al. (2010) to account for
1319 the Valhalla Orogeny. Xiao et al. (2010) summarise the geology and geochronology of rocks found in the
1320 Beishan area of China which record a protracted and complex history of multiple arc development and
1321 accretion through the late Neoproterozoic and Early Palaeozoic. Rocks in the Beishan area (Alxa, Fig. 15,

1322 16) range from low-grade sedimentary metamorphic assemblages to gneiss and eclogite complexes and
1323 intrusive granitic bodies that have late Neoproterozoic–Cambrian ages (Xiao et al., 2010). These rocks,
1324 inferred to represent an active subduction zone and accretionary complex, are unconformably overlain by
1325 Cambrian–Ordovician sediments. The earliest record of metamorphism in the area are from a series of
1326 SHRIMP U-Pb ages taken from the metamorphic rims of zircons of an eclogite unit at ca. 830–800 Ma
1327 (Yang et al., 2006).

1328
1329 With respect to the palaeomagnetic issues of Tarim we raised earlier (Section 4.2), we find that our
1330 conceptual model of this rotation of Tarim (e.g. Fig. 16) can fit either set of palaeomagnetic data equally as
1331 well, with the key factor being the time of subduction in the Beishan area. Under the cluster of three poles,
1332 the motion of Tarim occurs more quickly and peak subduction (possibly resulting in a collision?) would be
1333 earlier (ca. 650 Ma), while to fit the pole of Wen et al. (2017) it would occur later at between 600 and
1334 550 Ma. Based on the review of Xiao et al. (2010), we infer that the geological data support the later
1335 interpretation more strongly however, given the novelty of this scenario and the absence of identifiable
1336 piercing points, it could be revised in the future to fit the alternative scenario.

1337
1338 Late Neoproterozoic–Early Cambrian rifting events are inferred to have occurred within all the terranes
1339 (Kunlun, Qa-Qi, Chu Yili and Tianshan) that we have placed on this Indian-South Chinese accretionary
1340 margin, however, the high degree of reworking and suturing of crust from the terranes, coupled with the
1341 small size of these terranes makes it difficult to pin down precise rift times. We stress that our interpretation
1342 here is preliminary, especially when compared to specialised reviews of the tectonics of this area (Kroner
1343 et al., 2007; Wilhem et al., 2012; Windley et al., 2007; Xiao et al., 2013; Yakubchuk, 2017). We reiterate
1344 that our intention here is to provide a possible framework that connects and contextualises these terranes
1345 within a consistent kinematic and tectonic evolution between the Neoproterozoic and Palaeozoic (Fig. 16),
1346 which can be more tightly refined in the future. Ordovician–Silurian sutures between Qa-Qi-Kunlun and
1347 surrounding cratons preserve late Neoproterozoic–Cambrian ophiolites (Jian et al., 2014; Shi et al., 2018;
1348 Song et al., 2013, 2009) thus necessitating the existence of ocean basins, but there are few dates of ocean
1349 basin initiation. Xu et al. (2015) date Qilian-Qaidam continental rift basalts to 600–580 Ma, constraining
1350 ocean basin formation to the latest Ediacaran–earliest Cambrian, with the oldest ophiolite (the Yushigou
1351 Ophiolite) preserved in these terranes dated to 550 Ma (Shi et al., 2004). Evidence of rifting is more sparse
1352 in Kunlun, however, similar stratigraphy, ages and geochemistry of metavolcanic deposits between Kunlun
1353 and Qaidam-Qilian (Yuan et al., 2004) suggest coeval rifting is reasonable, though not definite. We follow
1354 some recent work (Peng et al., 2019; Zhao et al., 2018) in having separation of Tarim and these terranes in
1355 the late Ediacaran (550 Ma here, as a response to the closure of the Mozambique Ocean between India and

1356 Congo). Our model closely resembles the schematic framework outlined by Qiantao et al. (2001), while
1357 also following Domeier (2018) in maintaining a very close affinity between Kunlun, Q-Q and Alxa for the
1358 Early Palaeozoic, such that they conceptually form a single elongated terrane that rifts off Gondwana at ca.
1359 550 Ma and collides along the southern margin of Tarim by 440 Ma.

1360
1361 Comparably, rifting on the northern margin of Tarim is easier to constrain. Thick, late Neoproterozoic
1362 sedimentary sequences capped with carbonate and an unconformity on the Ediacaran–Early Cambrian
1363 imply a prolonged rift phase with breakup at ca. 550–540 Ma (Zhao et al., 2014; Zhu et al., 2017). Similarly,
1364 sedimentary assemblages preserved in the South Tianshan orogen are dated from 540–520 Ma (Alexeiev et
1365 al., 2020; Safonova et al., 2016), suggesting that ocean basin formation between Tarim and Kryguz Middle
1366 Tianshan begins in the Early–Middle Cambrian. Further north, the relationship between the Kryguz North
1367 Tianshan and Chu-Yili is also reasonably well established (e.g. Windley et al., 2007; Xiao et al., 2013).
1368 Late Ediacaran–Early Cambrian magmatism preserved in Chu-Yili and North Tianshan (Alexeiev et al.,
1369 2011; Degtyarev et al., 2017; Kroner et al., 2007) is interpreted to represent development of multiple
1370 contemporaneous arcs (e.g. Alexeiev et al., 2020). The Ordovician-aged sutures between Chu-Yili and
1371 North and Central Tianshan (Windley et al., 2007) are defined by ophiolitic slithers, implying an ocean
1372 basin (or a back-arc) existed between these terranes. We infer that in the late Neoproterozoic to Early
1373 Cambrian, the Kazakh and Tianshan terranes that accreted outboard of India-South China were fragmented
1374 and rifted off this margin forming a collage (not dissimilar to modern southeast Asia, or the NE Pacific in
1375 the Mesozoic, e.g. Sigloch and Mihalynuk (2013) that eventually re-assembled in the Ordovician. We
1376 model the time of fragmentation at 550 Ma, because this is the time of collision between India and Congo
1377 along the East African Orogen, so we infer that subduction relocated outboard of the northern margin.

1378
1379 Palaeomagnetic data from South China do not permit a fixed fit between South China and Gondwana for
1380 the early Palaeozoic. The data do, however, permit a close spatial relationship between them (<1000 km).
1381 Palaeomagnetic data from South China suggest it moved from mid to lower latitudes between the Cambrian
1382 and Devonian (Domeier, 2018; Han et al., 2015). Furthermore, shallow marine faunal data and detrital
1383 zircon arrays suggest that between the Cambrian and Devonian, South China shifted from an Indian-
1384 Himalayan-Iran affinity (Burrett et al., 1990) to Sibumasu-Australian affinity (Cocks and Fortey, 1997;
1385 Metcalfe, 2013, 2011), broadly consistent of the positions necessary to fit the palaeomagnetic data. Rift
1386 sequences in South China and in northern India (Himalayan terranes) are similar, but diverge strongly after
1387 the early Cambrian (Jiang et al., 2003), providing some kinematic support for invoking for relative motion
1388 between South China and Gondwana. The Sanya Block of Hainan Island (Fig. 15f) is linked through detrital
1389 zircon provenance and middle Cambrian trilobites to western Australia and Antarctica rather than South

1390 China in the Neoproterozoic (Cawood et al., 2018b; Xu et al., 2014). The presence of Early Ordovician
1391 trilobites in the Sanya block also common to South China and Australia (Torsvik and Cocks, 2009) support
1392 a close relationship between the three domains by this time (Cawood et al., 2018b). A late Cambrian–
1393 Ordovician (520–450 Ma) metabasaltic arc assemblage in Hainan Island (Xu et al., 2008, 2007) is
1394 interpreted to be the northerly extension of the Kungaen Orogen that sutured Australia-Antarctica and India
1395 (e.g. Xu et al., 2014). We introduce divergent motion between Gondwana and South China at 550 Ma,
1396 coinciding with the rift-to-drift sequences of Jiang et al. (2003). This divergent motion moves South China
1397 from a position outboard of Northern India at 550 Ma to one that is slightly further east and adjacent to
1398 western Australian at 500 Ma, accounting for the arc assemblage in Hainan as well as similar faunal
1399 patterns.

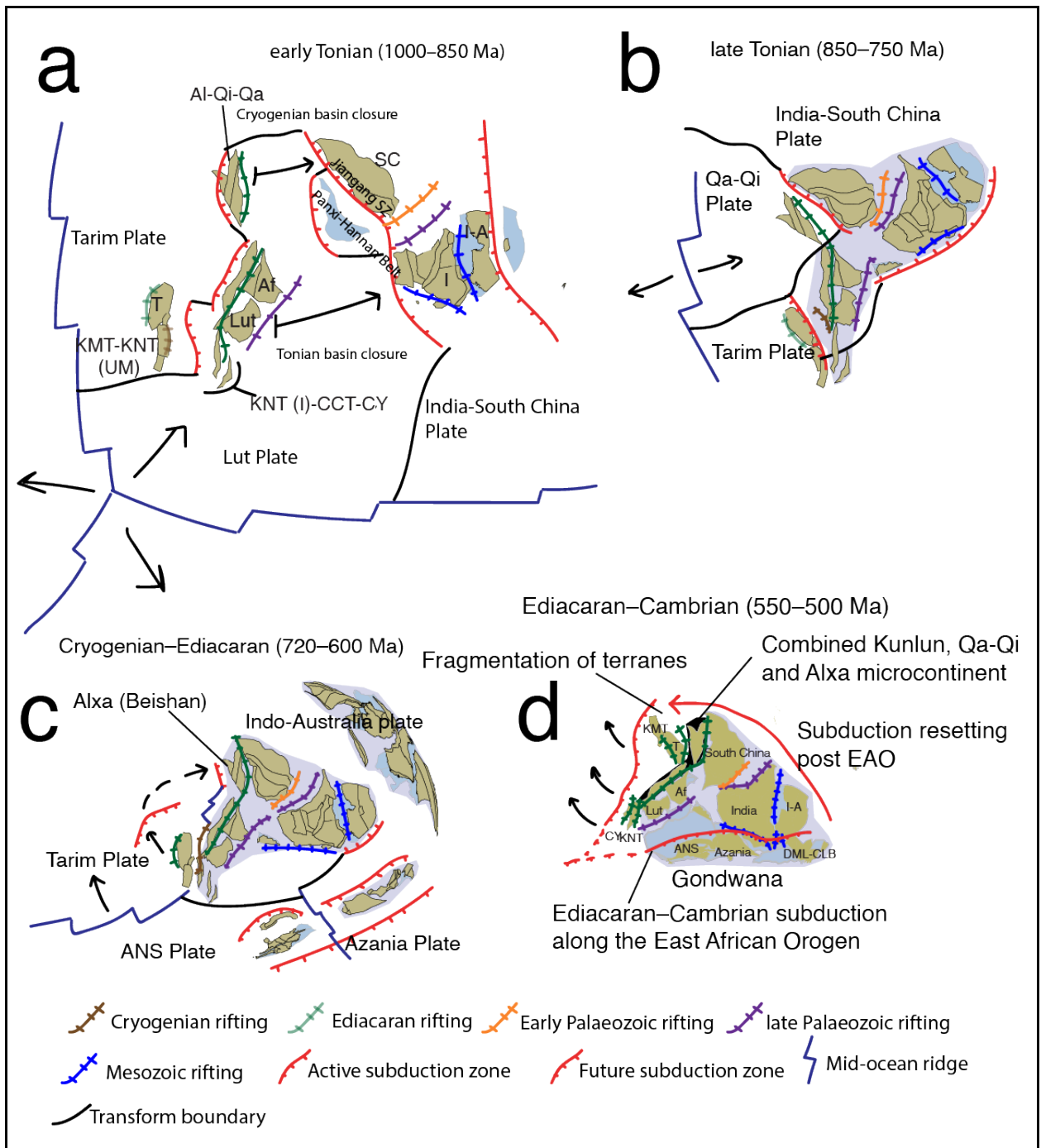


Figure 16

Schematic of our model for India-South China at key time steps, showing accretion of the Yangtze Craton and numerous smaller terranes and blocks to a large, Tonian subduction zone outboard of the north-western India and the northern margin of South China and their subsequent fragmentation and rifting off during the Ediacaran–Early Cambrian. (a) early Tonian; (b) late Tonian; (c) Cryogenian–Ediacaran, note if the model were adopted to fit the cluster of three palaeomagnetic poles from Tarim then collision would be at ca. 650 Ma, and; (d) Ediacaran–Cambrian. Af, Afghanistan; Al-Qi-Qa, Alxa, Qilian, Qaidam; ANS, Arabian Nubian Shield; CY, Chu Yili; DML-CLB, Dronning Maud Land-Coats Land Block; EAO, East African Orogen; I, India; I-A, Indo-Antarctica; KMT (I/UM), Krygyz Middle Tianshan (Issendonian/Ulutau-Moyunkum); KNT (I/UM), Krygyz North Tianshan (Issendonian/Ulutau-Moyunkum); SC, South China; T, Tarim.

1400

1401 5.4.3 ANS-Azania-TOAST

1402 We suggest that, to a first order, the central Arabian-Nubian Shield (ANS) accreted on the kernel of Azania
1403 and formed a semi-continuous archipelago outboard of the eastern margins of the Congo Craton and Sahara
1404 Metacraton (SM) (Fig. 17; Collins and Pisarevsky, 2005; Merdith et al., 2017a). Geological details and a
1405 regional plate model of the accretion of the ANS and Azania are adopted from Collins et al. (in revision),
1406 Blades et al. (2019a) and Johnson et al. (2011), though here we extend Azania to the south by attaching
1407 portions of the Tonian Aged Ocean Arc Super Terrane (TOAST—Jacobs et al. (2017, 2015)). The similarity
1408 in ages, petrology of rocks and $\delta^{18}\text{O}$ from zircons between the Dabolava Suite in Madagascar (Archibald et
1409 al., 2018) and TOAST (Jacobs et al., 2017, 2015; Wang et al., 2020) suggest a similar tectonic environment.
1410 As the southern tip of Azania is reconstructed to be adjacent to the location of the TOAST terrane in
1411 Gondwana, at the nexus between the East African Orogen and the Pinjarra/Kuunga Orogen, there is also a
1412 strong palaeogeographic argument for attaching TOAST to Azania, as their Rodinian reconstructed position
1413 requires no alteration for their position in Gondwana (Fig. 17b).

1414

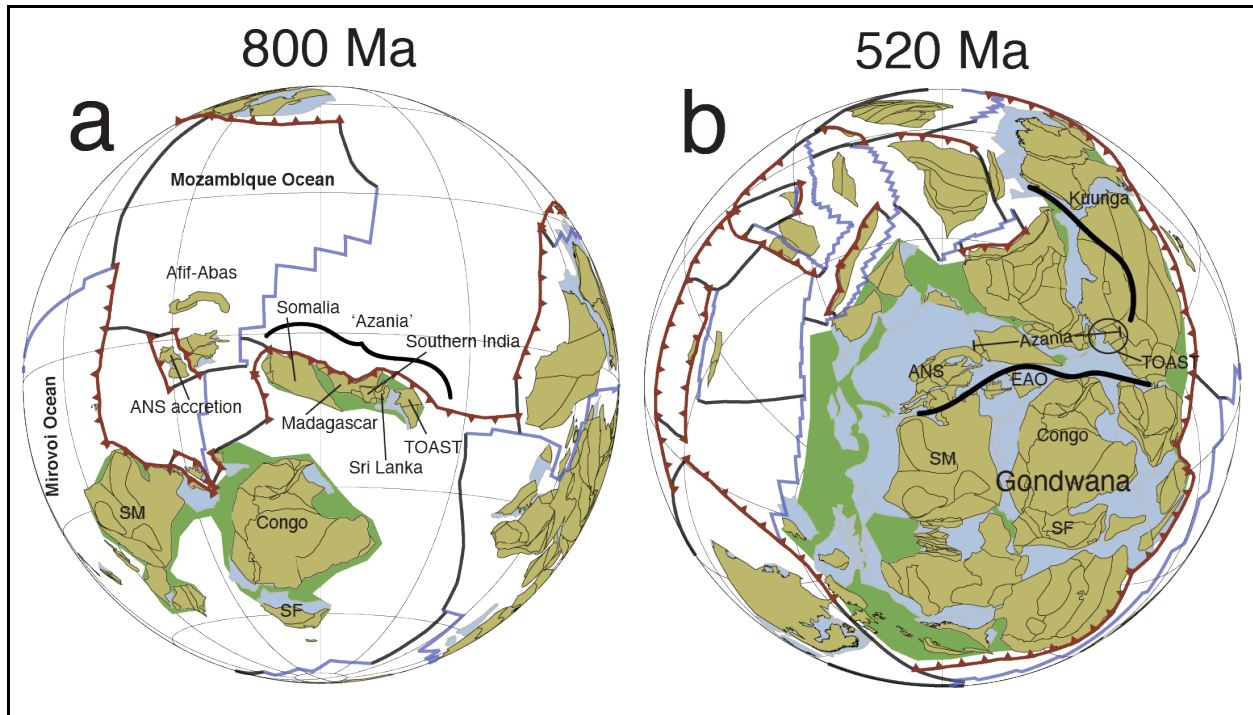


Figure 17

Amalgamation of the Arabian-Nubian Shield (ANS) after Blades et al. (2019b, 2015), Armistead et al. (2019) and Collins et al. (*submitted*) and the incorporation of the ANS, Azania and TOAST into Gondwana along the East African Orogen at: (a) 800 Ma and (b) 520 Ma. Tan polygons are areas of continental lithosphere in the Neoproterozoic that we model, blue polygons are areas of present-day continental lithosphere that are inferred to exist during the Neoproterozoic, but without having firm geological evidence or that have been affected by subsequent deformation (e.g. the distance between a present-day coastline and COB). Green polygons represent a schematic interpretation of congruent continental lithosphere, with intervening crust being subsequently deformed during future tectonic cycles. Thick black lines follow the suture of the East African Orogen and Kuunga Orogen. ANS, Arabian-Nubian Shield; EAO, East African Orogen; SF, Sao Francisco; SM, Sahara Metacraton.

1415

1416 5.4.4 Hoggar, Borborema, Avalonia and Ganderia

1417 The Hoggar Block is preserved between the Sahara Metacraton (SM) and the West African Craton (WAC)
 1418 in northwest Africa and records a long Neoproterozoic history of accretion of island arcs and continental
 1419 ribbons. The model incorporated here is based on fieldwork by Caby et al. (1989), Black et al. (1994) and
 1420 Liégeois et al. (1994) and involves three main constituents of present-day Hoggar (from west to east):
 1421 IOGU-IGU, LATEA and the Air Block (Fig. 18a, b).

1422

1423 The broad tectonic framework of the Hoggar block is an accretionary margin consisting of at least 23
 1424 individual terranes that were slowly compressed between two large tectonic units—the WAC and the SM—
 1425 as Gondwana amalgamated. The Air block, preserved in the east, is an amalgamation of three closely related
 1426 terranes: the Aouzegueur, Barghot and Assodé-Issalane terranes. The first two terranes accreted onto the

1427 margin of the SM by 650 Ma, with the Aouzegueur terrane preserving a tonalite-trondhjemite-granodiorite
1428 (TTG) suite dated at ca. 730 Ma and the Barghot terrane recording calc-alkaline granitoids from ca. 730 to
1429 660 Ma, with a post nappe pluton preserving a U-Pb zircon age of 664 ± 8 Ma, interpreted to provide a
1430 minimum age for deformation (Liégeois et al., 1994). Both these terranes were metamorphosed to
1431 greenschist or amphibolite facies and were cut by east-verging thrusts. In contrast, the Assodé-Issalane
1432 terranes exhibit younger magmatism (ca. 640–580 Ma) and amphibolite-facies metamorphism. They are
1433 thrust east over the Barghot terrane. Both Black et al. (1994) and Liégeois et al. (1994) suggest that the
1434 Aouzegueur terrane collided first with the SM, followed by the Barghot terrane, which is positioned slightly
1435 further south than the former, through an east-dipping subduction zone underneath the two terranes (Fig.
1436 18). Following collision, the Assodé-Issalane terrane (which until this time we position slightly west of the
1437 former terranes) was thrust above of the Barghot terrane in response to the closure of the ocean between
1438 the WAC and the SM. Our reconstruction implies that this motion was predominantly transpressive, along
1439 the dextral Raghane shear zone with plutons dating from ca. 630 to 580 Ma (Liégeois et al., 1994).

1440
1441 Further west from the Aïr block in central Hoggar, the LATEA terranes (Laouni, Azrou-n-Fad, Tefedest
1442 and Egéré-Aleksod) all consist of Archaean to Palaeoproterozoic basement, but preserve no
1443 Mesoproterozoic or early Neoproterozoic rocks. LATEA was a passive cratonic unit for most of the
1444 Neoproterozoic and acted as a nucleus for the accretion of juvenile terranes. The earliest Neoproterozoic
1445 activity is the accretion of the ca. 900 Ma juvenile Iskel island arc to the western margin of LATEA, with
1446 subduction inferred to be west dipping away from LATEA (Liégeois et al., 2003). The protolith of an
1447 eclogitic unit, currently preserved along the shear zone delineating the Iskel arc and LATEA, is dated to ca.
1448 870 to 850 Ma by U-Pb dating from zircons extracted from syn-to-late kinematic plutons (Caby et al.,
1449 1982). The combined In-Ouzzal and Iforas granulite units (IOGU/UGI), which are Palaeoproterozoic
1450 continental ribbons, preserve few Tonian rocks. From ca. 700 to 640 Ma magmatism is recorded throughout
1451 the entire region, suggesting that subduction occurred along both margins of the terranes (Caby, 2003) (Fig.
1452 18d, e). At 630 Ma, collision between the IOGU/UGI terranes and the LATEA block occurred, forming the
1453 combined present-day central-western Hoggar region.

1454
1455 The final tectonic events of this area involve a two-step amalgamation process of Western and Central
1456 Hoggar (i.e. IOGU/UGI and LATEA) to the Aïr Shield and SM, and the collision between this landmass
1457 (Hoggar and the SM) and the WAC, where collisional deformation is preserved in the Pharusian and
1458 Dahoymede belts (Merdith et al., 2017a) (Fig. 18f, g). Here, subduction is inferred to have occurred away
1459 from the WAC (i.e. underneath Hoggar) due to the absence of magmatic rocks preserved on the WAC.
1460 Continual dextral deformation is preserved throughout Hoggar until ca. 530 Ma, suggesting that there was

1461 still relative motion until the Cambrian (Liégeois et al., 2003; Paquette et al., 1998). The major regime of
1462 the Hoggar block between the Ediacaran and early Cambrian was transpressive, resulting in extensive
1463 faulting and upwelling of the asthenosphere; causing partial melting of lower Archaean crust in some areas
1464 (Hadj-Kaddour et al., 1998). We interpret the final amalgamation of Hoggar to occur at ca. 580 Ma, as this
1465 is the age of the syntectonic, deformed plutons found among the shear zones that bind the SM and the WAC.
1466 Here, a suite of ages include: Rb-Sr whole rock ages from dykes affected by the transpressive event yield
1467 an age of 592 ± 6 Ma (Hadj-Kaddour et al., 1998); a 583 ± 7 Ma U-Pb age on zircons extracted from the syn-
1468 to-late tectonic, elongated Imezzarene pluton (Lapique et al., 1986); a 594 ± 4 Ma and 593 ± 17 Ma U-Pb age
1469 of zircon extracted from the Ohergehem and Adaf plutons, respectively (Henry et al., 2009). Fezaa et al.
1470 (2010) identified younger (ca. 575–555 Ma) deformation in the Murzoq area of Hoggar, however, they
1471 suggested that it was unrelated to the main convergence between WAC and SM.

1472

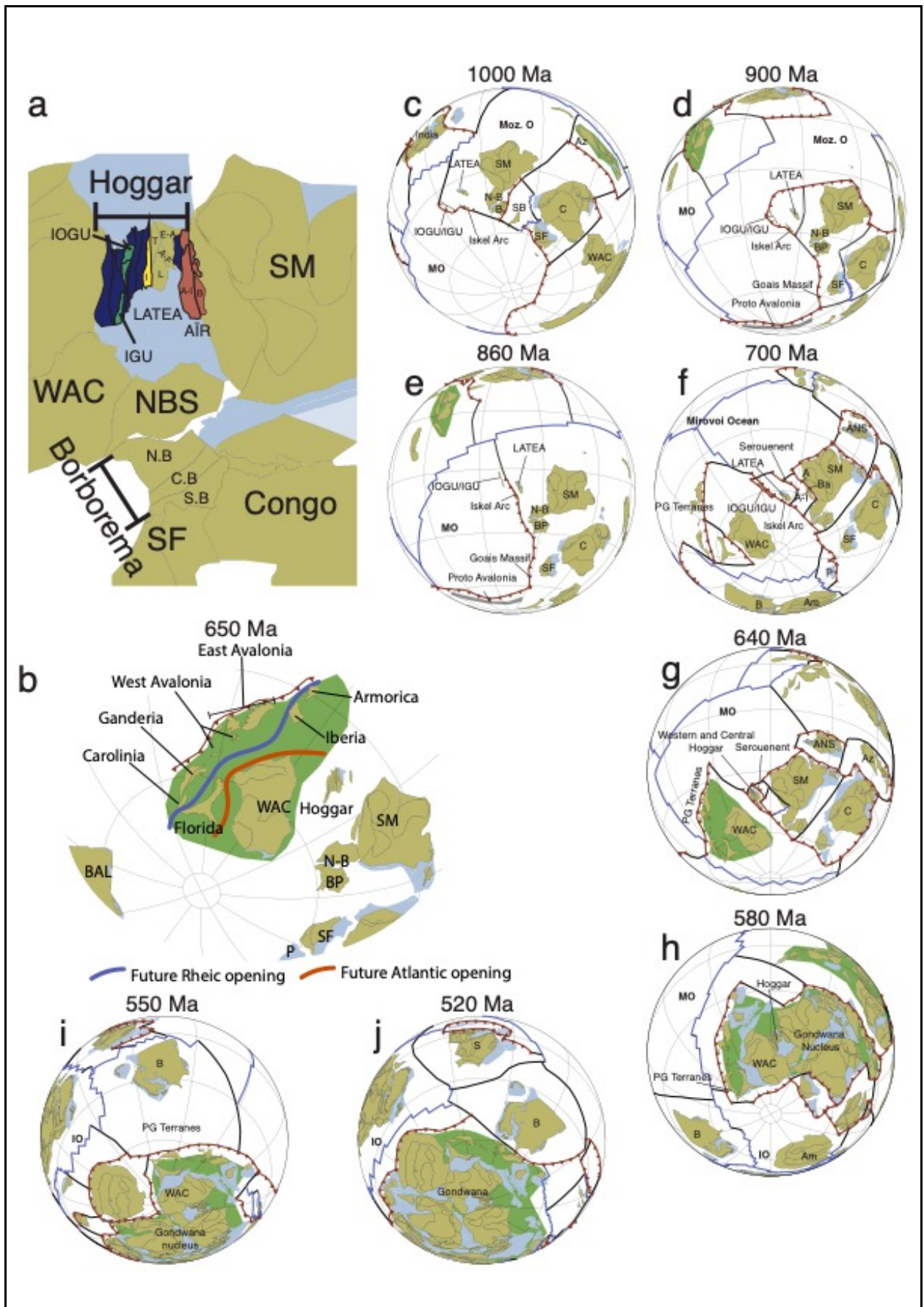


Figure 18

Amalgamation of Hoggar after Caby et al. (1989), Black et al. (1994) and Liégeois et al. (1994), Borborema and Peri-Gondwanan terranes after Nance et al. (2008) at key time slices. (a) map of key terranes in a reconstructed Gondwana (dark blue terranes are oceanic terranes); (b) map of reconstructed Peri-Gondwanan terranes at 650 Ma; (c) 1000 Ma; (d) 900 Ma; (e) 860 Ma; (f) 700 Ma; (g) 640 Ma; (h) 580 Ma; (i) 550 Ma and (j) 520 Ma. Tan polygons are areas of continental lithosphere in the Neoproterozoic that we model, blue polygons are areas of present-day continental lithosphere that are inferred to exist during the Neoproterozoic, but without having firm geological evidence or that have been affected by subsequent deformation (e.g. the distance between a present-day coastline and COB). Green polygons represent a schematic interpretation of congruent continental lithosphere, with intervening crust being subsequently deformed during future tectonic cycles A, Aouzegueur; A-I, Assodé-Issalane; Am, Amazonia; ANS, Arabian-Nubian Shield; B, Baltica; BP, Borborema Province; C, Congo; C-B, Central Borborema; IGU, Iforas granulite unit; IOGU, In Ouzzal granulite unit; IO, Iapetus Ocean; LATEA, Laouni, Azrou-n-Fad, Tefedest and Egéré-Aleksod terranes; MO, Mirovoi Ocean; Moz. O, Mozambique ocean; N-B, Niger-Benin Block; P, Paranapanema; PG, Peri-Gondwanan terranes; S-B, Southern Borborema; SF, Sao Francisco; SM, Sahara Metacraton; WAC, West African Craton.

1473

1474 The Borborema block sits between Congo-SF and the Nigeria-Benin Shield in a reconstructed Gondwana
1475 (Fig. 18a). This small block consists of Archaean–Proterozoic basement that was strongly reworked and
1476 deformed during the Gondwana amalgamation events between Africa and Amazonia (dos Santos et al.,
1477 2010). Magmatism in the Transversal Domain of Central Borborema is thought to represent a local, early
1478 Tonian orogeny called the Cariri Velhos Orogeny (da Silva Filho et al., 2002; dos Santos et al., 2010). Late
1479 Stenian rift deposits are preserved in the Cariri Velhos belt, suggesting that the Pernambuco-Alagoas
1480 domain (PEAL) (the crystalline basement of Southern Borborema) originally rifted from this margin
1481 (Guimarães et al., 2012), before the ocean inverted and closed. Our model places the Northern and
1482 Transversal Domains of Borborema fixed to the Nigeria-Benin-SM blocks, while the PEAL closed the
1483 small Stenian aged relict ocean basin as it collided with the northern and central Borborema provinces by
1484 ca. 920 Ma (Caxito et al., 2014a), forming the Cariri Velhos Orogen. An ocean basin remained on the
1485 southern margin of PEAL until the Ediacaran, as the final collision between Borborema and SF did not
1486 occur until this time forming the Sergipano belt, which preserves relict oceanic crust (e.g. Caxito et al.,
1487 2014b; Ganade de Araujo et al., 2014) (e.g. Fig. 9). To accommodate the Tonian closure, while maintaining
1488 an open ocean basin to the south of PEAL, we follow Caxito et al. (2014a, 2016) who suggested that the
1489 synchronous rifting and aulacogen formation preserved in SF (Pedrosa-Soares et al., 2001), which in our
1490 model is reconstructed to be adjacent to PEAL, are relicts of the divergent motion necessary to achieve this.

1491

1492 The Avalonian terranes, currently preserved in the east coast of modern day North American and western
1493 Europe, have a well-documented Neoproterozoic history (e.g. Murphy and Nance, 1989). The Avalonian
1494 terrane is interpreted to be underlain by ca. 1.0 Ga juvenile basement on the basis of 1.3–0.8 Ga Sm-Nd
1495 depleted mantle model ages in younger Neoproterozoic rocks (Murphy et al., 2000; Thorogood, 1990).

1496 These younger rocks consist of magmatic gneiss and plutonic complexes, along with tuffs, pelitic schists
1497 and quartzites. U-Pb ages of the complexes and tuffs range from ca. 750–650 Ma (Bevier et al., 1993; Doig
1498 et al., 1993; Keppie and Dostal, 1998; Krogh et al., 1988; O’Brien et al., 2001) and detrital zircons from
1499 the (meta-)sedimentary rocks suggest they were sourced from a juvenile arc (metapelites, Murphy, 2002)
1500 and a cratonic source (quartzite), typically inferred to be Amazonia or the WAC (Nance et al., 2008). This
1501 magmatism is followed by amphibolite–granulite metamorphism from 660–630 Ma (Keppie et al., 1998;
1502 Strachan et al., 2007). Younger magmatism (ca. 640–550 Ma) is more voluminous and includes abundant
1503 arc derived volcanic, plutonic complexes and coeval volcanic-sedimentary successions (Bevier et al., 1993;
1504 Compston et al., 2002; Doig et al., 1993; Nance et al., 2008; O’Brien et al., 2001; White et al., 2020).
1505 Subduction does not continue into the Cambrian, instead a clastic platform and transition to rift environment
1506 begins to form, culminating in the opening of the Rheic Ocean (Domeier, 2016; Nance et al., 2008; Nance
1507 and Linnemann, 2008).

1508

1509 To a first order, Ganderia and Carolina, both preserved in North America, record a similar Neoproterozoic
1510 history to Avalonia, differing predominantly in that key metamorphic and magmatic events are ca. 30–
1511 40 Ma younger than in Avalonia (Hibbard et al., 2007; Nance et al., 2008; van Staal et al., 2012). Depleted
1512 mantle model ages from Sm-Nd isotopes also hint at the presence of ca. 1.2–0.8 Ga juvenile crust in
1513 Carolina (Hibbard et al., 2007). However, the principal period of magmatism in both Ganderia and Carolina
1514 is preserved from 650 to 580 Ma and is inferred to have occurred in an ocean-arc environment (Hibbard et
1515 al., 2007). Metamorphism, up to eclogite facies, occurs at the end of this period and continues into the
1516 earliest Cambrian (580–540 Ma) (Barker et al., 1998; Shervais et al., 2003). Younger magmatism (to ca.
1517 520 Ma, White et al., 2002) linked to the rifting and opening of the Rheic Ocean, is only preserved in
1518 Ganderia (Hibbard et al., 2007). Finally, the Suwannee terrane of Florida is linked tectonically to both the
1519 West African Craton and Amazonia throughout the Neoproterozoic (Dallmeyer, 1989), lacking the
1520 Neoproterozoic arc development preserved in Avalonia, Ganderia and Carolina. Instead, 550 Ma calc-
1521 alkaline volcanic rocks are inferred to represent the remnants of a continental arc (Heatherington et al.,
1522 1996).

1523

1524 We follow the model of Nance et al. (2008) and Murphy et al. (2004) for the Neoproterozoic evolution of
1525 these terranes. An early Tonian (1–0.8 Ga) oceanic arc outboard of Baltica-Amazonia-WAC dipping under
1526 the Rodinian plate, formed the earliest portions of crust preserved in these terranes (Fig. 18c–e). The relative
1527 positioning of the terranes follows that of DOM16, with East Avalonia most easterly (Fig. 18b), then West
1528 Avalonia, and Ganderia and Carolina furthest west, with Ganderia sitting oceanward of Carolina. This
1529 arrangement follows the same logic outlined in Section 5.2.2, as by maintaining this relative positioning

1530 we avoid having to laterally re-organise the terranes during the Palaeozoic. This is slightly different from
1531 the positioning in Nance et al. (2008), who model West Avalonia more easterly (relative to a fixed WAC)
1532 than East Avalonia and invoke wrench-tectonics to laterally translate the terranes. Nonetheless, at ca. 750
1533 Ma this subduction polarity reversed and the adjacent ocean basin between WAC-Baltica began to subduct
1534 underneath Avalonia. We model Ganderia and Carolina slightly further away from the active subduction
1535 front–behind Western Avalonia, to account for their lack of Cryogenian magmatism. This arc front collided
1536 with WAC at ca. 650 Ma when the subduction ceased and reset outboard of the now amalgamated
1537 Avalonian-WAC continent as a continental arc (Fig. 18f, g). This subduction continued until the Cambrian
1538 when the area transitioned into a rift environment when the Rheic Ocean opened.

1539
1540 This last phase our model is preliminary and needs further development, though we hope that it provides a
1541 framework that can assist with testing alternative scenarios. By fitting the latitude of the ca. 520–500 Ma
1542 poles of Baltica (Section 5.2.1), subduction must consume most of the relic ocean basin immediately north
1543 of the Avalonian margin of Gondwana between 550 and 520 Ma. The magmatism in Ganderia easily
1544 accounts for this, however Baltica needs to be further east at 520 Ma, otherwise it must undergo 4000 km
1545 of dextral motion (relative to Gondwana) to allow for the initial stages of the Rheic Ocean opening at ca
1546 500 Ma (e.g. Domeier, 2016; von Raumer and Stampfli, 2008), which we suggest is not a reasonable
1547 scenario. As such, our model places a subduction zone slightly outboard of Avalonia, but acknowledge that
1548 this is a simplification that needs further refinement.

1549

1550 **6 Plate Model**

1551
1552 Having discussed the motions of the evolution of continental configurations in previous sections, here we
1553 discuss the more speculative elements of the reconstruction—the oceanic plates and plate boundaries. For
1554 further in-depth discussion of the continental portions of the model, in particular the major Gondwana
1555 forming sutures and evolution of the post-Cambrian world, we point readers to the studies that produced
1556 the base models used here (MER17, DOM16/18, YOU19, DT14). We also provide in our supplementary
1557 material the associated plate model files (SM2), as well we a tectonic summary of seafloor production and
1558 consumption rates, mid-ocean ridge length and subduction zone length (SM3).

1559

1560 **6.1 Synthetic ocean plates**

1561
1562 The construction of synthetic ocean plates is required to maintain tectonic congruency (Section 2.7) but,
1563 with few exceptions (e.g. ophiolites), there is no direct evidence of the configuration or tectonic parameters

1564 (e.g. spreading rate, asymmetry) of oceanic crust for the pre-Mesozoic due to the constant subduction of
1565 oceanic lithosphere. However, we know that oceanic crust typical of present-day (i.e. MORB) did exist in
1566 the Palaeozoic and Neoproterozoic, as evidenced by ophiolitic remains preserved in orogens (Furnes et al.,
1567 2014). We therefore use one key assumption when constructing oceanic plates: we assume that the
1568 production (rate of motion, orthogonal spreading etc.) and subduction of oceanic crust in the
1569 Neoproterozoic was fundamentally similar to the Cenozoic. We note that this may not be a valid assumption
1570 for the early Neoproterozoic, since abundant ophiolite preservation only occurs after Rodinia breakup
1571 (Stern and Miller, 2018) and pre-1 Ga ophiolites suggest thicker oceanic crust (Moores, 2002) which, along
1572 with secular changes in Earth's heat loss (Brown et al., 2020b) could have an influence on spreading and
1573 subduction dynamics. Nonetheless, we maintain that if available palaeomagnetic and geological data can
1574 be reconciled within a uniformitarian framework of oceanic crust production and destruction, then our
1575 model becomes a useful reference model for future models that explore alternative hypotheses.
1576 Measurements of seafloor production, crustal consumption, ridge length and subduction zone length are
1577 provided in the supplementary material.

1578

1579 *6.1.1 Early Tonian until Rodinia breakup (1000-750 Ma)*

1580

1581 In our model, three prominent ocean basins existed in the early Tonian: the Mirovoi Ocean (McMenamin
1582 et al., 1990; Meert and Lieberman, 2008), the Mawson Sea (Meert, 2003; Meert and Lieberman, 2008) and
1583 the Mozambique Ocean (Fig. 8) (Collins et al., 2003; Collins and Pisarevsky, 2005). These ocean basins
1584 have been defined previously in the same context as they appear in our model, however, given differences
1585 between our model and the original publications, the geographical boundaries of each ocean are slightly
1586 different.

1587

1588 We define the Mirovoi Ocean as the large ocean bordering Rodinia in its west and India-South China and
1589 the Sahara Metacraton in the north east and south east respectively. The Mirovoi is the largest and most
1590 prominent ocean basin for the Neoproterozoic in our model, existing until ca. 520 Ma with the opening of
1591 the Proto-Tethyan Ocean and Ran Sea (Fig. 9, Hartz and Torsvik, 2002). It is (conceptually) equivalent to
1592 the external Panthalassic and Pacific oceans of the Phanerozoic, as it consists almost entirely of oceanic
1593 lithosphere and is ringed by subduction for the majority of its existence. At 1000 Ma, we model a triple
1594 junction spreading ridge located roughly in the centre of the ocean basin. The triple junction provides three
1595 directions of spreading to account for convergence in three areas: (i) the closure of the ocean basin
1596 separating India-South China from Tarim, Qaidam-Qilian, Lut, Afghanistan, Kunlun and Tarim (*this study*);
1597 (ii) the Taimyr subduction zone outboard of *northern* Siberia (Metelkin et al., 2012; Vernikovskiy et al.,

1598 2004) and the Valhalla Orogen outboard of Greenland (Cawood et al., 2010), and; (iii) the Proto-Avalonian-
1599 Cadomian subduction zone outboard of Baltica and Amazonia (Murphy et al., 2000) that extends
1600 northwards to Sao Francisco and further north where it is preserved in the Iskel Island Arc of Hoggar
1601 (Liégeois et al., 2003).

1602
1603 The spreading arms of the triple junction span north, east-southeast and southwest. The northern arm
1604 separates Siberia and the India-China accretionary zone and extends partway into the Mawson Sea. The
1605 east-southeastern arm extends towards India, where we connect it via a transform fault to the mid-ocean
1606 ridge in the Mozambique Ocean. The southwestern arm intersects the Proto-Avalonian subduction zone.
1607 We model this configuration (triple junction) as being stable through the early Tonian until ca. 870–850
1608 Ma, where a plate-reorganisation event occurs. We link this organisation to a change in kinematics of
1609 Rodinia, suggested through palaeomagnetic data. At this time, palaeomagnetic data from the Baltica
1610 (Walderhaug et al., 2007) suggest that Rodinia had drifted to southerly latitudes, before returning to
1611 equatorial latitudes by ca. 750 Ma (Eyster et al., 2019). MER17 modelled significant relative dextral motion
1612 between Congo-SF-Azania and Rodinia during this time (870–750 Ma) as well, as suggested by
1613 palaeomagnetic data (Evans et al., 2016). Geological data from Congo-Azania also supports the rotation,
1614 with onset of sedimentation interpreted to be a rift event in the Damara region (Armstrong et al., 2005;
1615 McGee et al., 2012) and the onset of a massive subduction system outboard of Azania (Archibald et al.,
1616 2017; Handke et al., 1999). During this transition (850–800 Ma), we model the Mirovoi Ocean as a single
1617 spreading ridge, orientated sub-parallel to the *north*-facing arm in the original triple junction, extending
1618 northwards toward Siberia and intersecting an oceanic arc outboard of Baltica.

1619
1620 For the Tonian, until 750 Ma, the South China-India continent moved to polar latitudes on the north-eastern
1621 side of the Mirovoi Ocean basin. Comparably, Siberia started dextral motion relative to Rodinia, from a
1622 position near Australia-North China to one near Greenland (Pisarevsky et al., 2013). To account for this
1623 motion, alongside ongoing subduction in the Taimyr region of Siberia, we have extended the spreading
1624 ridge from the Mozambique Ocean into the Mirovoi Ocean (running E-W) and have a northern arm
1625 accounting for divergence between Tarim and the Taimyr subduction zone. This interpretation necessitates
1626 the presence of a triple junction, with a third ridge arm intersecting the subduction zone outboard of Baltica,
1627 similar to the configuration at the start of the Tonian.

1628
1629 The Mawson Sea is defined as the ocean basin between Australia and India-South China that closed with
1630 the amalgamation of Gondwana (Meert, 2003). In the early Tonian, this basin is large in our model,
1631 necessitated by MER17s removal of India-South China from Rodinia. The large size is because relative

1632 longitude prevents India-South China (at this point in time travelling north from the equator) from being
1633 any closer to Australia, as Azania occupied the same latitude as India and lay between India and Australia.
1634 We model a single spreading ridge in the centre of the ocean basin, accounting for the subduction on the
1635 India-South China margin as suggested in the Eastern Ghats of India and accretion of the Ruker Terrane to
1636 Indo-Antarctica (e.g. Corvino et al., 2008; Liu et al., 2017). In South China, this subduction is more sparse,
1637 but recent work has suggested that part of present-day Vietnam is associated with the southwestern Yangtze
1638 craton (Minh et al., 2020) and could record the late Tonian portion of a subduction system and be the focus
1639 of future work. At 930 Ma the spreading direction of the ridge changes, to compensate for the southerly
1640 drift of Rodinia. The change in spreading direction coincides with the docking of North China-Australia-
1641 Antarctica with Laurentia as the final amalgamation event of Rodinia (Mulder et al., 2018b). At this time
1642 we model subduction initiating outboard of Australia (against Lhasa, (e.g. Guynn et al., 2006) and into the
1643 ocean outboard of Antarctica further *south*. Preserved evidence of subduction here is sparse due to ice cover
1644 in Antarctica. However, this area of the ocean (just outboard of the western margin of the Mawson craton)
1645 is positioned at the centre of Antarctica in the nexus between the TOAST terrane and Mawson craton, so it
1646 could be possible some arcs are preserved in Antarctica. Further south, this subduction zone transitions into
1647 a transform boundary and separates relative motion between Azania-Congo and Rodinia between 930 Ma
1648 and 850 Ma. We model continual spreading in the Mawson Sea until 850 Ma, at which time the ocean basin
1649 begins to close and we do not model an active ridge. By 750 Ma the Mawson Sea is extremely narrow, with
1650 only 2500–3500 km of ocean basin separating Australia and India. A narrow ocean basin is supported
1651 geologically by the strong evidence suggesting that a large sinistral shear zone was present outboard of
1652 western Australia and Antarctica during the Cryogenian and Ediacaran, suggesting that there was close
1653 proximity without collision between Australia-Antarctica and another continent (Collins, 2003; Fitzsimons,
1654 2003; Halpin et al., 2017; Merdith et al., 2017b; Powell and Pisarevsky, 2002).

1655
1656 The Mozambique Ocean is described as the ocean that closed with the collision of India and Congo along
1657 the East African Orogen reacted to Gondwana amalgamation during the Cryogenian and Ediacaran (e.g.
1658 Collins and Pisarevsky, 2005). For the sake of continuity, we refer to this ocean as the Mozambique in the
1659 Tonian as well. A small ocean (in our model, roughly equivalent in size to the Tasman Sea between
1660 Australia and New Zealand), termed ‘Neomozambique Ocean’ also closed with the formation of the East
1661 African Orogen, however this ocean was located between ANS-Azania-TOAST and Congo (Fig. 8).

1662
1663 Geographically, the location of the Mozambique ocean is difficult to determine in the early Tonian due to
1664 overlapping latitudes between Azania and India (they are separated longitudinally by $\sim 120^\circ$ in our model).
1665 In our model there is no spreading in this ocean basin at this time, because Congo-Azania was latitudinally

1666 stable while India-South China moves towards the North Pole on a different longitude, accounted for by
1667 spreading in the Mirovoi Ocean. The spreading ridge in the Mawson Sea at ca. 900 Ma extends sufficiently
1668 south so that the ocean lithosphere generated here is subducted during closure of the Mozambique Ocean.
1669 We model active spreading in a clearly defined Mozambique Ocean beginning at 850 Ma, by which time
1670 India-South China had a similar longitude to Azania-Congo, making it easier to delineate the geographical
1671 extent of the ocean distinct from the Mawson Sea. Between 820 and 750 Ma the ocean basin closes rapidly,
1672 in order to fit palaeomagnetic constraints at 750 Ma that show India at $\sim 60^\circ\text{N}$ (Gregory et al., 2009; Torsvik
1673 et al., 2001) and Congo at 15°S (Meert et al., 1995) (placing Azania at the equator).

1674
1675 At 800 Ma, we model the birth of the Pacific/Panthalassic Ocean, here defined as the ocean basin separating
1676 Laurentia from North China, Australia and Antarctica, which most likely opened as Rodinia broke-up
1677 (although terrane migration across this ocean basin cannot be ruled out, e.g. Mulder et al. (2020)). We note
1678 here that the pre-Mesozoic Pacific Ocean is already universally referred to as the Panthalassic Ocean.
1679 Consequently, we refer to the ocean separating North China-Australia-Antarctica and Laurentia between
1680 Rodinia and Gondwana times (ca. 800–520 Ma) as the proto-Pacific Ocean, the ocean surrounding
1681 Gondwana as the Panthalassic Ocean ('Panthalassa', ca. 520–200 Ma) and the ocean that has existed from
1682 200 Ma to present-day as the Pacific Ocean, noting that all three of these oceans essentially refer to the
1683 same ocean basin (in a geographical sense) that existed between North China-Australia-Antarctica and
1684 Laurentia. From 800 to 720 Ma we have a single ridge system separating Australia-Antarctica and
1685 Laurentia. This ridge produces a highly angular divergence, with spreading rates faster towards northern
1686 Australia and Canada than in Antarctica, resulting in a wider ocean basin in the north and narrower in the
1687 south. These variable spreading rates are required fit the ca. 750 Ma palaeomagnetic data, which require
1688 Australia to be 'upright' (same orientation as present-day) and perpendicular to Laurentia (Wingate and
1689 Giddings, 2000).

1690

1691 *6.1.2 late Tonian–Cambrian (Rodinia breakup–Gondwana Assembly, 720–520 Ma)*

1692

1693 By 720 Ma, continental motions around the Mirovoi Ocean are latitudinally stable with no polar excursions
1694 thus, the simplest way to account for the necessary subduction is with a stable triple junction. At this time,
1695 we show subduction along the western margin of the Mirovoi Ocean, outboard of Siberia in the Taimyr
1696 region, as well further south outboard of the WAC and Baltica where the Avalonian and Cadomian terranes
1697 were coalescing (Murphy et al., 1999; Murphy and Nance, 1989) and along the *northern* margin of the
1698 Sahara Metacraton in the east. This latter subduction zone is speculative since there are no known rocks of
1699 this age in the Sahara Metacraton (Blades et al., submitted). The Mirovoi ocean basin does not grow

1700 appreciably during the Ediacaran due to onset of subduction around its periphery, however, at 590 Ma
1701 Baltica begins moving north, resulting in the consumption of the Mirovoi Ocean basin and necessitating a
1702 change in mid-ocean ridge configuration. At this point we model a single ridge parallel to the Gondwanan
1703 margin, from Amazonia in the west towards India in the northeast. This ridge also accommodates the final
1704 motion of India as it collides with Congo. It is difficult to identify when the Mirovoi Ocean ceased to exist,
1705 but by ca. 490 Ma, expansion in the Proto-Tethyan ocean basin outboard of northwest Gondwana (e.g. Fig.
1706 12), as well as the easterly drift of Siberia amalgamates the Siberian subduction zones outboard of North
1707 China and Chu-Yili-Tianshan, probably indicating that the majority of Mirovoi crust produced during the
1708 Cryogenian and Ediacaran has been consumed.

1709
1710 An obvious issue with this discussion on the size of the Mirovoi is the longitudinal uncertainty between the
1711 position of Congo and Laurentia during the Ediacaran. This uncertainty is because the distance between
1712 these two cratons dictates the size of the Adamastor Ocean (between Kalahari and Congo), which grew at
1713 expense of the Mirovoi Ocean. Earliest evidence of subduction in the Damara belt exists from 650 Ma, with
1714 final closure occurring at 550 Ma. A conservative convergence rate of 40–60 km/Ma (roughly equivalent
1715 to present-day Pacific convergence rates) would make the ocean basin at 4000–6000 km wide, roughly
1716 equivalent to the present-day Atlantic Ocean (this width is similar in our model to that of the Adamastor
1717 Ocean). However, faster divergence during Rodinia breakup would increase the size of this ocean basin, in
1718 turn reducing the size of the Mirovoi Ocean during the Ediacaran, similar to how the size of the modern
1719 Pacific Ocean would become smaller or larger depending on the changing size of the Atlantic Ocean.

1720
1721 The Mawson Sea remains very small in size during the Cryogenian due to the close proximity between
1722 India and Australia-Antarctica. There is no active ridge, instead a transform fault separates the two
1723 continents. There is little evidence of subduction-related magmatism on either cratonic Australia or India
1724 or this time (e.g. Halpin et al., 2017), suggesting the intervening lithosphere that eventually closed with
1725 Gondwana amalgamation could have also involved a more complex scenario of terrane accretion. The
1726 veracity of that statement is strongly dependent on the configuration and relative positioning of other
1727 terranes that are typically reconstructed to the north-western margin of Australia in the late Palaeozoic, such
1728 as Sibumasu and Indochina (Metcalf, 2011) or other terranes preserved in Antarctica that are speculated
1729 to have rifted off the Indo-Antarctica and accreted to the western margin of the Mawson Craton (Daczko et
1730 al., 2018; Mulder et al., 2019). Neither set of terranes are yet considered explicitly in our model. By 520
1731 Ma Australia-Antarctica is sutured with India, closing any remnants of the Mawson Sea.

1732

1733 Both the Mozambique and NeoMozambique oceans close orthogonally from 720 to 550 Ma due to the
1734 continual southward motion of India towards Congo-SM. We do not model an active spreading ridge during
1735 this time, as subduction is only preserved on the African side of the collision (Collins and Pisarevsky, 2005).
1736 The presence of an earlier ridge does, however, suggest that at least two ridges (in our model they are
1737 extinct) were subducted during the East African Orogeny.

1738
1739 The Proto-Pacific Ocean grows predominantly longitudinally during the Cryogenian–Cambrian. In our
1740 model, we show separation between Australia-Antarctica-North China and Laurentia using a single ridge
1741 system that propagates southwards, around *southern* Laurentia to eventually separate the Kalahari Craton
1742 and DML at ca. 700 Ma. We maintain a single ridge system until the Ediacaran, although when Kalahari
1743 begins drifting from Laurentia, we follow Merdith et al. (2017b) in inferring a ridge jump to re-align
1744 spreading between Australia and Laurentia with the incipient ridge separating Kalahari and Laurentia. This
1745 ridge jump also assists with reconciling the necessary motion of Australia to Ediacaran palaeomagnetic
1746 data, which require a $\sim 35\text{--}45^\circ$ counter-clockwise rotation from its present-day orientation (Schmidt and
1747 Williams, 2010). At 580 Ma we model a triple junction in the Proto-Pacific Ocean that coincides with the
1748 equatorial excursion of Baltica and cessation of triple junction spreading in the Mirovoi Ocean. The arms
1749 of this triple junction intersect sub-perpendicular to subduction outboard of Laurentia, a transform fault
1750 outboard of North China and another transform boundary outboard of Baltica.

1751
1752 Between 500 and 410 Ma, we refer to the ocean as the Panthalassic Ocean and for this time interval we
1753 extended the triple junction of YOU19 backwards through DOM16 and DOM18. We found at 500 Ma
1754 when Cuyania rifts off the promontory of Laurentia (Domeier, 2016), that the position of the triple junction
1755 and orientation of the ridges extended backwards from YOU19 was parallel to the direction of spreading
1756 separating Cuyania from Laurentia. While coincidental, given the arbitrary nature of pre-Mesozoic ocean
1757 plates, we find it useful to use the configuration at this time as a transition from the Proto-Pacific Ocean to
1758 the Panthalassic Ocean.

1759

1760 **7 Conclusions**

1761
1762 We present here the first continuous full-plate model from 1 Ga to present-day. The model traces the
1763 kinematic evolution of all cratonic crust and links the Neoproterozoic to the Phanerozoic, encompassing an
1764 entire supercontinent cycle, and enabling quantitative analysis of tectonic features for deep time. We present
1765 the model in a palaeomagnetic reference frame, including a new APWP for Gondwana from 540 to 320 Ma
1766 and a GAPWaP from 320 to 0 Ma. For the Neoproterozoic, the model uses a hybrid hierarchy, where

1767 relative plate motions are tied to a key plate, forming distinct nodes. This cluster-approach allows for the
1768 model to be iterated, constructed and modified in the future more easily in light of sparse palaeomagnetic
1769 data, but abundant geological data. Our revised Neoproterozoic model incorporates a late amalgamation of
1770 Rodinia with a novel configuration, in particular through the removal of India, South China and Tarim from
1771 the supercontinent. We incorporate major plate re-organisation events at ca. 850 Ma and again at ca. 750–
1772 700 Ma, corresponding to the counter-clockwise rotation of Congo-Sao Francisco-Sahara Metacraton
1773 relative to Rodinia and the initial closing of the Mozambique Ocean and coeval opening of the Proto-Pacific
1774 Ocean, respectively. Our model also includes preliminary interpretations of the Neoproterozoic history of
1775 many regional areas, such as terrane amalgamation outboard of India-South China, Hoggar and Avalonia,
1776 that then link coherently with their more established Phanerozoic histories. We reiterate that this model is
1777 a non-unique solution of global palaeogeography and tectonics for the Neoproterozoic but we hope it can
1778 provide a framework on which future studies can build upon. To facilitate this, we include in our
1779 supplementary material (SM3) the tectonic parameters of seafloor production and consumption as extracted
1780 from the model.

1781
1782 Because our model has continuous plate boundaries, it enables a range of new scientific experiments such
1783 as those seeking to link plate boundary processes to other aspects of the Earth system. This includes
1784 experiments related to the biosphere, hydrosphere and atmosphere investigating events surrounding
1785 oxygenation of Earth's atmosphere, Snowball Earth and animal radiation (e.g. (Gernon et al., 2016;
1786 Godd ris et al., 2017; He et al., 2019; Hoffman et al., 1998; Hoffman and Schrag, 2002; Lenton et al., 2016;
1787 Mills et al., 2019) and those studying the deep Earth (e.g. Heron et al., 2020). There are a number of
1788 limitations of this study, in particular, we do not address TPW in this model. Most previous studies looked
1789 at TPW purely from a palaeomagnetic framework, however the incorporation of geological data in the form
1790 of plate boundaries in this model (and others like it) open up opportunities for to analyse whole-lithospheric
1791 motion from other directions (e.g. Tetley et al., 2019).

1792

1793 **Acknowledgements**

1794
1795 The authors thank Sergei Pisarevsky for advice on palaeomagnetic data. ASM is currently supported by the
1796 Deep Energy Community of the Deep Carbon Observatory and the Richard Lounsbery Foundation. ASM,
1797 SEW, RDM and SZ were supported by Australian Research Council grant IH130200012. ASC and MLB
1798 are supported by Australian Research Council grants FT120100340 and LP160101353. MGT was
1799 supported by European Research Council Grant Agreement 617588 and Agence Nationale de la Recherche
1800 project ANR-18-ERC1-0005. JAM is supported by ARC grant FL160100168. AY and SA are supported

1801 by an Australian Government Research Training Program Scholarship. SZ was supported by Australian
1802 Research Council grant IH130200012, a University of Sydney Robinson Fellowship. SZ and RDM were
1803 supported by Alfred P. Sloan grants G-2017-9997 and G-2018-11296 through the Deep Carbon
1804 Observatory. JC and RDM were also supported by the AuScope National Collaborative Research
1805 Infrastructure System (NCRIS) program. pyGPlates and GPlates development is funded by the AuScope
1806 National Collaborative Research Infrastructure System (NCRIS) program. The authors are grateful for
1807 thorough reviews by D. J. J. van Hinsbergen, C. Scotese and B. Murphy, all of which greatly improved the
1808 focus and clarity of the manuscript.

1809

1810

1811 Table 1

Model	Time (Ma)	Scope	Reference Frame			LLSVPs	Hierarchy Structure
			Palaeomagnetic	Mantle	Details		
SET12	200–0	Global	No	Yes	TPW corrected palaeomagnetic data (200–100 Ma). Hotspot motion (100–0 Ma).	No assumption.	Branching.
DT14	410–250	Global	Yes	Yes	TPW corrected mantle reference from 410–250 Ma.	Assumes stable and long-lived.	Flat.
MUL16	230–200	Global	No	Yes	TPW corrected palaeomagnetic data (200–100 Ma). Hotspot motion (100–0 Ma).	No assumption.	Branching.
MAT16	410–0	Global	Yes	Yes	TPW corrected mantle reference from 410–0 Ma.	Assumes stable and long-lived.	Branching.
<i>DOM16</i>	500–410	Gondwana-Laurentia-Baltica	Yes	Yes	TPW corrected mantle reference from 500–410 Ma.	Assumes stable and long-lived.	Flat.
<i>MER17</i>	1000–520	Global	Yes	No		No assumption.	Nodal.
<i>DOM18</i>	500–410	Gondwana-Siberia-China	Yes	Yes	TPW corrected mantle reference from 500–410 Ma.	Assumes stable and long-lived.	Flat.
<i>YOU19</i>	410–0	Global	Yes	Yes	TPW corrected mantle reference frame from 250–0 Ma.	No assumption.	Branching.
MUL19	250–0	Global	No	Yes	Optimisation method after Tetley et al. (2019).	No assumption.	Branching.
This model	1000–0	Global	Yes	No		No assumption.	Nodal from 1000–410 Ma. Branching from 410–0 Ma.

1812

1813 **Table 2**

Key	Rockunit	OldAge	YoungAge	Glat	Glon	Plat	Plon	A95	Reference
<i>Laurentia</i>									
L1	Gunbarrel Intrusions combined	780	776	45	-110	14.6	127	3.2	Harlan et al. (2008).
L2	Uinta Formation	800	750	41	-110	0.8	161.3	4.7	Weil et al. (2006).
L3	Galeros - Carbon Canyon	764	750	35.15	-111.8	-0.5	166	9.7	Weil et al. (2004); Eyster et al. (2019).
L4	Kwagunt Formation	759	743	36.15	-112	14.2	163.8	3.5	Eyster et al. (2019).
L5	Kwagunt Formation 2	748	736	36.15	-112	18.2	166	7	Weil et al. (2004).
L6	Franklin Dykes	727	712	75	-82	8.4	163.8	2.8	Denyszyn et al. (2009).
L7	Long Range Dykes	617	613	53.5	-57.5	-19	175.3	17.4	Murthy et al. (1992); Hodych et al. (2004); Age: Kamo and Gower (1994).
L8	Skinner Cove Formation	554	548	50	-60	15	157	9	McCausland and Hodych (1998).
L9**	Andres Red Beds	423	393	41	-74	13	105	9	Miller and Kent (1988).
L10**	Wabash Reef	423	415	40.85	-85.7	17	125	5.3	McCabe et al. (1985); Torsvik et al. (1996).
L11**	Rose Hill formation	433	427	39	-79	19.1	128.3	5.8	French and Van der Voo (1979).
L12**	Ringgold Gap Sediments	456	433	34.51	-85.06	24	146.6	7.7	Morrison and Ellwood (1986).
L13**	Tablehead Group Limestone mean	470	456	48.33	-58.43	13.4	149.3	3.9	Hodych (1989); Hall and Evans (1988); Deutsch and Prasad (1987); Torsvik et al. (1996); Torsvik et al. (2012).
L14**	St George Group Limestone	485	456	48.3	-59	17.5	152.4	4.3	Deutsch and Prasad (1987).
L15**	Oneota Dolomite	485	470	43.41	-91.23	10.3	166.5	11.9	Jackson and Van der Voo (1985) .

L16**	Moore Hollow sediments	500	490	31	-99	-0.6	163	8.5	Far and Gose (1991).
L17**	Morgan Creek	497	470	30.25	-98.5	10.6	158	9.7	Loucks an Elmore (1986).
L18**	Point Peak	497	485	30.5	-99	5.2	165.8	6	Van der Voo et al. (1976).
L19**	Taum Sauk Limestone	497	485	37.55	-90.31	-3.4	175.1	7.1	Dunn and Elmore (1985).
L20**	Roywe dolomite	497	485	34.25	-97.11	12.6	157.3	4.3	Nick and Elmore (1990).
L21**	Florida Mountains	497	485	32.05	-107.37	-5.4	168.7	10	Geissman et al. (1991).
L22**	Tapeats Sandstone	520	497	36.11	-113.99	2.3	162.6	3.3	Elston and Bressler (1977).
L23**	Mount Rigaud and Chatham-Grenville	534	530	45.28	24.2	-11.9	184.5	6.2	McClausland et al. (2007).
<i>Baltica</i>									
B1	Southern Sweden Dykes	946	935	59	16	-0.9	240.7	6.7	Elming et al. (2014); Pisarevsky and Bylund (1998).
B2	Branton-Algo Anorthosite	927	905	58.5	6.5	5	249	3.9	Stearn and Piper, (1984); Age: Scherstén et al. (2000).
B3	Rogaland Igneous Complex	883	855	58.5	6	-46	238	18.1	Walderhaug et al. (2007).
B4	Hunnedalen Dykes	875	821	59	6.75	-41	222	10	Walderhaug et al. (1999).
B5	Egersund Dykes	619	613	58.5	6	-31.4	224.1	15.6	Walderhaug et al. (2007).
B6	Kurgashlya Formation	570	560	53.3	57.5	-51	135	4.9	Lubnina et al. (2014).
B7	Bakeevo Formation	570	560	54.5	58.2	-42	119	5.3	Lubnina et al. (2014).
B8	Winter coast sediments	558	552	65.5	40	-25.3	132.5	2.8	Popov et al. (2002); Age: Martin et al. (2000).
B9	Zolotitsa sediments I, Russia	560	550	65.5	40	-31.7	112.9	2.4	Popov et al. (2005).

B10	Verkhotina sediments	560	550	65.5	40	-32.2	107.1	2	Popov et al. (2005).
B11	Zolotitsa sediments II	560	550	65.5	40	-28.3	109.9	3.8	Iglesia Llanos et al. (2005).
B12	Zigan Formation	552	544	53.7	56.7	-16	138	3.7	Levashova et al. (2013).
B13	Swedish Limestone (1N)	467	458	58.3	13.9	3	35	13.4	Torsvik & Trench (1991).
B14	Swedish Limestone	480	470	58	13	30	55	9	Torsvik & Trench (1991).
B15	Swedish Limestone (1R)	480	470	59	15	18	46	5.1	Torsvik & Trench (1991).
B16	Narva Limestones	485	470	59	31	18	55	4	Khramov and Iosifidi (2009).
B17	St Petersburg Limestone	480	470	58	30	33	58	3.6	Smethurst et al., (1998).
B18+	Gotland Follingbo Limestone	430	420	57.5	18.5	21	164	6	Claesson (1979).
B19+	Dniestr Silurian Lmst.	428	416	48.6	27	14.3	169.3	7.4	Jelenska et al. (2005).
B20+	Gotland Medby Limest.	427	417	57.5	18.5	23	171	8	Claesson (1979).
B21+	Ringerike Sandst. Norway	426	410	60	10.2	19	164	6.7	Douglass. (1988).
B22+	Tiverskaya Series	419	411	48.6	27	0	149	13.3	Jelenska et al. (2015).
B23+	Ivaniev and Dniestr Sediments	419	393	48.7	26	-1	175	9.6	Lubnina et al (2007).
B24+	Devonian Seds. Podolia	416	406	48.7	26	-3.7	145.5	6.7	Smethurst and Khramov (1992).
B25+	Dniestrovskaya Series	416	407	48.6	27	2.3	158.4	7.4	Jelenska et al. (2005).
B26+	Zilair Sediments, Russia	411	375	54	59	-2	161	3.1	Danukalov et al. (1983).
B27+	Eifelian sedimentary rocks, Russia	398	392	50	5	19	173	2.9	Minibaev and Sulutdinov (1991).

B28+	Bashkirea Sediments, Russia	398	385	54	59	-7	162	4.8	Danukalov et al. (1983).
B29+	Kola Dykes, Russia	390	370	68	33	11	147.6	11.1	Veselovsky and Arzamastsev (2011).
<i>Siberia</i>									
S1	Ust-Kirba Formation	960	930	60	137.2	8.1	2.6	10.4	Popov et al. (2002).
S2	Kitoy Dykes	762	754	52	103	0.4	21.8	6.1	Pisarevsky et al. (2013).
S3	Kesyussa Formation	542	535	71	122.5	-37.6	165	5.2	Pisarevsky et al. (1997).
S4-	Moyero River sediments	459	439	68	104	-14	124	8	Gallet and pavlov (1996).
S5-	Angara River sediments*	460	450	58.5	99.8	-29.5	140.2	6.4	Pavlov et al. (2012).
S6-	Kulumbe section	466	456	68	88.8	-24.1	152.4	3.3	Pavlov et al. (2008).
S7-	Stolobovaya section	466	456	62.1	92.5	-22	158	4	Pavlov et al. (2008).
S8-	Moyero River sediments	468	458	68	104	-23	158	4	Gallet and Pavlov (1996).
S9-	Angara River sediments	473	463	58.5	99.8	-35.2	153.2	3.6	Pavlov et al. (2012).
S10-	Moyero River sediments	474	464	68	104	-30	157	4	Gallet and Pavlov (1996).
S11-	Guragir Formation	475	465	68	88.8	-30.9	152.7	3.2	Pavlov and Gallet(1998).
S12-	Angara River sediments	480	470	58.5	99.8	-36.4	158.2	6.5	Pavlov et al. (2012).
S13-	Moyero River sediments	483	473	67.5	104	-33.9	151.7	2.2	Gallet and Pavlov (1996).

S14-	Uigur and Nizhneiltyk Formations	488	478	68	88.8	-35.2	127.2	4.9	Pavlov and Gallet (1998).
S15-	Moyero River sediments	488	478	68	104	-40	138	9	Gallet and Pavlov (1996).
S16-	Kulumbinskaya Formation	505	495	68	88.8	-36.1	130.7	6	Pavlov and Gallet (1998).
S17-	Moyero River sediments	505	495	68	104	-37	138	9	Gallet and Pavlov (1996).
S18	Yunkyulyabit-Yuryakh Formation	512	502	70.9	122.6	-36.4	139.6	4.6	Pisarevsky et al. (1997).
S19-	Kulombe River section	512	502	68	88.4	-41.9	135.8	2.3	Pavlov and Gallet (1998).
S20-	Khorbusuonka Amgan and Mayan seds.	512	502	71.5	124	-43.7	140.5	2.6	Gallet et al. (2003).
S21-	Nyuya and Lena River sediments	437	427	60.6	116.3	-17.6	102	3.2	Powerman et al. (2013).
S22-	Nyuya and Lena River sediments	438	428	60.7	116.3	-18.6	101.9	4.6	Shatsillo et al. (2007).
S23-	Lena River sediments	454	444	60.5	116.4	-21	109	17.3	Torsvik et al. (1995).
S24-	Nyuya River sediments	456	446	60.6	116.3	-31.3	129.5	3.6	Powerman et al. (2013).
S25-	Kudrino section	466	456	57.7	107.99	-21.1	143.4	5	Pavlov et al. (2008).
S26-	Krivaya Luka Formation	469	459	59.7	118.1	-25.6	117.9	5.1	Iosifide et al. (1999).
S27-	Krivaya Luka Formation	469	459	59.7	118.1	-28.2	127.1	2.5	Iosifide et al. (1999).
S28-	Krivolutsky Suite	470	460	57.6	107.8	-32.6	137	8.3	Rodionov et al. (2003).
S29-	Lena River sediments	473	463	59.8	118.1	-32	139	3.1	Torsvik et al. (1995).

S30-	Lena River redbeds	475	465	60	114	-25	137	9	Rodionov et al. (1966).
S31-	Surinsk Formation	485	475	58.3	109.61	-42.2	128.1	5.8	Surkis et al. (1999).
S32-	Verkholensk Formation	506	496	58.5	109.8	-37.69	124	4.5	Rodionov et al. (1998).
S33-	Maya River sediments	515	505	60	132	-45.8	115	5	Pavlovi et al. (2008).
<i>West Australia</i>									
WA1	Browne Formation	830	730	-26	126	44.5	141.7	6.8	Pisarevsky et al. (2007).
WA2	Hussar Formation	800	730	-26	126	62.2	85.8	10.3	Pisarevsky et al. (2007).
WA3	Mundine Dykes	758	752	-23	115.8	45.3	135.4	4.1	Wingate and Giddings (2000).
<i>North Australia</i>									
NA1	Johnny's Creek Member	780	660	-24	133	15.8	83	13.5	Swanson-Hysell et al. (2012).
<i>South Australia</i>									
SA1	Angepena Formation	660	640	-32	138	47.1	176.6	5.3	Williams and Schmidt (2015).
SA2	Yaltipena Formation	650	635	-31.5	139	44.2	172.7	8.2	Sohl et al. (1999).
SA3	Elatina Formation, MEAN	645	635	-32	137.5	49.9	164.4	13.5	Embleton and Williams (1986); Schmidt et al. (1991); Schmidt and Williams (1995); Sohl et al. (1999).
SA4	Nuccaleena Formation	635	610	-31	139	32.3	170.8	2.9	Schmidt et al. (2009).
SA5	Brachina Formation	620	590	-32.2	138	46	135.4	3.3	Schmidt and Williams (2010).
SA6	Bunyeroo Formation	590	570	-31.6	138.4	18.1	196.3	8.8	Schmidt and Williams (1996).

SA7	Wonoka Formation	575	555	-31.3	138.6	5.2	210.5	4.9	Schmidt and Williams (2010).
<i>North China</i>									
NC1	Huaibei Sills 890 Ma	913	876	34	117	-52.3	149.3	3.5	Fu et al. (2015).
NC2	Wudaotang and Xinji Fm	541	521	35.6	110.5	18.5	341.9	6.5	Huang et al. (1999).
NC3	Hebei and Shandong Sediments	541	501	36	118	21.2	335.2	12.4	Zhao et al. (1992).
NC4	NE Sino-Korean Massif	541	485	35.6	110.5	26.8	334.5	8.9	Gao et al. (1983) (recalculated by Zhao et al. (1992)).
NC5-	Zhangxia and Xuzhuang Fms	510	496	35.6	110.5	37	326.7	5.5	Huang et al. (1999).
NC6-	Zhaogezhuang area carbonates	490	467	39.7	118.5	32.9	294.6	4.7	Yang et al. (2002).
NC7-	Changshan and Gushan Fms	496	485	35.6	110.5	31.7	329.6	5.4	Huang et al. (1999).
NC8-	Hebei and Shandong Sediments	499	461	36	118	28.8	310.9	12.3	Zhao et al. (1992).
NC9-	Liangjiashan and Lower Majiagou Fm	485	470	35.6	110.5	37.4	324.3	8.5	Huang et al. (1999).
NC10-	Jinghe	470	456	35.6	110.5	31.5	327.7	7	Huang et al. (1999).
NC11	Upper Majiagou Formation	470	456	35.6	110.5	27.9	310.4	9.2	Yang et al. (1996).
NC12-	Tianjinshan and Miboshan Formations	480	464	37.2	105.5	31.8	326.5	9.5	Huang et al. (1999).
<i>South China</i>									
SC1	Yanbian Dykes A	830	818	26.5	101.5	45.1	130.4	19	Niu et al. (2016).

SC2	Xiaofeng Dykes	812	792	31	111	13.5	91	10.9	Li et al. (2004).
SC3*	Yanbian Dykes B	814	798	26.5	101.5	14.1	32.5	20.4	Niu et al. (2016).
SC4	Liantuo Formation	735	705	30.8	111	9.9	160.3	4.6	Jing et al. (2015) and Evans et al. (2000), combined.
SC5	Nantuo Formation	641	631	28.5	110	7.5	161.6	5.9	Zhang et al. (2013); Zhang and Piper (1997).
SC6	Doushantuo Formation	614	590	30.8	111	25.9	185.5	6.7	Zhang et al. (2015).
SC7-	Douposi Formation (Wangcang)	510	496	32.1	106.2	-39.5	185.1	8.3	Lixin et al. (1998).
SC8-	Douposi Formation (Guangyuan)	510	496	32.4	106.3	-51.3	166	8.3	Yang et al. (2004).
SC9-	Shiqian Redbeds	440	425	27.5	108	4.9	194.7	5.6	Opdyke et al. (1987).
SC10-	Shiqian Redbeds	440	425	27.5	108	14.9	196.1	5.1	Huang et al. (2000).
SC11-	Pagoda Formation	458	445	32.4	106.3	-45.8	191.3	3.6	Han et al. (2015).
<i>Congo</i>									
C1	Luakela Volcanics A	770	757	-11.5	24.25	-40.2	122	14.1	Wingate et al. (2010).
C2	Mbozi Complex	773	713	-9.2	32.8	-46	145	6.7	Meert et al. (1995).
<i>Sao Francisco</i>									
SF1	Bahia Dykes (N+R)	928	912	-14	-39	7.3	106.4	6.2	Evans et al. (2016).
<i>Tarim</i>									
T1*	Sugetbrak Formation	635	550	40.9	79.4	19.1	149.7	9.3	Zhan et al. (2007).

T2*	Zhamoketi Andesite	621	609	41.5	87.8	-4.9	146.7	3.9	Zhao et al. (2014).
T3	Lower Sugetbrak Formation	640	615	41	79.5	-21.1	87.4	7	Wen et al. (2017).
T4*	Tereeken Cap Carbonate	640	630	41.5	87.8	27.6	140.4	9.9	Zhao et al. (2014).
T5	Qiaoenbrak Formation, Aksu	760	720	40.8	79.5	-6.3	17.5	9.1	Wen et al. (2013).
T6*	Aksu Dykes	819	795	41.15	80.1	19	128	4.5	Chen et al. (2004).
T7	Baiyisi Volcanics	770	717	41.6	86.54	-17.7	14.2	6	Huang et al. (2005).
T8-	Ordovician Limestones	485	470	41.3	83.4	-20.4	180.6	8.5	Fang et al. (1996).
T9-	Aksu-Kalpin-Bachu area sediments	455	445	40.6	78.9	-40.7	183.3	4.8	Sun and Huang (2009).
T10	Red Sandstone	433	427	40.6	79.4	12.8	159.8	7.3	Zhao et al. (2014)(2014) average of three poles from Fang et al. (1996); Li et al. (1990); Fang et al. (1998).
<i>India</i>									
I1	Malani Igneous Suite Grand Mean	770	734	26	72	69.4	75.7	6.5	Meert et al. (2013).
I2	Bhander and Rewa formations	650	530	26	78	47.3	212.7	5.8	McElhinny et al. (1978).
I3*	Jodphur Group	570	520	27	73	1	164	6.7	Davis et al. (2014).
<i>Seychelles</i>									
SE1	Mahe Dykes	753	747	-4.7	55.5	54.8	57.6	12.1	Torsvik et al. (2001).
<i>Rio de la Plata</i>									

RP1	Sierra de las Animas Complex	582	574	-34	-55.3	12.2	78.9	14.9	Rapalini et al. (2015).
RP2	Sierra de los Barrientos Redbeds	600	500	-37.8	-59	15.1	72.6	12.4	Rapalini et al. (2006).
<i>West African Craton</i>									
WAC1	Djebel Boho Volc.	547	526	30.4	-6.7	-27.3	207.1	14.9	Robert et al. (2017).
WAC2	Fajjoud and Tadoughast Volc.	572	551	30.2	-7.8	-21.9	211	15.6	Robert et al. (2017).
WAC3*	Adrar-n-takoucht Volc	577	564	30.4	-7.8	57.6	115.6	15.7	Robert et al. (2017).
<i>East Avalonia</i>									
EAV1# ₁	Treffgarne volcanics	482	472	52	-5	-56	126	5.5	Trench et al. (1992).
EAV2#	Stapeley volcanics	471	463	52.6	-3	-26.6	216.1	4.9	McCabe and Channell (1990).
EAV3#	Builth igneous and sediments	468	460	52.1	-3.3	-11	198	10	McCabe et al. (1992).
EAV4#	Tramore volcanics	461	449	52.1	-7.4	-11	198	8.5	Deutsch (1980); Trench and Torsvik (1991).
EAV5#	Borrowdale volcanics	448	438	54.4	-3.2	-8.1	186.2	6.9	Millward and Evans (2003); Channell and McCabe (1992).
EAV6# ₂	Midlands Minor Intrusives	442	432	52.5	-1.5	-52.5	181.5	10.4	Vizan et al. (2003).
EAV7# ₂	Browgill redbeds	439	433	54.3	-2.5	-13.6	133.9	12.4	Channell et al. (1993).
EAV8# ₂	Tortworth volcanics	437	431	51.7	-2.5	7	124	4.7	Torsvik et al. (1994).
EAV9# ₂	Mendips volcanics	435	429	51.2	-2.5	-13	91	8.8	Torsvik et al. (1993).

<i>Ganderia</i>									
GAN1#	Bourinot Group	510	496	46.1	-60.4	-21	160	8.1	Johnson and Van der Voo (1985).
<i>West Avalonia</i>									
WAV1#	Nahant intrusives	490	488	42.4	-70.9	-34	140	3.9	Thompson et al. (2010).
WAV2#	Dunn Point volcanics	463	457	45.8	-62.1	2	130	4.1	Johnson and Van Der Voo (1990); Hamilton and Murphy (2004).
WAV3#	Cape St. Mary sills	443	439	46.8	-54	10	140	9	Hodych and Buchan (1998).
<i>Carolinia</i>									
CAR1# ₂	Cid Formation metasediments	450	445	35	-80.2	29.6	122.1	5.1	Vick et al. (1987).
CAR2# ₂	Uwharrie and Cid Formation metaseds	450	445	35.5	-80	20	80	14.2	Noel et al. (1988).
<i>Cuyania</i>									
CUY1#	Pavon Formation sediments	458	452	-34.6	-68.6	-3.6	166.4	6.6	Rapalini and Cingolani (2004).
<p>* pole not fit by model # from compilation of Domeier (2016) + from compilation of S. Pisarevsky (<i>Pers. Comm.</i>) - from compilation of Domeier (2018) ** from compilation of Torsvik et al. (2012) 1 inclination only used 2 no upper age constraint (fits inclination data) Glat, sample site latitude; Glon, sample site longitude; Plat, pole latitude; Plon, pole longitude; A95, 95% confidence ellipse.</p>									

1814

1815

1816 References

1817

1818 Ahmad, M., Munson, T.J., 2013. Geology and mineral resources of the Northern Territory. Northern
1819 Territory Geological Survey Special Publication 5.

1820 Alessio, B.L., Blades, M.L., Murray, G., Thorpe, B., Collins, A.S., Kelsey, D.E., Foden, J., Payne, J., Al-
1821 Khirbash, S., Jourdan, F., 2018. Origin and tectonic evolution of the NE basement of Oman: a
1822 window into the Neoproterozoic accretionary growth of India? *Geol. Mag.* 155, 1150–1174.
1823 <https://doi.org/10.1017/S0016756817000061>

1824 Alexeiev, D.V., Biske, G.S., Kröner, A., Tretyakov, A.A., Kovach, V.P., Rojas-Agramonte, Y., 2020.
1825 Ediacaran, Early Ordovician and early Silurian arcs in the South Tianshan orogen of Kyrgyzstan.
1826 *J. Asian Earth Sci.* 190, 104194. <https://doi.org/10.1016/j.jseaes.2019.104194>

1827 Alexeiev, D.V., Kröner, A., Kovach, V.P., Tretyakov, A.A., Rojas-Agramonte, Y., Degtyarev, K.E.,
1828 Mikolaichuk, A.V., Wong, J., Kiselev, V.V., 2019. Evolution of Cambrian and Early Ordovician
1829 arcs in the Kyrgyz North Tianshan: Insights from U-Pb zircon ages and geochemical data.
1830 *Gondwana Res.* 66, 93–115. <https://doi.org/10.1016/j.gr.2018.09.005>

1831 Alexeiev, D.V., Ryazantsev, A.V., Kröner, A., Tretyakov, A.A., Xia, X., Liu, D.Y., 2011. Geochemical
1832 data and zircon ages for rocks in a high-pressure belt of Chu-Yili Mountains, southern
1833 Kazakhstan: Implications for the earliest stages of accretion in Kazakhstan and the Tianshan. *J.*
1834 *Asian Earth Sci.* 42, 805–820. <https://doi.org/10.1016/j.jseaes.2010.09.004>

1835 Archibald, D.B., Collins, A.S., Foden, J.D., 2017. Tonian arc magmatism in central Madagascar: the
1836 petrogenesis of the Imorona-Itsindro Suite. *The Journal of*.

1837 Archibald, D.B., Collins, A.S., Foden, J.D., Payne, J.L., Macey, P.H., Holden, P., Razakamanana, T.,
1838 2018. Stenian–Tonian arc magmatism in west–central Madagascar: the genesis of the Dabolava
1839 Suite. *J. Geol. Soc. London* 175, 111–129. <https://doi.org/10.1144/jgs2017-028>

1840 Armistead, S.E., Collins, A.S., Merdith, A.S., Payne, J.L., Cox, G.M., Foden, J.D., Razakamanana, T., De
1841 Waele, B., 2019. Evolving marginal terranes during Neoproterozoic supercontinent
1842 reorganisation: constraints from the Bemarivo Domain in northern Madagascar. *Tectonics*.
1843 <https://doi.org/10.1029/2018TC005384>

1844 Armstrong, R.A., Master, S., Robb, L.J., 2005. Geochronology of the Nchanga Granite, and constraints
1845 on the maximum age of the Katanga Supergroup, Zambian Copperbelt. *J. Afr. Earth. Sci.* 42, 32–
1846 40. <https://doi.org/10.1016/j.jafrearsci.2005.08.012>

1847 Arthaud, F., Matte, P., 1977. Late Paleozoic strike-slip faulting in southern Europe and northern Africa:
1848 Result of a right-lateral shear zone between the Appalachians and the Urals. *GSA Bulletin* 88,
1849 1305–1320. [https://doi.org/10.1130/0016-7606\(1977\)88<1305:LPSFIS>2.0.CO;2](https://doi.org/10.1130/0016-7606(1977)88<1305:LPSFIS>2.0.CO;2)

1850 Ashwal, L.D., Solanki, A.M., Pandit, M.K., Corfu, F., Hendriks, B.W.H., Burke, K., Torsvik, T.H., 2013.
1851 Geochronology and geochemistry of Neoproterozoic Mt. Abu granitoids, NW India: Regional
1852 correlation and implications for Rodinia paleogeography. *Precambrian Res.* 236, 265–281.
1853 <https://doi.org/10.1016/j.precamres.2013.07.018>

1854 Austermann, J., Ben-Avraham, Z., Bird, P., Heidbach, O., Schubert, G., Stock, J.M., 2011. Quantifying
1855 the forces needed for the rapid change of Pacific plate motion at 6Ma. *Earth Planet. Sci. Lett.* 307,
1856 289–297. <https://doi.org/10.1016/j.epsl.2011.04.043>

1857 Austermann, J., Kaye, B.T., Mitrovica, J.X., Huybers, P., 2014. A statistical analysis of the correlation
1858 between large igneous provinces and lower mantle seismic structure. *Geophys. J. Int.* 197, 1–9.
1859 <https://doi.org/10.1093/gji/ggt500>

1860 Barker, C.A., Secor, Jr., T., D., Pray, J.R., Wright, J.E., 1998. Age and Deformation of the Longtown
1861 Metagranite, South Carolina Piedmont: A Possible Constraint on the Origin of the Carolina
1862 Terrane. *J. Geol.* 106, 713–726. <https://doi.org/10.1086/516055>

1863 Bebout, G.E., 1995. The impact of subduction-zone metamorphism on mantle-ocean chemical cycling.
1864 *Chem. Geol.* 126, 191–218. [https://doi.org/10.1016/0009-2541\(95\)00118-5](https://doi.org/10.1016/0009-2541(95)00118-5)

1865 Berry, R.F., Steele, D.A., Meffre, S., 2008. Proterozoic metamorphism in Tasmania: Implications for
1866 tectonic reconstructions. *Precambrian Res.* 166, 387–396.
1867 <https://doi.org/10.1016/j.precamres.2007.05.004>

1868 Bevier, M.L., Barr, S.M., White, C.E., Macdonald, A.S., 1993. U–Pb geochronologic constraints on the
1869 volcanic evolution of the Mira (Avalon) terrane, southeastern Cape Breton Island, Nova Scotia.
1870 *Can. J. Earth Sci.* 30, 1–10. <https://doi.org/10.1139/e93-001>

1871 Black, L.P., 1997. Dating Tasmania’s oldest geological events. Australian Geological Survey
1872 Organisation.

1873 Black, R., Latouche, L., Liégeois, J.P., Caby, R., Bertrand, J.M., 1994. Pan-African displaced terranes in
1874 the Tuareg shield (central Sahara). *Geology* 22, 641–644.
1875 [https://doi.org/10.1130/0091-7613\(1994\)022<0641:PADTIT>2.3.CO;2](https://doi.org/10.1130/0091-7613(1994)022<0641:PADTIT>2.3.CO;2)

1876 Blades, M.L., Alessio, B.L., Collins, A.S., Foden, J., Payne, J.L., Glorie, S., Holden, P., Thorpe, B., Al-
1877 Khirbash, S., 2019a. Unravelling the Neoproterozoic accretionary history of Oman, using an
1878 array of isotopic systems in zircon. *J. Geol. Soc. London.* <https://doi.org/10.1144/jgs2018-125>

1879 Blades, M.L., Collins, A.S., Foden, J., Payne, J.L., Stüwe, K., Hassan, M., Abu-Alam, T., submitted. Age
1880 and Hafnium Isotope Evolution of Sudanese Butana and Chad Illuminates the Stenian to
1881 Ediacaran Evolution of the Southeast Sahara Metacraton. *Precambrian Res.*

1882 Blades, M.L., Collins, A.S., Foden, J., Payne, J.L., Xu, X., Alemu, T., Woldetinsae, G., Clark, C., Taylor,
1883 R.J.M., 2015. Age and hafnium isotopic evolution of the Didesa and Kemashi Domains, western

- 1884 Ethiopia. *Precambrian Res.* 270, 267–284. <https://doi.org/10.1016/j.precamres.2015.09.018>
- 1885 Blades, M.L., Foden, J., Collins, A.S., Alemu, T., Woldetinsae, G., 2019b. The origin of the ultramafic
1886 rocks of the Tulu Dimtu Belt, western Ethiopia--do they represent remnants of the Mozambique
1887 Ocean? *Geol. Mag.* 156, 62–82.
- 1888 Bleeker, W., 2003. The late Archean record: a puzzle in ca. 35 pieces. *Lithos* 71, 99–134.
1889 <https://doi.org/10.1016/j.lithos.2003.07.003>
- 1890 Bodorkos, S., Crowley, J.L., Claoué-Long, J.C., Anderson, J.R., Magee, C.W., 2020. Precise U–Pb
1891 baddeleyite dating of the Derim Derim Dolerite, McArthur Basin, Northern Territory: old and
1892 new SHRIMP and ID-TIMS constraints. *Aust. J. Earth Sci.* 1–15.
1893 <https://doi.org/10.1080/08120099.2020.1749929>
- 1894 Bower, D.J., Gurnis, M., Seton, M., 2013. Lower mantle structure from paleogeographically constrained
1895 dynamic Earth models. *Geochem. Geophys. Geosyst.* 14, 44–63.
1896 <https://doi.org/10.1029/2012GC004267>
- 1897 Boyden, J.A., Müller, R.D., Gurnis, M., Torsvik, T.H., Clark, J.A., Turner, M., Ivey-Law, H., Watson,
1898 R.J., Cannon, J.S., 2011. Next-generation plate tectonic reconstructions, in: Keller, G.R., Baru, C.
1899 (Eds.), *Geoinformatics: Cyberinfrastructure for the Solid Earth Sciences*. Cambridge University
1900 Press, Cambridge, pp. 95–113.
- 1901 Brenner, A.R., Fu, R.R., Evans, D.A.D., Smirnov, A.V., Trubko, R., Rose, I.R., 2020. Paleomagnetic
1902 evidence for modern-like plate motion velocities at 3.2 Ga. *Science Advances* 6, eaaz8670.
1903 <https://doi.org/10.1126/sciadv.aaz8670>
- 1904 Brown, M., Johnson, T.E., Gardiner, N.J., 2020a. Plate Tectonics and the Archean Earth. *Annu. Rev.*
1905 *Earth Planet. Sci.* 48, 291–320. <https://doi.org/10.1146/annurev-earth-081619-052705>
- 1906 Brown, M., Kirkland, C.L., Johnson, T.E., 2020b. Evolution of geodynamics since the Archean:
1907 Significant change at the dawn of the Phanerozoic. *Geology* 48, 488–492.
1908 <https://doi.org/10.1130/G47417.1>
- 1909 Brune, S., Williams, S.E., Müller, R.D., 2017. Potential links between continental rifting, CO₂ degassing
1910 and climate change through time. *Nat. Geosci.* 10, 941–946. [https://doi.org/10.1038/s41561-017-](https://doi.org/10.1038/s41561-017-0003-6)
1911 [0003-6](https://doi.org/10.1038/s41561-017-0003-6)
- 1912 Burke, K., Torsvik, T.H., 2004. Derivation of Large Igneous Provinces of the past 200 million years from
1913 long-term heterogeneities in the deep mantle. *Earth Planet. Sci. Lett.* 227, 531–538.
1914 <https://doi.org/10.1016/j.epsl.2004.09.015>
- 1915 Burrett, C., Khin Zaw, Meffre, S., Lai, C.K., Khositantont, S., Chaodumrong, P., Udchachon, M., Ekins,
1916 S., Halpin, J., 2014. The configuration of Greater Gondwana—Evidence from LA ICPMS, U–Pb
1917 geochronology of detrital zircons from the Palaeozoic and Mesozoic of Southeast Asia and China.

- 1918 Gondwana Res. 26, 31–51. <https://doi.org/10.1016/j.gr.2013.05.020>
- 1919 Burrett, C., Long, J., Stait, B., 1990. Early-Middle Palaeozoic biogeography of Asian terranes derived
1920 from Gondwana. Geological Society, London, Memoirs 12, 163–174.
1921 <https://doi.org/10.1144/GSL.MEM.1990.012.01.14>
- 1922 Caby, R., 2003. Terrane assembly and geodynamic evolution of central–western Hoggar: a synthesis. J.
1923 Afr. Earth. Sci. 37, 133–159. <https://doi.org/10.1016/j.jafrearsci.2003.05.003>
- 1924 Caby, R., Andreopoulos-Renaud, U., Gravelle, M., 1982. Cadre géologique et géochronologique U/Pb sur
1925 zircon des batholites précoces dans le segment pan-africain du Hoggar central (Algérie). Bulletin
1926 de la Société Géologique de France S7-XXIV, 677–684. <https://doi.org/10.2113/gssgfbull.S7-XXIV.4.677>
- 1927
- 1928 Caby, R., Andreopoulos-Renaud, U., Pin, C., 1989. Late Proterozoic arc–continent and continent–
1929 continent collision in the pan-African trans-Saharan belt of Mali. Can. J. Earth Sci. 26, 1136–
1930 1146. <https://doi.org/10.1139/e89-097>
- 1931 Calver, C.R., 2011. Neoproterozoic glacial deposits of Tasmania, in: Arnaud, E., Halverson, G.P.,
1932 Shields-Zhou, G. (Ed.), The Geological Record of Neoproterozoic Glaciations. Geological
1933 Society of London, pp. 649–658. <https://doi.org/10.1144/M36.64>
- 1934 Calver, C.R., Everard, J.L., Berry, R.F., Bottrill, R.S., Seymour, D.B., 2014. Proterozoic Tasmania.
1935 Geological Evolution of Tasmania: Geological Society of Australia Special Publication 24, 33–
1936 94.
- 1937 Calver, C.R., Meffre, S., Everard, J.L., 2013. Felsic Porphyry Sills in Surprise Bay Formation Near
1938 Currie, King Island, Dated at 775 Ma (LA-ICPMS, U-Pb on Zircon). Tasmanian Geological
1939 Survey.
- 1940 Cao, W., Williams, S., Flament, N., Zahirovic, S., Scotese, C., Dietmar Müller, R., 2019.
1941 Palaeolatitudinal distribution of lithologic indicators of climate in a palaeogeographic framework.
1942 Geol. Mag. 156, 331–354. <https://doi.org/10.1017/S0016756818000110>
- 1943 Cawood, P.A., Buchan, C., 2007. Linking accretionary orogenesis with supercontinent assembly. Earth-
1944 Sci. Rev. 82, 217–256. <https://doi.org/10.1016/j.earscirev.2007.03.003>
- 1945 Cawood, P.A., Hawkesworth, C.J., Dhuime, B., 2013a. The continental record and the generation of
1946 continental crust. GSA Bulletin 125, 14–32. <https://doi.org/10.1130/B30722.1>
- 1947 Cawood, P.A., Hawkesworth, C.J., Pisarevsky, S.A., Dhuime, B., Capitanio, F.A., Nebel, O., 2018a.
1948 Geological archive of the onset of plate tectonics. Philos. Trans. A Math. Phys. Eng. Sci. 376.
1949 <https://doi.org/10.1098/rsta.2017.0405>
- 1950 Cawood, P.A., Nemchin, A.A., Leverenz, A., Saeed, A., Balance, P.F., 1999. U/Pb dating of detrital
1951 zircons: Implications for the provenance record of Gondwana margin terranes. GSA Bulletin 111,

1952 1107–1119. 2.3.CO;2">[https://doi.org/10.1130/0016-7606\(1999\)111<1107:UPDODZ>2.3.CO;2](https://doi.org/10.1130/0016-7606(1999)111<1107:UPDODZ>2.3.CO;2)

1953 Cawood, P.A., Nemchin, A.A., Smith, M., Loewy, S., 2003. Source of the Dalradian Supergroup
1954 constrained by U–Pb dating of detrital zircon and implications for the East Laurentian margin. *J.*
1955 *Geol. Soc. London* 160, 231–246. <https://doi.org/10.1144/0016-764902-039>

1956 Cawood, P.A., Pisarevsky, S.A., 2006. Was Baltica right-way-up or upside-down in the Neoproterozoic?
1957 *J. Geol. Soc. London* 163, 753–759. <https://doi.org/10.1144/0016-76492005-126>

1958 Cawood, P.A., Strachan, R., Cutts, K., Kinny, P.D., Hand, M., Pisarevsky, S., 2010. Neoproterozoic
1959 orogeny along the margin of Rodinia: Valhalla orogen, North Atlantic. *Geology* 38, 99–102.
1960 <https://doi.org/10.1130/G30450.1>

1961 Cawood, P.A., Strachan, R.A., Pisarevsky, S.A., Gladkochub, D.P., Murphy, J.B., 2016. Linking
1962 collisional and accretionary orogens during Rodinia assembly and breakup: Implications for
1963 models of supercontinent cycles. *Earth Planet. Sci. Lett.* 449, 118–126.
1964 <https://doi.org/10.1016/j.epsl.2016.05.049>

1965 Cawood, P.A., Wang, W., Zhao, T., Xu, Y., Mulder, J.A., Pisarevsky, S.A., Zhang, L., Gan, C., He, H.,
1966 Liu, H., Qi, L., Wang, Y., Yao, J., Zhao, G., Zhou, M.-F., Zi, J.-W., 2020. Deconstructing South
1967 China and consequences for reconstructing Nuna and Rodinia. *Earth-Sci. Rev.* 204, 103169.
1968 <https://doi.org/10.1016/j.earscirev.2020.103169>

1969 Cawood, P.A., Wang, Y., Xu, Y., Zhao, G., 2013b. Locating South China in Rodinia and Gondwana: A
1970 fragment of greater India lithosphere? *Geology* 41, 903–906. <https://doi.org/10.1130/G34395.1>

1971 Cawood, P.A., Zhao, G., Yao, J., Wang, W., Xu, Y., Wang, Y., 2018b. Reconstructing South China in
1972 Phanerozoic and Precambrian supercontinents. *Earth-Sci. Rev.* 186, 173–194.
1973 <https://doi.org/10.1016/j.earscirev.2017.06.001>

1974 Caxito, F. de A., Uhlein, A., Dantas, E.L., 2014a. The Afeição augen-gneiss Suite and the record of the
1975 Cariris Velhos Orogeny (1000–960 Ma) within the Riacho do Pontal fold belt, NE Brazil. *J.*
1976 *South Amer. Earth Sci.* 51, 12–27. <https://doi.org/10.1016/j.jsames.2013.12.012>

1977 Caxito, F. de A., Uhlein, A., Stevenson, R., Uhlein, G.J., 2014b. Neoproterozoic oceanic crust remnants
1978 in northeast Brazil. *Geology* 42, 387–390. <https://doi.org/10.1130/G35479.1>

1979 Caxito, F.A., Uhlein, A., Dantas, E.L., Stevenson, R., Salgado, S.S., Dussin, I.A., Sial, A. da N., 2016. A
1980 complete Wilson Cycle recorded within the Riacho do Pontal Orogen, NE Brazil: Implications for
1981 the Neoproterozoic evolution of the Borborema Province at the heart of West Gondwana.
1982 *Precambrian Res.* 282, 97–120. <https://doi.org/10.1016/j.precamres.2016.07.001>

1983 Cayley, R.A., 2011. Exotic crustal block accretion to the eastern Gondwanaland margin in the Late
1984 Cambrian--Tasmania, the Selwyn Block, and implications for the Cambrian--Silurian evolution of
1985 the Ross, Delamerian, and Lachlan orogens. *Gondwana Res.* 19, 628–649.

- 1986 Channell, J.E.T., McCabe, C., 1992. Palaeomagnetic data from the Borrowdale Volcanic Group: volcano-
1987 tectonics and Late Ordovician palaeolatitudes. *J. Geol. Soc. London* 149, 881–888.
1988 <https://doi.org/10.1144/gsjgs.149.6.0881>
- 1989 Channell, J.E.T., McCabe, C., Woodcock, N.H., 1993. Palaeomagnetic study of Llandovery (Lower
1990 Silurian) red beds in north-west England. *Geophys. J. Int.* 115, 1085–1094.
- 1991 Charvet, J., Shu, L., Laurent-Charvet, S., Wang, B., Faure, M., Cluzel, D., Chen, Y., De Jong, K., 2011.
1992 Palaeozoic tectonic evolution of the Tianshan belt, NW China. *Sci. China Earth Sci.* 54, 166–184.
1993 <https://doi.org/10.1007/s11430-010-4138-1>
- 1994 Chen, Y., Xu, B., Zhan, S., Li, Y., 2004. First mid-Neoproterozoic paleomagnetic results from the Tarim
1995 Basin (NW China) and their geodynamic implications. *Precambrian Res.* 133, 271–281.
1996 <https://doi.org/10.1016/j.precamres.2004.05.002>
- 1997 Claesson, C., 1979. Early Palaeozoic geomagnetism of Gotland. *Geologiska Föreningen i Stockholm*
1998 *Förhandlingar* 101, 149–155. <https://doi.org/10.1080/11035897909452573>
- 1999 Clennett, E.J., Sigloch, K., Mihalynuk, M.G., Seton, M., Henderson, M.A., Hosseini, K.,
2000 Mohammadzaheri, A., Johnston, S.T., Müller, R.D., 2020. A Quantitative Tomotectonic Plate
2001 Reconstruction of Western North America and the Eastern Pacific Basin. *Geochem. Geophys.*
2002 *Geosyst., Geological Association of Canada Special Paper* 21, 2011–11.
2003 <https://doi.org/10.1029/2020GC009117>
- 2004 Cocks, L.R.M., Fortey, R.A., 1997. A new Hirnantia fauna from Thailand and the biogeography of the
2005 latest Ordovician of south-east Asia. *Geobios Mem. Spec.* 30, 117–126.
2006 [https://doi.org/10.1016/S0016-6995\(97\)80017-4](https://doi.org/10.1016/S0016-6995(97)80017-4)
- 2007 Cocks, L.R.M., Torsvik, T.H., 2007. Siberia, the wandering northern terrane, and its changing geography
2008 through the Palaeozoic. *Earth-Sci. Rev.* 82, 29–74.
2009 <https://doi.org/10.1016/j.earscirev.2007.02.001>
- 2010 Collins, A.S., 2006. Madagascar and the amalgamation of Central Gondwana. *Gondwana Res.* 9, 3–16.
2011 <https://doi.org/10.1016/j.gr.2005.10.001>
- 2012 Collins, A.S., 2003. Structure and age of the northern Leeuwin Complex, Western Australia: Constraints
2013 from field mapping and U–Pb isotopic analysis. *Aust. J. Earth Sci.* 50, 585–599.
2014 <https://doi.org/10.1046/j.1440-0952.2003.01014.x>
- 2015 Collins, A.S., Blades, M.L., Merdith, A.S., Foden, J.D., in revision. A late Tonian plate reorganization
2016 event revealed by a full-plate Proterozoic reconstruction. *Communications Earth and*
2017 *Environment.*
- 2018 Collins, A.S., Kröner, A., Fitzsimons, I.C.W., Razakamanana, T., 2003. Detrital footprint of the
2019 Mozambique ocean: U–Pb SHRIMP and Pb evaporation zircon geochronology of

2020 metasedimentary gneisses in eastern Madagascar. *Tectonophysics* 375, 77–99.

2021 [https://doi.org/10.1016/S0040-1951\(03\)00334-2](https://doi.org/10.1016/S0040-1951(03)00334-2)

2022 Collins, A.S., Pisarevsky, S.A., 2005. Amalgamating eastern Gondwana: The evolution of the Circum-
2023 Indian Orogens. *Earth-Sci. Rev.* 71, 229–270. <https://doi.org/10.1016/j.earscirev.2005.02.004>

2024 Collins, W.J., Belousova, E.A., Kemp, A.I.S., Murphy, J.B., 2011. Two contrasting Phanerozoic orogenic
2025 systems revealed by hafnium isotope data. *Nat. Geosci.* 4, 333–337.

2026 <https://doi.org/10.1038/ngeo1127>

2027 Colpron, M., Logan, J.M., Mortensen, J.K., 2002. U-Pb zircon age constraint for late Neoproterozoic
2028 rifting and initiation of the lower Paleozoic passive margin of western Laurentia. *Can. J. Earth*
2029 *Sci.* 39, 133–143.

2030 Compston, W., Wright, A.E., Toghil, P., 2002. Dating the Late Precambrian volcanicity of England and
2031 Wales. *J. Geol. Soc. London* 159, 323–339. <https://doi.org/10.1144/0016-764901-010>

2032 Corvino, A.F., Boger, S.D., Henjes-Kunst, F., Wilson, C.J.L., Fitzsimons, I.C.W., 2008. Superimposed
2033 tectonic events at 2450 Ma, 2100 Ma, 900 Ma and 500 Ma in the North Mawson Escarpment,
2034 Antarctic Prince Charles Mountains. *Precambrian Res.* 167, 281–302.

2035 Cox, G.M., Halverson, G.P., Denyszyn, S., Foden, J., Macdonald, F.A., 2018. Cryogenian magmatism
2036 along the north-western margin of Laurentia: Plume or rift? *Precambrian Res.* 319, 144–157.

2037 <https://doi.org/10.1016/j.precamres.2017.09.025>

2038 da Silva Filho, A.F., Guimarães, I.P., Van Schmus, W.R., 2002. Crustal Evolution of the Pernambuco-
2039 Alagoas Complex, Borborema Province, NE Brazil: Nd Isotopic Data from Neoproterozoic
2040 Granitoids. *Gondwana Res.* 5, 409–422. [https://doi.org/10.1016/S1342-937X\(05\)70732-2](https://doi.org/10.1016/S1342-937X(05)70732-2)

2041 Daczko, N.R., Halpin, J.A., Fitzsimons, I.C.W., Whittaker, J.M., 2018. A cryptic Gondwana-forming
2042 orogen located in Antarctica. *Sci. Rep.* 8, 8371. <https://doi.org/10.1038/s41598-018-26530-1>

2043 Dallmeyer, R.D., 1989. Contrasting accreted terranes in the southern Appalachian Orogen, basement
2044 beneath the Atlantic and Gulf Coastal Plains, and West African orogens. *Precambrian Res.* 42,
2045 387–409. [https://doi.org/10.1016/0301-9268\(89\)90021-1](https://doi.org/10.1016/0301-9268(89)90021-1)

2046 Dalziel, I.W., 1992. On the organization of American plates in the Neoproterozoic and the breakout of
2047 Laurentia. *GSA Today* 2.

2048 Dalziel, I.W.D., 1997. Neoproterozoic-Paleozoic geography and tectonics: Review, hypothesis,
2049 environmental speculation. *GSA Bulletin* 109, 16–42. [https://doi.org/10.1130/0016-7606\(1997\)109<0016:ONPGAT>2.3.CO;2](https://doi.org/10.1130/0016-7606(1997)109<0016:ONPGAT>2.3.CO;2)

2050

2051 Dalziel, I.W.D., 1991. Pacific margins of Laurentia and East Antarctica-Australia as a conjugate rift pair:
2052 Evidence and implications for an Eocambrian supercontinent. *Geology* 19, 598–601.

2053 Dalziel, I.W.D., Dewey, J.F., 2019. The classic Wilson cycle revisited. Geological Society, London,

2054 Special Publications 470, 19–38. <https://doi.org/10.1144/SP470.1>

2055 Danukalov, N.F., Kondruchina, L.S., Chernikov, A.P., 1983. Paleozoic paleomagnetism of the South and
2056 Central Urals. *BF AN SSSR, Ufa*.

2057 Davies, D.R., Goes, S., Sambridge, M., 2015. On the relationship between volcanic hotspot locations, the
2058 reconstructed eruption sites of large igneous provinces and deep mantle seismic structure. *Earth*
2059 *Planet. Sci. Lett.* 411, 121–130. <https://doi.org/10.1016/j.epsl.2014.11.052>

2060 Davies, R.G., Crawford, A.R., 1971. Petrography and age of the rocks of Bulland Hill, Kirana Hills,
2061 Sarghoda District, West Pakistan. *Geol. Mag.* 108, 235–246.
2062 <https://doi.org/10.1017/S001675680005158X>

2063 Davis, J.K., Meert, J.G., Pandit, M.K., 2014. Paleomagnetic analysis of the Marwar Supergroup,
2064 Rajasthan, India and proposed interbasinal correlations. *J. Asian Earth Sci.* 91, 339–351.
2065 <https://doi.org/10.1016/j.jseaes.2013.09.027>

2066 Deb, M., Thorpe, R.I., Krstic, D., Corfu, F., Davis, D.W., 2001. Zircon U–Pb and galena Pb isotope
2067 evidence for an approximate 1.0 Ga terrane constituting the western margin of the Aravalli–Delhi
2068 orogenic belt, northwestern India. *Precambrian Res.* 108, 195–213.
2069 [https://doi.org/10.1016/S0301-9268\(01\)00134-6](https://doi.org/10.1016/S0301-9268(01)00134-6)

2070 Degtyarev, K., Yakubchuk, A., Tretyakov, A., Kotov, A., Kovach, V., 2017. Precambrian geology of the
2071 Kazakh Uplands and Tien Shan: An overview. *Gondwana Res.* 47, 44–75.
2072 <https://doi.org/10.1016/j.gr.2016.12.014>

2073 Degtyarev, K.E., 2011. Tectonic evolution of Early Paleozoic island-arc systems and continental crust
2074 formation in the Caledonides of Kazakhstan and the North Tien Shan. *Geotectonics/Geotektonika*
2075 45, 23–50. <https://doi.org/10.1134/S0016852111010031>

2076 Degtyarev, K.E., Shatagin, K.N., Kotov, A.B., Sal’nikova, E.B., Luchitskaya, M.V., Tretyakov, A.A.,
2077 Yakovleva, S.Z., 2008. Late Precambrian volcanoplutonic association of the Aktau-Dzhungar
2078 massif, Central Kazakhstan: Structural position and age, in: *Doklady Earth Sciences*. Springer
2079 Nature BV, p. 879.

2080 Degtyarev, K.E., Tretyakov, A.A., Ryazantsev, A.V., Kotov, A.B., Sal’nikova, E.B., Aleksandrov, P.A.,
2081 Anisimova, I.V., 2011. Stenian granitoids of the west Kyrgyz Ridge (North Tien Shan): Position,
2082 structure, and age determination. *Dokl. Earth Sci.* 441, 1484–1488.
2083 <https://doi.org/10.1134/S1028334X11110134>

2084 Denyszyn, S.W., Halls, H.C., Davis, D.W., Evans, D.A.D., 2009. Paleomagnetism and U–Pb
2085 geochronology of Franklin dykes in High Arctic Canada and Greenland: a revised age and
2086 paleomagnetic pole constraining block rotations in the Nares Strait region. *Can. J. Earth Sci.* 46,
2087 689–705. <https://doi.org/10.1139/E09-042>

2088 Deutsch, E.R., 1980. Magnetism of the Mid-Ordovician Tramore Volcanics, SE Ireland, and the Question
2089 of a Wide Proto-Atlantic Ocean. *J. Geomagn. Geoelectr.* 32, SIII77–SIII98.
2090 https://doi.org/10.5636/jgg.32.Supplement3_SIII77

2091 Deutsch, E.R., Prasad, J.N., 1987. Ordovician paleomagnetic results from the St. George and Table Head
2092 carbonates of western Newfoundland. *Can. J. Earth Sci.* 24, 1785–1796.
2093 <https://doi.org/10.1139/e87-170>

2094 Direen, N.G., Crawford, A.J., 2003. Fossil seaward-dipping reflector sequences preserved in southeastern
2095 Australia: a 600 Ma volcanic passive margin in eastern Gondwanaland. *J. Geol. Soc. London* 160,
2096 985–990. <https://doi.org/10.1144/0016-764903-010>

2097 Doig, R., Murphy, J.B., Nance, R.D., 1993. Tectonic significance of the Late Proterozoic Economy River
2098 gneiss, Cobequid Highlands, Avalon Composite Terrane, Nova Scotia. *Can. J. Earth Sci.* 30, 474–
2099 479. <https://doi.org/10.1139/e93-035>

2100 Domeier, M., 2018. Early Paleozoic tectonics of Asia: Towards a full-plate model. *Geoscience Frontiers*
2101 9, 789–862. <https://doi.org/10.1016/j.gsf.2017.11.012>

2102 Domeier, M., 2016. A plate tectonic scenario for the Iapetus and Rheic oceans. *Gondwana Res.* 36, 275–
2103 295. <https://doi.org/10.1016/j.gr.2015.08.003>

2104 Domeier, M., Font, E., Youbi, N., Davies, J., Nemkin, S., Van der Voo, R., Perrot, M., Benabbou, M.,
2105 Boumehdi, M.A., Torsvik, T.H., 2020. On the Early Permian shape of Pangea from
2106 paleomagnetism at its core. *Gondwana Res.* <https://doi.org/10.1016/j.gr.2020.11.005>

2107 Domeier, M., Shephard, G.E., Jakob, J., Gaina, C., Doubrovine, P.V., Torsvik, T.H., 2017. Intraoceanic
2108 subduction spanned the Pacific in the Late Cretaceous-Paleocene. *Sci Adv* 3.
2109 <https://doi.org/10.1126/sciadv.aao2303>

2110 Domeier, M., Torsvik, T.H., 2017. Full-plate modelling in pre-Jurassic time. *Geol. Mag.* 1–20.
2111 <https://doi.org/10.1017/S0016756817001005>

2112 Domeier, M., Torsvik, T.H., 2014. Plate tectonics in the late Paleozoic. *Geoscience Frontiers* 5, 303–350.
2113 <https://doi.org/10.1016/j.gsf.2014.01.002>

2114 Domeier, M., Van der Voo, R., Torsvik, T.H., 2012. Paleomagnetism and Pangea: The road to
2115 reconciliation. *Tectonophysics* 514–517, 14–43. <https://doi.org/10.1016/j.tecto.2011.10.021>

2116 Dong, Y., Santosh, M., 2016. Tectonic architecture and multiple orogeny of the Qinling Orogenic Belt,
2117 Central China. *Gondwana Res.* 29, 1–40. <https://doi.org/10.1016/j.gr.2015.06.009>

2118 Dong, Y., Yang, Z., Liu, X., Zhang, X., He, D., Li, W., Zhang, F., Sun, S., Zhang, H., Zhang, G., 2014.
2119 Neoproterozoic amalgamation of the Northern Qinling terrain to the North China Craton:
2120 Constraints from geochronology and geochemistry of the Kuanping ophiolite. *Precambrian Res.*
2121 255, 77–95. <https://doi.org/10.1016/j.precamres.2014.09.008>

2122 dos Santos, E.J., Van Schmus, W.R., Kozuch, M., Neves, B.B. de B., 2010. The Cariris Velhos tectonic
2123 event in Northeast Brazil. *J. South Amer. Earth Sci.* 29, 61–76.
2124 <https://doi.org/10.1016/j.jsames.2009.07.003>

2125 Doubrovine, P.V., Steinberger, B., Torsvik, T.H., 2016. A failure to reject: Testing the correlation
2126 between large igneous provinces and deep mantle structures with EDF statistics. *Geochem.*
2127 *Geophys. Geosyst.* 17, 1130–1163.

2128 Doucet, L.S., Li, Z.-X., Gamal El Dien, H., Pourteau, A., Murphy, J.B., Collins, W.J., Mattielli, N.,
2129 Olierook, H.K.H., Spencer, C.J., Mitchell, R.N., 2020. Distinct formation history for deep-mantle
2130 domains reflected in geochemical differences. *Nat. Geosci.* 13, 511–515.
2131 <https://doi.org/10.1038/s41561-020-0599-9>

2132 Douglass, D.N., 1988. Paleomagnetism of Ringerike Old Red Sandstone and related rocks, southern
2133 Norway: implications for pre-Carboniferous separation of Baltica and British terranes.
2134 *Tectonophysics* 148, 11–27. [https://doi.org/10.1016/0040-1951\(88\)90157-6](https://doi.org/10.1016/0040-1951(88)90157-6)

2135 Dunn, W.J., Elmore, R.D., 1985. Paleomagnetic and petrographic investigation of the Taum Sauk
2136 Limestone, southeast Missouri. *J. Geophys. Res., Geodyn. Ser.* 90, 11469.
2137 <https://doi.org/10.1029/JB090iB13p11469>

2138 Dutkiewicz, A., Dietmar Müller, R., Cannon, J., Vaughan, S., Zahirovic, S., 2019. Sequestration and
2139 subduction of deep-sea carbonate in the global ocean since the Early Cretaceous. *Geology* 47, 91–
2140 94. <https://doi.org/10.1130/G45424.1>

2141 Elburg, M.A., Andersen, T., Jacobs, J., Läufer, A., Ruppel, A., Krohne, N., Damaske, D., 2015. One
2142 Hundred Fifty Million Years of Intrusive Activity in the Sør Rondane Mountains (East
2143 Antarctica): Implications for Gondwana Assembly. *J. Geol.* <https://doi.org/10.1086/684052>

2144 Elming, S.-Å., Pisarevsky, S.A., Layer, P., Bylund, G., 2014. A palaeomagnetic and ⁴⁰Ar/³⁹Ar study of
2145 mafic dykes in southern Sweden: A new Early Neoproterozoic key-pole for the Baltic Shield and
2146 implications for Sveconorwegian and Grenville loops. *Precambrian Res.* 244, 192–206.
2147 <https://doi.org/10.1016/j.precamres.2013.12.007>

2148 Elston, D.P., Bressler, S.L., 1977. Paleomagnetic poles and polarity zonation from Cambrian and
2149 Devonian strata of Arizona. *Earth Planet. Sci. Lett.* 36, 423–433. [https://doi.org/10.1016/0012-821X\(77\)90067-X](https://doi.org/10.1016/0012-821X(77)90067-X)

2150

2151 Embleton, B.J.J., Williams, G.E., 1986. Low palaeolatitude of deposition for late Precambrian periglacial
2152 varvites in South Australia: implications for palaeoclimatology. *Earth Planet. Sci. Lett.* 79, 419–
2153 430. [https://doi.org/10.1016/0012-821X\(86\)90197-4](https://doi.org/10.1016/0012-821X(86)90197-4)

2154 England, P., Molnar, P., 1990. Surface uplift, uplift of rocks, and exhumation of rocks. *Geology* 18,
2155 1173–1177. [https://doi.org/10.1130/0091-7613\(1990\)018<1173:SUUORA>2.3.CO;2](https://doi.org/10.1130/0091-7613(1990)018<1173:SUUORA>2.3.CO;2)

2156 Evans, D., 2003. True polar wander and supercontinents. *Tectonophysics*. <https://doi.org/10.1016/S0040->
2157 1951(02)00642-X

2158 Evans, D.A.D., 2013. Reconstructing pre-Pangean supercontinents. *Bull. Am. Assoc. Hist. Nurs.*

2159 Evans, D.A.D., 2009. The palaeomagnetically viable, long-lived and all-inclusive Rodinia supercontinent
2160 reconstruction. Geological Society, London, Special.

2161 Evans, D.A.D., Li, Z.X., Kirschvink, J.L., Wingate, M.T.D., 2000. A high-quality mid-Neoproterozoic
2162 paleomagnetic pole from South China, with implications for ice ages and the breakup
2163 configuration of Rodinia. *Precambrian Res.* 100, 313–334. <https://doi.org/10.1016/S0301->
2164 9268(99)00079-0

2165 Evans, D.A.D., Trindade, R.I.F., Catelani, E.L., D’Agrella-Filho, M.S., Heaman, L.M., Oliveira, E.P.,
2166 Söderlund, U., Ernst, R.E., Smirnov, A.V., Salminen, J.M., 2016. Return to Rodinia? Moderate to
2167 high palaeolatitude of the São Francisco/Congo craton at 920 Ma. Geological Society, London,
2168 Special Publications 424, 167–190. <https://doi.org/10.1144/SP424.1>

2169 Eyster, A., Weiss, B.P., Karlstrom, K., Macdonald, F.A., 2019. Paleomagnetism of the Chuar Group and
2170 evaluation of the late Tonian Laurentian apparent polar wander path with implications for the
2171 makeup and breakup of Rodinia. *GSA Bulletin*. <https://doi.org/10.1130/B32012.1>

2172 Fang, D., Wang, P., Shen, Z., Tan, X., 1998. Cenozoic paleomagnetic results and Phanerozoic apparent
2173 polar wandering path of Tarim Block. *Sci. China Ser. D Earth Sci.*

2174 Fang, D.-J., Jin, G.-H., Jiang, L.-P., Wang, P.-Y., Wang, Z.-L., 1996. Paleozoic paleomagnetic results and
2175 the tectonic significance of Tarim Plate. *Acta Geophysica Sinica* 39, 532–542.

2176 Farr, M.R., Gose, W.A., 1991. Paleomagnetism of the Cambrian Moore Hollow Group, Texas: Evidence
2177 for a primary magnetization carried by detrital magnetite. *J. Geophys. Res.* 96, 9895.
2178 <https://doi.org/10.1029/91JB00337>

2179 Fezaa, N., Liégeois, J.-P., Abdallah, N., Cherfouh, E.H., De Waele, B., Bruguier, O., Ouabadi, A., 2010.
2180 Late Ediacaran geological evolution (575–555 Ma) of the Djanet Terrane, Eastern Hoggar,
2181 Algeria, evidence for a Murzukian intracontinental episode. *Precambrian Res.* 180, 299–327.

2182 Fioretti, A.M., Black, L.P., Foden, J., Visonà, D., 2005. Grenville-age magmatism at the South Tasman
2183 Rise (Australia): A new piercing point for the reconstruction of Rodinia. *Geology* 33, 769–772.
2184 <https://doi.org/10.1130/G21671.1>

2185 Fitzsimons, I.C.W., 2003. Proterozoic basement provinces of southern and southwestern Australia, and
2186 their correlation with Antarctica. Geological Society, London, Special Publications 206, 93–130.
2187 <https://doi.org/10.1144/GSL.SP.2003.206.01.07>

2188 Flament, N., Williams, S., Müller, R.D., Gurnis, M., Bower, D.J., 2017. Origin and evolution of the deep
2189 thermochemical structure beneath Eurasia. *Nat. Commun.* 8, 14164.

2190 <https://doi.org/10.1038/ncomms14164>

2191 French, A.N., Van der Voo, R., 1979. The magnetization of the Rose Hill Formation at the classical site
2192 of Graham's Fold Test. *J. Geophys. Res.* 84, 7688–7696.
2193 <https://doi.org/10.1029/JB084iB13p07688>

2194 Fu, X., Zhang, S., Li, Haiyan, Ding, J., Li, Huaikun, Yang, T., Wu, H., Yuan, H., Lv, J., 2015. New
2195 paleomagnetic results from the Huaibei Group and Neoproterozoic mafic sills in the North China
2196 Craton and their paleogeographic implications. *Precambrian Res.* 269, 90–106.
2197 <https://doi.org/10.1016/j.precamres.2015.08.013>

2198 Furnes, H., de Wit, M., Dilek, Y., 2014. Four billion years of ophiolites reveal secular trends in oceanic
2199 crust formation. *Geoscience Frontiers* 5, 571–603. <https://doi.org/10.1016/j.gsf.2014.02.002>

2200 Gallet, Y., Pavlov, V., 1996. Magnetostratigraphy of the Moyero River Section (North-Western Siberia):
2201 Constraints On Geomagnetic Reversal Frequency During the Early Palaeozoic. *Geophys. J. Int.*
2202 125, 95–105. <https://doi.org/10.1111/j.1365-246X.1996.tb06536.x>

2203 Gallet, Y., Pavlov, V., Courtillot, V., 2003. Magnetic reversal frequency and apparent polar wander of the
2204 Siberian platform in the earliest Palaeozoic, inferred from the Khorbusuonka river section
2205 (northeastern Siberia). *Geophys. J. Int.* 154, 829–840.

2206 Ganade de Araujo, C.E., Cordani, U.G., Weinberg, R.F., Basei, M.A.S., Armstrong, R., Sato, K., 2014.
2207 Tracing Neoproterozoic subduction in the Borborema Province (NE-Brazil): Clues from U-Pb
2208 geochronology and Sr-Nd-Hf-O isotopes on granitoids and migmatites. *Lithos* 202–203, 167–
2209 189. <https://doi.org/10.1016/j.lithos.2014.05.015>

2210 Gao, J., Wang, X.-S., Klemm, R., Jiang, T., Qian, Q., Mu, L.-X., Ma, Y.-Z., 2015. Record of assembly and
2211 breakup of Rodinia in the Southwestern Altaids: Evidence from Neoproterozoic magmatism in
2212 the Chinese Western Tianshan Orogen. *J. Asian Earth Sci.* 113, 173–193.
2213 <https://doi.org/10.1016/j.jseaes.2015.02.002>

2214 Gao, R.F., Huang, H.L., Zhu, Z.W., Liu, H.S., Fan, Y.Q., Qing, X.J., 1983. The study of paleomagnetism
2215 in northeastern Sino-Korean massif during Pre-late Paleozoic. *Contr. Project of Plate Tectonics in*
2216 *North China* 1, 265–274.

2217 Garnero, E.J., Lay, T., McNamara, A., 2007. Implications of lower-mantle structural heterogeneity for the
2218 existence and nature of whole-mantle plumes. *Special Papers-Geological Society of America* 430,
2219 79.

2220 Ge, R., Zhu, W., Wilde, S.A., He, J., Cui, X., Wang, X., Bihai, Z., 2014. Neoproterozoic to Paleozoic
2221 long-lived accretionary orogeny in the northern Tarim Craton: accretionary orogeny in northern
2222 Tarim. *Tectonics* 33, 302–329. <https://doi.org/10.1002/2013TC003501>

2223 Geissman, J.W., Jackson, M., Harlan, S.S., Van Der Voo, R., 1991. Paleomagnetism of Latest Cambrian-

- 2224 Early Ordovician and Latest Cretaceous-Early Tertiary rocks of the Florida Mountains, southwest
2225 New Mexico. *J. Geophys. Res. [Solid Earth]* 96, 6053–6071.
- 2226 Gernon, T.M., Hincks, T.K., Tyrrell, T., Rohling, E.J., Palmer, M.R., 2016. Snowball Earth ocean
2227 chemistry driven by extensive ridge volcanism during Rodinia breakup. *Nat. Geosci.* 9, 242.
2228 <https://doi.org/10.1038/ngeo2632>
- 2229 Gerya, T., 2014. Precambrian geodynamics: Concepts and models. *Gondwana Res.* 25, 442–463.
2230 <https://doi.org/10.1016/j.gr.2012.11.008>
- 2231 Godd ris, Y., Le Hir, G., Macouin, M., Donnadieu, Y., Hubert-Th ou, L., Dera, G., Aretz, M., Fluteau,
2232 F., Li, Z.X., Halverson, G.P., 2017. Paleogeographic forcing of the strontium isotopic cycle in the
2233 Neoproterozoic. *Gondwana Res.* 42, 151–162. <https://doi.org/10.1016/j.gr.2016.09.013>
- 2234 Goodge, J.W., Fanning, C.M., Fisher, C.M., Vervoort, J.D., 2017. Proterozoic crustal evolution of central
2235 East Antarctica: Age and isotopic evidence from glacial igneous clasts, and links with Australia
2236 and Laurentia. *Precambrian Res.* 299, 151–176. <https://doi.org/10.1016/j.precamres.2017.07.026>
- 2237 Gordon, R.G., Cox, A., O’Hare, S., 1984. Paleomagnetic Euler poles and the apparent polar wander and
2238 absolute motion of North America since the Carboniferous. *Tectonics* 3, 499–537.
2239 <https://doi.org/10.1029/TC003i005p00499>
- 2240 Granot, R., 2016. Palaeozoic oceanic crust preserved beneath the eastern Mediterranean. *Nat. Geosci.* 9,
2241 701–705. <https://doi.org/10.1038/ngeo2784>
- 2242 Gregory, L.C., Meert, J.G., Bingen, B., Pandit, M.K., Torsvik, T.H., 2009. Paleomagnetism and
2243 geochronology of the Malani Igneous Suite, Northwest India: Implications for the configuration
2244 of Rodinia and the assembly of Gondwana. *Precambrian Res.* 170, 13–26.
2245 <https://doi.org/10.1016/j.precamres.2008.11.004>
- 2246 Guimar es, I.P., Van Schmus, W.R., de Brito Neves, B.B., Bretas Bittar, S.M., Silva Filho, A.F.,
2247 Armstrong, R., 2012. U–Pb zircon ages of orthogneisses and supracrustal rocks of the Cariris
2248 Velhos belt: Onset of Neoproterozoic rifting in the Borborema Province, NE Brazil. *Precambrian*
2249 *Res.* 192–195, 52–77. <https://doi.org/10.1016/j.precamres.2011.10.008>
- 2250 Gurnis, M., Turner, M., Zahirovic, S., DiCaprio, L., Spasojevic, S., M ller, R.D., Boyden, J., Seton, M.,
2251 Manea, V.C., Bower, D.J., 2012. Plate tectonic reconstructions with continuously closing plates.
2252 *Comput. Geosci.* 38, 35–42. <https://doi.org/10.1016/j.cageo.2011.04.014>
- 2253 Gurnis, M., Yang, T., Cannon, J., Turner, M., Williams, S., Flament, N., M ller, R.D., 2018. Global
2254 tectonic reconstructions with continuously deforming and evolving rigid plates. *Comput. Geosci.*
2255 116, 32–41. <https://doi.org/10.1016/j.cageo.2018.04.007>
- 2256 Guynn, J., Kapp, P., Gehrels, G.E., Ding, L., 2012. U–Pb geochronology of basement rocks in central
2257 Tibet and paleogeographic implications. *J. Asian Earth Sci.* 43, 23–50.

2258 <https://doi.org/10.1016/j.jseaes.2011.09.003>

2259 Guynn, J.H., Kapp, P., Pullen, A., Heizler, M., Gehrels, G., Ding, L., 2006. Tibetan basement rocks near
2260 Amdo reveal “missing” Mesozoic tectonism along the Bangong suture, central Tibet. *Geology* 34,
2261 505–508. <https://doi.org/10.1130/G22453.1>

2262 Hadj-Kaddour, Z., Liégeois, J.-P., Demaiffe, D., Caby, R., 1998. The alkaline–peralkaline granitic post-
2263 collisional Tin Zebane dyke swarm (Pan-African Tuareg shield, Algeria): prevalent mantle
2264 signature and late agpaitic differentiation. *Lithos* 45, 223–243. [https://doi.org/10.1016/S0024-](https://doi.org/10.1016/S0024-4937(98)00033-4)
2265 [4937\(98\)00033-4](https://doi.org/10.1016/S0024-4937(98)00033-4)

2266 Haldar, S.K., Deb, M., 2001. Geology and mineralization of Rajpura-Dariba lead-zinc belt, Rajasthan, in:
2267 Deb, M., Goodfellow, W.D. (Eds.), *Sediment-Hosted Lead-Zinc Deposit Modeling Program*.
2268 Delhi-Udaipur, Elsevier, New Dehli, pp. 177–187.

2269 Hall, S.A., Evans, I., 1988. Paleomagnetic study of the Ordovician Table Head Group, Port au Port
2270 Peninsula, Newfoundland. *Can. J. Earth Sci.* 25, 1407–1419. <https://doi.org/10.1139/e88-135>

2271 Halpin, J.A., Daczko, N.R., Kobler, M.E., Whittaker, J.M., 2017. Strike-slip tectonics during the
2272 Neoproterozoic–Cambrian assembly of East Gondwana: Evidence from a newly discovered
2273 microcontinent in the Indian Ocean *Gondwana Res.*

2274 Halpin, J.A., Jensen, T., McGoldrick, P., Meffre, S., Berry, R.F., Everard, J.L., Calver, C.R., Thompson,
2275 J., Goemann, K., Whittaker, J.M., 2014. Authigenic monazite and detrital zircon dating from the
2276 Proterozoic Rocky Cape Group, Tasmania: Links to the Belt-Purcell Supergroup, North America.
2277 *Precambrian Res.* 250, 50–67. <https://doi.org/10.1016/j.precamres.2014.05.025>

2278 Hamilton, M.A., Murphy, J.B., 2004. Tectonic significance of a Llanvirn age for the Dunn Point volcanic
2279 rocks, Avalon terrane, Nova Scotia, Canada: implications for the evolution of the Iapetus and
2280 Rheic Oceans. *Tectonophysics* 379, 199–209. <https://doi.org/10.1016/j.tecto.2003.11.006>

2281 Han, Z., Yang, Z., Tong, Y., Jing, X., 2015. New paleomagnetic results from Late Ordovician rocks of the
2282 Yangtze Block, South China, and their paleogeographic implications. *J. Geophys. Res. [Solid*
2283 *Earth]* 120, 4759–4772.

2284 Handke, M.J., Tucker, R.D., Ashwal, L.D., 1999. Neoproterozoic continental arc magmatism in west-
2285 central Madagascar. *Geology* 27, 351–354. [https://doi.org/10.1130/0091-](https://doi.org/10.1130/0091-7613(1999)027<0351:NCAMIW>2.3.CO;2)
2286 [7613\(1999\)027<0351:NCAMIW>2.3.CO;2](https://doi.org/10.1130/0091-7613(1999)027<0351:NCAMIW>2.3.CO;2)

2287 Hargraves, R.B., Dawson, E.M., Houten, F.B., 1987. Palaeomagnetism and age of mid-Palaeozoic ring
2288 complexes in Niger, West Africa, and tectonic implications. *Geophys. J. Int.* 90, 705–729.
2289 <https://doi.org/10.1111/j.1365-246X.1987.tb00750.x>

2290 Harlan, S.S., Geissman, J.W., Snee, L.W., 2008. Paleomagnetism of Proterozoic mafic dikes from the
2291 Tobacco Root Mountains, southwest Montana. *Precambrian Res.* 163, 239–264.

2292 <https://doi.org/10.1016/j.precamres.2007.12.002>

2293 Hartz, E.H., Torsvik, T.H., 2002. Baltica upside down: A new plate tectonic model for Rodinia and the
2294 Iapetus Ocean. *Geology* 30, 255–258. [2.0.CO;2">https://doi.org/10.1130/0091-](https://doi.org/10.1130/0091-7613(2002)030<0255:BUDANP>2.0.CO;2)
2295 [7613\(2002\)030<0255:BUDANP>2.0.CO;2](https://doi.org/10.1130/0091-7613(2002)030<0255:BUDANP>2.0.CO;2)

2296 He, T., Zhu, M., Mills, B.J.W., Wynn, P.M., Zhuravlev, A.Y., Tostevin, R., Pogge von Strandmann,
2297 P.A.E., Yang, A., Poulton, S.W., Shields, G.A., 2019. Possible links between extreme oxygen
2298 perturbations and the Cambrian radiation of animals. *Nat. Geosci.* 12, 468–474.
2299 <https://doi.org/10.1038/s41561-019-0357-z>

2300 Heatherington, A.L., Mueller, P.A., Nutman, A.P., 1996. Neoproterozoic magmatism in the Suwannee
2301 terrane: Implications for terrane correlation. *Geological Society of America Special Papers* 304,
2302 257–268.

2303 Henry, B., Liégeois, J.P., Nouar, O., Derder, M.E.M., Bayou, B., Bruguier, O., Ouabadi, A., Belhai, D.,
2304 Amenna, M., Hemmi, A., Ayache, M., 2009. Repeated granitoid intrusions during the
2305 Neoproterozoic along the western boundary of the Saharan metacraton, Eastern Hoggar, Tuareg
2306 shield, Algeria: An AMS and U–Pb zircon age study. *Tectonophysics* 474, 417–434.
2307 <https://doi.org/10.1016/j.tecto.2009.04.022>

2308 Heron, P.J., Murphy, J.B., Nance, D.R., Pysklywec, R.N., 2020. Pannotia’s mantle signature: the quest for
2309 supercontinent identification. *Geological Society, London, Special Publications* 503.
2310 <https://doi.org/10.1144/SP503-2020-7>

2311 Hibbard, J.P., van Staal, C.R., Miller, B.V., 2007. Links among Carolina, Avalonia, and Ganderia in the
2312 Appalachian peri-Gondwanan realm. *Geological Society of America Special Papers* 433, 291–
2313 311.

2314 Hochmuth, K., Gohl, K., Uenzelmann-Neben, G., 2015. Playing jigsaw with large igneous provinces—A
2315 plate tectonic reconstruction of Ontong Java Nui, West Pacific. *Geochem. Geophys. Geosyst.* 16,
2316 3789–3807.

2317 Hodych, J.P., 1989. Limestones of western Newfoundland that magnetized before Devonian folding but
2318 after Middle Ordovician lithification. *Geophys. Res. Lett.* 16, 93–96.
2319 <https://doi.org/10.1029/GL016i001p00093>

2320 Hodych, J.P., Buchan, K.L., 1998. Palaeomagnetism of the ca. 440 Ma Cape St Mary’s sills of the Avalon
2321 Peninsula of Newfoundland: implications for Iapetus Ocean closure. *Geophys. J. Int.* 135, 155–
2322 164. <https://doi.org/10.1046/j.1365-246X.1998.00263.x>

2323 Hodych, J.P., Cox, R.A., Košler, J., 2004. An equatorial Laurentia at 550 Ma confirmed by Grenvillian
2324 inherited zircons dated by LAM ICP-MS in the Skinner Cove volcanics of western
2325 Newfoundland: implications for inertial interchange true polar wander. *Precambrian Res.* 129,

2326 93–113. <https://doi.org/10.1016/j.precamres.2003.10.012>

2327 Hoffman, P.F., 1991. Did the breakout of Laurentia turn Gondwanaland inside-out? *Science* 252, 1409–
2328 1412. <https://doi.org/10.1126/science.252.5011.1409>

2329 Hoffman, P.F., Kaufman, A.J., Halverson, G.P., Schrag, D.P., 1998. A Neoproterozoic snowball earth.
2330 *Science* 281, 1342–1346. <https://doi.org/10.1126/science.281.5381.1342>

2331 Hoffman, P.F., Schrag, D.P., 2002. The snowball Earth hypothesis: testing the limits of global change.
2332 *Terra Nova* 14, 129–155. <https://doi.org/10.1046/j.1365-3121.2002.00408.x>

2333 Hofmann, M., Linnemann, U., Rai, V., Becker, S., Gärtner, A., Sagawe, A., 2011. The India and South
2334 China cratons at the margin of Rodinia—Synchronous Neoproterozoic magmatism revealed by
2335 LA-ICP-MS zircon analyses. *Lithos* 123, 176–187.

2336 Hopper, E., Fischer, K.M., Wagner, L.S., Hawman, R.B., 2017. Reconstructing the end of the
2337 Appalachian orogeny. *Geology* 45, 15–18. <https://doi.org/10.1130/G38453.1>

2338 Hounslow, M.W., Domeier, M., Biggin, A.J., 2018. Subduction flux modulates the geomagnetic polarity
2339 reversal rate. *Tectonophysics* 742–743, 34–49. <https://doi.org/10.1016/j.tecto.2018.05.018>

2340 Hu, P.-Y., Zhai, Q.-G., Wang, J., Tang, Y., Wang, H.-T., Hou, K.-J., 2018. Precambrian origin of the
2341 North Lhasa terrane, Tibetan Plateau: Constraint from early Cryogenian back-arc magmatism.
2342 *Precambrian Res.* 313, 51–67. <https://doi.org/10.1016/j.precamres.2018.05.014>

2343 Hu, X., Garzanti, E., Wang, J., Huang, W., An, W., Webb, A., 2016. The timing of India-Asia collision
2344 onset—Facts, theories, controversies. *Earth-Sci. Rev.* 160, 264–299.

2345 Huang, B., He, Z., Zong, K., Zhang, Z., 2014. Zircon U–Pb and Hf isotopic study of Neoproterozoic
2346 granitic gneisses from the Alatage area, Xinjiang: constraints on the Precambrian crustal
2347 evolution in the Central Tianshan Block. *Chin. Sci. Bull.* 59, 100–112.
2348 <https://doi.org/10.1007/s11434-013-0010-y>

2349 Huang, B., Xu, B., Zhang, C., Li, Y., Zhu, R., 2005. Paleomagnetism of the Baiyisi volcanic rocks (ca.
2350 740Ma) of Tarim, Northwest China: A continental fragment of Neoproterozoic Western
2351 Australia? *Precambrian Res.* 142, 83–92. <https://doi.org/10.1016/j.precamres.2005.09.006>

2352 Huang, B., Yang, Z., Otofujii, Y.-I., Zhu, R., 1999. Early Paleozoic paleomagnetic poles from the western
2353 part of the North China Block and their implications. *Tectonophysics* 308, 377–402.
2354 [https://doi.org/10.1016/S0040-1951\(99\)00098-0](https://doi.org/10.1016/S0040-1951(99)00098-0)

2355 Huang, B.C., Otofujii, Y., Yang, Z.Y., 1999. Paleomagnetic constraints on the tectonic relationship
2356 between the Alashan/Hexi Corridor Terrane and the North China Block. *Geophys. Res. Lett.* 26,
2357 787–790. <https://doi.org/10.1029/1999GL900097>

2358 Huang, H., Cawood, P.A., Hou, M., Xiong, F., Ni, S., 2019. Provenance of latest Mesoproterozoic to
2359 early Neoproterozoic (meta)-sedimentary rocks and implications for paleographic reconstruction

2360 of the Yili Block. *Gondwana Res.*

2361 Huang, K., Opdyke, N.D., Zhu, R., 2000. Further paleomagnetic results from the Silurian of the Yangtze
2362 Block and their implications. *Earth Planet. Sci. Lett.* 175, 191–202.
2363 [https://doi.org/10.1016/S0012-821X\(99\)00302-7](https://doi.org/10.1016/S0012-821X(99)00302-7)

2364 Huang, Z., Long, X., Kröner, A., Yuan, C., Wang, Y., Chen, B., Zhang, Y., 2015. Neoproterozoic granitic
2365 gneisses in the Chinese Central Tianshan Block: Implications for tectonic affinity and
2366 Precambrian crustal evolution. *Precambrian Res.* 269, 73–89.
2367 <https://doi.org/10.1016/j.precamres.2015.08.005>

2368 Iosifidi, A.G., Khramov, A.N., Rodionov, V.P., Pisarevskii, S.A., Popov, V.V., 1999. Geomagnetic
2369 reversals in the Early Paleozoic: 2. A nonsynchronous record of Middle Ordovician reversals in
2370 the Berezovskaya section, southern Siberian Platform. *Izv. Phys. Solid Earth* 35, 24–32.

2371 Jackson, M., Van der Voo, R., 1985. A Lower Ordovician paleomagnetic pole from the Oneota dolomite,
2372 Upper Mississippi River Valley. *J. Geophys. Res., Geol. Soc. Am.* 90, 10449.
2373 <https://doi.org/10.1029/JB090iB12p10449>

2374 Jacobs, J., Elburg, M., Läufer, A., Kleinhanns, I.C., Henjes-Kunst, F., Estrada, S., Ruppel, A.S.,
2375 Damaske, D., Montero, P., Bea, F., 2015. Two distinct Late Mesoproterozoic/Early
2376 Neoproterozoic basement provinces in central/eastern Dronning Maud Land, East Antarctica: The
2377 missing link, 15–21°E. *Precambrian Res.* 265, 249–272.
2378 <https://doi.org/10.1016/j.precamres.2015.05.003>

2379 Jacobs, J., Opås, B., Elburg, M.A., Läufer, A., Estrada, S., Ksienzyk, A.K., Damaske, D., Hofmann, M.,
2380 2017. Cryptic sub-ice geology revealed by a U-Pb zircon study of glacial till in Dronning Maud
2381 Land, East Antarctica. *Precambrian Res.* 294, 1–14.
2382 <https://doi.org/10.1016/j.precamres.2017.03.012>

2383 Jarrard, R.D., 2003. Subduction fluxes of water, carbon dioxide, chlorine, and potassium. *Geochem.*
2384 *Geophys. Geosyst., Geophys. Monogr. Ser.* 4. <https://doi.org/10.1029/2002GC000392>

2385 Jeleńska, M., Bakhmutov, V., Konstantinienko, L., 2005. Paleomagnetic and rock magnetic data from the
2386 Silurian succession of the Dniester basin, Ukraine. *Phys. Earth Planet. Inter.* 149, 307–320.
2387 <https://doi.org/10.1016/j.pepi.2004.10.005>

2388 Jeleńska, M., Kądziałko-Hofmokr, M., Bakhmutov, V., Poliachenko, I., Ziółkowski, P., 2015.
2389 Palaeomagnetic and rock magnetic study of Lower Devonian sediments from Podolia, SW
2390 Ukraine: remagnetization problems. *Geophys. J. Int.* 200, 557–573.
2391 <https://doi.org/10.1093/gji/ggu411>

2392 Jian, P., Kröner, A., Jahn, B.-M., Windley, B.F., Shi, Y., Zhang, W., Zhang, F., Miao, L., Tomurhuu, D.,
2393 Liu, D., 2014. Zircon dating of Neoproterozoic and Cambrian ophiolites in West Mongolia and

2394 implications for the timing of orogenic processes in the central part of the Central Asian Orogenic
2395 Belt. *Earth-Sci. Rev.* 133, 62–93. <https://doi.org/10.1016/j.earscirev.2014.02.006>

2396 Jiang, G., Sohl, L.E., Christie-Blick, N., 2003. Neoproterozoic stratigraphic comparison of the Lesser
2397 Himalaya (India) and Yangtze block (south China): Paleogeographic implications. *Geology* 31,
2398 917–920. <https://doi.org/10.1130/G19790.1>

2399 Jing, X.-Q., Yang, Z., Tong, Y., Han, Z., 2015. A revised paleomagnetic pole from the mid-
2400 Neoproterozoic Liantuo Formation in the Yangtze block and its paleogeographic implications.
2401 *Precambrian Res.* 268, 194–211. <https://doi.org/10.1016/j.precamres.2015.07.007>

2402 Johnson, P.R., Andresen, A., Collins, A.S., Fowler, A.R., Fritz, H., Ghebreab, W., Kusky, T., Stern, R.J.,
2403 2011. Late Cryogenian--Ediacaran history of the Arabian--Nubian Shield: a review of
2404 depositional, plutonic, structural, and tectonic events in the closing stages of the northern East
2405 African Orogen. *J. Afr. Earth. Sci.* 61, 167–232.

2406 Johnson, R.J.E., Van Der Voo, R., 1990. Pre-folding magnetization reconfirmed for the Late Ordovician-
2407 Early Silurian Dunn Point volcanics, Nova Scotia. *Tectonophysics* 178, 193–205.
2408 [https://doi.org/10.1016/0040-1951\(90\)90146-Y](https://doi.org/10.1016/0040-1951(90)90146-Y)

2409 Johnson, R.J.E., Van der Voo, R., 1985. Middle Cambrian paleomagnetism of the Avalon Terrane in
2410 Cape Breton Island, Nova Scotia. *Tectonics* 4, 629–651.
2411 <https://doi.org/10.1029/TC004i007p00629>

2412 Just, J., Schulz, B., de Wall, H., Jourdan, F., Pandit, M.K., 2011. Monazite CHIME/EPMA dating of
2413 Erinpura granitoid deformation: Implications for Neoproterozoic tectono-thermal evolution of
2414 NW India. *Gondwana Res.* 19, 402–412. <https://doi.org/10.1016/j.gr.2010.08.002>

2415 Kamo, S.L., Gower, C.F., 1994. Note: U-Pb baddeleyite dating clarifies age of characteristic
2416 paleomagnetic remanence of Long Range dykes, southeastern Labrador.

2417 Karlsen, K.S., Conrad, C.P., Magni, V., 2019. Deep Water Cycling and Sea Level Change Since the
2418 Breakup of Pangea. *Geochem. Geophys. Geosyst.* 20, 2919–2935.
2419 <https://doi.org/10.1029/2019GC008232>

2420 Keppie, J.D., Davis, D.W., Krogh, T.E., 1998. U-Pb geochronological constraints on Precambrian
2421 stratified units in the Avalon Composite Terrane of Nova Scotia, Canada: tectonic implications.
2422 *Can. J. Earth Sci.* 35, 222–236. <https://doi.org/10.1139/e97-109>

2423 Keppie, J.D., Dostal, J., 1998. Birth of the Avalon arc in Nova Scotia, Canada: geochemical evidence for
2424 700--630 Ma back-arc rift volcanism off Gondwana. *Geol. Mag.* 135, 171–181.

2425 Khramov, A.N., Iosifidi, A.G., 2009. Paleomagnetism of the Lower Ordovician and Cambrian
2426 sedimentary rocks in the section of the Narva river right bank: For the construction of the Baltic
2427 kinematic model in the Early Paleozoic. *Izv. Phys. Solid Earth* 45, 465–481.

2428 Kirschvink, J.L., Ripperdan, R.L., Evans, D.A., 1997. Evidence for a Large-Scale Reorganization of Early
2429 Cambrian Continental Masses by Inertial Interchange True Polar Wander. *Science* 277, 541–545.
2430 <https://doi.org/10.1126/science.277.5325.541>

2431 Knesel, K.M., Cohen, B.E., Vasconcelos, P.M., Thiede, D.S., 2008. Rapid change in drift of the
2432 Australian plate records collision with Ontong Java plateau. *Nature* 454, 754–757.
2433 <https://doi.org/10.1038/nature07138>

2434 Konstantinovskaya, E.A., 2002. The mechanism of continental crust accretion: an example of Western
2435 Kamchatka. *Geotectonics/Geotektonika* 36, 393–411.

2436 Krogh, T.E., Strong, D.F., O'Brien, S.J., Papezik, V.S., 1988. Precise U–Pb zircon dates from the Avalon
2437 Terrane in Newfoundland. *Can. J. Earth Sci.* 25, 442–453. <https://doi.org/10.1139/e88-045>

2438 Kröner, A., Alexeiev, D.V., Hegner, E., Rojas-Agramonte, Y., Corsini, M., Chao, Y., Wong, J., Windley,
2439 B.F., Liu, D., Tretyakov, A.A., 2012. Zircon and muscovite ages, geochemistry, and Nd–Hf
2440 isotopes for the Aktyuz metamorphic terrane: Evidence for an Early Ordovician collisional belt in
2441 the northern Tianshan of Kyrgyzstan. *Gondwana Res.* 21, 901–927.
2442 <https://doi.org/10.1016/j.gr.2011.05.010>

2443 Kroner, A., Windley, B.F., Badarch, G., Tomurtogoo, O., Hegner, E., Jahn, B.M., Gruschka, S., Khain,
2444 E.V., Demoux, A., Wingate, M.T.D., 2007. Accretionary growth and crust formation in the
2445 Central Asian Orogenic Belt and comparison with the Arabian-Nubian shield. *Memoirs-*
2446 *Geological Society of America* 200, 181.

2447 Lapique, F., Bertrand, J.M., Meriem, D., 1986. A major Pan-African crustal decoupling zone in the
2448 Timgaouine area (Western Hoggar, Algeria). *Journal of African Earth Sciences* (1983).
2449 [https://doi.org/10.1016/0899-5362\(86\)90028-x](https://doi.org/10.1016/0899-5362(86)90028-x)

2450 Lenton, T.M., Dahl, T.W., Daines, S.J., Mills, B.J.W., Ozaki, K., Saltzman, M.R., Porada, P., 2016.
2451 Earliest land plants created modern levels of atmospheric oxygen. *Proc. Natl. Acad. Sci. U. S. A.*
2452 113, 9704–9709. <https://doi.org/10.1073/pnas.1604787113>

2453 Levashova, N.M., Bazhenov, M.L., Meert, J.G., Kuznetsov, N.B., Golovanova, I.V., Danukalov, K.N.,
2454 Fedorova, N.M., 2013. Paleogeography of Baltica in the Ediacaran: Paleomagnetic and
2455 geochronological data from the clastic Zigan Formation, South Urals. *Precambrian Res.* 236, 16–
2456 30. <https://doi.org/10.1016/j.precamres.2013.06.006>

2457 Li, M., McNamara, A.K., 2013. The difficulty for subducted oceanic crust to accumulate at the Earth's
2458 core-mantle boundary. *J. Geophys. Res. [Solid Earth]* 118, 1807–1816.

2459 Li, Yianping, McWilliams, M., Sharps, R., Cox, A., Li, Yongan, Li, Q., Gao, Z., Zhang, Z., Zhai, Y.,
2460 1990. A Devonian paleomagnetic pole from red beds of the Tarim Block, China. *J. Geophys.*
2461 *Res., Geodyn. Ser.* 95, 19185. <https://doi.org/10.1029/JB095iB12p19185>

- 2462 Li, Z., Ding, L., Lippert, P.C., Song, P., Yue, Y., van Hinsbergen, D.J.J., 2016. Paleomagnetic constraints
2463 on the Mesozoic drift of the Lhasa terrane (Tibet) from Gondwana to Eurasia. *Geology* 44, 727–
2464 730. <https://doi.org/10.1130/G38030.1>
- 2465 Li, Z., Ding, L., Song, P., Fu, J., Yue, Y., 2017. Paleomagnetic constraints on the paleolatitude of the
2466 Lhasa block during the Early Cretaceous: implications for the onset of India--Asia collision and
2467 latitudinal shortening estimates across Tibet and stable Asia. *Gondwana Res.* 41, 352–372.
- 2468 Li, Z.X., Bogdanova, S.V., Collins, A.S., Davidson, A., De Waele, B., Ernst, R.E., Fitzsimons, I.C.W.,
2469 Fuck, R.A., Gladkochub, D.P., Jacobs, J., Karlstrom, K.E., Lu, S., Natapov, L.M., Pease, V.,
2470 Pisarevsky, S.A., Thrane, K., Vernikovsky, V., 2008. Assembly, configuration, and break-up
2471 history of Rodinia: A synthesis. *Precambrian Res.* 160, 179–210.
2472 <https://doi.org/10.1016/j.precamres.2007.04.021>
- 2473 Li, Z.-X., Evans, D.A.D., Halverson, G.P., 2013. Neoproterozoic glaciations in a revised global
2474 palaeogeography from the breakup of Rodinia to the assembly of Gondwanaland. *Sediment.*
2475 *Geol.* 294, 219–232. <https://doi.org/10.1016/j.sedgeo.2013.05.016>
- 2476 Li, Z.X., Evans, D.A.D., Zhang, S., 2004. A 90° spin on Rodinia: possible causal links between the
2477 Neoproterozoic supercontinent, superplume, true polar wander and low-latitude glaciation. *Earth*
2478 *Planet. Sci. Lett.* 220, 409–421. [https://doi.org/10.1016/S0012-821X\(04\)00064-0](https://doi.org/10.1016/S0012-821X(04)00064-0)
- 2479 Li, Z.X., Mitchell, R.N., Spencer, C.J., Ernst, R., Pisarevsky, S., Kirscher, U., Murphy, J.B., 2019.
2480 Decoding Earth's rhythms: modulation of supercontinent cycles by longer superocean episodes.
2481 *Precambrian Res.* 323, 1–5.
- 2482 Li, Z.-X., Zhang, L., Powell, C.M., 1995. South China in Rodinia: Part of the missing link between
2483 Australia–East Antarctica and Laurentia? *Geology* 23, 407–410.
2484 [2.3.CO;2">https://doi.org/10.1130/0091-7613\(1995\)023<0407:SCIRPO>2.3.CO;2](https://doi.org/10.1130/0091-7613(1995)023<0407:SCIRPO>2.3.CO;2)
- 2485 Li, Z.-X., Zhong, S., 2009. Supercontinent–superplume coupling, true polar wander and plume mobility:
2486 Plate dominance in whole-mantle tectonics. *Phys. Earth Planet. Inter.* 176, 143–156.
2487 <https://doi.org/10.1016/j.pepi.2009.05.004>
- 2488 Liégeois, J.P., Black, R., Navez, J., Latouche, L., 1994. Early and late Pan-African orogenies in the Air
2489 assembly of terranes (Tuareg shield, Niger). *Precambrian Res.* 67, 59–88.
2490 [https://doi.org/10.1016/0301-9268\(94\)90005-1](https://doi.org/10.1016/0301-9268(94)90005-1)
- 2491 Liégeois, J.P., Latouche, L., Boughrara, M., Navez, J., Guiraud, M., 2003. The LATEA metacraton
2492 (Central Hoggar, Tuareg shield, Algeria): behaviour of an old passive margin during the Pan-
2493 African orogeny. *J. Afr. Earth. Sci.* 37, 161–190. <https://doi.org/10.1016/j.jafrearsci.2003.05.004>
- 2494 Liu, L., Gurnis, M., Seton, M., Saleeby, J., Müller, R.D., Jackson, J.M., 2010. The role of oceanic plateau
2495 subduction in the Laramide orogeny. *Nat. Geosci.* 3, 353–357. <https://doi.org/10.1038/ngeo829>

- 2496 Liu, L., Spasojevic, S., Gurnis, M., 2008. Reconstructing Farallon plate subduction beneath North
2497 America back to the Late Cretaceous. *Science* 322, 934–938.
2498 <https://doi.org/10.1126/science.1162921>
- 2499 Liu, X., Zhao, Y., Chen, H., Song, B., 2017. New zircon U–Pb and Hf–Nd isotopic constraints on the
2500 timing of magmatism, sedimentation and metamorphism in the northern Prince Charles
2501 Mountains, East Antarctica. *Precambrian Res.* 299, 15–33.
2502 <https://doi.org/10.1016/j.precamres.2017.07.012>
- 2503 Lixin, B., Rixiang, Z., Harming, W., Bin, G., Jianjun, L., 1998. New Cambrian paleomagnetic pole for
2504 Yangtze Block. *Sci. China Ser. D Earth Sci.* 41, 66–71. <https://doi.org/10.1007/BF02984514>
- 2505 Llanos, M.P.I., Tait, J.A., Popov, V., Abalmassova, A., 2005. Palaeomagnetic data from Ediacaran
2506 (Vendian) sediments of the Arkhangelsk region, NW Russia: An alternative apparent polar
2507 wander path of Baltica for the Late Proterozoic–Early Palaeozoic. *Earth Planet. Sci. Lett.* 240,
2508 732–747. <https://doi.org/10.1016/j.epsl.2005.09.063>
- 2509 Loucks, V., Elmore, D.R., 1986. Absolute dating of dedolomitization and the origin of magnetization in
2510 the Cambrian Morgan Creek Limestone, central Texas. *GSA Bulletin* 97, 486–496.
2511 [https://doi.org/10.1130/0016-7606\(1986\)97<486:ADODAT>2.0.CO;2](https://doi.org/10.1130/0016-7606(1986)97<486:ADODAT>2.0.CO;2)
- 2512 Lubnina, N.V., Iosifidi, A.G., Khramov, A.N., Popov, V.V., Lewandowski, M., 2007. Paleomagnetism of
2513 the Silurian and Devonian sedimentary formations of Podolia, Ukraine, in: Khramov, A.N. (Ed.),
2514 Paleomagnetism of the Northern Eurasia Sedimentary Basins (IN RUSSIAN). pp. 105–125.
- 2515 Lubnina, N.V., Pisarevsky, S.A., Puchkov, V.N., Kozlov, V.I., Sergeeva, N.D., 2014. New paleomagnetic
2516 data from Late Neoproterozoic sedimentary successions in Southern Urals, Russia: implications
2517 for the Late Neoproterozoic paleogeography of the Iapetan realm. *Int. J. Earth Sci.* 103, 1317–
2518 1334. <https://doi.org/10.1007/s00531-014-1013-x>
- 2519 Macdonald, F.A., Prave, A.R., Petterson, R., Smith, E.F., Pruss, S.B., Oates, K., Waechter, F., Trotzok,
2520 D., Fallick, A.E., 2013. The Laurentian record of Neoproterozoic glaciation, tectonism, and
2521 eukaryotic evolution in Death Valley, California. *GSA Bulletin* 125, 1203–1223.
2522 <https://doi.org/10.1130/B30789.1>
- 2523 Martin, M.W., Grazhdankin, D.V., Bowring, S.A., Evans, D.A., Fedonkin, M.A., Kirschvink, J.L., 2000.
2524 Age of Neoproterozoic bilaterian body and trace fossils, White Sea, Russia: implications for
2525 metazoan evolution. *Science* 288, 841–845. <https://doi.org/10.1126/science.288.5467.841>
- 2526 Matthews, K.J., Maloney, K.T., Zahirovic, S., Williams, S.E., Seton, M., Müller, R.D., 2016. Global plate
2527 boundary evolution and kinematics since the late Paleozoic. *Glob. Planet. Change* 146, 226–250.
2528 <https://doi.org/10.1016/j.gloplacha.2016.10.002>
- 2529 Matthews, K.J., Williams, S.E., Whittaker, J.M., Müller, R.D., Seton, M., Clarke, G.L., 2015. Geologic

2530 and kinematic constraints on Late Cretaceous to mid Eocene plate boundaries in the southwest
2531 Pacific. *Earth-Sci. Rev.* 140, 72–107. <https://doi.org/10.1016/j.earscirev.2014.10.008>

2532 McCabe, C., Channell, J.E.T., 1990. Paleomagnetic results from volcanic rocks of the Shelve Inlier,
2533 Wales: evidence for a wide Late Ordovician Iapetus Ocean in Britain. *Earth Planet. Sci. Lett.* 96,
2534 458–468. [https://doi.org/10.1016/0012-821X\(90\)90020-X](https://doi.org/10.1016/0012-821X(90)90020-X)

2535 McCabe, C., Channell, J.E.T., Woodcock, N.H., 1992. Further paleomagnetic results from the Builth
2536 Wells Ordovician inlier, Wales. *J. Geophys. Res. [Solid Earth]* 97, 9357–9370.

2537 McCabe, C., Van der Voo, R., Wilkinson, B.H., Devaney, K., 1985. A Middle/Late Silurian
2538 paleomagnetic pole from limestone reefs of the Wabash Formation, Indiana, USA. *J. Geophys.*
2539 *Res. [Solid Earth]* 90, 2959–2965.

2540 McCausland, P.J.A., Hodych, J.P., 1998. Paleomagnetism of the 550 Ma Skinner Cove volcanics of
2541 western Newfoundland and the opening of the Iapetus Ocean. *Earth Planet. Sci. Lett.* 163, 15–29.
2542 [https://doi.org/10.1016/S0012-821X\(98\)00171-X](https://doi.org/10.1016/S0012-821X(98)00171-X)

2543 McCausland, P.J.A., Van der Voo, R., Hall, C.M., 2007. Circum-Iapetus paleogeography of the
2544 Precambrian–Cambrian transition with a new paleomagnetic constraint from Laurentia.
2545 *Precambrian Res.* 156, 125–152. <https://doi.org/10.1016/j.precamres.2007.03.004>

2546 McElhinny, M.W., Cowley, J.A., Edwards, D.J., 1978. Palaeomagnetism of some rocks from Peninsular
2547 India and Kashmir. *Tectonophysics* 50, 41–54. [https://doi.org/10.1016/0040-1951\(78\)90198-1](https://doi.org/10.1016/0040-1951(78)90198-1)

2548 McGee, B., Halverson, G.P., Collins, A.S., 2012. Cryogenian rift-related magmatism and sedimentation:
2549 South-western Congo Craton, Namibia. *J. Afr. Earth. Sci.* 76, 34–49.
2550 <https://doi.org/10.1016/j.jafrearsci.2012.09.003>

2551 McKenzie, D.P., Parker, R.L., 1967. The North Pacific: an Example of Tectonics on a Sphere. *Nature*
2552 216, 1276–1280. <https://doi.org/10.1038/2161276a0>

2553 McKenzie, R.N., Hughes, N.C., Gill, B.C., Myrow, P.M., 2014. Plate tectonic influences on
2554 Neoproterozoic–early Paleozoic climate and animal evolution. *Geology* 42, 127–130.
2555 <https://doi.org/10.1130/G34962.1>

2556 McKerrow, W.S., Mac Niocaill, C., Ahlberg, P.E., Clayton, G., Cleal, C.J., Eagar, R.M.C., 2000. The
2557 Late Palaeozoic relations between Gondwana and Laurussia. *Geological Society, London, Special*
2558 *Publications* 179, 9–20. <https://doi.org/10.1144/GSL.SP.2000.179.01.03>

2559 McMenamin, M.A., McMenamin, M.A., McMenamin, D.L.S., 1990. *The emergence of animals: the*
2560 *Cambrian breakthrough*. Columbia University Press.

2561 Meert, J.G., 2014. Ediacaran–Early Ordovician paleomagnetism of Baltica: A review. *Gondwana Res.* 25,
2562 159–169. <https://doi.org/10.1016/j.gr.2013.02.003>

2563 Meert, J.G., 2003. A synopsis of events related to the assembly of eastern Gondwana. *Tectonophysics*

2564 362, 1–40. [https://doi.org/10.1016/S0040-1951\(02\)00629-7](https://doi.org/10.1016/S0040-1951(02)00629-7)

2565 Meert, J.G., 2002. Paleomagnetic Evidence for a Paleo-Mesoproterozoic Supercontinent Columbia.
2566 *Gondwana Res.* 5, 207–215. [https://doi.org/10.1016/S1342-937X\(05\)70904-7](https://doi.org/10.1016/S1342-937X(05)70904-7)

2567 Meert, J.G., Lieberman, B.S., 2008. The Neoproterozoic assembly of Gondwana and its relationship to
2568 the Ediacaran–Cambrian radiation. *Gondwana Res.* 14, 5–21.
2569 <https://doi.org/10.1016/j.gr.2007.06.007>

2570 Meert, J.G., Pandit, M.K., Kamenov, G.D., 2013. Further geochronological and paleomagnetic constraints
2571 on Malani (and pre-Malani) magmatism in NW India. *Tectonophysics* 608, 1254–1267.
2572 <https://doi.org/10.1016/j.tecto.2013.06.019>

2573 Meert, J.G., Pandit, M.K., Pradhan, V.R., Banks, J., Sirianni, R., Stroud, M., Newstead, B., Gifford, J.,
2574 2010. Precambrian crustal evolution of Peninsular India: A 3.0 billion year odyssey. *J. Asian*
2575 *Earth Sci.* 39, 483–515. <https://doi.org/10.1016/j.jseaes.2010.04.026>

2576 Meert, J.G., van der Voo, R., Ayub, S., 1995. Paleomagnetic investigation of the Neoproterozoic Gagwe
2577 lavas and Mbozi complex, Tanzania and the assembly of Gondwana. *Precambrian Res.* 74, 225–
2578 244. [https://doi.org/10.1016/0301-9268\(95\)00012-T](https://doi.org/10.1016/0301-9268(95)00012-T)

2579 Meffre, S., Direen, N.G., Crawford, A.J., Kamenetsky, V., 2004. Mafic volcanic rocks on King Island,
2580 Tasmania: evidence for 579 Ma break-up in east Gondwana. *Precambrian Res.* 135, 177–191.

2581 Merdith, A.S., Atkins, S.E., Tetley, M.G., 2019a. Tectonic Controls on Carbon and Serpentinite Storage
2582 in Subducted Upper Oceanic Lithosphere for the Past 320 Ma. *Front Earth Sci. Chin.* 7, 332.
2583 <https://doi.org/10.3389/feart.2019.00332>

2584 Merdith, A.S., Collins, A.S., Williams, S.E., Pisarevsky, S., Foden, J.D., Archibald, D.B., Blades, M.L.,
2585 Alessio, B.L., Armistead, S., Plavsa, D., Clark, C., Müller, R.D., 2017a. A full-plate global
2586 reconstruction of the Neoproterozoic. *Gondwana Res.* 50, 84–134.
2587 <https://doi.org/10.1016/j.gr.2017.04.001>

2588 Merdith, A.S., Williams, S.E., Brune, S., Collins, A.S., Müller, R.D., 2019b. Rift and plate boundary
2589 evolution across two supercontinent cycles. *Glob. Planet. Change* 173, 1–14.
2590 <https://doi.org/10.1016/j.gloplacha.2018.11.006>

2591 Merdith, A.S., Williams, S.E., Müller, R.D., Collins, A.S., 2017b. Kinematic constraints on the Rodinia to
2592 Gondwana transition. *Precambrian Res.* 299, 132–150.
2593 <https://doi.org/10.1016/j.precamres.2017.07.013>

2594 Metcalfe, I., 2013. Gondwana dispersion and Asian accretion: Tectonic and palaeogeographic evolution
2595 of eastern Tethys. *J. Asian Earth Sci.* 66, 1–33. <https://doi.org/10.1016/j.jseaes.2012.12.020>

2596 Metcalfe, I., 2011. Palaeozoic–Mesozoic history of SE Asia. Geological Society, London, Special
2597 Publications 355, 7–35. <https://doi.org/10.1144/SP355.2>

2598 Metelkin, D.V., Vernikovskiy, V.A., Kazansky, A.Y., 2012. Tectonic evolution of the Siberian
2599 paleocontinent from the Neoproterozoic to the Late Mesozoic: paleomagnetic record and
2600 reconstructions. *Russ. Geol. Geophys.* 53, 675–688. <https://doi.org/10.1016/j.rgg.2012.05.006>

2601 Miller, J.D., Kent, D.V., 1988. Paleomagnetism of the Silurian-Devonian Andreas redbeds: Evidence for
2602 an Early Devonian supercontinent? *Geology* 16, 195–198.
2603 2.3.CO;2">[https://doi.org/10.1130/0091-7613\(1988\)016<0195:POTSDA>2.3.CO;2](https://doi.org/10.1130/0091-7613(1988)016<0195:POTSDA>2.3.CO;2)

2604 Mills, B., Watson, A.J., Goldblatt, C., Boyle, R., Lenton, T.M., 2011. Timing of Neoproterozoic
2605 glaciations linked to transport-limited global weathering. *Nat. Geosci.* 4, 861–864.
2606 <https://doi.org/10.1038/ngeo1305>

2607 Mills, B.J.W., Krause, A.J., Scotese, C.R., Hill, D.J., Shields, G.A., Lenton, T.M., 2019. Modelling the
2608 long-term carbon cycle, atmospheric CO₂, and Earth surface temperature from late
2609 Neoproterozoic to present day. *Gondwana Res.* 67, 172–186.
2610 <https://doi.org/10.1016/j.gr.2018.12.001>

2611 Millward, D., Evans, J.A., 2003. U–Pb chronology and duration of late Ordovician magmatism in the
2612 English Lake District. *J. Geol. Soc. London* 160, 773–781. [https://doi.org/10.1144/0016-764902-](https://doi.org/10.1144/0016-764902-160)
2613 160

2614 Minh, P., Hieu, P.T., Thuy, N.T.B., Dung, L.T., Kawaguchi, K., Dung, P.T., 2020. Neoproterozoic
2615 granitoids from the Phan Si Pan Zone, NW Vietnam: geochemistry and geochronology
2616 constraints on reconstructing South China--India Palaeogeography. *Int. Geol. Rev.* 1–16.

2617 Minibaev, R.A. and Sulutdinov, R.M., 1991. Paleomagnitniye kharakteristiki siluriyskikh obrazovaniy
2618 sakmarskoy zoni Yuzhnogo Urala. *Bashkirian Natl.Cttee.Ural.Branch Acad.Sci.USSR (Ufa)* 30.

2619 Mitchell, R.N., Kilian, T.M., Evans, D.A.D., 2012. Supercontinent cycles and the calculation of absolute
2620 palaeolongitude in deep time. *Nature* 482, 208–211. <https://doi.org/10.1038/nature10800>

2621 Moores, E.M., 2002. Pre–1 Ga (pre-Rodinian) ophiolites: Their tectonic and environmental implications.
2622 *GSA Bulletin* 114, 80–95. 2.0.CO;2">[https://doi.org/10.1130/0016-](https://doi.org/10.1130/0016-7606(2002)114<0080:PGPROT>2.0.CO;2)
2623 7606(2002)114<0080:PGPROT>2.0.CO;2

2624 Moores, E.M., 1991. Southwest U.S.-East Antarctic (SWEAT) connection: A hypothesis. *Geology* 19,
2625 425–428. 2.3.CO;2">[https://doi.org/10.1130/0091-7613\(1991\)019<0425:SUSEAS>2.3.CO;2](https://doi.org/10.1130/0091-7613(1991)019<0425:SUSEAS>2.3.CO;2)

2626 Morgan, W.J., 1968. Rises, trenches, great faults, and crustal blocks. *J. Geophys. Res.* 73, 1959–1982.
2627 <https://doi.org/10.1029/JB073i006p01959>

2628 Morrison, J., Ellwood, B.B., 1986. Paleomagnetism of Silurian-Ordovician sediments from the Valley
2629 and Ridge province, northwest Georgia. *Geophys. Res. Lett.* 13, 189–192.

2630 Mulder, J.A., Berry, R.F., Halpin, J.A., Meffre, S., Everard, J.L., 2018a. Depositional age and correlation
2631 of the Oonah Formation: refining the timing of Neoproterozoic basin formation in Tasmania.

2632 Aust. J. Earth Sci. 65, 391–407. <https://doi.org/10.1080/08120099.2018.1426629>

2633 Mulder, J.A., Everard, J.L., Cumming, G., Meffre, S., Bottrill, R.S., Merdith, A.S., Halpin, J.A., McNeill,
2634 A.W., Cawood, P.A., 2020. Neoproterozoic opening of the Pacific Ocean recorded by multi-stage
2635 rifting in Tasmania, Australia. *Earth-Sci. Rev.* 201, 103041.
2636 <https://doi.org/10.1016/j.earscirev.2019.103041>

2637 Mulder, J.A., Halpin, J.A., Daczko, N.R., 2015. Mesoproterozoic Tasmania: Witness to the East
2638 Antarctica–Laurentia connection within Nuna. *Geology* 43, 759–762.
2639 <https://doi.org/10.1130/G36850.1>

2640 Mulder, J.A., Halpin, J.A., Daczko, N.R., Orth, K., Meffre, S., Thompson, J.M., Morrissey, L.J., 2019. A
2641 Multiproxy provenance approach to uncovering the assembly of East Gondwana in Antarctica.
2642 *Geology* 47, 645–649. <https://doi.org/10.1130/G45952.1>

2643 Mulder, J.A., Karlstrom, K.E., Halpin, J.A., Merdith, A.S., Spencer, C.J., Berry, R.F., McDonald, B.,
2644 2018b. Rodinian devil in disguise: Correlation of 1.25–1.10 Ga strata between Tasmania and
2645 Grand Canyon. *Geology* 46, 991–994. <https://doi.org/10.1130/G45225.1>

2646 Müller, R.D., Cannon, J., Qin, X., Watson, R.J., Gurnis, M., Williams, S., Pfaffelmoser, T., Seton, M.,
2647 Russell, S.H.J., Zahirovic, S., 2018. GPlates: Building a Virtual Earth Through Deep Time.
2648 *Geochem. Geophys. Geosyst.* 19, 2243–2261. <https://doi.org/10.1029/2018GC007584>

2649 Müller, R.D., Royer, J.-Y., Lawver, L.A., 1993. Revised plate motions relative to the hotspots from
2650 combined Atlantic and Indian Ocean hotspot tracks. *Geology* 21, 275–278.
2651 [2.3.CO;2">https://doi.org/10.1130/0091-7613\(1993\)021<0275:RPMRTT>2.3.CO;2](https://doi.org/10.1130/0091-7613(1993)021<0275:RPMRTT>2.3.CO;2)

2652 Müller, R.D., Sdrolias, M., Gaina, C., Steinberger, B., Heine, C., 2008. Long-term sea-level fluctuations
2653 driven by ocean basin dynamics. *Science* 319, 1357–1362.
2654 <https://doi.org/10.1126/science.1151540>

2655 Müller, R.D., Seton, M., Zahirovic, S., Williams, S.E., Matthews, K.J., Wright, N.M., Shephard, G.E.,
2656 Maloney, K.T., Barnett-Moore, N., Hosseinpour, M., Bower, D.J., Cannon, J., 2016. Ocean Basin
2657 Evolution and Global-Scale Plate Reorganization Events Since Pangea Breakup. *Annu. Rev.*
2658 *Earth Planet. Sci.* 44, 107–138. <https://doi.org/10.1146/annurev-earth-060115-012211>

2659 Müller, R.D., Zahirovic, S., Williams, S.E., Cannon, J., Seton, M., Bower, D.J., Tetley, M., Heine, C., Le
2660 Breton, E., Liu, S., Russell, S.H.J., Yang, T., Leonard, J., Gurnis, M., 2019. A global plate model
2661 including lithospheric deformation along major rifts and orogens since the Triassic. *Tectonics*.
2662 <https://doi.org/10.1029/2018TC005462>

2663 Murphy, J.B., 2002. Geochemistry of the Neoproterozoic metasedimentary Gamble Brook Formation,
2664 Avalon terrane, Nova Scotia: evidence for a rifted-arc environment along the west Gondwanan
2665 margin of Rodinia. *J. Geol.* 110, 407–419.

2666 Murphy, J.B., Keppie, J.D., Dostal, J., Nance, R.D., 1999. Neoproterozoic-early Paleozoic evolution
2667 of Avalonia. *Laurentia-Gondwana Connections Before Pangea* 336, 253.

2668 Murphy, J.B., Nance, R.D., 1989. Model for the evolution of the Avalonian-Cadomian belt. *Geology* 17,
2669 735–738. [https://doi.org/10.1130/0091-7613\(1989\)017<0735:MFTEOT>2.3.CO;2](https://doi.org/10.1130/0091-7613(1989)017<0735:MFTEOT>2.3.CO;2)

2670 Murphy, J.B., Pisarevsky, S.A., Nance, R.D., Keppie, J.D., 2004. Neoproterozoic—Early Paleozoic
2671 evolution of peri-Gondwanan terranes: implications for Laurentia-Gondwana connections. *Int. J.*
2672 *Earth Sci.* 93, 659–682. <https://doi.org/10.1007/s00531-004-0412-9>

2673 Murphy, J.B., Strachan, R.A., Nance, R.D., Parker, K.D., Fowler, M.B., 2000. Proto-Avalonia: A 1.2–1.0
2674 Ga tectonothermal event and constraints for the evolution of Rodinia. *Geology* 28, 1071–1074.
2675 [https://doi.org/10.1130/0091-7613\(2000\)28<1071:PAGTEA>2.0.CO;2](https://doi.org/10.1130/0091-7613(2000)28<1071:PAGTEA>2.0.CO;2)

2676 Murphy, J.B., Waldron, J.W.F., Kontak, D.J., Pe-Piper, G., Piper, D.J.W., 2011. Minas Fault Zone: Late
2677 Paleozoic history of an intra-continental orogenic transform fault in the Canadian Appalachians.
2678 *J. Struct. Geol.* 33, 312–328. <https://doi.org/10.1016/j.jsg.2010.11.012>

2679 Murthy, G., Gower, C., Tubrett, M., Pätzold, R., 1992. Paleomagnetism of Eocambrian Long Range
2680 dykes and Double Mer Formation from Labrador, Canada. *Can. J. Earth Sci.* 29, 1224–1234.
2681 <https://doi.org/10.1139/e92-098>

2682 Nance, R.D., Linnemann, U., 2008. The Rheic Ocean: origin, evolution, and significance. *GSA Today* 18,
2683 4–12.

2684 Nance, R.D., Murphy, J.B., Strachan, R.A., Keppie, J.D., Gutiérrez-Alonso, G., Fernández-Suárez, J.,
2685 Quesada, C., Linnemann, U., D’lemos, R., Pisarevsky, S.A., 2008. Neoproterozoic-early
2686 Palaeozoic tectonostratigraphy and palaeogeography of the peri-Gondwanan terranes: Amazonian
2687 v. West African connections. Geological Society, London, Special Publications 297, 345–383.

2688 Nick, K.E., Elmore, R.D., 1990. Paleomagnetism of the Cambrian Royer Dolomite and Pennsylvanian
2689 Collings Ranch Conglomerate, southern Oklahoma: An early Paleozoic magnetization and
2690 nonpervasive remagnetization by weathering. *Geol. Soc. Am. Bull.* 102, 1517–1525.

2691 Niu, J., Li, Z.-X., Zhu, W., 2016. Palaeomagnetism and geochronology of mid-Neoproterozoic Yanbian
2692 dykes, South China: implications for a c. 820–800 Ma true polar wander event and the
2693 reconstruction of Rodinia. Geological Society, London, Special Publications 424, 191–121.
2694 <https://doi.org/http://doi.org/10.1144/SP424.11>

2695 Noel, J.R., Spariosu, D.J., Dallmeyer, R.D., 1988. Paleomagnetism and $^{40}\text{Ar}/^{39}\text{Ar}$ ages from the
2696 Carolina slate belt, Albemarle, North Carolina: Implications for terrane amalgamation with North
2697 America. *Geology* 16, 64–68.

2698 O’Brien, S.J., Dunning, G.R., Dube, B., O’Driscoll, C.F., Sparkes, B., Israel, S., Ketchum, J., 2001. New
2699 insights into the Neoproterozoic geology of the central Avalon Peninsula (parts of NTS map areas

2700 1N/6, 1N/7 and 1N/3), eastern Newfoundland. Current Research, Government of Newfoundland
2701 and Labrador, Department of Mines and Energy, Geological Survey 2001, 169–189.

2702 O'Neill, C., Müller, D., Steinberger, B., 2005. On the uncertainties in hot spot reconstructions and the
2703 significance of moving hot spot reference frames. *Geochem. Geophys. Geosyst.*, Spec. Pap. Geol.
2704 Soc. Am. 6. <https://doi.org/10.1029/2004GC000784>

2705 Opdyke, N.D., Huang, K., Xu, G., Zhang, W.Y., Kent, D.V., 1987. Paleomagnetic results from the
2706 Silurian of the Yangtze paraplatform. *Tectonophysics* 139, 123–132.
2707 [https://doi.org/10.1016/0040-1951\(87\)90201-0](https://doi.org/10.1016/0040-1951(87)90201-0)

2708 Palin, R.M., Santosh, M., Cao, W., Li, S.S., 2020. Secular change and the onset of plate tectonics on
2709 Earth. *Earth-Sci. Rev.*

2710 Pan, B., Brock, G.A., Skovsted, C.B., Betts, M.J., Topper, T.P., Li, G., 2018. *Paterimitra pyramidalis*
2711 Laurie, 1986, the first tomotiid discovered from the early Cambrian of North China. *Gondwana*
2712 *Res.* 63, 179–185. <https://doi.org/10.1016/j.gr.2018.05.014>

2713 Pandit, M.K., Carter, L.M., Ashwal, L.D., Tucker, R.D., Torsvik, T.H., Jamtveit, B., Bhushan, S.K.,
2714 2003. Age, petrogenesis and significance of 1 Ga granitoids and related rocks from the Sendra
2715 area, Aravalli Craton, NW India. *J. Asian Earth Sci.* 22, 363–381.

2716 Paquette, J.L., Caby, R., Djouadi, M.T., Bouchez, J.L., 1998. U–Pb dating of the end of the Pan-African
2717 orogeny in the Tuareg shield: the post-collisional syn-shear Tioueine pluton (Western Hoggar,
2718 Algeria). *Lithos* 45, 245–253. [https://doi.org/10.1016/S0024-4937\(98\)00034-6](https://doi.org/10.1016/S0024-4937(98)00034-6)

2719 Parsons, A.J., Hosseini, K., Palin, R.M., Sigloch, K., 2020. Geological, geophysical and plate kinematic
2720 constraints for models of the India-Asia collision and the post-Triassic central Tethys oceans.
2721 *Earth-Sci. Rev.* 208, 103084. <https://doi.org/10.1016/j.earscirev.2020.103084>

2722 Pavlov, V., Bachtadse, V., Mikhailov, V., 2008. New Middle Cambrian and Middle Ordovician
2723 palaeomagnetic data from Siberia: Llandelian magnetostratigraphy and relative rotation between
2724 the Aldan and Anabar--Angara blocks. *Earth Planet. Sci. Lett.* 276, 229–242.

2725 Pavlov, V., Gallet, Y., 1998. Upper Cambrian to Middle Ordovician magnetostratigraphy from the
2726 Kulumbe river section (northwestern Siberia). *Phys. Earth Planet. Inter.* 108, 49–59.
2727 [https://doi.org/10.1016/S0031-9201\(98\)00087-9](https://doi.org/10.1016/S0031-9201(98)00087-9)

2728 Pavlov, V.E., Shatsillo, A.V., Petrov, P.Y., 2015. Paleomagnetism of the upper Riphean deposits in the
2729 Turukhansk and Olenek uplifts and Uda Pre-Sayan region and the neoproterozoic drift of the
2730 Siberian Platform. *Izv. Phys. Solid Earth* 51, 716–747.
2731 <https://doi.org/10.1134/S1069351315050092>

2732 Pavlov, V.E., Veselovskiy, R.V., Shatsillo, A.V., Gallet, Y., 2012. Magnetostratigraphy of the Ordovician
2733 Angara/Rozhkova River section: Further evidence for the Moyero reversed superchron. *Izv. Phys.*

2734 Solid Earth 48, 297–305. <https://doi.org/10.1134/S1069351312040052>

2735 Pedrosa-Soares, A.C., Noce, C.M., Wiedemann, C.M., Pinto, C.P., 2001. The Aracuai-West-Congo
2736 Orogen in Brazil: an overview of a confined orogen formed during Gondwanaland assembly.
2737 Precambrian Res. 110, 307–323.

2738 Pehrsson, S.J., Berman, R.G., Eglinton, B., Rainbird, R., 2013. Two Neoproterozoic supercontinents
2739 revisited: The case for a Rae family of cratons. Precambrian Res. 232, 27–43.
2740 <https://doi.org/10.1016/j.precamres.2013.02.005>

2741 Peng, Y., Yu, S., Li, S., Zhang, J., Liu, Y., Li, Y., Santosh, M., 2019. Early Neoproterozoic magmatic
2742 imprints in the Altun-Qilian-Kunlun region of the Qinghai-Tibet Plateau: Response to the
2743 assembly and breakup of Rodinia supercontinent. Earth-Sci. Rev. 199, 102954.
2744 <https://doi.org/10.1016/j.earscirev.2019.102954>

2745 Pisarevsky, S., Bylund, G., 1998. Neoproterozoic palaeomagnetic directions in rocks from a key section
2746 of the Protogine Zone, southern Sweden. Geophys. J. Int. 133, 185–200.
2747 <https://doi.org/10.1046/j.1365-246X.1998.1331497.x>

2748 Pisarevsky, S.A., Elming, S.-Å., Pesonen, L.J., Li, Z.-X., 2014. Mesoproterozoic paleogeography:
2749 Supercontinent and beyond. Precambrian Res. 244, 207–225.
2750 <https://doi.org/10.1016/j.precamres.2013.05.014>

2751 Pisarevsky, S.A., Gladkochub, D.P., Konstantinov, K.M., Mazukabzov, A.M., Stanevich, A.M., Murphy,
2752 J.B., Tait, J.A., Donskaya, T.V., Konstantinov, I.K., 2013. Paleomagnetism of Cryogenian Kitoi
2753 mafic dykes in South Siberia: Implications for Neoproterozoic paleogeography. Precambrian Res.
2754 231, 372–382. <https://doi.org/10.1016/j.precamres.2013.04.007>

2755 Pisarevsky, S.A., Gurevich, E.L., Khramov, A.N., 1997. Palaeomagnetism of Lower Cambrian sediments
2756 from the Olenek River section (northern Siberia): palaeopoles and the problem of magnetic
2757 polarity in the Early Cambrian. Geophys. J. Int. 130, 746–756. <https://doi.org/10.1111/j.1365-246X.1997.tb01869.x>

2759 Pisarevsky, S.A., Murphy, J.B., Cawood, P.A., Collins, A.S., 2008. Late Neoproterozoic and Early
2760 Cambrian palaeogeography: models and problems. Geological Society, London, Special
2761 Publications 294, 9–31. <https://doi.org/10.1144/SP294.2>

2762 Pisarevsky, S.A., Natapov, L.M., 2003. Siberia and Rodinia. Tectonophysics 375, 221–245.
2763 <https://doi.org/10.1016/j.tecto.2003.06.001>

2764 Pisarevsky, S.A., Wingate, M.T.D., Stevens, M.K., Haines, P.W., 2007. Palaeomagnetic results from the
2765 Lancer 1 stratigraphic drillhole, Officer Basin, Western Australia, and implications for Rodinia
2766 reconstructions. Aust. J. Earth Sci. 54, 561–572. <https://doi.org/10.1080/08120090701188962>

2767 Plavsa, D., Collins, A.S., Foden, J.D., Clark, C., 2015. The evolution of a Gondwanan collisional orogen:

2768 A structural and geochronological appraisal from the Southern Granulite Terrane, South India.
2769 *Tectonics* 34, 820–857.

2770 Popov, V., Iosifidi, A., Khramov, A., Tait, J., Bachtadse, V., 2002. Paleomagnetism of Upper Vendian
2771 sediments from the Winter Coast, White Sea region, Russia: implications for the paleogeography
2772 of Baltica during Neoproterozoic times. *J. Geophys. Res. [Solid Earth]* 107, EPM-10.

2773 Popov, V.V., Khramov, A.N., Bachtadse, V., 2005. Palaeomagnetism, magnetic stratigraphy, and
2774 petromagnetism of the Upper Vendian sedimentary rocks in the sections of the Zolotitsa River
2775 and in the Verkhotina Hole, Winter Coast of the White Sea, Russia. *Russian Journal of Earth
2776 Sciences* 7.

2777 Powell, C.M., Pisarevsky, S.A., 2002. Late Neoproterozoic assembly of East Gondwana. *Geology* 30, 3–
2778 6. [https://doi.org/10.1130/0091-7613\(2002\)030<0003:LNAOEG>2.0.CO;2](https://doi.org/10.1130/0091-7613(2002)030<0003:LNAOEG>2.0.CO;2)

2779 Powerman, V., Shatsillo, A., Coe, R., Zhao, X., Gladkochub, D., Buchwaldt, R., Pavlov, V., 2013.
2780 Palaeogeography of the Siberian platform during middle Palaeozoic Times (450–400 Ma): new
2781 palaeomagnetic evidence from the Lena and Nyuya rivers. *Geophys. J. Int.* 194, 1412–1440.

2782 Qiantao, B., Shanlin, G., Dihui, L., Zhengren, Y., Chengfa, C., Xiaoquan, L., 2001. A study of the
2783 Kunlun-Qilian-Qinling suture system. *Acta Geologica Sinica-English Edition* 75, 364–374.

2784 Rapalini, A.E., 2006. New late Proterozoic paleomagnetic pole for the Rio de la Plata craton: Implications
2785 for Gondwana. *Precambrian Res.* 147, 223–233. <https://doi.org/10.1016/j.precamres.2006.01.016>

2786 Rapalini, A.E., Cingolani, C.A., 2004. First Late Ordovician Paleomagnetic Pole for the Cuyania
2787 (Precordillera) Terrane of Western Argentina: a Microcontinent or a Laurentian Plateau.
2788 *Gondwana Res.* 7, 1089–1104. [https://doi.org/10.1016/S1342-937X\(05\)71086-8](https://doi.org/10.1016/S1342-937X(05)71086-8)

2789 Rapalini, A.E., Tohver, E., Bettucci, L.S., Lossada, A.C., Barcelona, H., Pérez, C., 2015. The late
2790 Neoproterozoic Sierra de las Ánimas Magmatic Complex and Playa Hermosa Formation,
2791 southern Uruguay, revisited: Paleogeographic implications of new paleomagnetic and precise
2792 geochronologic data. *Precambrian Res.* 259, 143–155.
2793 <https://doi.org/10.1016/j.precamres.2014.11.021>

2794 Raub, T.D., Kirschvink, J.L., Evans, D.A.D., 2007. True polar wander: Linking deep and shallow
2795 geodynamics to hydro- and biospheric hypotheses. *Treatise on Geophysics* 5, 565–589.

2796 Raza, M., Khan, A., Bhardwaj, V.R., Rais, S., 2012. Geochemistry of Mesoproterozoic sedimentary rocks
2797 of upper Vindhyan Group, southeastern Rajasthan and implications for weathering history,
2798 composition and tectonic setting of continental crust in the northern part of Indian shield. *J. Asian
2799 Earth Sci.* 48, 160–172.

2800 Robert, B., Besse, J., Blein, O., Greff-Lefftz, M., Baudin, T., Lopes, F., Meslouh, S., Belbadaoui, M.,
2801 2017. Constraints on the Ediacaran inertial interchange true polar wander hypothesis: A new

2802 paleomagnetic study in Morocco (West African Craton). *Precambrian Res.* 295, 90–116.
2803 <https://doi.org/10.1016/j.precamres.2017.04.010>

2804 Robert, B., Domeier, M., Jakob, J., 2020. Iapetan Oceans: An analog of Tethys? *Geology*.
2805 Rodionov, V.P., 1966. Dipole character of the Geomagnetic field in the Late Cambrian and the
2806 Ordovician in the south of the Siberian Platform. *Geol. Geofiz.* 1, 94–101.

2807 Rodionov, V.P., Dekkers, M.J., Khramov, A.N., Gurevich, E.L., Krijgsman, W., Duermeijer, C.E.,
2808 Heslop, D., 2003. Paleomagnetism and cyclostratigraphy of the Middle Ordovician Krivolutsky
2809 suite, Krivaya Luka section, southern Siberian platform: record of non-synchronous NRM-
2810 components or a non-axial geomagnetic field? *Studia Geophys. Geodaetica* 47, 255–274.

2811 Rodionov, V.P., Khramov, A.N., Pisarevskii, S.A., Popov, V.V., Iosifidi, A.G., 1998. Geomagnetic
2812 Reversals in the Early Paleozoic. 1. A Late Cambrian Reversal Recorded in the Ichera Section,
2813 Southern Siberian Platform. *Izv. Phys. Solid Earth* 34, 1009–1017.

2814 Rogers, J.J.W., Santosh, M., 2002. Configuration of Columbia, a Mesoproterozoic Supercontinent.
2815 *Gondwana Res.* 5, 5–22. [https://doi.org/10.1016/S1342-937X\(05\)70883-2](https://doi.org/10.1016/S1342-937X(05)70883-2)

2816 Ross, M.I., Scotese, C.R., 1988. A hierarchical tectonic model of the Gulf of Mexico and Caribbean
2817 region. *Tectonophysics*.

2818 Ruppel, A., Jacobs, J., Eagles, G., Läufer, A., Jokat, W., 2018. New geophysical data from a key region in
2819 East Antarctica: Estimates for the spatial extent of the Tonian Oceanic Arc Super Terrane
2820 (TOAST). *Gondwana Res.* 59, 97–107. <https://doi.org/10.1016/j.gr.2018.02.019>

2821 Safonova, I., Biske, G., Romer, R.L., Seltmann, R., Simonov, V., Maruyama, S., 2016. Middle Paleozoic
2822 mafic magmatism and ocean plate stratigraphy of the South Tianshan, Kyrgyzstan. *Gondwana*
2823 *Res.* 30, 236–256. <https://doi.org/10.1016/j.gr.2015.03.006>

2824 Schellart, W.P., Lister, G.S., Toy, V.G., 2006. A Late Cretaceous and Cenozoic reconstruction of the
2825 Southwest Pacific region: Tectonics controlled by subduction and slab rollback processes. *Earth-*
2826 *Sci. Rev.* 76, 191–233. <https://doi.org/10.1016/j.earscirev.2006.01.002>

2827 Scherstén, A., Årebäck, H., Cornell, D., Hoskin, P., Åberg, A., Armstrong, R., 2000. Dating mafic–
2828 ultramafic intrusions by ion-microprobing contact-melt zircon: examples from SW Sweden.
2829 *Contrib. Mineral. Petrol.* 139, 115–125. <https://doi.org/10.1007/s004100050577>

2830 Schmidt, P.W., Williams, G.E., 2010. Ediacaran palaeomagnetism and apparent polar wander path for
2831 Australia: no large true polar wander. *Geophys. J. Int.* 182, 711–726.
2832 <https://doi.org/10.1111/j.1365-246X.2010.04652.x>

2833 Schmidt, P.W., Williams, G.E., 1996. Palaeomagnetism of the ejecta-bearing Bunyeroo Formation, late
2834 Neoproterozoic, Adelaide fold belt, and the age of the Acraman impact. *Earth Planet. Sci. Lett.*
2835 144, 347–357. [https://doi.org/10.1016/S0012-821X\(96\)00169-0](https://doi.org/10.1016/S0012-821X(96)00169-0)

2836 Schmidt, P.W., Williams, G.E., 1995. The Neoproterozoic climatic paradox: Equatorial palaeolatitude for
2837 Marinoan glaciation near sea level in South Australia. *Earth Planet. Sci. Lett.* 134, 107–124.
2838 [https://doi.org/10.1016/0012-821X\(95\)00106-M](https://doi.org/10.1016/0012-821X(95)00106-M)

2839 Schmidt, P.W., Williams, G.E., Embleton, B.J.J., 1991. Low palaeolatitude of Late Proterozoic
2840 glaciation: early timing of remanence in haematite of the Elatina Formation, South Australia.
2841 *Earth Planet. Sci. Lett.* 105, 355–367. [https://doi.org/10.1016/0012-821X\(91\)90177-J](https://doi.org/10.1016/0012-821X(91)90177-J)

2842 Schmidt, P.W., Williams, G.E., McWilliams, M.O., 2009. Palaeomagnetism and magnetic anisotropy of
2843 late Neoproterozoic strata, South Australia: Implications for the palaeolatitude of late Cryogenian
2844 glaciation, cap carbonate and the Ediacaran System. *Precambrian Res.* 174, 35–52.
2845 <https://doi.org/10.1016/j.precamres.2009.06.002>

2846 Scotese, C.R., 2016. PALEOMAP PaleoAtlas for GPlates and the PaleoData Plotter Program,
2847 PALEOMAP Project. See <http://www.earthbyte.org/paleomap-paleoatlas-for-gplates>.

2848 Scotese, C.R., 2004. A Continental Drift Flipbook. *J. Geol.* 112, 729–741. <https://doi.org/10.1086/424867>

2849 Seton, M., Müller, R.D., Zahirovic, S., Gaina, C., Torsvik, T., Shephard, G., Talsma, A., Gurnis, M.,
2850 Turner, M., Maus, S., Chandler, M., 2012. Global continental and ocean basin reconstructions
2851 since 200 Ma. *Earth-Sci. Rev.* 113, 212–270. <https://doi.org/10.1016/j.earscirev.2012.03.002>

2852 Shapiro, M.N., Solov'ev, A.V., 2009. Formation of the Olyutorsky–Kamchatka foldbelt: a kinematic
2853 model. *Russ. Geol. Geophys.* 50, 668–681. <https://doi.org/10.1016/j.rgg.2008.10.006>

2854 Shatsillo, A.V., Paverman, V.I., Pavlov, V.E., 2007. Middle paleozoic segment of the apparent polar
2855 wander path from the Siberian platform: New paleomagnetic evidence for the Silurian of the
2856 Nyuya-Berezovskii facial province. *Izv. Phys. Solid Earth* 43, 880–889.
2857 <https://doi.org/10.1134/S1069351307100102>

2858 Shephard, G.E., Müller, R.D., Seton, M., 2013. The tectonic evolution of the Arctic since Pangea
2859 breakup: Integrating constraints from surface geology and geophysics with mantle structure.
2860 *Earth-Sci. Rev.* 124, 148–183. <https://doi.org/10.1016/j.earscirev.2013.05.012>

2861 Shervais, J.W., Dennis, A.J., McGee, J.J., Secor, D., 2003. Deep in the heart of Dixie: Pre-Alleghanian
2862 eclogite and HP granulite metamorphism in the Carolina Terrane, South Carolina, USA. *J.*
2863 *Metamorph. Geol.* 21, 65–80.

2864 Shi, R., Yang, J., Wu, C., Wooden, J., 2004. First SHRIMP dating for the formation of the late Sinian
2865 Yushigou Ophiolite, North Qilian Mountains. *ACTA GEOLOGICA SINICA-CHINESE*
2866 *EDITION-* 78, 649–657.

2867 Shi, Y., Zhang, W., Kröner, A., Li, L., Jian, P., 2018. Cambrian ophiolite complexes in the Beishan area,
2868 China, southern margin of the Central Asian Orogenic Belt. *J. Asian Earth Sci.* 153, 193–205.
2869 <https://doi.org/10.1016/j.jseaes.2017.05.021>

2870 Sigloch, K., Mihalynuk, M.G., 2013. Intra-oceanic subduction shaped the assembly of Cordilleran North
2871 America. *Nature* 496, 50–56. <https://doi.org/10.1038/nature12019>

2872 Slagstad, T., Kulakov, E., Kirkland, C.L., Roberts, N.M.W., Ganerød, M., 2019. Breaking the Grenville–
2873 Sveconorwegian link in Rodinia reconstructions. *Terra Nova* 31, 430–437.
2874 <https://doi.org/10.1111/ter.12406>

2875 Smethurst, M.A., Khramov, A.N., 1992. A new Devonian palaeomagnetic pole for the Russian platform
2876 and Baltica, and related apparent polar wander. *Geophys. J. Int.* 108, 179–192.
2877 <https://doi.org/10.1111/j.1365-246X.1992.tb00848.x>

2878 Smethurst, M.A., Khramov, A.N., Pisarevsky, S., 1998. Palaeomagnetism of the Lower Ordovician
2879 Orthoceras Limestone, St. Petersburg, and a revised drift history for Baltica in the early
2880 Palaeozoic. *Geophys. J. Int.* 133, 44–56. <https://doi.org/10.1046/j.1365-246X.1998.1331463.x>

2881 Smirnov, A.V., Evans, D.A.D., Ernst, R.E., Söderlund, U., Li, Z.-X., 2013. Trading partners: Tectonic
2882 ancestry of southern Africa and western Australia, in Archean supercratons Vaalbara and
2883 Zimgarn. *Precambrian Res.* 224, 11–22. <https://doi.org/10.1016/j.precamres.2012.09.020>

2884 Sohl, L.E., Christie-Blick, N., Kent, D.V., 1999. Paleomagnetic polarity reversals in Marinoan (ca. 600
2885 Ma) glacial deposits of Australia: Implications for the duration of low-latitude glaciation in
2886 Neoproterozoic time. *GSA Bulletin* 111, 1120–1139. [https://doi.org/10.1130/0016-7606\(1999\)111<1120:PPRIMC>2.3.CO;2](https://doi.org/10.1130/0016-7606(1999)111<1120:PPRIMC>2.3.CO;2)

2888 Soldati, G., Boschi, L., Piersanti, A., Spada, G., 2001. The effect of global seismicity on the polar motion
2889 of a viscoelastic Earth. *J. Geophys. Res.* 106, 6761–6767. <https://doi.org/10.1029/2000JB900354>

2890 Song, S., Li, X.-H., 2019. A positive test for the Greater Tarim Block at the heart of Rodinia: Mega-
2891 dextral suturing of supercontinent assembly: COMMENT. *Geology* 47, e453–e453.

2892 Song, S., Niu, Y., Su, L., Xia, X., 2013. Tectonics of the North Qilian orogen, NW China. *Gondwana*
2893 *Res.* 23, 1378–1401. <https://doi.org/10.1016/j.gr.2012.02.004>

2894 Song, S., Niu, Y., Zhang, L., Wei, C., Liou, J.G., Su, L., 2009. Tectonic evolution of early Paleozoic HP
2895 metamorphic rocks in the North Qilian Mountains, NW China: New perspectives. *J. Asian Earth*
2896 *Sci.* 35, 334–353. <https://doi.org/10.1016/j.jseaes.2008.11.005>

2897 Song, S., Su, L., Li, X.-H., Niu, Y., Zhang, L., 2012. Grenville-age orogenesis in the Qaidam-Qilian
2898 block: The link between South China and Tarim. *Precambrian Res.* 220–221, 9–22.
2899 <https://doi.org/10.1016/j.precamres.2012.07.007>

2900 Stampfli, G.M., Borel, G.D., 2002. A plate tectonic model for the Paleozoic and Mesozoic constrained by
2901 dynamic plate boundaries and restored synthetic oceanic isochrons. *Earth Planet. Sci. Lett.* 196,
2902 17–33. [https://doi.org/10.1016/S0012-821X\(01\)00588-X](https://doi.org/10.1016/S0012-821X(01)00588-X)

2903 Stearn, J.E.F., Piper, J.D.A., 1984. Sub-Department of Geophysics, University of Liverpool, Liverpool

2904 L69 3BX (Gt. Britain). *Precambrian Res.* 23, 201–246.

2905 Steinberger, B., Torsvik, T.H., 2008. Absolute plate motions and true polar wander in the absence of
2906 hotspot tracks. *Nature* 452, 620–623. <https://doi.org/10.1038/nature06824>

2907 Stern, R.J., 1994. Arc Assembly and Continental Collision in the Neoproterozoic East African Orogen:
2908 Implications for the Consolidation of Gondwanaland. *Annu. Rev. Earth Planet. Sci.* 22, 319–351.
2909 <https://doi.org/10.1146/annurev.ea.22.050194.001535>

2910 Stern, R.J., Miller, N.R., 2018. Did the transition to plate tectonics cause Neoproterozoic Snowball Earth?
2911 *Terra Nova* 30, 87–94. <https://doi.org/10.1111/ter.12321>

2912 Strachan, R.A., Collins, A.S., Buchan, C., Nance, R.D., Murphy, J.B., D’Lemos, R.S., 2007. Terrane
2913 analysis along a Neoproterozoic active margin of Gondwana: insights from U–Pb zircon
2914 geochronology. *J. Geol. Soc. London* 164, 57–60. <https://doi.org/10.1144/0016-76492006-014>

2915 Sun, L.-S., Huang, B.-C., 2009. New paleomagnetic result for Ordovician rocks from the Tarim Block,
2916 Northwest China and its tectonic implications.

2917 Surkis, Y.F., Rodionov, V.P., Khramov, A.N., Gurevich, E.L., Westfahl, M., 1999. Geomagnetic
2918 reversals in the early Paleozoic: 3. Reversals recorded in redbeds of the lower Ordovician Mandra
2919 section, Siberia. *Izv. Phys. Solid Earth* 35, 347–357.

2920 Sutherland, R., Dickens, G.R., Blum, P., Agnini, C., Alegret, L., Asatryan, G., Bhattacharya, J.,
2921 Bordenave, A., Chang, L., Collot, J., Cramwinckel, M.J., Dallanave, E., Drake, M.K., Etienne,
2922 S.J.G., Giorgioni, M., Gurnis, M., Harper, D.T., Huang, H.-H.M., Keller, A.L., Lam, A.R., Li, H.,
2923 Matsui, H., Morgans, H.E.G., Newsam, C., Park, Y.-H., Pascher, K.M., Pekar, S.F., Penman,
2924 D.E., Saito, S., Stratford, W.R., Westerhold, T., Zhou, X., 2020. Continental-scale geographic
2925 change across Zealandia during Paleogene subduction initiation. *Geology* 48, 419–424.
2926 <https://doi.org/10.1130/G47008.1>

2927 Swanson-Hysell, N.L., Maloof, A.C., Kirschvink, J.L., Evans, D.A.D., Halverson, G.P., Hurtgen, M.T.,
2928 2012. Constraints on Neoproterozoic paleogeography and Paleozoic orogenesis from
2929 paleomagnetic records of the Bitter Springs Formation, Amadeus Basin, central Australia. *Am. J.*
2930 *Sci.* 312, 817–884. <https://doi.org/10.2475/08.2012.01>

2931 Tetley, M.G., 2018. Constraining Earth’s plate tectonic evolution through data mining and knowledge
2932 discovery (PhD). The University of Sydney.

2933 Tetley, M.G., Williams, S.E., Gurnis, M., Flament, N., Müller, R.D., 2019. Constraining absolute plate
2934 motions since the Triassic. *J. Geophys. Res. [Solid Earth]*. <https://doi.org/10.1029/2019JB017442>

2935 Thomas, R.J., De Waele, B., Schofield, D.I., Goodenough, K.M., Horstwood, M., Tucker, R., Bauer, W.,
2936 Annells, R., Howard, K., Walsh, G., Rabarimanana, M., Rafahatelo, J.M., Ralison, A.V.,
2937 Randriamananjara, T., 2009. Geological evolution of the Neoproterozoic Bemarivo Belt, northern

2938 Madagascar. *Precambrian Res.* 172, 279–300. <https://doi.org/10.1016/j.precamres.2009.04.008>

2939 Thompson, M.D., Grunow, A.M., Ramezani, J., 2010. Cambro-Ordovician paleogeography of the
2940 Southeastern New England Avalon Zone: Implications for Gondwana breakup. *GSA Bulletin*
2941 122, 76–88. <https://doi.org/10.1130/B26581.1>

2942 Thorogood, E.J., 1990. Provenance of the pre-Devonian sediments of England and Wales: Sm-Nd
2943 isotopic evidence. *J. Geol. Soc. London* 147, 591–594. <https://doi.org/10.1144/gsjgs.147.4.0591>

2944 Torsvik, T.H., Ashwal, L.D., Tucker, R.D., Eide, E.A., 2001. Neoproterozoic geochronology and
2945 palaeogeography of the Seychelles microcontinent: the India link. *Precambrian Res.* 110, 47–59.
2946 [https://doi.org/10.1016/S0301-9268\(01\)00180-2](https://doi.org/10.1016/S0301-9268(01)00180-2)

2947 Torsvik, T.H., Burke, K., Steinberger, B., Webb, S.J., Ashwal, L.D., 2010a. Diamonds sampled by
2948 plumes from the core-mantle boundary. *Nature* 466, 352–355.
2949 <https://doi.org/10.1038/nature09216>

2950 Torsvik, T.H., Cocks, L.R.M., 2017. The integration of palaeomagnetism, the geological record and
2951 mantle tomography in the location of ancient continents. *Geol. Mag.* 1–19.
2952 <https://doi.org/10.1017/S001675681700098X>

2953 Torsvik, T.H., Cocks, L.R.M., 2016. *Earth History and Palaeogeography*. Cambridge University Press.

2954 Torsvik, T.H., Cocks, L.R.M., 2009. The Lower Palaeozoic palaeogeographical evolution of the
2955 northeastern and eastern peri-Gondwanan margin from Turkey to New Zealand. *Geological*
2956 *Society, London, Special Publications* 325, 3–21. <https://doi.org/10.1144/SP325.2>

2957 Torsvik, T.H., Dietmar Muller, R., Van der Voo, R., Steinberger, B., Gaina, C., 2008. Global Plate
2958 Motion Frames: Toward a Unified Model. *Reviews of Geophysics* 46.
2959 <https://doi.org/10.1029/2007RG000227>

2960 Torsvik, T.H., Domeier, M., 2017. Correspondence: Numerical modelling of the PERM anomaly and the
2961 Emeishan large igneous province. *Nat. Commun.* 8, 821. [https://doi.org/10.1038/s41467-017-](https://doi.org/10.1038/s41467-017-00125-2)
2962 [00125-2](https://doi.org/10.1038/s41467-017-00125-2)

2963 Torsvik, T.H., Rehnström, E.F., 2001. Cambrian palaeomagnetic data from Baltica: implications for true
2964 polar wander and Cambrian palaeogeography. *J. Geol. Soc. London* 158, 321–329.
2965 <https://doi.org/10.1144/jgs.158.2.321>

2966 Torsvik, T.H., Smethurst, M.A., 1989. GMAP32—Geographic Mapping and Reconstruction System.
2967 *Geol. Surv. of Norway, Oslo* 1997.

2968 Torsvik, T.H., Smethurst, M.A., Meert, J.G., Van der Voo, R., McKerrow, W.S., Brasier, Sturt, B.A.,
2969 Walderhaug, H.J., 1996. Continental break-up and collision in the Neoproterozoic and Palaeozoic
2970 — A tale of Baltica and Laurentia. *Earth-Sci. Rev.* 40, 229–258. [https://doi.org/10.1016/0012-](https://doi.org/10.1016/0012-8252(96)00008-6)
2971 [8252\(96\)00008-6](https://doi.org/10.1016/0012-8252(96)00008-6)

- 2972 Torsvik, T.H., Steinberger, B., Gurnis, M., Gaina, C., 2010b. Plate tectonics and net lithosphere rotation
2973 over the past 150My. *Earth Planet. Sci. Lett.* 291, 106–112.
2974 <https://doi.org/10.1016/j.epsl.2009.12.055>
- 2975 Torsvik, T.H., Tait, J., Moralev, V.M., McKerrow, W.S., Sturt, B.A., Roberts, D., 1995. Ordovician
2976 palaeogeography of Siberia and adjacent continents. *J. Geol. Soc. London* 152, 279–287.
- 2977 Torsvik, T.H., Trench, A., 1991. The Lower—Middle Ordovician palaeofield of Scandinavia: southern
2978 Sweden “revisited.” *Phys. Earth Planet. Inter.* 65, 283–291.
- 2979 Torsvik, T.H., Trench, A., McKerrow, W.S., 1994. Implications of palaeomagnetic data from the
2980 Tortworth Silurian inlier (southern Britain) to palaeogeography and Variscan tectonism. *Geophys.*
2981 *J. Int.* 119, 91–100.
- 2982 Torsvik, T.H., Trench, A., Svensson, I., Walderhaug, H.J., 1993. Palaeogeographic significance of mid-
2983 Silurian palaeomagnetic results from southern Britain—major revision of the apparent polar
2984 wander path for eastern Avalonia. *Geophys. J. Int.* 113, 651–668.
- 2985 Torsvik, T.H., Van der Voo, R., 2002. Refining Gondwana and Pangea palaeogeography: estimates of
2986 Phanerozoic non-dipole (octupole) fields. *Geophys. J. Int.* 151, 771–794.
2987 <https://doi.org/10.1046/j.1365-246X.2002.01799.x>
- 2988 Torsvik, T.H., van der Voo, R., Doubrovine, P.V., Burke, K., Steinberger, B., Ashwal, L.D., Trønnes,
2989 R.G., Webb, S.J., Bull, A.L., 2014. Deep mantle structure as a reference frame for movements in
2990 and on the Earth. *Proc. Natl. Acad. Sci. U. S. A.* 111, 8735–8740.
2991 <https://doi.org/10.1073/pnas.1318135111>
- 2992 Torsvik, T.H., Van der Voo, R., Preeden, U., Mac Niocaill, C., Steinberger, B., Doubrovine, P.V., van
2993 Hinsbergen, D.J.J., Domeier, M., Gaina, C., Tohver, E., Meert, J.G., McCausland, P.J.A., Cocks,
2994 L.R.M., 2012. Phanerozoic polar wander, palaeogeography and dynamics. *Earth-Sci. Rev.* 114,
2995 325–368. <https://doi.org/10.1016/j.earscirev.2012.06.007>
- 2996 Trench, A., Torsvik, T.H., 1991. A revised Palaeozoic apparent polar wander path for Southern Britain
2997 (Eastern Avalonia). *Geophys. J. Int.* 104, 227–233. [https://doi.org/10.1111/j.1365-](https://doi.org/10.1111/j.1365-246X.1991.tb02506.x)
2998 [246X.1991.tb02506.x](https://doi.org/10.1111/j.1365-246X.1991.tb02506.x)
- 2999 Trench, A., Torsvik, T.H., Dentith, M.C., Walderhaug, H., Traynor, J.-J., 1992. A high southerly
3000 palaeolatitude for Southern Britain in Early Ordovician times: palaeomagnetic data from the
3001 Treffgarne Volcanic Formation SW Wales. *Geophys. J. Int.* 108, 89–100.
- 3002 Tretyakov, A.A., Degtyarev, K.E., Kovach, V.P., Kotov, A.B., Salnikova, E.B., Pilitsyna, A.V.,
3003 Yakovleva, S.Z., 2016. The migmatite–gneiss complex of the Chuya–Kendyktas sialic massif
3004 (Southern Kazakhstan): Structure and age. *Dokl. Earth Sci.* 467, 236–240.
3005 <https://doi.org/10.1134/S1028334X16030156>

3006 Tucker, R.D., Ashwal, L.D., Torsvik, T.H., 2001. U–Pb geochronology of Seychelles granitoids: a
3007 Neoproterozoic continental arc fragment. *Earth Planet. Sci. Lett.* 187, 27–38.
3008 [https://doi.org/10.1016/S0012-821X\(01\)00282-5](https://doi.org/10.1016/S0012-821X(01)00282-5)

3009 Tucker, R.D., Roig, J.Y., Macey, P.H., Delor, C., Amelin, Y., Armstrong, R.A., Rabarimanana, M.H.,
3010 Ralison, A.V., 2011. A new geological framework for south-central Madagascar, and its
3011 relevance to the “out-of-Africa” hypothesis. *Precambrian Res.* 185, 109–130.
3012 <https://doi.org/10.1016/j.precamres.2010.12.008>

3013 Tung, K., Yang, H.-J., Yang, H.-Y., Liu, D., Zhang, J., Wan, Y., Tseng, C.-Y., 2007. SHRIMP U-Pb
3014 geochronology of the zircons from the Precambrian basement of the Qilian Block and its
3015 geological significances. *Chin. Sci. Bull.* 52, 2687–2701. [https://doi.org/10.1007/s11434-007-](https://doi.org/10.1007/s11434-007-0356-0)
3016 [0356-0](https://doi.org/10.1007/s11434-007-0356-0)

3017 Vaes, B., Van Hinsbergen, D.J.J., Boschman, L.M., 2019. Reconstruction of subduction and back-arc
3018 spreading in the NW Pacific and Aleutian Basin: Clues to causes of Cretaceous and Eocene plate
3019 reorganizations. *Tectonics* 38, 1367–1413.

3020 van der Meer, D.G., Spakman, W., van Hinsbergen, D.J.J., Amaru, M.L., Torsvik, T.H., 2010. Towards
3021 absolute plate motions constrained by lower-mantle slab remnants. *Nat. Geosci.* 3, 36–40.
3022 <https://doi.org/10.1038/ngeo708>

3023 Van der Voo, R., 1990. The reliability of paleomagnetic data. *Tectonophysics* 184, 1–9.
3024 [https://doi.org/10.1016/0040-1951\(90\)90116-P](https://doi.org/10.1016/0040-1951(90)90116-P)

3025 Van der Voo, R., French, R.B., Williams, D.W., 1976. Paleomagnetism of the Wilberns Formation
3026 (Texas) and the late Cambrian paleomagnetic field for North America. *J. Geophys. Res.* 81,
3027 5633–5638.

3028 van Hinsbergen, D.J.J., Lippert, P.C., Dupont-Nivet, G., McQuarrie, N., Doubrovine, P.V., Spakman, W.,
3029 Torsvik, T.H., 2012. Greater India Basin hypothesis and a two-stage Cenozoic collision between
3030 India and Asia. *Proc. Natl. Acad. Sci. U. S. A.* 109, 7659–7664.
3031 <https://doi.org/10.1073/pnas.1117262109>

3032 van Hinsbergen, D.J.J., Torsvik, T.H., Schmid, S.M., Mañenco, L.C., Maffione, M., Vissers, R.L.M.,
3033 Gürer, D., Spakman, W., 2020. Orogenic architecture of the Mediterranean region and kinematic
3034 reconstruction of its tectonic evolution since the Triassic. *Gondwana Res.* 81, 79–229.
3035 <https://doi.org/10.1016/j.gr.2019.07.009>

3036 Van Lente, B., Ashwal, L.D., Pandit, M.K., Bowring, S.A., Torsvik, T.H., 2009. Neoproterozoic
3037 hydrothermally altered basaltic rocks from Rajasthan, northwest India: Implications for late
3038 Precambrian tectonic evolution of the Aravalli Craton. *Precambrian Res.* 170, 202–222.
3039 <https://doi.org/10.1016/j.precamres.2009.01.007>

3040 van Staal, C.R., Barr, S.M., Brendan Murphy, J., 2012. Provenance and tectonic evolution of Ganderia:
3041 Constraints on the evolution of the Iapetus and Rheic oceans. *Geology* 40, 987–990.
3042 <https://doi.org/10.1130/G333302.1>

3043 Vernikovskiy, V.A., Vernikovskaya, A.E., 2001. Central Taimyr accretionary belt (Arctic Asia): Meso–
3044 Neoproterozoic tectonic evolution and Rodinia breakup. *Precambrian Res.* 110, 127–141.
3045 [https://doi.org/10.1016/S0301-9268\(01\)00184-X](https://doi.org/10.1016/S0301-9268(01)00184-X)

3046 Vernikovskiy, V.A., Vernikovskaya, A.E., Kotov, A.B., Sal’nikova, E.B., Kovach, V.P., 2003.
3047 Neoproterozoic accretionary and collisional events on the western margin of the Siberian craton:
3048 new geological and geochronological evidence from the Yenisey Ridge. *Tectonophysics* 375,
3049 147–168. [https://doi.org/10.1016/S0040-1951\(03\)00337-8](https://doi.org/10.1016/S0040-1951(03)00337-8)

3050 Vernikovskiy, V.A., Vernikovskaya, A.E., Pease, V.L., Gee, D.G., 2004. Neoproterozoic Orogeny along
3051 the margins of Siberia. *Geological Society, London, Memoirs* 30, 233–248.
3052 <https://doi.org/10.1144/GSL.MEM.2004.030.01.18>

3053 Veselovskiy, R.V., Arzamastsev, A.A., 2011. Evidence for the Mesozoic endogenous activity in the
3054 northeastern part of the Fennoscandian Shield. *Dokl. Earth Sci.* 438, 754–758.
3055 <https://doi.org/10.1134/S1028334X11060377>

3056 Vick, H.K., Channell, J.E.T., Opdyke, N.D., 1987. Ordovician docking of the Carolina Slate Belt:
3057 Paleomagnetic data. *Tectonics* 6, 573–583. <https://doi.org/10.1029/TC006i005p00573>

3058 Vizan, H., Carney, J.N., Turner, P., Ixer, R.A., Tomasso, M., Mullen, R.P., Clarke, P., 2003. Late
3059 Neoproterozoic to Early Palaeozoic palaeogeography of Avalonia: some palaeomagnetic
3060 constraints from Nuneaton, central England. *Geol. Mag.* 140, 685–705.
3061 <https://doi.org/10.1017/S001675680300832X>

3062 von Raumer, J.F., Stampfli, G.M., 2008. The birth of the Rheic Ocean—Early Palaeozoic subsidence
3063 patterns and subsequent tectonic plate scenarios. *Tectonophysics* 461, 9–20.

3064 Walderhaug, H.J., Torsvik, T.H., Eide, E.A., Sundvoll, B., Bingen, B., 1999. Geochronology and
3065 palaeomagnetism of the Hunnedalen dykes, SW Norway: implications for the Sveconorwegian
3066 apparent polar wander loop. *Earth Planet. Sci. Lett.* 169, 71–83. [https://doi.org/10.1016/S0012-821X\(99\)00066-7](https://doi.org/10.1016/S0012-821X(99)00066-7)

3067

3068 Walderhaug, H.J., Torsvik, T.H., Halvorsen, E., 2007. The Egersund dykes (SW Norway): a robust Early
3069 Ediacaran (Vendian) palaeomagnetic pole from Baltica. *Geophys. J. Int.* 168, 935–948.
3070 <https://doi.org/10.1111/j.1365-246X.2006.03265.x>

3071 Wang, C., Liu, L., Wang, Y.-H., He, S.-P., Li, R.-S., Li, M., Yang, W.-Q., Cao, Y.-T., Collins, A.S., Shi,
3072 C., Wu, Z.-N., 2015. Recognition and tectonic implications of an extensive Neoproterozoic
3073 volcano-sedimentary rift basin along the southwestern margin of the Tarim Craton, northwestern

3074 China. *Precambrian Res.* 257, 65–82. <https://doi.org/10.1016/j.precamres.2014.11.022>

3075 Wang, C.-C., Jacobs, J., Elburg, M.A., Läufer, A., Thomas, R.J., Elvevold, S., 2020. Grenville-age
3076 continental arc magmatism and crustal evolution in central Dronning Maud Land (East
3077 Antarctica): Zircon geochronological and HfO isotopic evidence. *Gondwana Res.*
3078 <https://doi.org/10.1016/j.gr.2019.12.004>

3079 Weil, A.B., Geissman, J.W., Ashby, J.M., 2006. A new paleomagnetic pole for the Neoproterozoic Uinta
3080 Mountain supergroup, Central Rocky Mountain States, USA. *Precambrian Res.* 147, 234–259.
3081 <https://doi.org/10.1016/j.precamres.2006.01.017>

3082 Weil, A.B., Geissman, J.W., Van der Voo, R., 2004. Paleomagnetism of the Neoproterozoic Chuar
3083 Group, Grand Canyon Supergroup, Arizona: implications for Laurentia’s Neoproterozoic APWP
3084 and Rodinia break-up. *Precambrian Res.* 129, 71–92.

3085 Weil, A.B., Van der Voo, R., Mac Niocaill, C., Meert, J.G., 1998. The Proterozoic supercontinent
3086 Rodinia: paleomagnetically derived reconstructions for 1100 to 800 Ma. *Earth Planet. Sci. Lett.*
3087 154, 13–24. [https://doi.org/10.1016/S0012-821X\(97\)00127-1](https://doi.org/10.1016/S0012-821X(97)00127-1)

3088 Wen, B., Evans, D.A.D., Li, Y.-X., 2017. Neoproterozoic paleogeography of the Tarim Block: An
3089 extended or alternative “missing-link” model for Rodinia? *Earth Planet. Sci. Lett.* 458, 92–106.
3090 <https://doi.org/10.1016/j.epsl.2016.10.030>

3091 Wen, B., Evans, D.A.D., Wang, C., Li, Y.-X., Jing, X., 2019. A positive test for the Greater Tarim Block
3092 at the heart of Rodinia: Mega-dextral suturing of supercontinent assembly: REPLY. *Geology* 47,
3093 e454–e454.

3094 Wen, B., Evans, D.A.D., Wang, C., Li, Y.-X., Jing, X., 2018. A positive test for the Greater Tarim Block
3095 at the heart of Rodinia: Mega-dextral suturing of supercontinent assembly. *Geology* 46, 687–690.
3096 <https://doi.org/10.1130/G40254.1>

3097 Wen, B., Li, Y.-X., Zhu, W., 2013. Paleomagnetism of the Neoproterozoic diamictites of the Qiaoenbrak
3098 formation in the Aksu area, NW China: Constraints on the paleogeographic position of the Tarim
3099 Block. *Precambrian Res.* 226, 75–90. <https://doi.org/10.1016/j.precamres.2012.10.018>

3100 White, C.E., Barr, S.M., Hamilton, M.A., Murphy, J.B., 2020. Age and tectonic setting of Neoproterozoic
3101 granitoid rocks, Antigonish Highlands, Nova Scotia, Canada: Implications for Avalonia in the
3102 northern Appalachian orogen. *Can. J. Earth Sci.*

3103 White, C.E., Barr, S.M., Miller, B.V., Hamilton, M.A., 2002. Granitoid plutons of the Brookville terrane,
3104 southern New Brunswick: petrology, age, and tectonic setting.

3105 Wilhelm, C., Windley, B.F., Stampfli, G.M., 2012. The Altaids of Central Asia: A tectonic and
3106 evolutionary innovative review. *Earth-Sci. Rev.* 113, 303–341.
3107 <https://doi.org/10.1016/j.earscirev.2012.04.001>

3108 Williams, G.E., Schmidt, P.W., 2015. Low paleolatitude for the late Cryogenian interglacial succession,
3109 South Australia: paleomagnetism of the Angepena Formation, Adelaide Geosyncline. *Aust. J.*
3110 *Earth Sci.* 62, 243–253. <https://doi.org/10.1080/08120099.2015.1003967>

3111 Williams, S., Flament, N., Dietmar Müller, R., Butterworth, N., 2015. Absolute plate motions since 130
3112 Ma constrained by subduction zone kinematics. *Earth Planet. Sci. Lett.* 418, 66–77.
3113 <https://doi.org/10.1016/j.epsl.2015.02.026>

3114 Windley, B.F., Alexeiev, D., Xiao, W., Kröner, A., Badarch, G., 2007. Tectonic models for accretion of
3115 the Central Asian Orogenic Belt. *J. Geol. Soc. London* 164, 31–47. [https://doi.org/10.1144/0016-](https://doi.org/10.1144/0016-76492006-022)
3116 [76492006-022](https://doi.org/10.1144/0016-76492006-022)

3117 Wingate, M.T.D., Giddings, J.W., 2000. Age and palaeomagnetism of the Mundine Well dyke swarm,
3118 Western Australia: implications for an Australia–Laurentia connection at 755 Ma. *Precambrian*
3119 *Res.* 100, 335–357. [https://doi.org/10.1016/S0301-9268\(99\)00080-7](https://doi.org/10.1016/S0301-9268(99)00080-7)

3120 Wingate, M.T.D., Pisarevsky, S.A., De Waele, B., 2010. Paleomagnetism of the 765 Ma Luakela
3121 volcanics in Northwest Zambia and implications for Neoproterozoic positions of the Congo
3122 Craton. *Am. J. Sci.* 310, 1333–1344. <https://doi.org/10.2475/10.2010.05>

3123 Wu, C., Zuza, A.V., Yin, A., Liu, C., Reith, R.C., Zhang, J., Liu, W., Zhou, Z., 2017. Geochronology and
3124 geochemistry of Neoproterozoic granitoids in the central Qilian Shan of northern Tibet:
3125 Reconstructing the amalgamation processes and tectonic history of Asia. *Lithosphere* 9, 609–636.
3126 <https://doi.org/10.1130/L640.1>

3127 Wu, J., Suppe, J., Lu, R., Kanda, R., 2016. Philippine Sea and East Asian plate tectonics since 52 Ma
3128 constrained by new subducted slab reconstruction methods. *J. Geophys. Res. [Solid Earth]* 121,
3129 4670–4741.

3130 Wu, L., Murphy, J.B., Quesada, C., Li, Z.-X., Waldron, J.W.F., Williams, S., Pisarevsky, S., Collins,
3131 W.J., 2020. The amalgamation of Pangea: Paleomagnetic and geological observations revisited.
3132 *GSA Bulletin*. <https://doi.org/10.1130/B35633.1>

3133 Xia, B., Zhang, L., Du, Z., Xu, B., 2017. Petrology and age of Precambrian Aksu blueschist, NW China.
3134 *Precambrian Res.* <https://doi.org/10.1016/j.precamres.2017.12.041>

3135 Xiao, W., Windley, B.F., Allen, M.B., Han, C., 2013. Paleozoic multiple accretionary and collisional
3136 tectonics of the Chinese Tianshan orogenic collage. *Gondwana Res.* 23, 1316–1341.
3137 <https://doi.org/10.1016/j.gr.2012.01.012>

3138 Xiao, W., Windley, B.F., Yong, Y., Yan, Z., Yuan, C., Liu, C., Li, J., 2009. Early Paleozoic to Devonian
3139 multiple-accretionary model for the Qilian Shan, NW China. *J. Asian Earth Sci.* 35, 323–333.
3140 <https://doi.org/10.1016/j.jseaes.2008.10.001>

3141 Xiao, W.J., Mao, Q.G., Windley, B.F., Han, C.M., Qu, J.F., Zhang, J.E., Ao, S.J., Guo, Q.Q., Cleven,

3142 N.R., Lin, S.F., Shan, Y.H., Li, J.L., 2010. Paleozoic multiple accretionary and collisional
3143 processes of the Beishan orogenic collage. *Am. J. Sci.* 310, 1553–1594.
3144 <https://doi.org/10.2475/10.2010.12>

3145 Xu, D., Xia, B., Bakun-Czubarow, N., Bachlinski, R., Li, P., Chen, G., Chen, T., 2008. Geochemistry and
3146 Sr-Nd isotope systematics of metabasites in the Tunchang area, Hainan Island, South China:
3147 implications for petrogenesis and tectonic setting. *Mineral. Petrol.* 92, 361–391.
3148 <https://doi.org/10.1007/s00710-007-0198-0>

3149 Xu, D.-R., Xia, B., Li, P.-C., Chen, G.-H., Ma, C., Zhang, Y.-Q., 2007. Protolith natures and U-Pb
3150 sensitive high mass-resolution ion microprobe (SHRIMP) zircon ages of the metabasites in
3151 Hainan Island, South China: Implications for geodynamic evolution since the late Precambrian.
3152 *Island Arc* 16, 575–597.

3153 Xu, X., Song, S., Su, L., Li, Z., Niu, Y., Allen, M.B., 2015. The 600–580Ma continental rift basalts in
3154 North Qilian Shan, northwest China: Links between the Qilian-Qaidam block and SE Australia,
3155 and the reconstruction of East Gondwana. *Precambrian Res.* 257, 47–64.
3156 <https://doi.org/10.1016/j.precamres.2014.11.017>

3157 Xu, Y., Cawood, P.A., Du, Y., Zhong, Z., Hughes, N.C., 2014. Terminal suturing of Gondwana along the
3158 southern margin of South China Craton: Evidence from detrital zircon U-Pb ages and Hf isotopes
3159 in Cambrian and Ordovician strata, Hainan Island. *Tectonics* 33, 2490–2504.

3160 Yakubchuk, A., 2017. Evolution of the Central Asian Orogenic Supercollage since Late Neoproterozoic
3161 revised again. *Gondwana Res.* 47, 372–398. <https://doi.org/10.1016/j.gr.2016.12.010>

3162 Yang, B., Collins, A.S., Blades, M.L., 2019. Middle–late Mesoproterozoic tectonic geography of the
3163 North Australia Craton: U–Pb and Hf isotopes of detrital zircon grains in the Beetaloo Sub-basin,
3164 Northern *Journal of the*

3165 Yang, B., Collins, A.S., Cox, G.M., Jarrett, A.J.M., Denyszyn, S., Blades, M.L., Farkaš, J., Glorie, S.,
3166 2020. Using Mesoproterozoic sedimentary geochemistry to reconstruct basin tectonic geography
3167 and link organic carbon productivity to nutrient flux from a Northern Australian large igneous
3168 Province. *Basin Res.* 60, 175. <https://doi.org/10.1111/bre.12450>

3169 Yang, J.S., Wu, C.L., Chen, S.Y., Shi, R.D., Zhang, J.X., Meng, F.C., Zuo, G.C., Wu, H.Q.,
3170 Constantinovskaya, E., 2006. Neoproterozoic eclogitic metamorphic age of the Beishan eclogite
3171 of Gansu, China: evidence from SHRIMP U--Pb isotope dating. *Geology in China* 33, 317–325.

3172 Yang, Z., Otofujii, Y.-I., Sun, Z., Huang, B., 2002. Magnetostratigraphic constraints on the Gondwanan
3173 origin of North China: Cambrian/Ordovician boundary results. *Geophys. J. Int.* 151, 1–10.
3174 <https://doi.org/10.1046/j.1365-246X.2002.01656.x>

3175 Yang, Z., Sun, Z., Yang, T., Pei, J., 2004. A long connection (750–380 Ma) between South China and

3176 Australia: paleomagnetic constraints. *Earth Planet. Sci. Lett.* 220, 423–434.
3177 [https://doi.org/10.1016/S0012-821X\(04\)00053-6](https://doi.org/10.1016/S0012-821X(04)00053-6)

3178 Yang, Z.-Y., Sun, Z.M., Ma, X.H., Huang, B.C., Dong, J.M., Zhou, Y.X., Zhu, H., 1996. Preliminary
3179 paleomagnetic results from the Lower Paleozoic of North China (Henan Province) and its
3180 implications. *Chinese Science Bulletin (in Chinese)* 42, 401.

3181 Yin, A., Harrison, T.M., 2000. Geologic Evolution of the Himalayan-Tibetan Orogen. *Annu. Rev. Earth*
3182 *Planet. Sci.* 28, 211–280. <https://doi.org/10.1146/annurev.earth.28.1.211>

3183 Young, A., Flament, N., Maloney, K., Williams, S., Matthews, K., Zahirovic, S., Müller, R.D., 2019.
3184 Global kinematics of tectonic plates and subduction zones since the late Paleozoic Era.
3185 *Geoscience Frontiers* 10, 989–1013. <https://doi.org/10.1016/j.gsf.2018.05.011>

3186 Yuan, C., Sun, M., Yang, J., Zhou, H., Zhou, M.-F., 2004. Nb-depleted, continental rift-related Akaz
3187 metavolcanic rocks (West Kunlun): implication for the rifting of the Tarim Craton from
3188 Gondwana. *Geological Society, London, Special Publications* 226, 131–143.
3189 <https://doi.org/10.1144/GSL.SP.2004.226.01.07>

3190 Zeng, Y.-C., Chen, Q., Xu, J.-F., Chen, J.-L., Huang, F., Yu, H.-X., Zhao, P.-P., 2018. Petrogenesis and
3191 geodynamic significance of Neoproterozoic (~925 Ma) high-Fe–Ti gabbros of the RenTso
3192 ophiolite, Lhasa Terrane, central Tibet. *Precambrian Res.* 314, 160–169.
3193 <https://doi.org/10.1016/j.precamres.2018.06.005>

3194 Zhan, S., Chen, Y., Xu, B., Wang, B., Faure, M., 2007. Late Neoproterozoic paleomagnetic results from
3195 the Sugetbrak Formation of the Aksu area, Tarim basin (NW China) and their implications to
3196 paleogeographic reconstructions and the snowball Earth hypothesis. *Precambrian Res.* 154, 143–
3197 158. <https://doi.org/10.1016/j.precamres.2007.01.001>

3198 Zhang, C.-L., Li, H.-K., Santosh, M., Li, Z.-X., Zou, H.-B., Wang, H., Ye, H., 2012. Precambrian
3199 evolution and cratonization of the Tarim Block, NW China: Petrology, geochemistry, Nd-isotopes
3200 and U–Pb zircon geochronology from Archaean gabbro-TTG–potassic granite suite and
3201 Paleoproterozoic metamorphic belt. *J. Asian Earth Sci.* 47, 5–20.
3202 <https://doi.org/10.1016/j.jseaes.2011.05.018>

3203 Zhang, C.-L., Li, Z.-X., Li, X.-H., Ye, H.-M., 2009. Neoproterozoic mafic dyke swarms at the northern
3204 margin of the Tarim Block, NW China: Age, geochemistry, petrogenesis and tectonic
3205 implications. *J. Asian Earth Sci.* 35, 167–179. <https://doi.org/10.1016/j.jseaes.2009.02.003>

3206 Zhang, C.-L., Zou, H.-B., Li, H.-K., Wang, H.-Y., 2013. Tectonic framework and evolution of the Tarim
3207 Block in NW China. *Gondwana Res.* 23, 1306–1315. <https://doi.org/10.1016/j.gr.2012.05.009>

3208 Zhang, J., Mattinson, C.G., Meng, F., Wan, Y., Tung, K., 2008. Polyphase tectonothermal history
3209 recorded in granulitized gneisses from the north Qaidam HP/UHP metamorphic terrane, western

3210 China: Evidence from zircon U-Pb geochronology. *Geol. Soc. Am. Bull.* 120, 732–749.

3211 Zhang, N., Zhong, S., Leng, W., Li, Z.X., 2010. A model for the evolution of the Earth's mantle structure
3212 since the Early Paleozoic. *J. Geophys. Res.*

3213 Zhang, Q.R., Piper, J.D.A., 1997. Palaeomagnetic study of Neoproterozoic glacial rocks of the Yangzi
3214 Block: palaeolatitude and configuration of South China in the late Proterozoic Supercontinent.
3215 *Precambrian Res.* 85, 173–199. [https://doi.org/10.1016/S0301-9268\(97\)00031-4](https://doi.org/10.1016/S0301-9268(97)00031-4)

3216 Zhang, S., Evans, D.A.D., Li, H., Wu, H., Jiang, G., Dong, J., Zhao, Q., Raub, T.D., Yang, T., 2013.
3217 Paleomagnetism of the late Cryogenian Nantuo Formation and paleogeographic implications for
3218 the South China Block. *J. Asian Earth Sci.* 72, 164–177.
3219 <https://doi.org/10.1016/j.jseaes.2012.11.022>

3220 Zhang, S., Li, H., Jiang, G., Evans, D.A.D., Dong, J., Wu, H., Yang, T., Liu, P., Xiao, Q., 2015. New
3221 paleomagnetic results from the Ediacaran Doushantuo Formation in South China and their
3222 paleogeographic implications. *Precambrian Res.* 259, 130–142.
3223 <https://doi.org/10.1016/j.precamres.2014.09.018>

3224 Zhang, S.-H., Zhao, Y., Li, X.-H., Ernst, R.E., Yang, Z.-Y., 2017. The 1.33–1.30 Ga Yanliao large
3225 igneous province in the North China Craton: Implications for reconstruction of the Nuna
3226 (Columbia) supercontinent, and specifically with the North Australian Craton. *Earth Planet. Sci.*
3227 *Lett.* 465, 112–125.

3228 Zhao, G., Cawood, P.A., Wilde, S.A., Sun, M., 2002. Review of global 2.1–1.8 Ga orogens: implications
3229 for a pre-Rodinia supercontinent. *Earth-Sci. Rev.* 59, 125–162. [https://doi.org/10.1016/S0012-](https://doi.org/10.1016/S0012-8252(02)00073-9)
3230 [8252\(02\)00073-9](https://doi.org/10.1016/S0012-8252(02)00073-9)

3231 Zhao, G., Wang, Y., Huang, B., Dong, Y., Li, S., Zhang, G., Yu, S., 2018. Geological reconstructions of
3232 the East Asian blocks: From the breakup of Rodinia to the assembly of Pangea. *Earth-Sci. Rev.*
3233 186, 262–286. <https://doi.org/10.1016/j.earscirev.2018.10.003>

3234 Zhao, P., Chen, Y., Zhan, S., Xu, B., Faure, M., 2014. The Apparent Polar Wander Path of the Tarim
3235 block (NW China) since the Neoproterozoic and its implications for a long-term Tarim–Australia
3236 connection. *Precambrian Res.* 242, 39–57. <https://doi.org/10.1016/j.precamres.2013.12.009>

3237 Zhao, X., Coe, R.S., Liu, C., Zhou, Y., 1992. New Cambrian and Ordovician paleomagnetic poles for the
3238 North China Block and their paleogeographic implications. *J. Geophys. Res., Studi. Geol.* 97,
3239 1767–1788. <https://doi.org/10.1029/91JB02742>

3240 Zhong, S., Liu, X., 2016. The long-wavelength mantle structure and dynamics and implications for large-
3241 scale tectonics and volcanism in the Phanerozoic. *Gondwana Res.* 29, 83–104.
3242 <https://doi.org/10.1016/j.gr.2015.07.007>

3243 Zhong, S., Rudolph, M.L., 2015. On the temporal evolution of long-wavelength mantle structure of the

- 3244 Earth since the early Paleozoic. *Geochem. Geophys. Geosyst.* 16, 1599–1615.
- 3245 Zhong, S., Zhang, N., Li, Z.-X., Roberts, J.H., 2007. Supercontinent cycles, true polar wander, and very
3246 long-wavelength mantle convection. *Earth Planet. Sci. Lett.* 261, 551–564.
3247 <https://doi.org/10.1016/j.epsl.2007.07.049>
- 3248 Zhu, D.-C., Zhao, Z.-D., Niu, Y., Dilek, Y., Hou, Z.-Q., Mo, X.-X., 2013. The origin and pre-Cenozoic
3249 evolution of the Tibetan Plateau. *Gondwana Res.* 23, 1429–1454.
3250 <https://doi.org/10.1016/j.gr.2012.02.002>
- 3251 Zhu, D.-C., Zhao, Z.-D., Niu, Y., Dilek, Y., Mo, X.-X., 2011. Lhasa terrane in southern Tibet came from
3252 Australia. *Geology* 39, 727–730. <https://doi.org/10.1130/G31895.1>
- 3253 Zhu, G.-Y., Ren, R., Chen, F.-R., Li, T.-T., Chen, Y.-Q., 2017. Neoproterozoic rift basins and their
3254 control on the development of hydrocarbon source rocks in the Tarim Basin, NW China. *J. Asian
3255 Earth Sci.* 150, 63–72. <https://doi.org/10.1016/j.jseaes.2017.09.018>